The isolation, culture-expansion, cryopreservation, characterization, and properties of umbilical cord-derived mesenchymal stromal cells and their extracellular vesicles

by

Adrienne Beth Wright

B.S., University of Kentucky, 2012
M.A., Kansas State University, 2020

AN ABSTRACT OF A DISSERTATION

submitted in partial fulfillment of the requirements for the degree

DOCTOR OF PHILOSOPHY

Department of Anatomy & Physiology
College of Veterinary Medicine

KANSAS STATE UNIVERSITY
Manhattan, Kansas

2021

Abstract

Mesenchymal stromal cells (MSCs) are of therapeutic interest due to their immunomodulatory and regenerative properties. As a therapeutic, MSCs have limitations such as variability among tissue and species source, low survival, and risk of thrombosis or embolism following intravenous administration. Preclinical data supports MSCs as a therapeutic but has not translated to consistent, successful clinical trial results possibly due in part to aforementioned limitations. Extracellular vesicles (EVs) have been shown to be involved with physiological cell signaling and communication and may play a role in MSC's therapeutic effect. In addition, EVs purified from cell culture conditioned media have been shown to retain some properties of the parent cell type, such as cargo and protein surface marker expression, thus making EVs a potential therapeutic target. Although a cell-free product, EVs come with their own limitations such as the inability to produce sufficient and consistent EVs. Similar to MSCs from other species, EVs purified from these cell types are not well understood. Here, an optimized protocol for the isolation, expansion, cryopreservation, and characterization of canine umbilical cord-derived MSCs (UC-MSCs) is presented. This protocol addresses shortcomings in the canine MSC field by employing the coating of tissue culture surfaces to increase cellular adherence and the use of basic fibroblast growth factor in cell culture medium to allow canine MSCs to be maintained in culture longer than published methods before senescing. In addition, the effect of storage temperature of human UC-MSC conditioned media (CM) on subsequent purified EVs is presented demonstrating that comparable numbers of EVs could be isolated from CM following storage at room temperature, 4ºC, -20ºC, and -80ºC compared to fresh CM. Storage of CM at -80ºC resulted in a more homogeneous population of particles, with similar surface potential and hydrodynamic size. Although the presence of EVs were confirmed in all CM storage conditions by transmission electron

microscopy, only EVs from CM stored at -80ºC exhibited similar morphology and size to EVs purified from fresh CM. EVs from CM stored at -80ºC displayed stronger overall protein expression of tetraspanins CD9, CD63, and CD81, as well as heat shock protein 70, indicating that storage of CM at -80ºC is comparable to fresh CM for downstream EV purification. Lastly, it is demonstrated here that EVs purified from canine and human UC-MSC CM retain surface tissue factor expression from parental cells and display tissue factor-mediated procoagulant activity in the form of FXa generation. Thus, EV administration is a safety concern and poses a risk of thromboembolism. This is concerning since MSCs, and possibly MSC-EVs, are being investigated as a therapeutic, specifically with respiratory complications associated with COVID-19. We suggest that the procoagulant activity of EVs may serve as a safety screening tool in clinical use.

The isolation, culture-expansion, cryopreservation, characterization, and properties of umbilical cord-derived mesenchymal stromal cells and their extracellular vesicles

by

Adrienne Beth Wright

B.S., University of Kentucky, 2012
M.A., Kansas State University, 2020

A DISSERTATION

submitted in partial fulfillment of the requirements for the degree

DOCTOR OF PHILOSOPHY

Department of Anatomy & Physiology
College of Veterinary Medicine

KANSAS STATE UNIVERSITY
Manhattan, Kansas

2021

Approved by:

Major Professor
Dr. Mark Weiss

Copyright

Abstract

Mesenchymal stromal cells (MSCs) are of therapeutic interest due to their immunomodulatory and regenerative properties. As a therapeutic, MSCs have limitations such as variability among tissue and species source, low survival, and risk of thrombosis or embolism following intravenous administration. Preclinical data supports MSCs as a therapeutic but has not translated to consistent, successful clinical trial results possibly due in part to aforementioned limitations. Extracellular vesicles (EVs) have been shown to be involved with physiological cell signaling and communication and may play a role in MSC's therapeutic effect. In addition, EVs purified from cell culture conditioned media have been shown to retain some properties of the parent cell type, such as cargo and protein surface marker expression, thus making EVs a potential therapeutic target. Although a cell-free product, EVs come with their own limitations such as the inability to produce sufficient and consistent EVs. Similar to MSCs from other species, EVs purified from these cell types are not well understood. Here, an optimized protocol for the isolation, expansion, cryopreservation, and characterization of canine umbilical cord-derived MSCs (UC-MSCs) is presented. This protocol addresses shortcomings in the canine MSC field by employing the coating of tissue culture surfaces to increase cellular adherence and the use of basic fibroblast growth factor in cell culture medium to allow canine MSCs to be maintained in culture longer than published methods before senescing. In addition, the effect of storage temperature of human UC-MSC conditioned media (CM) on subsequent purified EVs is presented demonstrating that comparable numbers of EVs could be isolated from CM following storage at room temperature, 4ºC, -20ºC, and -80ºC compared to fresh CM. Storage of CM at -80ºC resulted in a more homogeneous population of particles, with similar surface potential and hydrodynamic size. Although the presence of EVs were confirmed in all CM storage conditions by transmission electron

microscopy, only EVs from CM stored at -80ºC exhibited similar morphology and size to EVs purified from fresh CM. EVs from CM stored at -80ºC displayed stronger overall protein expression of tetraspanins CD9, CD63, and CD81, as well as heat shock protein 70, indicating that storage of CM at -80ºC is comparable to fresh CM for downstream EV purification. Lastly, it is demonstrated here that EVs purified from canine and human UC-MSC CM retain surface tissue factor expression from parental cells and display tissue factor-mediated procoagulant activity in the form of FXa generation. Thus, EV administration is a safety concern and poses a risk of thromboembolism. This is concerning since MSCs, and possibly MSC-EVs, are being investigated as a therapeutic, specifically with respiratory complications associated with COVID-19. We suggest that the procoagulant activity of EVs may serve as a safety screening tool in clinical use.

Table of Contents

List of Figures xv
List of Tables xvii
List of Abbreviations xviii
Acknowledgements xx
Dedication xxii
Chapter 1 - Introduction 1
Mesenchymal Stromal Cells (MSCs) 1
History of MSC Research 1
Definition 2
Tissue Sources 3
Clinical Significance 4
Canines 6
Significance of Canines as a Model for Diseases and Genetic Disorders 6
Canine MSCs 6
Extracellular Vesicles (EVs) 7
Definition 8
Classification of EVs 8
Sources of EVs 9
Clinical Significance of EVs 10
Isolation of EVs 10
Centrifugation-Based Methods 11
Ultrafiltration 13
Size-Exclusion Chromatography 13
Characterization of EVs 14
Procoagulant Activity of MSCs 15
MSC *In Vivo* Survival 15
Instant Blood-Mediated Reaction 16
Tissue Factor 16

Chapter 2 - A Protocol for the Isolation, Culture, and Cryopreservation of Umbilical Cord-Derived Canine Mesenchymal Stromal Cells: Role of Cell Attachment in Long-Term Maintenance 20
Introduction 20
Materials and Methods 22
Umbilical Cord Collection 23
Gelatin Coating of Tissue Culture Plastic 23
Isolation of Canine UC-MSCs 24
Culture 26
Cryopreservation 26
Trilineage Differentiation 27
Colony-Forming Unit-Fibroblast Assay 28
Flow Cytometry 29
Reverse Transcriptase-Polymerase Chain Reaction 31
Statistics 34
Results 35
Isolation of MSCs from Canine Umbilical Cords 35
Stage 1 37
Stage 2 38
Stage 3 38
Effect of Gelatin-Coated Plates 41
Comparing Method of Lifting Cells for Passage 43
Cryopreservation Effects and Ability to Revive UC-MSCs from Cryostorage 44
Trilineage Differentiation 47
Immunophenotyping by Flow Cytometry 49
Confirmation of CD34 Expression by RT-PCR 50
Evaluation of Cell Cycle by Flow Cytometry 51
Discussion 52
Chapter 3 - Effect of Conditioned Media Storage Temperature on Extracellular Vesicles Isolated from Human Umbilical Cord-Derived Mesenchymal Stromal Cells 59
Introduction 59

Materials and Methods 62
Preparation of Conditioned Media from Human UC-MSCs 62
Preparation of Size-Exclusion Chromatography (SEC) Column 66
EV Isolation by a Combination of Ultrafiltration and SEC 66
Lyophilization of EVs for Transmission Electron Microscopy and Dot Blots 67
Nanoparticle Tracking Analysis 68
Dynamic Light Scattering 69
Transmission Electron Microscopy 70
Determination of Protein Concentration 70
Characterization by Dot Blot 71
MicroRNA Isolation and Reverse Transcriptase-Polymerase Chain Reaction 72
Statistics 76
Results 77
EV Analysis by Nanoparticle Tracking Analysis 77
EV Characterization by Dynamic Light Scattering 81
EV Analysis by TEM 82
EV Characterization by Dot Blots 85
Analysis of EV-Associated miRNAs 87
Discussion 90
Chapter 4 - Procoagulant Activity of Canine MSC-EVs 100
Introduction 100
Materials and Methods 103
Experimental Design 103
Preparation of Conditioned Media from Canine UC-MSCs 104
Preparation of Size-Exclusion Chromatography Column 107
EV Isolation by a Combination of Ultrafiltration and SEC 107
EV Isolation by Ultracentrifugation 108
Lyophilization of EVs 109
Nanoparticle Tracking Analysis 109
Dynamic Light Scattering 111
Transmission Electron Microscopy 112

Determination of Protein Concentration 112
Immunocytochemistry 113
Protein Expression by Dot Blots 114
Procoagulant Assay 115
Statistics 117
Results 118
Isolation of EVs 118
EV Analysis by NTA 118
EV Characterization by Dynamic Light Scattering 122
EV Analysis by Transmission Electron Microscopy 126
Comparison of Protein Content in EV Samples 127
Expression of Tissue Factor by MSCs 129
Tissue Factor Expression by EVs 129
EVs Possess Procoagulant Activity 132
Discussion 137
Chapter 5 - Therapeutic Use of Mesenchymal Stromal Cells: The Need for Inclusive Characterization Guidelines to Accommodate All Tissue Sources and Species 154
Introduction 154
Challenges for Clinical Translation of Mesenchymal Stromal Cells 156
Outdated Characterization Guidelines 156
Biological Variability Translates to MSC Inconsistencies 158
Regulatory Gaps in MSC Therapy 159
MSC-Based Products Also Suffer from Lack of Standardization 163
Tissue Source Differences 165
Species Differences 167
MSC Heterogeneity 172
Purity vs. Potency 173
Need for an Expanded Surface Marker Characterization Panel 173
Metrology Standards 176
Research Driven by Commercial Applicability 177
Allogeneic MSC Therapy Represents a Viable Business Model 179

Conclusion 185
Chapter 6 - Conclusion 187
References 191
Appendix A - Supplementary Data from Chapter 2 224
Appendix B - Supplementary Data from Chapter 3 233
Appendix C - Supplementary Data from Chapter 4 234
Appendix D - Human Umbilical Cord Mesenchymal Stromal Cell Isolation, Expansion, Cryopreservation, and Characterization 235
Introduction 235
Strategic Planning 238
Basic Protocol 1: Isolation of Cells from Umbilical Cord 238
Materials 241
Umbilical Cord 243
Setup 243
Wash and Sanitize 243
Cutting and Rinsing 244
Dissociation with Enzyme and Incubation 244
BSC Setup and After Incubation 244
Filtration 245
RBC Lysis 245
Cell Counting with ViaStain 245
Plating Cells 246
Basic Protocol 2: Culturing and Passaging UC-MSCs 247
Materials 249
Passaging the Cells 249
Counting and Plating UC-MSCs 250
Culturing UC-MSCs 251
Basic Protocol 3: Cryopreservation and Thawing of UC-MSCs 251
Materials 251
Cryopreservation 252
Thawing Frozen Cells 253

Basic Protocol 4: Flow Cytometry 253
Materials 254
Cell Culture 255
Cell Detachment for Flow Cytometry 256
Strain Cells 256
Counting 256
Staining for Flow Cytometry 257
Perform Flow Cytometry 257
Basic Protocol 5: Osteogenic, Adipogenic, and Chondrogenic Differentiation of UC-MSCs 260
Materials 261
Cell Culture and Passaging 261
Differentiation Media 262
Adipogenesis 262
Osteogenesis 262
Chondrogenesis 263
Basic Protocol 6: Staining for MSC Differentiation 264
Materials 264
Fixing the Cells 264
Osteogenic Staining 265
Adipogenesis Staining 265
Chondrogenic Staining 265
Basic Protocol 7: Colony Forming-Units-Fibroblast (CFU-F) 266
Materials 267
Cell Culture and Passaging 267
Plating for CFU-F Assay 267
Methanol Fixation 268
Methylene Blue Staining 268
Reagents and Solutions 269
Commentary 274
Background Information 274
Critical Parameters and Troubleshooting 276

Anticipated Results 277
Time Considerations 278
Appendix E - Copyright Releases 280
Chapter 2 Copyright Release 280
Chapter 5 Copyright Release 280

List of Figures

Figure 1: A schematic of the isolation procedure showing the major steps involved for obtaining MSCs from the canine umbilical cord. 36
Figure 2: Isolation efficiency from umbilical cord. 37
Figure 3: Stepwise improvement of canine MSC expansion. 39
Figure 4: Effect of gelatin coating of plates on canine MSCs morphology 41
Figure 5: Effect of gelatin coating of plates on canine MSCs expansion. 42
Figure 6: Nattokinase improved MSC passage compared to TrypLE Express. 44
Figure 7: Cryostorage reduces the viability of canine MSCs. 46
Figure 8: Trilineage differentiation of canine MSCs. 48
Figure 9: Immunophenotyping of canine UC-MSCs. 50
Figure 10: Flow cytometric analysis of canine MSC cell cycle and polyploidy. 52
Figure 11: Storage Experimental Schematic 65
Figure 12: Effect of CM Storage Temperature on Particle Count 78
Figure 13: Particles per MSC by CM Storage Condition 80
Figure 14: Dynamic Light Scattering Analysis of EVs 82
Figure 15: TEM Analysis of EVs 84
Figure 16: Effect of CM Storage Condition on EV Dot Blot Staining 86
Figure 17: Total miRNA Yield from EVs 87
Figure 18: Effect of CM Storage Condition on miRNA Expression 89
Figure 19: Experimental Design 104
Figure 20: Experimental Schematic 106
Figure 21: Nanoparticle Tracking Analysis Particle Counts 119
Figure 22: Nanoparticle Tracking Analysis of the Size of Canine MSC-EVs 120
Figure 23: Effect of Cell Passage on the Number of EVs Released per Canine UC-MSC 122
Figure 24: Dynamic Light Scattering Polydispersity Index of Canine EVs 123
Figure 25: The Effect of Passage and Isolation Method on Canine EVs Zeta Potential 124
Figure 26: Hydrodynamic Size of Canine EVs 125
Figure 27: Transmission Electron Microscopy Analysis of Canine EVs 127

Figure 28: Relationship Between Soluble Protein Concentration and EVs by Isolation Method 128
Figure 29: Tissue Factor Expression by Human and Canine MSCs 129
Figure 30: Dot Blot Analysis for Canine MSC-EVs 131
Figure 31: Comparing the Procoagulant Activity of Human and Canine EVs 132
Figure 32: Procoagulant Activity of MSC-EVs 134
Figure 33: Inhibition of Procoagulant Activity of EVs 137
Figure 34: Canine Expression of MSC Markers in the Literature 170
Figure 35: Porter's Five Forces Analysis 181
Figure 36: Supplementary Figure S1 224
Figure 37: Supplementary Figure S2 225
Figure 38: Supplementary Figure S3 226
Figure 39: Supplementary Figure S4 227
Figure 40: Supplementary Figure S5 228
Figure 41: Supplementary Figure S6 229
Figure 42: Supplementary Figure S7 230
Figure 43: Supplementary Figure S8 233
Figure 44: Supplementary Figure S9 234
Figure 45: Isolation Flowchart 237
Figure 46: Cell Numbers for Isolation and Expansion 248
Figure 47: Flow Cytometry Characterization of Human UC-MSCs 259
Figure 48: Trilineage Differentiation of Human UC-MSCs 260
Figure 49: Human UC-MSC CFU-F 266
Figure 50: Chapter 2 Copyright Release 280

List of Tables

Table 1: Antibodies Tested in Flow Cytometry 30
Table 2: Reverse Transcriptase-Polymerase Chain Reaction Primers 33
Table 3: Calculation of Viable Cell Number 69
Table 4: RT-PCR Primers 75
Table 5: NTA Size Estimate of EVs by CM Storage Condition 77
Table 6: EVs Released per MSC by Cell Line 79
Table 7: Calculation of Viable Cell Number for Canine MSCs 111
Table 8: Antibodies Used for Dot Blots 115
Table 9: Procoagulant Activity per Million Cells and EVs 135
Table 10: MSC Products with Regulatory Approval 160
Table 11: Supplementary Table S1. Media Formulations Tested for Trilineage Differentiation 231
Table 12: Supplementary Table S2. Antibody Clone Discrepancies Noted 232
Table 13: Umbilical Cord Isolation Numbers Averaged per Variable 240
Table 14: Passaging and Culturing Component Volume for Plate Size 246
Table 15: Flow Cytometry Antibodies for each Test 254

List of Abbreviations

A/A: antibiotic/antimycotic

ABs: apoptotic bodies

ACB: canine MSC cell culture medium

ANOVA: analysis of variance

AOPI: acridine orange propidium iodide

AT: adipose tissue

AT-MSCs: adipose tissue-derived mesenchymal stromal cells

bFGF: basic fibroblast growth factor

BM: bone marrow

BM-MSCs: bone marrow-derived mesenchymal stromal cells

BSA: bovine serum albumin

BSC: biological safety cabinet

CD: cluster of differentiation

CFU-F: colony forming units-fibroblast

CPD: cumulative population doublings

CUC: canine umbilical cord

DG: density gradient

DLA: dog leukocyte antigen

DMEM: Dulbecco's Modified Eagle Medium

DNA: deoxyribonucleic acid

DOE: design of experiments

DPBS: Dulbecco's phosphate-buffered saline

EDTA: ethylenediaminetetraacetic acid

EMF: Enhanced MetaFile

EVs: extracellular vesicles

FVII: factor VII

FVIIa: factor VIIa

FX: factor X

HBSS: Hank's balanced salt solution

HLA-DR: human leukocyte antigen—DR isotype

HSP: heat shock protein

HUC: human umbilical cord

IACUC: Institutional Animal Care and Use Committee

IBMIR: instant blood-mediated inflammatory reaction

IBMX: 3-Isobutyl-1-methylxanthine

IFATS: International Federation for Adipose Therapeutics

ILVs: intraluminal vesicles

ISCT: International Society for Cellular Therapy

ISEV: International Society for Extracellular Vesicles

MAPCs: multipotent adult progenitor cells

MHC: major histocompatibility complex

miRNA: microRNA

mRNA: messenger RNA

MSC: mesenchymal stromal cell

MSC-EVs: mesenchymal stromal cell-derived extracellular vesicles

MVBs: multivesicular bodies

MVs: microvesicles

PEG: polyethylene glycol

PVDF: polyvinylidene difluoride

RBC: red blood cells

RNA: ribonucleic acid

RT-PCR: reverse transcriptase-polymerase chain reaction

SEC: size-exclusion chromatography

SVF: stromal vascular fraction

TF: tissue factor

TIFF: tag image file format

TSG101: tumor susceptibility gene 101

TSP: thrombospondin

UC: ultracentrifugation

UC-MSCs: umbilical cord-derived mesenchymal stromal cells

Acknowledgements

First and foremost, I would like to thank Dr. Mark Weiss for his guidance, wisdom, and patience. He always believed in me and realized my potential, even when I did not. Without him, this achievement would not have been possible. A special thanks to Tian Bao (Dr. Hong He), for sharing his wisdom and knowledge. It is an honor to be a part of the He family. I will take the "no hurry, no mistake" philosophy with me throughout all of my endeavors. I would also like to extend my deepest gratitude to Dr. Larry Snyder for always being willing and able to lend a hand. Because of his contributions, I was able to continue my work during the COVID pandemic and not lose progress. I would also like to thank Ellen Weiss for always being willing and able to provide beautiful illustrations for our publications and this work.

I would also like to thank Dr. Sherry Fleming for being a mentor and committee member. Dr. Fleming was always available and gave me an example of a woman in science to look up to and for that, I am so appreciative. I would like to thank my graduate committee members, Dr. Ansley Chua and Dr. Don Cohen, for their time, support, and wisdom. I would also like to thank the faculty and staff at the College of Business for allowing me to pursue my MBA alongside my PhD. Specifically, I would like to thank Drs. Marne Arthaud-Day and Chwen Sheu, two wonderful mentors. They both went above and beyond to offer me support and guidance. I am most appreciative for the perspectives and skills I gained during my time with the College of Business and will take these skills with me throughout my career. I also want to thank the Department of Anatomy and Physiology for their support over the years.

To my husband, Jacob. Words cannot express how thankful I am for you. You have stood by me since my first day of classes. Your unwavering love and support were the motivation I

needed to get through the hardest days. You have sacrificed a lot to see me through this journey, and for that, I am forever grateful. I thank you for always understanding and being willing to listen. I could not have done this without you. I love you and now I am ready for us to begin the next chapter.

Last, but certainly not least, to all of my friends and family. It would be impossible for me to express my gratitude to each and every one of you. Just know that you were an integral part of this process. I thank you for standing by my side during it all and I could not have been successful without your love and support.

Dedication

I dedicate this dissertation in loving memory of my wonderful mother, Patricia, whose unconditional love and support shaped me into the person I am. Without her and her sacrifices, this work would not have been possible. My only wish is that she was here to share this accomplishment with me. Not a day goes by that I do not miss you. I love you to pieces, Mom.

To my son, Benjamin. Being your mother is my greatest achievement. You have made me a better person. Please know it was never easy to sacrifice my time with you for research and writing, but I did it to give you the best life possible. I hope that one day you look at what I have accomplished and realize that anything is possible with hard work and determination.

Chapter 1 - Introduction

Mesenchymal Stromal Cells (MSCs)

History of MSC Research

In the late 1960s and 1970s, through a series of experiments, Alexander Friedenstein detailed a fibroblastic population of tissue culture treated plastic-adherent cells from bone marrow (BM) that was unlike the hematopoietic cells typically found in that niche [1-3]. These cells, which had the potential to form osteoblasts and fibrous tissue, were referred to as osteogenic stem cells [3, 4]. During the 1980s, several researchers demonstrated that the osteogenic stem cells described by Friedenstein were multipotent and capable of differentiating into osteoblasts, chondroblasts, adipocytes, and myoblasts [5]. The first use of the term "mesenchymal stem cell" appeared in the literature in 1991 by Arnold Caplan when he described the potential therapeutic use of these cells for skeletal tissue repair [6]. Arguments as to whether these cells could be considered a true stem cell went on for years [4]. One side of the argument claimed that "stem" referred to multipotent nature of the cells and their ability to self-renew and differentiate to cells of mesenchymal lineages (i.e., adipocytes, chondrocytes, and osteoblasts) [2, 7, 8]. In contrast, some argued that the BM contained a heterogeneous population of multipotent progenitor cells that vary in their response to differentiation factors, not a homogeneous stem cell population as proposed by others [4, 9]. Work by Dennis et al. indicated that not all of the cells in the BM population were true "stem cells" and thus referring to them as such was not physiologically accurate [9]. Alternative names that exclude the word "stem" were suggested, and the consensus or compromise term "multipotent mesenchymal stromal cell" was proposed by the International Society for Cellular Therapy (ISCT)

in 2005 [2, 4, 10, 11]. This term has been adopted in the literature and is predominantly used to the present day.

Definition

A stem cell is defined as a long-lived, self-renewing cell with the potential for differentiation into more specialized cells. Mesenchymal stromal cells (MSCs) are a heterogeneous, multipotent population of cells theoretically composed of stem (multipotent), progenitor (bipotent or unipotent), and differentiated (null potent) cell subpopulations [4, 12]. The ISCT original definition, released in 2005, was a "minimal defining criteria" of MSCs isolated from human BM [11]. These guidelines include 1.) Adherence to tissue culture plastic and self-renewal (inferring clonal expansion capability as demonstrated by the colony-forming unit-fibroblast assay); 2.) Positive (≥95%) for surface antigen markers CD105, CD90, and CD73; and negative (≤2%) for CD45 (pan-leukocyte), CD34 (hematopoietic and endothelial cells), CD14 or CD11b (monocytes and macrophages), CD79α or CD19 (B cells), and human leukocyte antigen—DR isotype (HLA-DR); and 3.) Capacity for tri-lineage differentiation to adipocytes, chondroblasts, and osteoblasts [11]. As discussed in Chapter 5, this definition does not require clonal expansion and does not account for tissue or species differences, donor age, nor the effect of cell passage at the time of characterization yet is commonly applied to all MSCs [13]. In 2013, the ISCT amended the MSC definition to include a function assay, such as a bioassay of immunosuppressive properties, but it did not further refine the original definition. In the same year, the International Federation for Adipose Therapeutics (IFATS) and the ISCT released a joint statement amending the minimal criteria for a freshly-isolated stromal vascular fraction (SVF) and

cultured stromal cells from adipose tissue, most importantly by adding surface expression of CD34 in SVF [14].

Tissue Sources

Since their discovery in the BM, MSCs (or MSC-like cells that I will refer to as MSCs, here) have been successfully isolated from other tissues including, but not limited to, adipose tissue (AT); extra-embryonic tissues, such as the placenta and the umbilical cord stroma; umbilical cord blood; muscle; and other decidual tissues such as teeth (dental pulp) and menstrual blood [15-22].

Owing to the human BM being the "defining-standard" MSC tissue source, other tissue sources come with a unique set of advantages and disadvantages, and the MSCs isolated from these other tissues (and other species) may differ in physiology, morphology, multi-lineage differentiation potential, or gene expression [13]. BM harvest is a painful, invasive procedure while other tissues, such as AT and extra-embryonic, can be harvested easily and painlessly as part of routine or elective procedures [13]. Further, as extra-embryonic tissue is deemed medical waste generated as part of routine births, it can be considered an inexhaustible source for MSCs [23]. Compared to adult tissues, e.g., BM and AT, extra-embryonic tissues may represent the ideal source for MSCs as they come from donors of a consistent young age [13, 23, 24]. BM-MSCs isolated from elderly donors have been shown to be less "stemmy" as they are difficult to expand in culture and senesce rapidly [7, 25]. Here, "stemmy" refers to the capacity of the cells to demonstrate stem cell-like properties.

Within the umbilical cord, MSCs have been isolated from umbilical cord blood, perivascular cells, and the Wharton's jelly (WJ) [15, 24]. WJ is the loose connective tissue matrix between umbilical cord blood vessels that functions to provide support and contains high amounts

of extracellular matrix components, such as collagen, hyaluronic acid, and sulfated proteoglycans [26-28]. The WJ includes three indistinct regions, the perivascular space, intravascular space, and the subamnion; it is unknown if these contain distinct cell populations [24]. MSCs isolated from the WJ have been shown to be both similar to and different from BM-MSCs. For example, similar to BM-MSCs, WJ-MSCs are tissue culture plastic-adherent, undergo self-renewal, possess multilineage differentiation potential, and express CD73, CD90, CD105, CD10, CD13, CD29, and CD44 but are negative for CD34, CD45, CD14, CD33, CD56, CD31, and HLA-DR/MHC class II [24, 29-33]. In contrast to BM-MSCs, WJ-MSCs appear to have a greater proliferative capacity, increased immunomodulatory potential, decreased population doubling time, and a decreased potential to differentiate into adipocytes [24, 29-31, 34]. In addition to humans and rodents, MSCs have successfully been isolated from the umbilical cord and umbilical cord blood from several veterinary species including canines [12, 35-37], porcine [38], bovine [39], caprine [40], and equines [41-43].

Clinical Significance

MSCs have been used as a therapeutic modality in tissue injuries, chronic degenerative disorders, and inflammatory diseases due to their regenerative potential and anti-inflammatory effects [44-49]. In recent late phase clinical trials, MSCs have demonstrated efficacy in treating complex perianal fistulas in Crohn's disease patients as well as a reduction in both morbidity and mortality in graft-versus-host-disease pediatric patients [44, 50]. Despite these successes and promising preclinical studies in animals, MSCs have not been able to meet efficacy endpoints in many human early- and late-phase clinical trials [13, 51, 52]. It is unclear as to why the strong positive results of preclinical MSC studies have not translated in human MSC clinical studies.

While reasons for the clinical translation barrier are discussed in Chapter 5, this matter will require additional research to hash out.

The consensus is that allogeneic MSCs are "safe" due to the low incidence of serious adverse events when tested as an experimental modality in a variety of disorders [50, 53-56]. A meta-analysis demonstrated that a single injection of allogeneic BM-MSCs is safe, but a toxic dose has yet to be established [48, 54, 57]. Adverse events have occurred as a result of MSC administration and there is speculation that adverse events may be under-reported [58-62]. There are gaps in the understanding of the safety of allogeneic MSCs when derived from tissue sources other than BM, culture-expanded in various conditions, repeatedly administered, administered in various dose sizes, administered in methods other than intravenous, and how they interact with the immune system.

For years it was believed that allogeneic MSCs were immune-privileged and that this would allow MSCs to be administered with no respect to major histocompatibility (MHC) markers and with no risk of immune rejection [44, 63]. Under this premise, allogeneic MSCs could be mass-produced and used to treat a large number of patients as an off-the-shelf product, with little risk of adverse effects. Since then, this immune-privileged philosophy has been debunked and the modified idea that MSCs are "immune-evasive" has been proposed [63]. MSCs express MHC class I antigens and lack expression of MHC class II, although MHC class II expression can be induced following exposure to inflammatory cytokines and a freeze/thaw cycle [64-68]. Data from animal studies suggest that allogeneic use of MSCs may not be safe due to immune response and rejection [64, 69-72]. Humoral alloimmunization has been reported in humans and equines when infused with non-matched MSCs [44, 73, 74]. In contrast, MSCs exhibit strong immunomodulatory properties that inhibit an allogeneic response and that there is no difference in the immune response

between allogeneic and autologous MSCs [75, 76]. Further, studies involving autologous (syngeneic) or MHC-matched MSCs in mice are almost unanimous in support of their use due to low risk [44].

Canines

Significance of Canines as a Model for Diseases and Genetic Disorders

Canines represent a sizable domestic population with over 350 distinct breeds recognized around the world [77]. Over 450 hereditary diseases have been reported in canines with approximately 360 of those analogous to humans, making the dog an excellent naturally-occurring disease and genetic disorders model [12, 77-81]. In addition, canines share the living environment with humans, breeds represent a distinct phenotype, canines have a highly conserved synteny to the human genome, and they are a large animal making them more physiologically similar than small animal models [77, 82, 83]. Canines disease models are widely used in aging [84, 85], cancer [77, 86], inherited muscle diseases [87, 88], cardiovascular exercise studies [89], retinal dystrophies [90], dementia and Alzheimer's disease [91, 92], osteoarthritis [93-95], and other anatomical injuries, especially those involving large joints [96]. In early clinical studies, canine MSCs have been tested as a treatment for orthopedic injuries and have been demonstrated to be safe and effective [12, 97-101].

Canine MSCs

Despite having potential as a well-suited disease model for multiple human diseases and genetic disorders, MSCs derived from canines remain marginalized in the literature compared to

rodents [12]. There are numerous barriers that may delay the widespread use of canine MSCs. First, it has been noted that canine MSCs may have a limited lifespan when maintained in culture due to rapid senescence at or before passage six [98, 101-110]. Few groups have been able to demonstrate canine MSCs culture-expanded for more than six passages [12, 35, 111, 112]. This highlights the lack of standardized isolation and culture protocols for canine MSCs that can aid in providing canine MSCs that can survive longer than six passages without senescing. Further, it highlights the inconsistencies regarding the overall health of the canine MSCs make it challenging to compare results and forces researchers to characterize at lower passages (< P3). Characterization of human MSCs is typically performed between passages 3 and 6 to allow for purification of the MSC population via product by process and expansion-related deletion of unattached endothelial cells, as well as surface marker maturation [113-116]. Second, canine surface marker antibody availability is more limited compared to humans and rodents, specifically for antibodies that are not used as part of routine diagnostics. Poor resource availability makes it difficult to characterize and accurately analyze canine MSCs, thus impeding widespread use of canine MSCs. Standardized protocols for isolation, culture, and characterization could support the use of canine MSCs by providing consistent canine MSC studies that allow for comparison among researchers. Here, we have provided a recommended protocol for isolation, culture, characterization, and cryopreservation to serve as a standard [12].

Extracellular Vesicles (EVs)

Definition

Although it was once believed that MSCs exerted their therapeutic effect via engrafting and differentiation, much of their therapeutic effect is due to the production and secretion of soluble factors and extracellular vesicles [117-122]. Extracellular vesicles (EVs) are a family of nanosized particles with a glycosylated phospholipid bilayer membrane released by many cell types, including MSCs [117, 123-125]. EVs have been grouped based on their size and mechanism of cellular release into three subpopulations: microvesicles (MVs), apoptotic bodies (ABs), and exosomes [120, 126].

Classification of EVs

MVs, or shedding particles, are formed by the outward budding of the plasma membrane and range in size from 50 to 1000 nm in diameter [120, 127-129]. ABs are the largest EVs (diameter 50 - 5000 nm) and are released into the extracellular space by apoptotic cells [120, 127]. Exosomes (30 - 150 nm in diameter) are formed when early endosomes are transferred into multivesicular bodies (MVBs)/late endosomes via formation of intraluminal vesicles (ILVs) from inward budding of the lumen and finally fusion with the plasma membrane and extracellular release of the ILV as an exosome [118, 120, 127, 130-133].

Although the size ranges overlap, EV subpopulations vary in proteins, membrane composition, and density (i.e., sedimentation speed). MVs membranes are identified based upon integrins, selectins, and CD40 composition [134, 135]. The MV membrane is made up of cholesterol, diacylglycerol, and phosphatidylserine in larger amounts when compared to exosomes [130, 135]. MVs can be sedimented by centrifugation at 10,000-20,000 *g* [136, 137]. ABs are identified using histones, thrombospondin (TSP), and C3b [135, 138]. ABs have

phosphatidylserine on the surface and can be sedimented by centrifugation at 10,000 - 100,000 *g* [135]. Unlike MVs and exosomes, ABs contain fragmented genomic DNA and cell organelles [135, 138-140]. Exosomes are identified by tetraspanins (e.g., CD9, CD63, CD81, and CD82), flotillin, TSG101, Alix, and heat shock proteins (e.g., HSP60, HSP70, HSPA5, CCT2, and HSP90) [134, 135, 141-143]. Exosome membranes are composed of cholesterol, sphingomyelin, phosphatidylinositol, ceramide, lipid rafts, phosphatidylethanolamine, and phosphatidylserine [134, 135, 142, 144]. Exosomes can be sedimented by centrifugation at 100,000 - 200,000 *g* [135-137].

Due to the absence of an identifying marker, the overlapping size ranges of subpopulations, and the lack of standards, it is near impossible to distinguish the subpopulations from one another unless the method of biogenesis is known. Ergo, the International Society for Extracellular Vesicles (ISEV) has encouraged the use of the term EV when referring to all secreted vesicles [145]. Here, the term EV will be used to refer to any secreted vesicles, although the vesicle of interest is exosomes.

Sources of EVs

EVs have been isolated from a variety of biological fluids and conditioned media from a diverse assortment of cultured cells [120, 146-158]. The EV membrane, composed of the phospholipid bilayer and proteins, protects the cargo of the EVs from degradation by proteases and nucleases [135]. The cargo of EVs includes proteins, lipids, sugars, DNA (both genomic and mitochondrial), and small RNAs (mainly mRNA, miRNA) [120, 159-164]. EVs may signal via interactions with cell surface receptors linked to second messenger systems or they may be endocytosed and their contents activate signaling pathways. EVs have been shown to be involved

with metabolic processes as well as correlate to changes within the internal and external cellular environment [117, 165-168]. Further, EV cargo supplies information regarding the differentiation and functional state of the parental cells, making them ideal biological markers for diagnosis [135]. In addition, the cargo may differ among EV subpopulations and become a tool used for identification and characterization [159, 169].

Clinical Significance of EVs

EVs have been shown to be critical in intercellular signaling and communication, as part of normal physiological and pathological processes [159, 170-176]. In addition, EVs have also been implicated in the regulation of the immune response, antigen presentation, blood coagulation, inflammation, cell adhesion, gene silencing, tissue remodeling, tumorigenesis and metastasis, and angiogenesis [117, 128, 176-182]. Clinically, EVs have been studied as a potential therapeutic modality [126, 183-186], a diagnostic marker for diseases [140, 183, 187-191], and as a drug delivery vessel [192-194].

Isolation of EVs

EVs may be isolated from a variety of biological fluids including, urine, plasma, serum, saliva, or cell conditioned medium [128, 140, 147, 149, 158, 191, 195-199]. There are at least five different methods that have been described to isolate EVs, including centrifugation-based methods, size exclusion chromatography, ultrafiltration, precipitation, and immune-affinity methods. Not only does the isolation technique of choice vary, but the specific protocols within each class of isolation method also vary, creating inconsistencies and lack of replication within the EV field. Without a standard isolation method, it is difficult to characterize or confirm the presence of EVs

and to compare results among groups. To move forward in an efficient manner generating reproducible research involving the use of EVs, EVs must be able to be recovered efficiently from various volumes of starting material, with minimal damage and contamination that would affect downstream use. For diagnostic purposes, a quick and reproducible purification process, at a relatively low cost, is ideal. In contrast, for therapeutic purposes, the ideal process would produce a product that is not contaminated with proteins and lipoproteins and that remains intact.

Centrifugation-Based Methods

Centrifugation-based methods, such as ultracentrifugation (UC) and differential centrifugation, are the most common and use centrifugal force to separate particles by their density [135, 176, 200]. EVs can be sedimented at high g-force (100,000 - 200,000 g), with no standard protocol for isolation [135-137, 176]. Differential centrifugation is simply a modified version of UC that uses consecutive centrifugation steps that increase in g-force to produce a purer product by pelleting apoptotic bodies and cell debris, MVs, and exosomes [176, 201]. Additional steps to UC and differential centrifugation, e.g, ultrafiltration, can increase the purity of the sample but also decrease the isolation quantity [135, 201-204]. The effectiveness of UC and differential centrifugation is variable and dependent on speed (g-force), rotor type (fixed angle or swinging bucket, rotor specifications (k factor, the radius of rotation, and sedimentation path length), and sample viscosity [135, 136, 176, 201, 205-207]. The number of components to consider make it very difficult to create a standard protocol as individuals are constrained by not only equipment factors but also biological factors. Regarding equipment factors, the overall efficiency of the rotor, k factor, which takes both the g-force and particle pathlength into consideration, is the main indicator for the time needed to pellet EVs [176, 206]. However, even with the same time and

speed, variance in yield has been observed and can be primarily attributed to rotors with different k factors, highlighting centrifuge performance inconsistencies [137, 176]. In addition to equipment factors, biological factors, such as sample viscosity, must also be adjusted for in centrifugation-based protocols. As the sample viscosity increases, the efficiency of sedimentation decreases, meaning that it takes a lower speed and time to pellet EVs from conditioned media samples than plasma samples [134, 135, 205]. In addition to the number of parameters to account for, EV samples from UC and differential centrifugation are contaminated with proteins and lipoproteins and the effects on the membrane of EVs being sedimented against a solid surface for extended periods of time are unknown [135, 176, 208-210].

Density gradient (DG) ultracentrifugation is another centrifugation-based approach that uses buoyant density to enhance particle separation [135, 197, 211-213]. A DG is established so that it increases from the top of a centrifuge tube to the bottom, commonly using materials such as sucrose or iodixanol [133, 176]. Once the gradient has been established, a small amount of sample can be loaded, centrifugal force is exerted, and the particles will travel through the gradient until they reach their density [176, 214, 215]. The centrifugal force needs to be applied at a high speed for an extended period of time so this protocol can range from 16 to 90 hours [176, 215, 216]. Differential fraction collection is then used to collect the particles of the desired density [215-218]. Although DG ultracentrifugation has the potential to produce a purer sample, it also has several limitations that make the process not ideal for many uses. The main limitation is that this process is limited to a small sample volume so it is not ideal for larger volume samples (e.g., conditioned media) or for samples that require a large sample volume in order to obtain a large amount of EVs. Second, the process itself is very long, limiting its diagnostic value in a field where rapid results are desired.

Ultrafiltration

Ultrafiltration (UF) is a purification method based on the size of the particles that can be used either in conjunction with another method or as a standalone technique [127, 135, 137, 218]. Filters with various pore sizes are commercially available for purchase that have a defined size cut-off [202, 218, 219]. Consecutive UF steps, with decreasing filter pore size, are typically performed, especially when isolating EVs from conditioned media [176]. UF allows for the removal of larger particles, such as cell debris (100 nm), and soluble proteins (500 kDa), and a final concentration filtration step (100 kDa) [202, 220]. Following UF, samples can be used immediately or further purified using an additional technique. The sequential UF technique has the ability to produce a purified sample while also maintaining functional integrity for downstream usage [202-204, 220]. UF is a valuable method for EV isolation as it is quick, requires no special equipment, and can be used alone or in conjunction with other methods to produce a highly enriched product [135, 202, 204, 218].

Size-Exclusion Chromatography

Size-exclusion chromatography (SEC), also referred to as gel filtration chromatography, is a classic technique used to separate proteins and other biological compounds based on their molecular size [160, 221, 222]. SEC is an attractive alternative to centrifugation methods because it has been shown to successfully separate proteins from EVs [200]. In SEC, a solid-phase stationary matrix of porous beads is packed into a column with a mobile liquid phase that flows through the column [221]. As the mobile phase flows through the column, molecules that are larger than the pores on the beads pass directly through while smaller molecules enter the pores and are

kept in the column longer [160, 221-223]. Larger molecules stay on the external side of the pores and elude from the column first as their path to elution is shorter [200, 221, 222]. SEC has successfully been used to isolate EVs from many biological fluids including sera, plasma, ascites, saliva, urine, and cell culture-conditioned medium [160, 200, 202, 215, 222, 224-231]. Compared to other methods, SEC does not require special equipment, is applicable to all biological samples, can easily be scaled up, separates proteins, and subjects the sample to minimal stress thus producing a highly purified and intact end product suitable for downstream use [135, 176, 200, 227]. To scale-up SEC isolation for therapeutic use, increasing the length of the column used enhances resolution for separation while increasing the diameter increases the sample volume that can be loaded and separated on the column [135].

Characterization of EVs

Similar to ISCT characterization guidelines for MSCs, the International Society for Extracellular Vesicles (ISEV) proposed Minimal Information for Studies of Extracellular Vesicles ("MISEV2014") in 2014 [232]. The ISEV guidelines suggest that to claim the presence of EVs in a sample the following must be demonstrated: (1) isolated from extracellular fluids, (2) the presence of at least 3 transmembrane or lipid-bound extracellular proteins (e.g., CD9, CD63, CD81), cytosolic proteins (e.g., TSG101), or extracellular proteins known to be present or enriched in EVs, (3) characterization of single vesicles within the sample using at least two methods (transmission electron microscopy or atomic force microscopy and nanoparticle tracking analysis, dynamic light scattering, or resistive pulse sensing), and (4) for functional studies, a quantitative analysis of dose-function relationship [232]. In 2018, the ISEV guidelines were updated to include a checklist of suggested protocols and documentation approaches [233]. The checklist expands

upon MISEV2014 and includes: (1) nomenclature, (2) collection and pre-processing, (3) EV separation and concentration, (4) EV characterization (quantification, global characterization, and single EV characterization), (5) functional studies, and (6) reporting [233].

Procoagulant Activity of MSCs

MSC *In Vivo* Survival

It is widely accepted that MSCs have a finite life span in vitro and that MSCs have a low survival rate or low engraftment potential once administered in vivo [234]. Following administration to both humans and rodents, MSCs are likely trapped in the lung, if this is the first capillary bed they encounter, or other capillary organs (e.g., the liver) [234-238]. As a result, they are cleared from circulation by mechanical trapping or by encounters with the immune system within hours [58, 234, 236-243]. Once MSCs are trapped in the lung there is the potential for thrombosis and the formation of microemboli has the potential to be lethal [53, 58, 240, 244]. The trapping of MSCs in the lung has been explained as the effect of a high concentration of large or adhesive MSCs entering the lung capillaries, which have a small diameter [58, 245]. However, this anomaly was not reduced by decreasing the concentration of cells or by treatment with antibodies against integrins in an attempt to reduce stickiness [58, 246]. In further work, thrombus formation was found to be a direct result of the total cell number administered, not the concentration of cells [247]. This evidence suggests that another mechanism may be responsible for thrombus formation.

Instant Blood-Mediated Reaction

In early work involving human intra-portal Langerhans' islet transplantations, it was discovered that instant blood-mediated inflammatory reaction (IBMIR) was primarily responsible for cell loss following transplantation despite identical histocompatibility barriers, leading to a lower success rate compared to pancreas transplantation [58, 248, 249]. IBMIR is mainly characterized by platelet consumption, activation of the coagulation cascade, and activation of the complement cascade [248, 250, 251]. Following this work, Moll et al. suggested that IBMIR may also be involved with early cell loss and the absence of engraftment shown following MSC administration in a donor-dependent fashion [58]. IBMIR was also shown to be the likely cause of adverse effects and no therapeutic effect in felines administered repeat doses of AT-MSCs to treat chronic kidney disease [252].

Tissue Factor

Tissue factor (TF), also known as CD142 or coagulation factor III, is membrane-bound single polypeptide chain (45-47 kDa) that consists of extracellular, transmembrane, and cytoplasmic domains [253]. TF can be found expressed in many extravascular cells and circulating in the blood in the non-cell associated soluble form [253-256]. TF functions in the body to provide supplementary protection to organs that are susceptible to mechanical injury, as well as to activate the extrinsic coagulation cascade through binding of its extracellular domain to factor VII and factor VIIa, creating a TF-FVIIa covalent complex [253, 254]. Once the TF-FVIIa complex forms it triggers the extrinsic pathway of the coagulation cascade, factors IX and X of the intrinsic and common pathways are activated, and this leads to the generation of a clot via thrombin, platelet activation, and fibrin deposition [253, 254, 257]. In addition, TF has been associated with the

induction of inflammation, angiogenesis, atherosclerosis, and tumorigenesis signaling cascades and found to be critical for embryonic development [258, 259]. TF has been shown to be upregulated by numerous factors such as vascular injury; inflammatory cytokines, such as interferons; culture expansion; and blood products (e.g., serum, plasma, and platelets) [53, 253, 260].

MSCs from various tissue sources have been shown to highly express TF on their surfaces and to have strong procoagulant activity [53, 58, 247, 260-262]. In work by Oeller et al., AT- and UC-MSCs were shown to have significantly higher TF expression compared to BM-MSCs [260]. Further, TF expression was shown to be altered by cell culture medium serum supplementation [260]. Christy et al. reported that AT-MSCs expressed higher levels than BM-MSCs and that the percentage of CD142+ AT-MSCs declined over time in culture starting at approximately 20 population doublings while the percentage of CD142+ BM-MSCs had no clear expansion-related pattern with high donor variability [53]. Work by George et al. looked at the TF load of MSCs as defined by the product of the mean fluorescence intensity and the percentage of cells expressing CD142, presented as relative units, and found amniotic fluid-derived MSCs and AT-MSCs to be significantly higher than BM-MSCs, UC-MSCs, multipotent adult progenitor cells (MAPCs), and BM mononuclear cells [261].

MSCs have been shown to be functionally procoagulant when exposed to blood or plasma [53, 244, 260, 261]. Work by Christy et al. demonstrated that the percentage of cells in a given MSC population expressing TF roughly correlates with functional procoagulant activity [53]. George et al. demonstrated the procoagulant activity is partially dependent on TF expression since the TF neutralizing antibody TF8-5G9 caused a loss of functional procoagulant activity [261]. In mice, Tatsumi et al. showed that intravenous administration of cultured AT-MSCs resulted in

~85% mortality within 24 hours due to the formation of a pulmonary embolism, while all mice administered with freshly isolated AT-MSCs survived [244]. Further, the procoagulant activity of mouse AT-MSCs was suppressed by exposing MSCs to an anti-TF antibody or by use of factor VII-deficient plasma and the procoagulant activity of human AT-MSCs was suppressed using human recombinant thrombomodulin [244]. This work suggests that procoagulant activity of MSCs is associated with culture-expansion and is primarily due to TF expression by MSCs. In work by Gleeson et al., BM-MSCs were shown to have procoagulant activity in a porcine intracoronary injection with decreased therapeutic effects, but when co-administered with heparin, procoagulant activity was inhibited and therapeutic effects were restored [262]. Although co-administration of heparin has been shown to ameliorate the procoagulant activity of MSCs, heparin use comes with its own side effects such as thrombocytopenia, increased bleeding and bruising, and osteopenia [263].

EVs are considered by many to be immunologically inert [135, 264, 265]. However, it is known that EVs share many cell surface proteins with that of their parental cells, which makes them ideal for disease biomarkers [135]. Given that MSCs highly express TF, it is reasonable to postulate that EVs derived from MSCs may also express TF and harbor procoagulant activity. TF-exposing EVs have been noted in the blood, urine, and saliva [266]. It is believed that multiple cell types release TF-exposing EVs including activated monocytes, endothelial, and many cancer types, yet nothing is known regarding EVs derived from MSCs [266-268]. Increased levels of EVs, and TF-positive EVs, in particular, have been found in patients with cancer, endotoxemia, and atrial fibrillation [269, 270]. Further, EVs derived from multiple tumor types have been shown to have procoagulant activity [271-275]. As EVs gain popularity as a potential therapeutic agent, their procoagulant activity must be elucidated as they pose a safety risk.

Because of the gaps in our understanding of MSC therapy, questions remain centered around the overall safety of MSCs and MSC-based products. MSCs may express tissue factor on their surface and exhibit procoagulant activity in the presence of blood or plasma [53, 58, 209, 244, 247, 260, 261, 276, 277]. In addition, EVs from other cell types have been shown to express TF and possess procoagulant activity, yet this has not been explored in MSC-derived EVs. Taken together, these facts call for a greater understanding and demonstration of safety regarding MSCs for use in clinical trials. Others have demanded safety screening before MSCs can be used systemically in patients but this presents a sizable hurdle as it will require a consensus safety assay or process to be developed and added to the current ISCT guidelines [11, 57, 261, 278].

Here, an optimized protocol for the isolation, culture, and cryopreservation of canine UC-MSCs is presented that utilizes gelatin as a cell-attachment factor to enable long-term maintenance of canine UC-MSCs. This protocol increases cell attachment, increases colony-forming units-fibroblast efficiency, and decreases population doubling time. Second, the impact of storage temperature of cell culture conditioned media on EV isolation efficiency and morphology is discussed. Third, a comparison of canine EVs isolated using UC and a combination of UF and SEC is conducted to examine the effect isolation method on EV efficiency and morphology. Lastly, canine MSCs and EVs derived from MSC cell culture conditioned media are shown not only to express TF, but to also have TF-mediated procoagulant activity.

Chapter 2 - A Protocol for the Isolation, Culture, and Cryopreservation of Umbilical Cord-Derived Canine Mesenchymal Stromal Cells: Role of Cell Attachment in Long-Term Maintenance

I contributed to all figures and tables. A modified version of Chapter 2 is published in Stem Cells and Development [12].

Wright, A., L. Snyder, K. Knights, H. He, N. L. Springer, J. Lillich and M. L. Weiss (2020). "A Protocol for the Isolation, Culture, and Cryopreservation of Umbilical Cord-Derived Canine Mesenchymal Stromal Cells: Role of Cell Attachment in Long-Term Maintenance." Stem Cells Dev 29(11): 695-713.

Introduction

Multipotent mesenchymal stromal cells (MSCs) are a heterogeneous population of cells that includes stem, progenitor, and differentiated cells. MSCs were originally described the 1960's as the fibroblastic population of adherent cells derived from bone marrow that are distinct from the hematopoietic cells found in that niche [1]. Since then MSCs have been isolated from adult tissues, such as adipose (AT) and bone marrow (BM), and extraembryonic tissues such as the placenta and umbilical cord. While there may be differences in the MSC populations isolated from each source that could impact their value for regenerative medicine applications, MSCs derived from umbilical cords have several advantages over adult tissue sources: umbilical cords are collected non-surgically from a discarded tissue, they can be collected with no risk or pain to the

donor, and they are collected from individuals of a consistent, young age [24, 31]. Thus, umbilical cord-derived MSCs (UC-MSCs) are a limitless and non-controversial source of MSCs.

We [23, 279] and others [280-283] have isolated human UC-MSCs, cryogenically banked, and expanded the cells for potential therapeutic applications. For regenerative medicine applications, UC-MSCs might be preferred to adult tissue-derived MSCs due to age-related or disease-related changes that affect MSCs [284-286]. UC-MSCs are in human clinical testing both in the United States and abroad (clinicaltrials.gov website, accessed March 2019). UC-MSCs have been successfully isolated from veterinary species including swine [38], cattle [39], goats [40], horses [41], and canines [35-37, 104, 287, 288]. The literature reveals that the efficiency of UC-MSC isolation and expansion differs between species and laboratories. The lack of reproducibility is a source of concern in the MSC field [289, 290].

Many factors affect the efficiency to generate MSCs. These factors include isolation method, donor pool, efficiency (cell yield per donor), expansion potential of isolated cells, medium formulation, cell plating density, passaging protocol, cryopreservation efficiency, characterization procedures, senescence, and thawing procedure. Based upon the lack of consistency in manufacturing between laboratories, we suggest that MSC protocols need to be both optimized and standardized.

Many common human genetic disorders and many naturally occurring diseases in humans have canine homologs, adding to the importance of canines as a model for human disease [291]. In addition, canines are an important model species for human anatomical injuries, especially those involving large joints [96]. Canine MSCs have been used as an experimental treatment for orthopedic injuries and show positive clinical results in pilot studies [97-100]. A recent uncontrolled nonblinded clinical trial in 22 dogs indicated the safety and efficacy of neonatal

MSCs in canines with arthritis for a 2-year follow-up period [101]. Canine MSCs are under-represented in the scientific literature compared with human and rodent MSCs [PubMed search February 11, 2019; search terms MSCs and (canine or dog) = 317; MSCs and human = 13,070; MSCs and (rat or mouse) = 8,821].

Here, barriers that impede canine MSC testing are addressed. First, some tissue-specific canine MSCs are slower to expand in culture or undergo senescence around passage 6 [98, 102, 104, 287, 291], with some groups surpassing six passages [35, 111, 112]. Second, a consensus set of canine MSC antibodies for characterization has not been established [11]. Having a standardized panel of monoclonal antibodies for cell surface markers CD105, CD44, CD73, CD90, DLA class I and II, CD31, CD45, and CD34 would constitute a minimal set of MSC characterization antibodies. Third, trilineage differentiation has been demonstrated by some groups [98, 110, 287, 291-296], but not by other groups [35, 36, 104, 106, 297-300], which suggests that standardized osteogenic, chondrogenic, and adipogenic differentiation protocols for MSCs are needed.

As we provided for human UC-MSCs [23, 279], in this study we provide protocols for isolation, expansion, and characterization for canine UC-MSCs. Standardizing protocols may improve the ability to compare results across laboratories and enable clinical translation. Our methods provide healthy viable canine MSCs that can be cryopreserved, thawed, and expanded. The characterization standards for canine MSCs provided here are not comprehensive. However, the protocols provided here remove key barriers and, thus, enable canine UC-MSCs research.

Materials and Methods

Umbilical Cord Collection

Institutional animal care and use committee (IACUC) reviewed and approved the current research. The current protocol was deemed an ‘‘exempt animal use activity’’ under guideline no. 21 exemption policy 2.3 ‘‘studies that do not use live animals provided that the tissue is obtained from an IACUC-approved source and is discarded in accordance with all relevant state laws and institutional policies governing disposal of hazardous waste.’’

Canine umbilical cords donated after cesarean-section births with owner–informed consent were used. In brief, the dam was anesthetized and placed in lateral recumbence; the abdomen was shaved and surgically prepared for a lateral celiotomy approach to the uterus. The uterus was exteriorized, a single hysterotomy was made, and the pups were delivered. The umbilical cords were separated from the placenta and placed in a sterile transport medium made from an isotonic neutral buffered solution supplemented with 1% antibiotic–antimycotic (Catalog No. 15240062; Gibco) and placed into a 4ºC refrigerator. Cords were kept in a styrofoam cooler during transport. Once received in the laboratory, cords were refrigerated at 4ºC until processing. All cords were processed within 5 days of birth. Donor breed information was recorded when provided by the clinic, but is not evaluated here.

Gelatin Coating of Tissue Culture Plastic

A solution of 0.1% w/w porcine skin gelatin (Catalog No. G2500-100G; Sigma Aldrich) dissolved in distilled water was sterilized and cooled before use. Gelatin solution was added to the flask or well and swirled for 10–15 s. Gelatin was removed and the plate or flask was air dried in the biological safety cabinet (BSC). The dried plates were sealed tightly and stored refrigerated until use, or they were used immediately after drying.

Isolation of Canine UC-MSCs

Umbilical cords were collected from an entire litter and litter size was not considered as a variable. In contrast to human cords, puppies' cords have a complex vascular structure that arborizes making it difficult to determine the vascular material of an individual (boxes in Supplementary Fig. S1, Appendix A). Furthermore, the umbilical cords from littermates were intertwined within the fetal adnexa tissue. The cords were stripped away from the adnexa without stretching or ripping (Appendix A, Supplementary Fig. S1), and pooled, then the length was measured for a desired amount per tube.

Processing of umbilical cords and trimming were performed in the BSC. The cords were rinsed repeatedly in 37ºC Dulbecco's phosphate-buffered saline (DPBS) containing 1% antibiotic-antimycotic (1% A/A; Catalog Nos. 14-190-250, 15-240-062; Gibco). The cord length was measured and it was cut into 0.25 cm sections, then transferred into a C-tube (Catalog No. 130-096-334; Miltenyi Biotech) containing 10mL of 37ºC enzyme solution. The length of umbilical cord placed in each C-tube was recorded and classified into <30 cm or >30 cm length. The enzyme solution contained 1 mg/mL hyaluronidase (Catalog No. 02151272; MP Biomedicals), 300 U/mL collagenase type I (Catalog No. 17-100-017; Life Technologies), and 300U of deoxyribonuclease I (Catalog No. D4263-5VL; Sigma Aldrich) in Hank's balanced salt solution (Catalog No. MT21021CM; Corning).

The cord tissue weight was estimated by subtracting the weight of the C-tube with enzyme from the weight of the tube containing the enzyme and the umbilical cords. The C-tubes were processed in a GentleMACS Dissociator (Catalog No. 130-093-235; Miltenyi Biotech) using standard program ''C,'' once. The C-tubes were centrifuged at 200 g for 5 min, then incubated at

37ºC on a Pelco R2 rotator with a 1,051-sample platform at 12 rpm for 3 h. Next, the C-tubes were processed using the GentleMACS Dissociator standard program B, once, and the solution was filtered (100 µm cell strainer, Catalog No. 22-363-549; Fisher Scientific). The filter was washed with an additional 5mL of DPBS with 1% A/A solution. The cells were pelleted by centrifugation (200 *g* for 5 min, room temperature), and the supernatant was discarded.

Red blood cells (RBCs) were lysed by resuspending the cells in 0.5mL of culture medium and addition of 0.5mL of lysing buffer (Catalog No. R7757-100ML; Hybri-Max, Sigma Aldrich). Cells were mixed by gentle pipetting for 60 s then diluted with 8mL of DPBS with 1% A/A solution. Cells were pelleted by centrifugation (200 *g* for 5 min, room temperature), and the supernatant was discarded. Cell pellet was resuspended in 1mL of 37ºC ACB culture medium (recipe provided hereunder).

An aliquot was removed for live/dead cell count using acridine orange/propidium iodide staining solution (Catalog No. CS2-0106-5ML; Nexcelom Bioscience), on a Nexcelom Auto 2000 Cellometer (immune cells, low RBC program). Cells were plated at a density of 20,000—30,000 cells/cm^2 on the gelatin-coated tissue culture T-75 flasks (Catalog No. 7202000; Corning) in ACB culture medium (ACB consists of Dulbecco's modified Eagle's medium (DMEM, high glucose; Catalog No. 11965092; Gibco) supplemented with 10% fetal bovine serum (FBS) (Catalog No. SH3007103; HyClone, GE Healthcare Life Sciences), 1% antibiotic–antimycotic (Catalog No. 15240096; Gibco), 1% Glutamax (Catalog No. 35-050-061; Gibco), with or without 10 ng/mL basic fibroblast growth factor (bFGF; Catalog No. PHG0264; Gibco).

Culture

After the first passage, canine UC-MSCs were plated at 20,000 cells/cm^2 on tissue culture plates or flasks (with or without prior gelatin coating) using ACB cell culture medium warmed to 37ºC. The cells were grown at 37ºC, 5% CO_2, condensing humidity in a Heracell 150i, or Nuaire AutoFlow 4950 incubator. Half of the volume of medium was replaced every 3 days until the cells reached 80%–95% confluency before passage.

Canine UC-MSCs were lifted with either TrypLE Express (Catalog No. 12605028; Gibco) or 1.75% nattokinase (Catalog No. NATT100; Bulk Supplements) for 30 min at 37ºC. Cells were dislodged with gentle tapping to completely remove them from the plate. If few cells remained adherent to the plate, an additional 5 min of incubation was used. Detached MSCs were collected and pelleted by centrifugation (200 g for 5 min at room temperature). The supernatant was discarded and the cell pellet was resuspended in 1mL of fresh warm ACB medium. A live/dead cell count was performed at passage, and the cells were plated in fresh medium on gelatin-coated plates at a density of 20,000 cells/cm^2, cryopreserved, or discarded. Population doubling time was calculated using the following formula:

$$Population\ Doubling\ Time = \frac{Duration\ of\ culture\ (days)\ \times \log(2)}{\log(final\ cell\ count) - \log(initial\ cell\ count)}$$

Cryopreservation

To cryopreserve, UC-MSCs were suspended in 1:1 v/v ratio of ACB cell culture medium and freezing medium (Human Embryonic Stem Cell Cryopreservative, MTIGlobalStem) at 0ºC. MSCs were kept ice cold and immediately transferred to a controlled rate freezing apparatus (Mr.

Frosty) and then onto the bottom shelf of a -80ºC freezer. After 24 h, the vials were moved to the vapor phase of liquid nitrogen tank for long-term storage.

Trilineage Differentiation

UC-MSCs between passages 6 and 10 were differentiated to chondrogenic, osteogenic, and adipogenic lineages after testing 3 different media for chondrogenic, 3 different media for adipogenic, and 2 different media for osteogenic lineages (Appendix A, Supplementary Figs. S2–S4). The formulations tested are given in Supplementary Table S1 (Appendix A).

The formulations used in the article were high-glucose DMEM, 1% antibiotic–antimycotic, 10 ng transforming growth factor beta 1 (TGF-β1) (Catalog No. GF346; Sigma Aldrich), 1% FBS, 100 nM dexamethasone (Catalog No. D4902; Sigma Aldrich), 1mM sodium pyruvate (Catalog No. 11360070; Gibco), and 40 mg l-Proline (Catalog No. P8865; Sigma Aldrich) for 21 days for chondrogenesis; high-glucose DMEM, 1% A/A, 5% rabbit serum (Catalog No. R9133; Sigma Aldrich), 100nM dexamethasone, 200 µM indomethacin (Catalog No. I7378; Sigma Aldrich), 10 µM insulin (Catalog No. 12585014; Gibco), and 0.5mM 3-isobutyl-1-methylxanthine (Catalog No. I7018; Sigma Aldrich) exposure for 14 days for adipogenesis; and StemPro osteogenesis differentiation kit (Catalog No. A1007201; ThermoFisher, StemPro) using manufacturer's protocol for 21 days for osteogenesis.

In brief, 12-well gelatin-coated plates (Catalog No. CC7682-7512; CytoOne) were used to plate UC-MSCs in triplicate at a lineage-specific density. For chondrogenesis, UC-MSCs are concentrated to $8x10^6$ cells/mL, and a 5mL droplet is plated in each well that causes the formation of a micromass of MSC [23]. For osteogenesis, a density of 20,000 UC-MSCs were plated per well, and 76,000 cells per well were used for adipogenesis. Cells remained in culture for 24 to 48

h in standard cell culture medium before changing to differentiation medium. Half the volume of medium was replaced every 3 days.

After 14–21 days of differentiation, medium was removed and cells were washed using DPBS with calcium and magnesium (Catalog No. 14040-133; Gibco). The cells were fixed with freshly prepared 4% paraformaldehyde in 10mM phosphate buffer (pH 7.4) for 30 min at room temperature, and then triple washed with DPBS. MSCs were stained with Oil Red O to visualize lipid droplets in adipocytes (Catalog No. HT904-8F0Z; Sigma Aldrich), or with Alizarin Red S to detect calcium crystal in osteocytes (Catalog No. A5533-25G; Sigma Aldrich), or with Safranin O to visualize sulfated glycosaminoglycans in chondrocytes (Catalog No. O0625-100G; Sigma Aldrich). After staining, brightfield images were captured using an Evos FL Auto microscope (Life Technologies).

Colony-Forming Unit-Fibroblast Assay

Canine UC-MSCs were plated at 50, 100, and 500 cells/cm^2 in triplicate on gelatin-coated 6-well tissue culture plates (Catalog No. CC7682-7506; CytoOne) in ACB medium and incubated undisturbed for at least 3 days. The medium was changed every 3 days. Cells grew 10–14 days before fixation with ice-cold 100% methanol for 15 min. Methanol was removed and the plates were washed twice for 5 min with room temperature, sterile Sorenson's phosphate buffered saline (pH 7.4). The colonies were then stained with 1% w/v aqueous methylene blue for 20 min at room temperature, gently washed three times with distilled water, and air dried overnight.

The colonies were counted manually using 4–10X magnification. Colonies were defined as ''clonal'' groups consisting of >10 cells. The number of colonies per well was averaged from

the technical triplicates at each plating density. By dividing the number of cells plated by the previously-averaged number of colonies, the colony forming efficiency was calculated.

Flow Cytometry

Flow cytometry analysis of canine UC-MSCs was adapted from the human UC-MSC protocol we have previously published [23, 279]. All antibody clones were previously tested for their use in immunophenotyping canine MSCs (Supplementary Table S2) or are in routine use by the Kansas State University Veterinary Diagnostic Flow Cytometry core for canines.

In brief, UC-MSCs were cultured until 90%–95% confluent, passaged using 1.75% nattokinase, and reconstituted in blocking buffer containing 1% bovine serum albumin (BSA). An aliquot was removed for viability and cell count, whereas the remainder of the cells were incubated in blocking buffer for 15 min at 4ºC. Canine UC-MSCs were centrifuged (200 *g* for 5 min at room temperature) and reconstituted in 1% BSA with the addition of primary antibody at a dilution of 1:100 (Table 1). Canine UC-MSCs were incubated for 1 h at 4ºC protected from light, washed, and centrifuged. If antibody was unconjugated, then secondary antibody was added to 1% BSA at a concentration of 2 µg/mL and incubated at 4ºC for 30 min protected from light. Finally, cells were washed with 1% BSA and resuspended in 500 mL of 1% BSA and stored at 4ºC protected from light until ran on cytometer.

Table 1: Antibodies Tested in Flow Cytometry

Antibody	*Clone*	*Fluorophore*	*Catalog No.*
CD5	YKIX322.3	PerCP-eFluor 710	46-5050-42
CD11b	M1170	V450	560456
CD14	TUK4	Alexa Fluor® 700	MCA1568A700
CD21	CA2.1D6	Alexa Fluor® 647	MCA1781A647
CD34	1H6	PE	12-0340-42
CD44	IM7	BV786	563736
CD45	YKIX716.13	Alexa Fluor® 488	MCA1042F
CD73	7G2	Purified	41-0200
CD90	5E10	PE-Cy7	25-0909-42
CD90	YKIX337.217	APC	12-5900-42
CD105	OTI8A1	Purified	AB156756
HLA-DR	L243	BV650	307602
Goat anti-mouse IgG H + L	Polyclonal	Alexa Fluor® 488	A-11001

DNA staining was based on published protocols [301, 302]. In brief, canine UC-MSCs were cultured and passaged for flow cytometry analysis as previously described, then fixed in glacial ethanol for 1 h at -20ºC. UC-MSCs were washed twice with DPBS. Then, 50 mg/mL of RNAse H (Catalog No. EN0201; Thermo Scientific) in DPBS was added to canine UC-MSCs for 30 min at 37ºC. RNAse was removed by aspirating the supernatant after pelleting the cells using low-speed centrifugation (200 *g* for 5 min at room temperature). The cell pellet was washed with

DPBS, and the UC-MSCs were resuspended in DPBS containing 50 µg/mL of propidium iodide (PI) (Catalog No. P3566; Invitrogen). The cells were stored at 4ºC protected from light until they were analyzed on the cytometer.

The samples were analyzed on a BD LSR Fortessa X-20 SORP flow cytometer (BD Biosciences, San Jose, CA) equipped with 405, 488, 561, and 633 nm lasers and appropriate filters to detect all fluorophores listed in Table 1. Data were acquired, recorded, and analyzed utilizing BD FACSDiva 8.0 software (BD Biosciences). For multicolor labeled samples, the compensation matrix was calculated by the software from individually labeled UltraComp eBeads (ThermoFischer Scientific, Waltham, MA) and applied to the cell sample before data acquisition. Cells were identified by forward and side scatter properties and used as the primary gate to exclude debris and doublets. Unstained cells established background fluorescence and acted as a negative control for cell surface markers. At least 10,000 gated data points were recorded for all samples. Results were generated by overlaying the appropriate fluorescence channel of unlabeled and labeled cell samples. For DNA analysis, cells were identified by setting the detection threshold to be based off fluorescence in a 610/20 bandpass filter, which would identify only PI stained cells. Positively identified cells were gated using pulse geometry to not only exclude doublets but also reveal the presence, if any, of cells with aberrant DNA content. A histogram was generated from the aforementioned gate for cell cycle analysis.

Reverse Transcriptase-Polymerase Chain Reaction

Reverse transcriptase-polymerase chain reaction (RT-PCR) was conducted as previously described [303]. In brief, total RNA was isolated using an RNeasy kit (Qiagen). RNA was treated with DNase before storage and measured using a NanoDrop spectrophotometer. Complementary

DNA was synthesized from total RNA using Superscript III First-Strand Synthesis Supermix kit (Invitrogen) primed with oligo-dT 12–18 per the manufacturer's protocol. PCR was performed using a BioRad iCycler: initial denaturation at 95ºC for 3 min, 30 cycles of (94ºC for 1 min, 53ºC–55ºC for 30 s, and 72ºC for 30 s), and the final extension at 72ºC for 10 min. After PCR, the products were resolved on a 1%–2% agarose gel with 100 bp DNA ladder and imaged using ethidium bromine. Primer sequences and amplicon size are listed in Table 2.

For sequencing, the amplicon of the anticipated size from a randomly selected MSC line was cut from the agarose gel (e.g., CD34 409 bp, CD34 356 bp, CD73 422 bp, CD73 434 bp, CD90 440 bp, CD90 420 bp, CD105 424 bp, and CD105 378 bp), and the DNA was extracted and purified. Next, the DNA was cloned into a plasmid and expanded. After expansion, five to eight clones were selected and plasmid DNA was isolated and submitted to the KSU Integrated Genomics core for Illumina sequencing. The DNA sequences were checked for quality before alignment. The DNA sequences were aligned with canine sequences in PubMed.

Table 2: Reverse Transcriptase-Polymerase Chain Reaction Primers

Gene	*Primer Sequence*	*Product Length (bp)*	*Tm (ºC)*	*Accession No.*
CD34-1	GTGCCAACCTCCACAGAAAT TGATGGTACTTGGGGTGTCA	409	55.6 55.8	NM_001003341
CD34-2	CCCTTTGGGTTCACAAACAC TCCGAACCATTTCCAGGTAG	356	54.5 54.2	NM_001003341
CD45-1	CCATACAACTGCTCCCACAA ACAAAGCCTTCCCATTCAAA	438	55.0 52.7	XM_005622278
CD45-2	AACAGCACTGTTGCCCTTCT TGGTCACAATTCACGGTATCA	386	57.3 54.0	XM_005622278
CD73-1	ACTGGGACACTCTGGTTTCG ATTCCTTAAAGCGGCAGGAT	422	56.9 54.4	XM_532221
CD73-2	TGCATTGCAGCCTGAAGTAG CTGTTTTCCCCAATTCCTGA	434	55.6 52.7	XM_532221
CD90-1	ACATGTGAACTCCGGCTCTC AGAAGCGACTCTGGGACAAA	420	57.0 56.2	NM_001287129
CD90-2	CGTGATCTATGGCACTGTGG GCAGCACTGGGATTCCTTAG	440	55.6 55.7	NM_001287129
CD105-1	AGGAGTCAACACCACGGAAC GATCTGCATGTTGTGGTTGG	424	57.2 54.3	XM_005625330
CD105-2	CCAATGCTACCGTGGAAGTT GATTGCAGAAGGACGGTGAT	378	55.3 55.0	XM_005625330

Statistics

After validating that the analysis of variance (ANOVA) assumptions were met, it was used to evaluate significant main effects and/or interactions. After finding significant ANOVA terms, post hoc testing of planned comparisons was performed using either the Bonferroni correction or the Holm–Sidak method. Those data are presented as average ±1 standard deviation (SD). For pairwise comparisons, Student's t-test was used after confirmation of statistical assumptions. If the ANOVA assumptions were not met, then Kruskal–Wallis ANOVA on ranks was used. Those data are presented in box and whisker plots showing median and 25th and 75th percentile in the box and whiskers showing 10th and 90th percentile, with potential outliers indicated by circles. In text, the data are presented as average ±1 SD unless stated otherwise.

Regression analysis was conducted using Sigma Plot v12.5, and significant relationships were reported (regression line is plotted in cases of significant relationship). In one case, regression analysis indicated nonsignificant trends, and was indicated in text (no regression line is shown in graph). Throughout this article, the entire data set was used, and it included potential outliers. The original data set is available. SigmaPlot version12.5 (Systat Software, Inc.) was used for statistics and generating graphs. The graphs created using SigmaPlot were saved as EMF files. These EMF files were labeled and edited for clarity using ACD Systems of America's Canvas (version 15.5, build 1770) and rendered in TIFF format. In all cases, hypothesis testing was two-tailed and $P < 0.05$ was considered ''significant."

Results

Isolation of MSCs from Canine Umbilical Cords

MSCs were isolated from umbilical cords from 30 litters of pups. The schematic for processing canine umbilical cords is shown in Figure 1. When necessary the fetal placenta was trimmed away from the UC before processing (Appendix A, Supplementary Fig. S1). Two isolation methods were compared: the explant method and the dissociation method (Figure 2A). The explant method involves mincing the UC into 0.2–0.5 mm pieces and adhering those pieces to the plastic plate before adding medium. The explant method produced the lowest cell yields but produced >90% viable cells (open circle shown in Figure 2A, B). MSCs from the explant method did not expand after attaching to the culture plate. This method was not tested further, and the remaining umbilical cords from 29 litters were mechanically and enzymatic disrupted before culturing, as we described previously for human umbilical cords [23, 279].

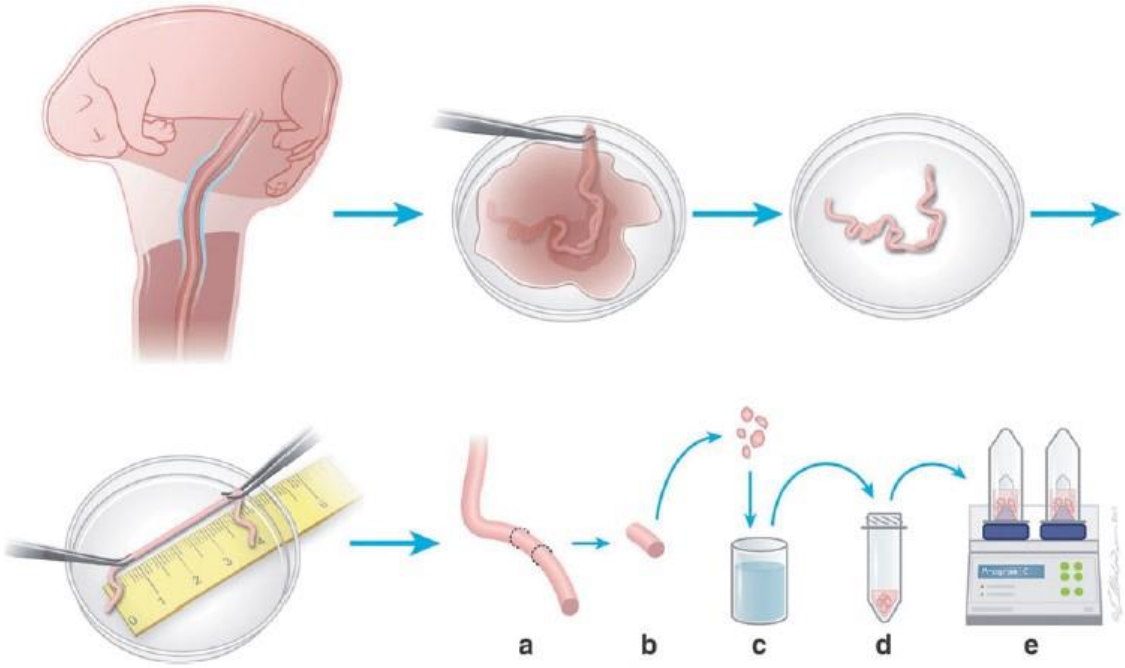

Figure 1: A schematic of the isolation procedure showing the major steps involved for obtaining MSCs from the canine umbilical cord.

After caesarian section delivery, the cord is removed from each puppy and placed into storage solution. The non-cord tissues are dissected and discarded using sterile technique. The length of the cord material is measured (a) and it is ligated into lengths (b), rinsed (c), and minced briefly. A fixed length is added to a Milliteny C-tube with enzymes (d). The tube is processed using a standard program (e) and the tube is incubated before cell pellet isolation, counting, and plating. MSC, mesenchymal stromal cells.

To evaluate the effect of tissue volume on cell yield and viability, either <30 cm of umbilical cord (black circles shown in Figure 2A, B) or >30 cm of umbilical cord was loaded into the disruptor (red circles shown in Figure 2A, B). The isolation yield and viability were not significantly changed by tissue volume. Although there was a significant trend for cell yield at isolation to increase over the course of this study (regression line shown in Figure 2A), there was no significant trend in cell viability (Figure 2B).

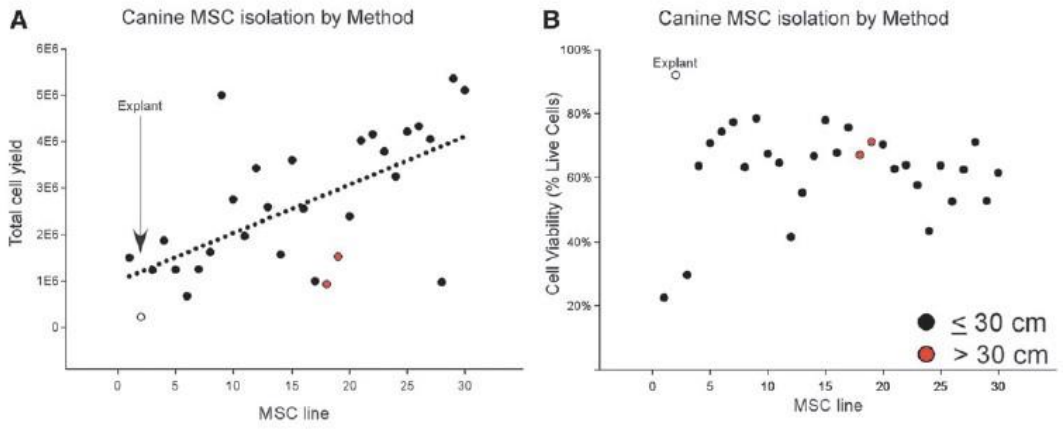

Figure 2: Isolation efficiency from umbilical cord.

(A) Total cell yields from three different variables tested: explant methods (n = 1, white circle), mechanical and enzymatic extraction of <30 cm of cord tissue (red circles) or >30 cm of cord tissue (black circles). Note that over the course of this experiment, our isolation efficiency improved statistically (positive and significant regression line). Note that the explant method was too inefficient to consider for scale-up. Note that adding more tissue to the C-tube did not improve yield or cell viability. This suggests that scale-up might be by using more C-tubes. (B) Cell viability after isolation. Note that the explant method produced the highest cell viability. This was offset by the lowest yield (in A). In contrast, the mechanical and enzymatic methods produced a viability of between 50% and 80%.

Stage 1

The first 10 canine UC-MSC lines were isolated and expanded using previously described protocols (labeled Stage 1 in Figure 3). Specifically, the MSCs were plated on tissue culture plastic, exposed to 10% FBS containing DMEM and other standard supplements, and passaged using 0.025% trypsin-ethylenediaminetetraacetic acid (EDTA). Using these methods, only 1 MSC line of the 10 could be expanded beyond 20 cumulative population doublings (CPDs), 50% of the MSC lines were able to expand beyond 10 CPDs, and only 1 line of 10 was able to be expanded to 15 passages (Figure 3B, C).

In Stage 1, we learned that when compared with human UC-MSCs, canine UC-MSCs require higher plating density to expand (20,000 cells/cm^2 for canine UC-MSCs vs. 10,000 cells/cm^2 for human UC-MSCs). In Stage 1, we performed pilot experiments with different agents for lifting MSCs off the tissue culture plate for passage (discussed hereunder).

Stage 2

Two modifications in UC-MSC expansion were made in Stage 2. First, tissue culture plastic was modified by coating the plates with gelatin. Second, nattokinase was used for lifting the MSCs at time of passage [304, 305]. In Stage 2, the expansion potential of UC-MSC was improved based upon the following observations: first, a significant positive trend line was found for the total cell yield, the ultimate number of passages reached by MSC lines, and the CPDs achieved (Figure 3A). Second, 6 of 9 (66%) MSC lines expanded beyond 10 CPDs and 3 of 9 (33%) MSC lines expanded beyond 20 CPDs) (Figure 3B). Third, 3 of 9 MSCs lines expanded to 15 passages without senescence (Figure 3B, C).

Stage 3

One modification was made in UC-MSC expansion in Stage 3 compared with Stage 2: a growth supplement, bFGF, was added to the medium (ACB medium) together with plating on gelatin-coated plates [306-308]. This modification further improved in UC-MSC expansion capability. This enhancement was indicated by better yield at initial isolation (9 out of 11 exceeded $3x10^6$ cells at isolation) (Figure 3A), and an increase to 9 out of 11 (90%) of the MSC lines expanding beyond 10 CPDs, 5 out of 11 (50%) of the MSC lines expanding beyond 20 CPDs, and 5 of 11 MSC lines expanded to 15 passages (Figure 3B, C).

The faster growth than Stage 2 was indicated by 5 of 11 MSC lines reaching or surpassing 20 CPDs by 60 days of culture (Figure 3B), and by significantly faster population doubling time, especially in the first five passages (labeled early in Figure 3D). The relative efficiency to maintain MSCs by stage of development is shown in Figure 3F.

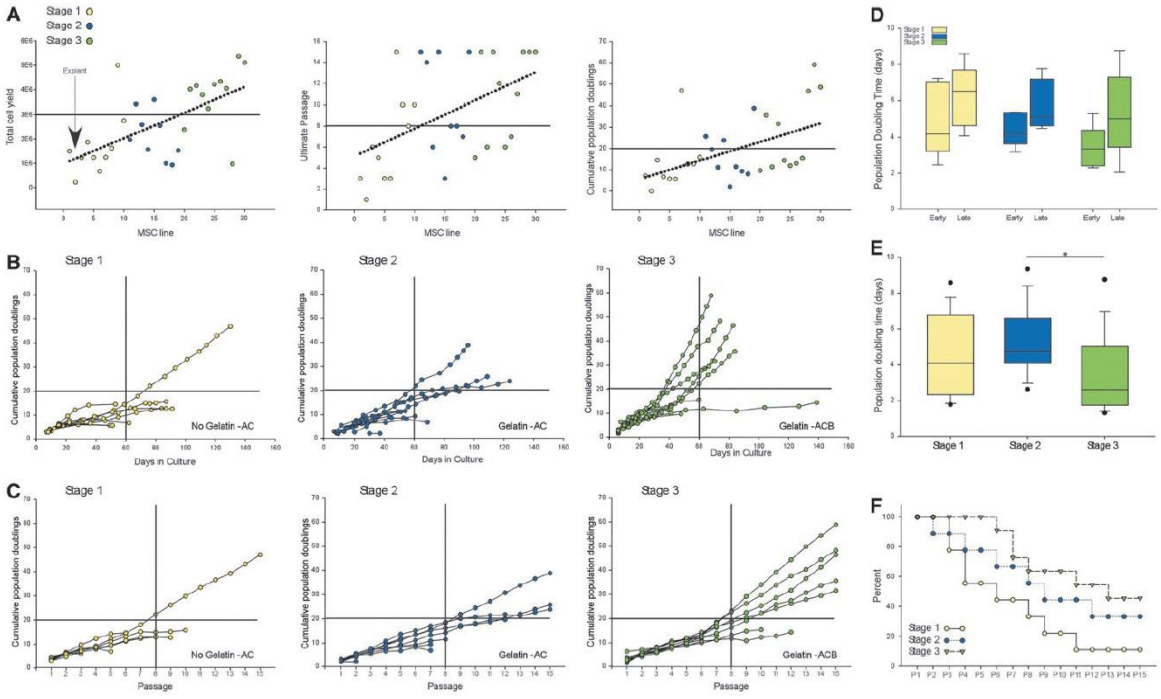

Figure 3: Stepwise improvement of canine MSC expansion.

Stepwise improvement of canine MSC expansion. (A) Left panel: Comparison of the three stages for cell yield at isolation. Horizontal bar indicates $3x10^6$ cells, as a criterion for suitable starting number for expansion. Over the course of the project our methods improved as evidenced by increasing cell yield over time, indicated by a significant positive regression line. Note also that the three stages, indicated by color code, roughly group and follow the trend line. Middle panel: Ultimate passage achieved for 30 canine MSC lines by stage. Horizontal bar indicates eight passages, as a criterion for minimum expansion capacity of MSCs. Note that at each stage of the project there is a significant increase in the number of ultimate passages achieved per cell line. Right panel: CPDs achieved by 30 MSC lines. Horizontal bar indicates 20 CPDs, as a criterion for minimum expansion of MSCs. Note that positive and significant trend line indicating improvement

of MSC manufacturing over project. (B) CPDs for all cell lines versus days in culture for all 30 MSC lines by stage (Stage 1, left panel; Stage 2, middle panel; Stage 3, right panel). These graphs give an indication of how rapidly MSCs expanded per passage, and the number of CPDs achieved by Stage. (C) CPDs for all cell lines versus passage for all 30 MSC lines by stage (Stage 1, left panel; Stage 2, middle panel; Stage 3, right panel). Note that 15 passages were set as a maximum number of passages, arbitrarily. Note that over stage, more MSC lines were able to reach the arbitrary maximum of 15 passages. In (B, C) horizontal bar indicates 20 CPDs, as a criterion for minimum expansion of MSCs, and vertical bar indicates 60 days in culture, as a target to try to keep manufacturing times as short as possible. (D) Population doubling time by stage and time in culture (Stage 1, yellow boxes; Stage 2, blue boxes; Stage 3, green boxes). Note that the box plots indicate median and 25th and 75th percentile and the whiskers indicate 10th and 90th percentiles. Each stage is further broken into early and late passages. ‘‘Early’’ is defined as passages 0–4 and ‘‘late’’ is defined as passages 5–10. From this, we can see that moving to Stage 2, the addition of gelatin coating and nattokinase for lifting MSCs, but no change to medium did not greatly change MSC growth rate, but tended to reduce senescence. In contrast, in Stage 3, changing the medium formulation increased MSC growth, especially in the early passage epoch. (E) Population doubling time by stage (Stage 1, yellow boxes; Stage 2, blue boxes; Stage 3, green boxes). When population doubling time was averaged (over all passages by stage), a significant increase in growth rate was observed between Stages 2 and 3. The median growth rate of Stage 3 was ~2.5 days. (F) Loss of MSC proliferation over passage by stage. Percentage of expanding MSC lines by passage and by stage (Stage 1, yellow dot; Stage 2, blue dots; Stage 3, green triangles). Note that while sustaining MSCs in culture showed a marked improvement over the three stages (in F), just 50% of the lines were able to achieve 15 passages in Stage 3. This suggests that improvements in culture conditions may be identified in future study. Dotted lines in (A) indicate statistically significant, positive regression lines indicate improvement over the project. Box plots in (D, E) indicate median, 25^{th}, and 75^{th} percentiles; whiskers indicate 10th and 90th percentiles (potential outliers indicated by filled circles). *Indicates significant ($P < 0.05$) using a two-tailed test. CPDs, cumulative population doublings.

Effect of Gelatin-Coated Plates

The effect of gelatin-coated tissue culture plates was apparent during culture based upon cellular morphology (Figure 4) and cumulatively over passage (Figure 5), but it did not significantly affect the growth rate of MSCs during the first five passages (comparing the population doubling time between Stages 1 and 2 shown in Figure 3D), or over entire culture period (comparing Stages 1 and 2 shown in Figure 3E).

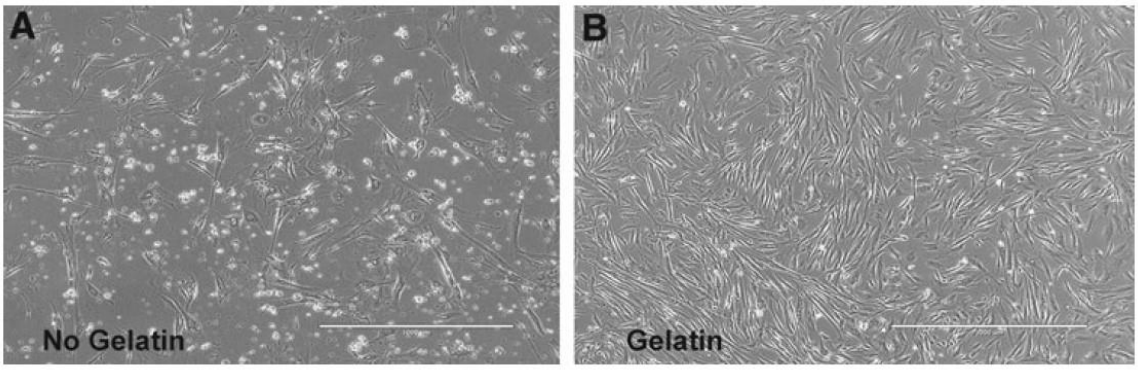

Figure 4: Effect of gelatin coating of plates on canine MSCs morphology.
(A) Canine MSC grown on tissue culture-treated plastic (Stage 1). Note the heterogeneity of the culture and the presence of large flattened cells with stress fibers and debris. (B) Canine MSCs grown on gelatin-coated plastic. Note the more homogeneous appearance of fusiform cells and the smaller cell size. Calibration bar is 1 mm.

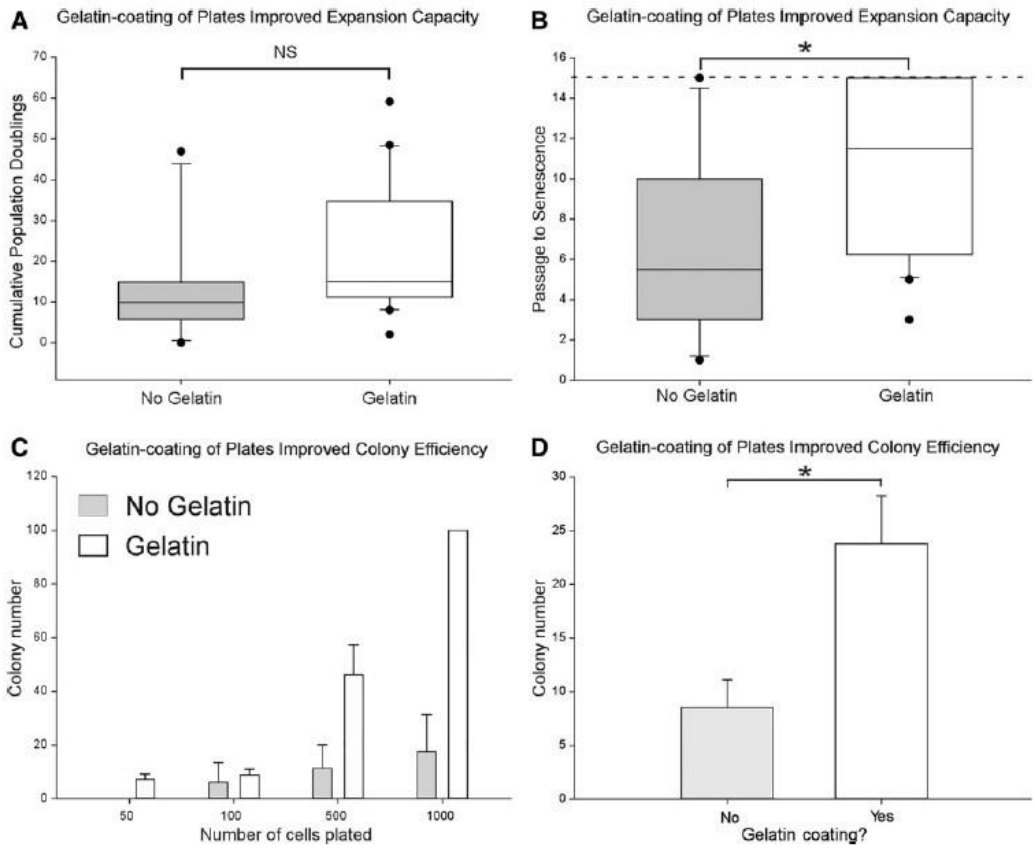

Figure 5: Effect of gelatin coating of plates on canine MSCs expansion.

(A) When comparing canine MSCs from Stage 1 and Stage 2, gelatin coating of the plate tended to improve the CPDs achieved, but this was not statistically significant. (B) In contrast, when comparing the number of passages with senescence for Stages 1 and 2, gelatin-coated plates significantly improved MSC's ability to achieve more passages. (C) Gelatin coating of the tissue culture plastic also improved the ability to perform colony-forming unit-fibroblast assays, as indicated by the number of colonies obtained per number of cells seeded. (D) Improved colony forming efficiency by gelatin coating. Gelatin coating significantly improves number of colonies compared with uncoated plates. Box plots indicate median, 25th, and 75th percentiles; whiskers indicate 10th and 90th percentiles (potential outliers indicated by filled circles). *Indicates significant ($P < 0.05$) using a two-tailed test.

Subjectively, UC-MSCs grown on gelatin-coated plates appear to experience less stress than MSCs grown on standard tissue culture plates (compare Figure 4A and B). For example, UC-MSCs grown on tissue culture plastic had more debris, and more of the large flattened cells with

stress fibers (Figure 4A) than MSCs grown on gelatin-coated plates (Figure 4B). This subjective observation was supported by other observations. As shown in Fig. 5A, there was a trend for MSCs grown on gelatin-coated plates to have greater CPDs, and as shown in Fig. 5B, there were significantly more passages until senescence when MSCs were grown on gelatin-coated plates. The attachment of MSCs to gelatin-coated plates also enhanced the colony forming fibroblast efficiency (Fig. 5C, D). As MSCs grew on gelatin-coated plates, a pattern in the arrangement of their cell bodies was observed when the same field was observed from day to day (Appendix A, Supplementary Fig. S5).

Comparing Method of Lifting Cells for Passage

Based upon our experience with human MSCs (data not shown) [23] and based on the canine MSC literature, we assumed that 0.025% trypsin-EDTA was suitable for canine MSCs. To evaluate this hypothesis, pilot experiments were conducted using 0.025% trypsin-EDTA compared with TrypLE, dispase, TrypLE Express, and 1.75% nattokinase. We determined that dispase, TrypLE, and Trypsin-EDTA negatively impact yield, viability, and downstream effects (comparison data not shown). Trypsin-EDTA and dispase were not successful and resulted in failure to proliferate after passage (data not shown). TrypLE was unable to efficiently lift canine MSCs from the plate for passage (data not shown).

In contrast, nattokinase improved MSC viability at passage compared with TrypLE Express (Figure 6A, B). The difference between cell viability and MSC yield between TrypLE Express (0.05%) versus nattokinase (1.75%) was significant (Figure 6B, D). Nattokinase was used to lift MSCs in Stages 2 and 3.

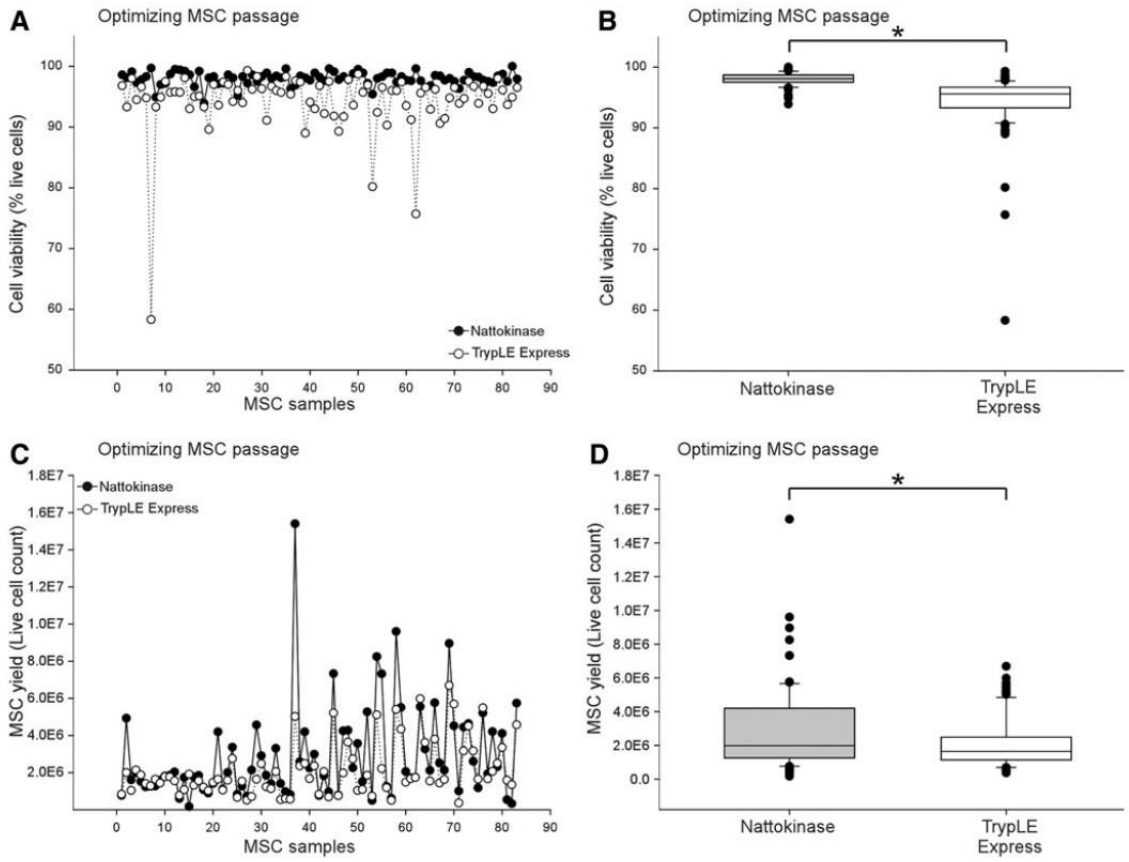

Figure 6: Nattokinase improved MSC passage compared to TrypLE Express.

(A) Side-by-side comparison of cell viability when MSCs at the same passage were lifted by TrypLE Express or nattokinase (83 independent trials). (B) Summarized data from (A). Nattokinase significantly improved MSC viability at passage (median of 98.1% for nattokinase, median of 95.6% for TrypLE Express). (C) Side-by-side comparison of MSC yield at passage when MSCs of the same passage were lifted with TrypLE Express or nattokinase. (D) Summarized data from (C). Nattokinase significantly improved cell yield at passage (median of $1.99x10^6$ cells for nattokinase, median of $1.64x10^6$ for TrypLE Express, a 21.3% improvement). Box plots indicate median, 25th, and 75th percentiles; whiskers indicate 10th and 90th percentiles (potential outliers indicated by filled circles). *Indicates significant ($P < 0.05$) using a two-tailed test.

Cryopreservation Effects and Ability to Revive UC-MSCs from Cryostorage

It appears that canine UC-MSCs are less robust than human UC-MSCs in terms of their expansion potential, response to chemical stress, and attachment ability. We then queried whether

canine UC-MSCs were sensitive to cryopreservation and could be revived and expanded after cryostorage. To answer this question, 33 UC-MSC samples were frozen and stored for an average of 185 days (median 191 days, range 4–448 days, 25th percentile 34.5 and 75th percentile 292.5 days) in vapor phase liquid nitrogen then thawed and tested for viability. As expected, there was a significant drop in MSC viability of 7.9% – 4.8% after thawing (Figure 7A, B). Although viability decreased due to freeze/thaw, there was no significant effects of length of storage on change in MSC viability (Figure 7C, D). Note that the regression line shown in Figure 7D is not significant. All thawed cell lines expanded for multiple passages after thaw.

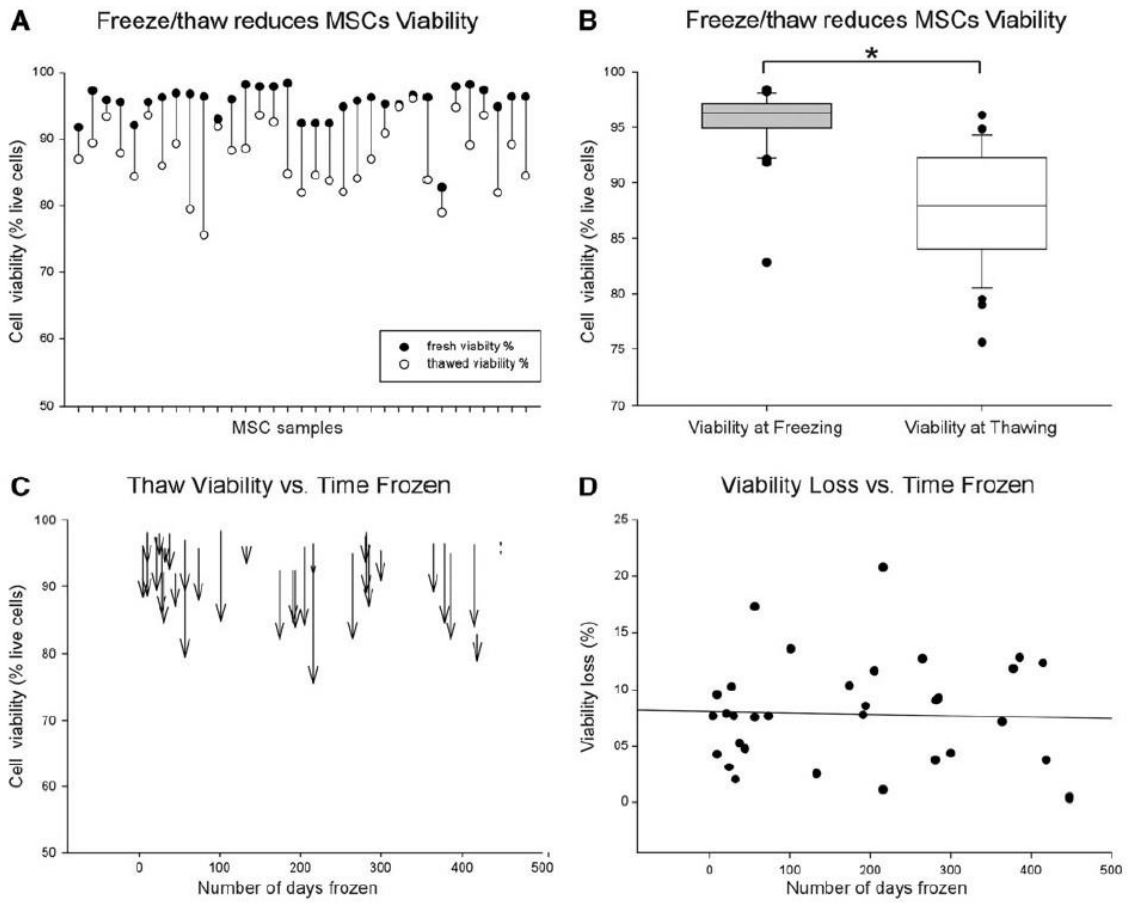

Figure 7: Cryostorage reduces the viability of canine MSCs.

(A) Side-by-side comparison of the viability of 33 MSC samples before (black circles) and after cryostorage (white circles) shows consistent loss of viability resulting from freeze/thaw cycle. (B) Summarized data from (A). As expected, cryostorage significantly reduces canine MSC viability. (C) Side-by-side comparison of the effect of time on MSC viability at thaw. Each vector indicates the change in viability from fresh to after thaw for an individual canine MSC sample. X-axis indicates the number of days in cryostorage before thaw. By inspection, there did not appear to be a time-dependent loss in viability due to cryostorage. (D) Change in viability (indicated by vector length in C) versus days frozen. Regression analysis reveals no significant relationship between change in viability over time (although a negative trend line is observed). Box plots indicate median, 25th, and 75th percentiles; whiskers indicate 10th and 90th percentiles (potential outliers indicated by filled circles). *Indicates significant ($P < 0.05$) using a two-tailed test.

Trilineage Differentiation

Many articles in the canine MSC literature do not demonstrate trilineage differentiation, and for that reason, some have argued that differentiation to two lineages is sufficient to demonstrate multipotent progenitors in canine MSCs. In pilot testing, eight different differentiation methods gleaned from the literature were compared for trilineage differentiation (Supplementary Figures S2–S4 and Supplementary Table S1). As shown in Figure 8, canine UC-MSCs successfully differentiate to bone-forming, cartilage-forming, and fat-forming lineages. The efficiency to differentiate canine UC-MSCs to adipocytes was low, but this probably reflected cell loss during differentiation and further optimization is likely possible.

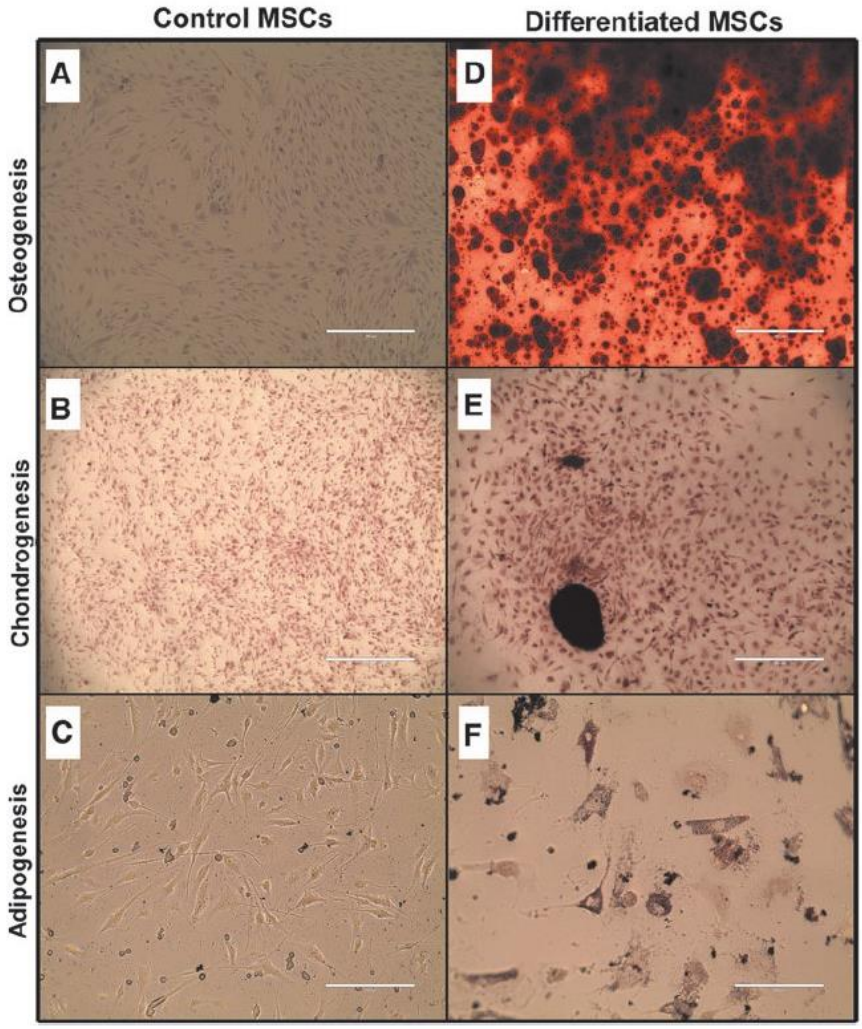

Figure 8: Trilineage differentiation of canine MSCs.

(A–C) Negative control (control MSCs): MSCs in normal culture medium and stained to demonstrate background levels of calcium deposition using Alizarin Red S (A, for osteogenic differentiation), acidic proteoglycan staining using Safranin O (B, for chondrogenic differentiation), and lipid droplets using Oil Red O (C, for adipogenic differentiation). (D–F) MSCs after trilineage differentiation (differentiated MSCs). Calcium matrix deposition after 21 days of osteogenic differentiation (D). MSC micromasses form and stain intensely for acidic proteoglycans after 14 days of chondrogenic differentiation (E). Lipid droplets within MSCs after 14 days of adipogenic differentiation (F). In all cases, staining was performed after fixation. Representative wells shown from technical duplicates. Calibration bar is 400µm in (A, D), 1,000µm in (B, E), and 200µm in (C, F).

Immunophenotyping by Flow Cytometry

We performed extensive testing of antibodies to find those that work best for canine UC-MSCs (Table 1). While representative data are shown in Figure 9, we validated the staining patterns provided here in two or three different canine UC-MSC lines at passages 5 to 8. Canine UC-MSCs positively labeled for CD90, CD73, CD44, and CD105, as indicated by the mean fluorescence intensity shift in the monomodal population of gated cells, but the size of the positive shifts was not as large as we have seen previously when working with human UC-MSCs [15, 23, 279]. We wondered whether the smaller shift was due to using a mouse anti-human CD90 (clone 5E10), instead of a canine-specific antibody. To address this concern, we repeated the flow cytometry using a rat anti-canine CD90 (clone YKIX337.217). As shown in Supplementary Figure S6 (Appendix A), the positive shift in CD90 was not frankly affected by using a canine-specific rat anti-CD90 compared with the mouse human-specific anti-CD90. We conclude that the surface expression of canine UC-MSCs is less than that of human UC-MSCs. Another observation that confused us was that canine UC-MSCs displayed positive labeling for CD34, which is typically considered a hematopoietic stem cell marker. To confirm whether CD34 was expressed by canine MSCs, we performed follow-up experiments that are described in the next section. As expected, canine MSCs had negative labeling for MHC class II, CD11b, CD14, CD21, CD5, and CD45.

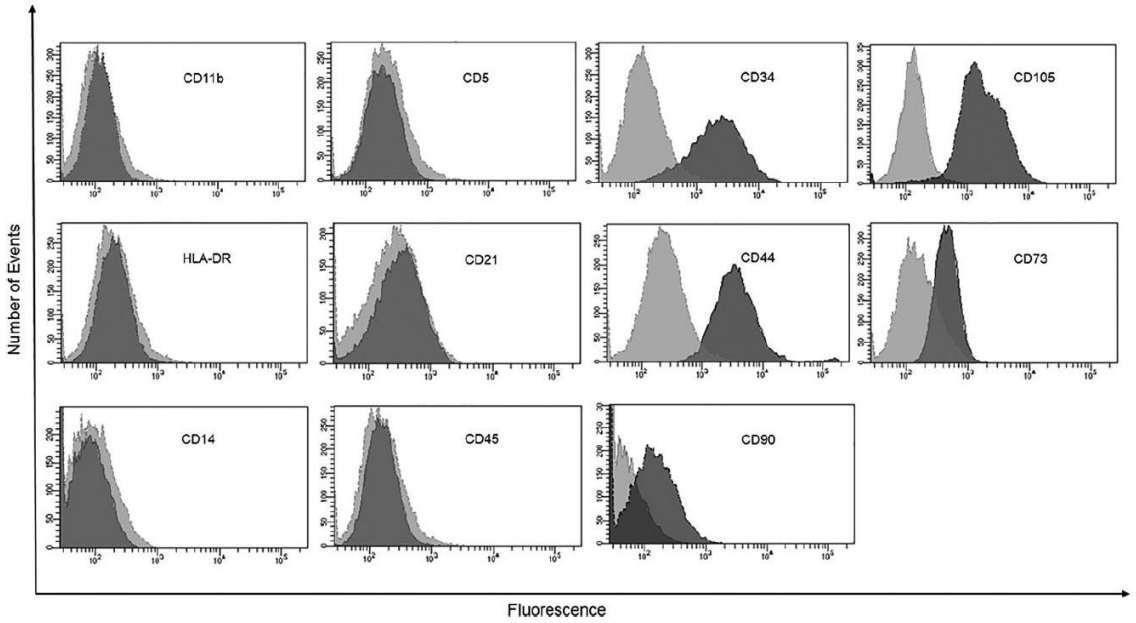

Figure 9: Immunophenotyping of canine UC-MSCs.

Representative flow cytometry histograms with unstained cells (light gray) versus antibody labeled sample (dark gray) for two or three canine MSC cell lines, depending on surface marker. Based on the prominent shift in fluorescence intensity for the entire population, the data are interpreted as follows: MSCs were positive for CD34, CD105, CD44, CD73, and CD90. MSCs were negative for CD11b, CD5, HLA-DR (MHC-II), CD21, CD14, and CD45.

Confirmation of CD34 Expression by RT-PCR

Since we observed CD34-positive labeling for canine UC-MSCs, we confirmed this by alternative means. Two PCR primer pairs, spanning an intron, were designed for CD73, CD90, CD105, CD34, and CD45 to perform RT-PCR on RNA samples obtained from 12 different canine MSC lines. As shown in Supplementary Fig. S7, canine MSCs express mRNA for CD73, CD90, CD105, and CD34, as indicated by the finding the appropriately sized amplicon after RT-PCR amplification for both primer pairs tested. As shown in Supplementary Fig. S6, both PCR primer sets confirm expression of CD73, CD90, CD105, and CD34 mRNA. However, the 434 bp PCR primer pair for CD73 showed multiple bands, a strong band between 400 and 500 bp of the

expected product, and in lanes 2,3, and 11, a second, larger product, suggesting nonspecific amplification.

Therefore, we confirmed the specificity of the PCR findings for CD34, CD73, CD90, and CD105 by sequencing. The sequences were verified to be 99%–100% matches to the expected canine mRNA (Supplementary Table S3). In contrast, canine MSCs did not express mRNA for CD45 to a detectable amount. This suggests that the flow cytometry results are valid since 11 of 12 lines tested (>91%) of the canine UC-MSC lines expanded using our culture, and passage conditions express CD34 mRNA and protein.

Evaluation of Cell Cycle by Flow Cytometry

Canine UC-MSC ploidy and cell cycle partitioning were evaluated using flow cytometry, as shown in Figure 10. The analysis of cell cycle revealed ~78% of the cells in G0/G1, ~16% cells in G2/M phase, and ~8% of the cells in S phase. Note that no tetraploid or aneuploid cells were detected.

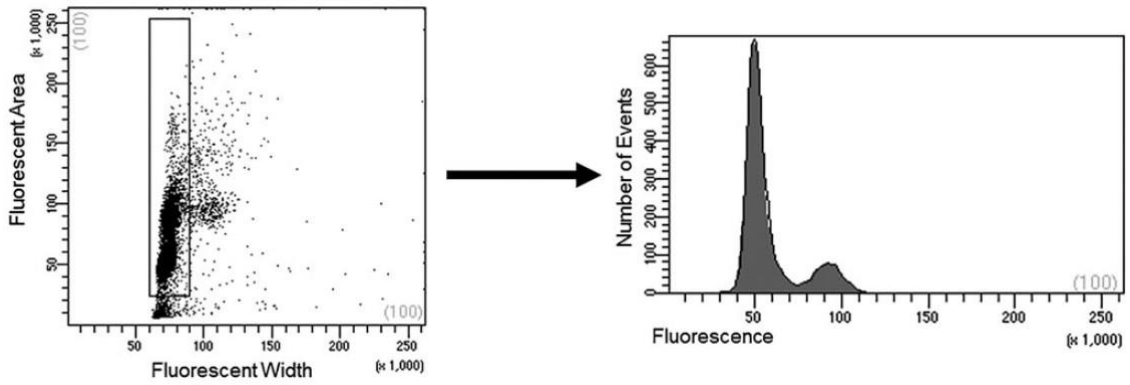

Figure 10: Flow cytometric analysis of canine MSC cell cycle and polyploidy.
The left panel illustrates the gating strategy to exclude doublets and debris. The histogram in the right panel indicates the stage of cell cycle based upon DNA staining. The majority of canine MSCs (~78%) were in the G0/G1 phase with fewer cells in the G2/M phase (~16%), and ~6% in the S phase.

Discussion

In this study, canine UC-MSC isolation and manufacturing protocols were generated using umbilical cords from 30 litters. Five new findings encapsulate this study. First, the manufacturing of canine UC-MSCs was fundamentally different from that of human UC-MSCs. By using human UC-MSC manufacturing protocols on canine cells, as done in Stage 1, most lines cease proliferation or senesce rapidly, since only 50% of the MSC lines could be maintained beyond passage 4.

Second, canine UC-MSC manufacturing was improved by adding cell attachment factors, such as gelatin-coating to tissue culture plates. A study by Devireddy et al. had previously indicated that gelatin coating was important for canine MSCs when they are expanded in serum-free defined medium [309]. This study indicates that addition of this attachment factor extends the longevity of MSC culture and improves colony-forming unit-fibroblast efficiency when MSCs are

grown with FBS-supplemented medium. When human MSCs are cultured in serum-free conditions, the addition of attachment factors is critical for their expansion [309].

These changes, represented here by shift from Stages 1 to 2, enabled 50% of the MSC lines expand to passage 8. Furthermore, use of gelatin coating significantly enhanced longevity of MSCs' self-renewal capability indicated by higher CPDs, and improved colony forming efficiency.

Third, an improvement was noted when nattokinase was used for lifting MSCs for passage. Nattokinase is a serine protease and a fibrinolytic enzyme isolated from Bacillus subtillis natto B-12 in traditionally fermented Japanese soybean. Previously, Carrion et al. reported that nattokinase could extract BM-derived MSCs out of a fibrin gel better than trypsin-EDTA or TrypLE [305]. We found nattokinase to be more effective for lifting canine MSCs than standard lifting agents, terms of yield, and viability. Lifting MSCs and passaging through trypsin-EDTA, dispase, or TrypLE reduced passage yield and viability. In short, nattokinase significantly improved cell viability and canine UC-MSC yield at passage.

Fourth, canine UC-MSC viability is reduced by cryopreservation, as expected. However, the impact of cryopreservation on canine UC-MSCs is no worse than that on human UC-MSCs (data not shown), and all 33 canine UC-MSC lines tested here re-entered the cell cycle and expanded after cryostorage. Importantly, the length of cryostorage had no significant impact on revival viability or expansion capability of canine UC-MSCs.

Fifth, we evaluated antibodies to be used as a standardized panel for evaluation of canine UC-MSCs. While overcoming the early senescence of canine MSC was a critical hurdle, the next challenge is to characterize canine MSCs. This is called a challenge because no consensus set of antibodies has been described for canine MSC surface markers. In this study, we addressed this

issue, and the monoclonal antibodies used in the canine MSC field were reviewed, and a list of antibodies that have been tested for canine MSC characterization is provided in Supplementary Table S2 [35, 36, 101-105, 287, 293, 299, 300, 309-317]. Antibodies used here are highlighted on this list. As can be seen when reviewing this table, the flow cytometry results using these antibodies were conflicting: Some of the antibodies performed well, meaning that they produced consistent results across different laboratories, and others were less consistent. In Table 1, the antibodies that worked in this study, and henceforth might be considered for a standard flow cytometry marker set for canine MSC immunophenotype characterization, are provided.

Two points raised by our flow cytometry study bear additional discussion. First, the positive shift for CD73 and CD90 staining was less than what we have seen in human UC-MSCs [23, 279]. We tested whether using an anti-canine-specific CD90 would improve the flow cytometry positive shift, compared with the anti-human CD90. As shown in Supplementary Figure S6, the positive shift was not frankly different, suggesting that the expression of CD90 was not as high in canine MSCs. Second, canine UC-MSCs appear to express CD34. This observation is controversial, since it is in contrast to the International Society for Cell and Gene Therapy (ISCT) consensus marker set for human MSCs [11]. However, it should be noted that three other laboratories have reported CD34 staining of canine MSCs, while most laboratories do not observe CD34 staining (Supplementary Table S2). Note also that the flow cytometry results for CD34 were confirmed by RT-PCR, and 11 out of 12 UC-MSC lines expressed CD34 mRNA (shown in Supplementary Figure S6), and further verified by DNA sequencing of the amplicons (data not shown). Together, this suggests that our cell source, culture, and passaging conditions result in CD34 expression by UCMSCs. These five new findings indicate the importance for optimizing

cell culture conditions and may have downstream impact on the clinical testing of canine UC-MSCs.

In the human MSC field, commercial human MSC flow cytometry characterization kits provide as a ‘‘standard’’ for comparison of MSC surface markers per the ISCT definition across the field. In contrast, no standardized antibody kit is available for the canine to facilitate between laboratory MSC comparisons. Canine MSCs positive surface marker expression, for example, the shift in mean fluorescence intensity, is less robust than that observed in human MSCs. Specifically, the shift in fluorescence intensity for canine MSCs for markers CD73, CD90, CD105, and CD44 is smaller than that observed in human MSCs. This could be due to differences in the affinity of the antibody for canine versus human molecule, or differences in the expression level between species, or due to cell culture-related ‘‘artifact.’’

Canine UC-MSCs were negative for hematopoietic markers CD45, CD5, CD21, CD14, and CD11b, and for HLA-DR (MHC class II), like human MSCs. Review of the literature provided in Supplementary Table S2 revealed that some laboratories reported CD34-positive canine MSCs [104, 297, 311, 314], and other laboratories, using the same CD34 clone, find no MSCs staining for CD34. Our review found that CD34-positive cells did not break cleanly such that CD34 expression was found only in tissue-specific MSCs, or only in early passage MSCs. For example, one article found CD34-positive cells in 18.4% AT-derived MSCs and in 3.6% BM-derived MSCs [104]. Another article reported 29.2% CD34-positive AT-derived MSCs [311]. A third article shows that CD34 expression (10%) AT-derived MSCs compared with 1% of the MSCs were CD105 positive [297]. Finally, Ryu et al. indicated that CD34 was expressed at low level in passage 1 AT-derived MSCs, but the expression was lost by passage 7 [314].

Based upon our results and the previous reports, some possible explanations for the disparity in CD34 expression can be considered. First, the observed CD34 staining here is real and CD34 expression in MSCs may be induced by culture or passaging conditions used here, since CD34 antibody clone we used performs consistently with high specificity in canine peripheral blood and BM immunophenotyping (K.K. and N.S., pers. comm.). Flow cytometry results for CD34 are supported by our RT-PCR (shown in Supplementary Figure S6) and DNA sequencing results (data not shown), which demonstrated CD34 expression in 11 of 12 canine UC-MSC lines. Second, as indicated by 3D cell culture work, it is possible that cell–substrate and cell–cell interactions may alter surface marker phenotype [318-320]. Follow-up study is needed to determine whether CD34 expression is due to using UC-MSCs, and to determine whether MSCs from other tissue sources can be induced to express CD34 by altered culture conditions.

Previous reports indicated that expanding canine MSCs was problematic, for example, that canine MSCs cannot proliferate beyond passage 7, and that canine MSCs must be characterized around passage 3 [105]. Some previous studies did not demonstrate trilineage differentiation or they performed RT-PCR to demonstrate gene expression in lieu of flow cytometry. We attribute these ‘‘problems,’’ for example, lack of multi-lineage differentiation, loss of differentiation potential, and to senescence associated with inappropriate cell attachment and passaging conditions. This was supported in our pilot studies (data not shown) where UC-MSCs from Stage 1 failed to differentiate or did so at very low efficiency whereas UC-MSCs from Stages 2 and 3 were able to differentiate at high efficiency.

Canine UC-MSCs have different medium requirements than human UC-MSCs, and that the addition of bFGF to the medium formulation significantly improved population doubling time and longevity in culture such that lines could be maintained beyond passage 11. The addition of

bFGF is known to have a mitogenic effect on MSCs of other species [306-308]. In summary, we demonstrated that bFGF not only improved growth rate, but it also may play a role in preventing UC-MSC senescence and improving differentiation efficiency.

Canine UC-MSCs were capable of differentiation to bone-, cartilage-, and fat-producing cells. Note that trilineage differentiation of canine MSCs is a point wherein laboratories have not consistently demonstrated the ISCT MSC definition. While saying this, we also observed low efficiency to differentiate UC-MSCs to adipocytes. We suggest that trilineage differentiation be adopted as part of standard for defining canine MSCs to meet the ISCT ‘‘multipotent cell’’ definition. We also suggest that further refinement in differentiation protocols would improve compliance. Note that more recently the ISCT released revised MSC characterization criterion that includes functional bioassays. We consider the addition of a functional bioassay important for canine UC-MSC characterization but it is beyond the scope of the present report.

Canine MSCs derived from different tissues such as AT, BM, or tissues discarded at birth such as placenta, amniotic membranes, or umbilical cord have been compared by others. In that regard, the advantages of MSCs derived from umbilical cords are clear. For example, MSCs from the umbilical cord are isolated from subjects of a consistent young age, and there is the potential to create banks of allogeneic cells for clinical use. Therefore, manufactured and banked UC-MSCs have the potential as an off-the-shelf allogeneic product, similar to umbilical cord blood hematopoietic stem cells. In that regard, this report provides an important contribution to the canine MSC literature.

MSCs are widely investigated in the field of regenerative medicine, as indicated by the number of MSC clinical trials listed on the ClinicalTrials.gov website. This clinical research ‘‘push’’ is not limited to human medicine, since there have been MSC trials conducted in

veterinary medicine, too. Thus, the demand for MSCs in large quantities and of ‘‘clinical grade’’ is present in both human and veterinary medicine. This demand for MSCs, however, is not well met. There is no standardized method to isolate, expand, characterize, and freeze/thaw MSCs that is universally accepted. There is no standard to compare MSC quality for their clinical potency. The lack of such standards might be an impediment for clinical translation, since each laboratory argues its case separately with the FDA. It seems likely that new manufacturing and qualification processes are needed to produce both large numbers but also MSCs manufactured of a quality standard [321].

In conclusion, this report addresses some limitations associated with manufacturing canine MSCs for clinical applications. Although significant improvements are reported here, further optimization might be possible. The knowledge gap between human UC-MSCs and canine UC-MSCs should be closed to maximize the usefulness of this companion animal species as a model for human UC-MSC clinical translation.

Chapter 3 - Effect of Conditioned Media Storage Temperature on Extracellular Vesicles Isolated from Human Umbilical Cord-Derived Mesenchymal Stromal Cells

Introduction

Mesenchymal stromal cells (MSCs) hold promise as a regenerative cellular therapeutic due to their ability to self-renew and differentiate. MSCs have been isolated from many tissues including, but not limited to, bone marrow (BM), adipose tissue, and extraembryonic tissues including the placenta and umbilical cord. The umbilical cord tissue has advantages as a MSC source of MSCs since it is collected painlessly and non-surgically at birth and from donors of a consistent young age [24, 31].

It was once believed that MSCs exerted their regenerative effects via engraftment and differentiation post-implantation. More recently it has been demonstrated that MSCs' effects are attributed in large part to the signaling via secreted factors and extracellular vesicles (EVs) that act in a paracrine manner, and in a smaller part by contact-mediated signaling [118-121, 322]. EVs are nanoparticles that may be divided into three major subpopulations by size and function: microvesicles (50-1000 nm), apoptotic bodies (50-5000 nm), and exosomes (30-150 nm) [118, 120, 127, 130-133]. EVs have been shown to be involved in both physiological and pathological signaling and communication [323-328]. In addition, EVs have been implicated in immune responses via antigen presentation and complement activation, cell adhesion, tissue remodeling, and in cancer progression and metastasis [117, 198, 329, 330].

EVs are produced by prokaryotic and eukaryotic cells and can be isolated from many biological fluids, including cell culture-conditioned media (CM). An impediment in EV clinical research is the scale-up and reproducible production of EVs [209, 322, 331, 332]. MSC-EVs are proceeding to clinical trials despite questions that remain concerning their production, isolation, and storage [333]. We hypothesize that CM will serve as a reproducible and scalable source of EVs for clinical translation. Here we investigate the effects of CM storage temperature in downstream EV isolation based upon the assumption that proper storage of cells and EVs affects their biological activity.

We used the immediate isolation of EVs as the "standard" method for comparison since there is little opportunity for degradation of EVs or their contents. Immediate isolation is not always feasible, especially as sample quantity and/or collection frequency are scaled-up. We reviewed the literature on this topic and found no systemic evaluation of storage conditions of sample prior to EV isolation. Some laboratories argue that EVs are resistant to the effects of a single freeze/thaw, and thus cryopreservation and storage are not critical considerations prior to isolation [199, 334, 335]. In contrast, others contend that EVs are subject to freeze/thaw damage, and that cryopreservation and proper storage are important considerations for their downstream application [128, 210, 336-340]. For example, Romanov et al. showed that storage temperature of human UC-MSC CM affects the isolated microvesicles (MVs) [128]. Storage at 4°C did not result in degradation of MVs for the first week, but beyond a week of storage, degradation was observed [128]. In addition, degradation was observed from a freeze/thaw cycle regardless of the storage temperature used [128]. Zhou et al. demonstrated that storage condition affects the quantity of exosomes recovered from urine, and storage at -80°C was the ideal storage temperature since it

resulted in a similar recovery of exosomes compared to fresh urine, while, in contrast, storage at -20°C resulted in significant exosome loss [338].

More research has been focused on the storage of EVs once they are isolated from CM or other biological fluids. After EVs isolated from HEK 293 CM were stored at temperatures ranging from -70°C, 4°C, to room temperature for 10 days, Lee et al. demonstrated that protein and RNA amounts were reduced after room temperature storage compared to storage at -70°C and 4°C [183]. Furthermore, storage at 4°C and room temperature resulted in loss of the exosome surface marker CD63 expression while storage at room temperature caused the loss of Hsp70 expression [183]. From this work Lee et al. concluded that -70°C was the ideal storage temperature [183]. Cheng et al. demonstrated that EVs isolated from HEK293T cell CM had the highest number of particles and levels of EV characterization proteins (ALIX, Hsp70, and TSG101) when stored at 4°C compared to EVs stored at higher temperatures or subjected to freeze/thaw cycles [341]. Using nanoparticle tracking analysis (NTA), Sokolova et al. demonstrated that EVs isolated from HEK 293T CM had a greater reduction in size when stored at 37°C compared to 4°C [225].

In contrast to EVs isolated from CM, EVs derived from cerebrospinal fluid of glioblastoma patients were found to be stable at room temperature for seven days as well as after a single cycle of freeze-thawing, while a second freeze-thaw cycle resulted in significant alterations of EV number, morphology, and RNA content or miRNA levels [195]. Lorincz et al. demonstrated that storage of EVs isolated from neutrophilic granulocytes at 4°C and 20°C resulted in a decrease in both the number of EVs and the antimicrobial effect of EVs, while storage at -80°C had no significant effect on either number or antimicrobial effect [339]. In a patent owned by Capricor Therapeutics, the number of EVs isolated from the cardiosphere-derived cells CM remained stable

when stored for one week at 4°C, -20°C, and -80°C, the miRNA concentration decreased significantly in EVs stored at 4°C and -20°C yet remain unchanged in those stored at -80°C [342].

The International Society for Extracellular Vesicles (ISEV) currently recommends that EVs should be stored in phosphate-buffered saline at -80°C in siliconized vessels, yet no recommendation exists regarding the storage of biological fluids prior to EV isolation [137, 232, 233]. Based upon the results presented here, we suggest that the optimal storage temperature for human UC-MSC CM is -80°C prior to downstream EV isolation. In addition, our findings suggest that storage at room temperature, 4°C, and -20°C did not result in complete degradation of EVs from human UC-MSC CM and thus research findings utilizing these storage conditions cannot be disregarded because of CM storage conditions.

Materials and Methods

Preparation of Conditioned Media from Human UC-MSCs

Here, MSCs derived from human umbilical cords were used. The research protocol was reviewed and approved by the Kansas State University human subject research committee and was considered exempted human subjects research under exemption 4. Human UC-MSCs were isolated, culture-expanded, characterized, and cryopreserved using a previously described protocol [23]. Thus, a cryobank of 57 HUC-MSC cell lines was generated and available for use. From the banked MSC lines, 18 lines were selected randomly and subjected to full MSC characterization in accordance with the International Society of Cellular Therapy (ISCT) recommendations [11]. All lines demonstrated (1) plastic adherence and self-renewal via tissue culture expansion and clonal expansion capability, (2) tri-lineage differentiation capacity via qualitative differentiation assays to bone, cartilage, and fat lineages, and (3) positive surface marker expression (defined as > 95%

positive over isotype control) of CD73, CD90, and CD105 alongside negative surface marker expression (defined as < 2% positive over isotype control) of CD34 and CD45. For the work described herein, five cryopreserved MSC lines were selected randomly from the 57 MSC lines for use and three of the selected lines had been fully characterized previously as MSCs. There were no frank differences observed between these five MSC lines in EV production.

The human UC-MSC lines (P3-P5) were thawed and plated individually at a density of $1x10^4$ cells/cm^2 on tissue culture-treated T-150 flask (Corning, Cat. No. 430825) and allowed to recover from cryostorage for one passage before use in experiments. The cells were maintained in culture and passed as previously described [23]. For quality control purposes, only cell lines with >95% viability during the passage prior to serum-starvation were used for CM production (all five lines passed this criterion).

As shown in the experimental schematic (Figure 11), following passage, human UC-MSCs were plated at a density of $1x10^4$ cells per cm^2 in five T-150 flasks and incubated at 37°C, 90% humidity, and 5% CO2 in a HeraCell 150i incubator in a growth medium containing platelet lysate [23]. Once cells reached 60-70% confluence (~48 hours), medium was removed and replaced with 30 mL low glucose Dulbecco's Modified Eagle Medium (DMEM, Gibco, Cat. No. 11885). After 24 hours the medium was considered conditioned (i.e., CM), and it was transferred to a sterile 50mL centrifuge tube. The tubes were pre-labeled with experimental conditions (immediate, room temperature, 4°C, -20°C, and -80°C) and the order was randomized and blinded prior to CM collection. CM in the immediate group was collected and processed for EV isolation within 24 hours. CM in the room temperature, 4°C, and -20°C groups were stored for 7 days at their designated temperature and were then processed for EV isolation within 24 hours. Due to COVID, core facilities were forced to close and the CM samples in the -80°C group were stored up to 1

month before being processed for EV isolation. The experimental design was balanced to ensure that there was an equal number of observations for all possible level combinations thus, CM from all lines was collected for every storage temperature. This was done to control for line-to-line variations in EV production.

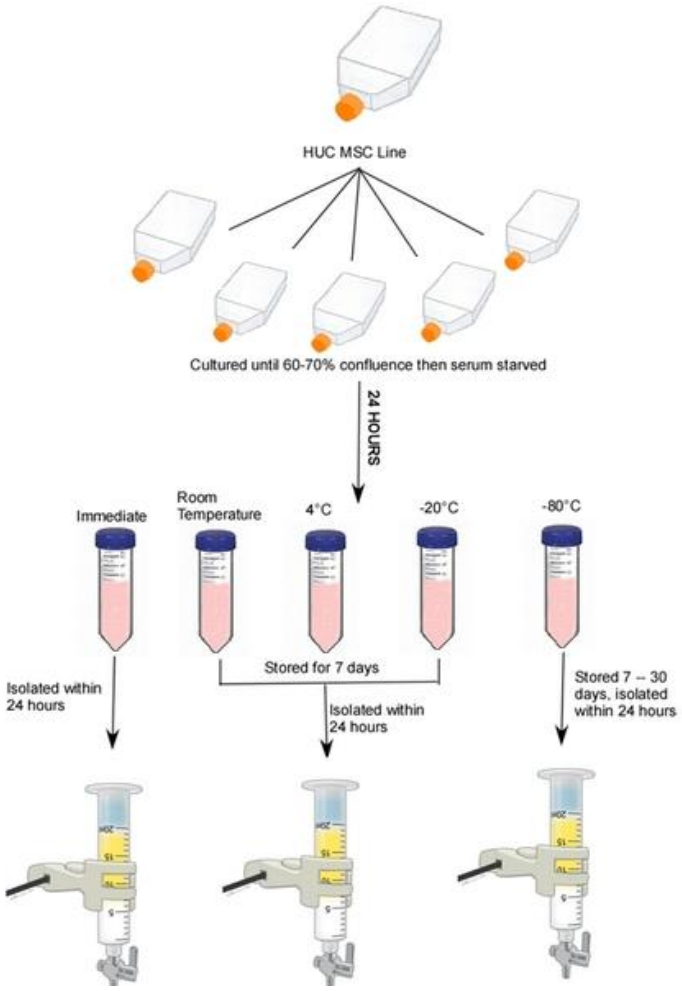

Figure 11: Storage Experimental Schematic

A schematic of the balanced experimental design showing the major steps involved for isolation of extracellular vesicles (EVs) from the human umbilical cord-derived mesenchymal stromal cell (UC-MSC) culture conditioned media. Following cryopreservation, human UC-MSCs were allowed one passage of recovery before being passaged and split into five T-150 tissue culture-treated flasks and incubated at 37°C, 90% humidity, and 5% CO2 until 60-70% confluence was reached. Medium was removed and replaced with serum-free medium. After 24 hours, conditioned media was collected in a sterile 50mL centrifuge tube and randomly assigned one of the five storage conditions (immediate, room temperature, 4°C, -20°C, and -80°C). Samples in the immediate group were isolated within 24 hours by a combination of ultrafiltration and size-exclusion chromatography. Samples in the room temperature, 4°C, and -20°C were stored for seven days at the assigned temperature and isolated within 24 hours. Samples in the -80°C group were stored up to one month before EV isolation.

Preparation of Size-Exclusion Chromatography (SEC) Column

A slurry of Sepharose CL-2B (GE Healthcare, Cat. No. 65099-79-8) was prepared and degassed using sterile Dulbecco's phosphate-buffered saline (DPBS, Gibco, Cat. No. 14-190-250) according to the manufacturer's instructions. A 20 mL syringe (EXELINT, Cat. No. 26280) was stuffed with cotton wool and the column was poured with 20 mL of Sepharose CL-2B slurry similar to [200]. After settling overnight in a cold room, the column height was 7.5 cm and the column diameter was 2.21 cm. At least three volumes of DPBS were run through the column to ensure consistent packing. The void volume and column packing and separation efficiency were determined by passing a solution containing 0.25 mL of both blue dextran solution (Sigma Aldrich, Cat. No. D5751) and bovine serum albumin (BSA, Sigma Aldrich, Cat. No. A3912-500G) through the column. Fractions of 0.25 mL were collected after the void volume up until those containing BSA (identified by protein concentration).

EV Isolation by a Combination of Ultrafiltration and SEC

EVs were isolated using a combination of ultrafiltration and SEC similar to Benedikter et al. with some modifications [202]. CM was centrifuged at 3200 *g* for 30 minutes at 4°C (Eppendorf 5810R using a swing bucket rotor A-4-62, Cat. No. FL08517291) to pellet cells and cellular debris. The supernatant was collected and filtered through a 0.22 µm syringe filter (Fisherbrand, Cat. No. 09-720-004). CM was transferred to an Amicon Ultra-15 filter unit with Ultracel-100 membrane (MWCO = 100 kDa, Merck Millipore, Cat. No. UFC910024) and centrifuged at 3200 *g* until the retained sample volume was approximately 300 µL. This represented approximately a 1:100 concentration factor. The retentate was collected in a sterile microcentrifuge tube. The membrane

was subsequently rinsed with 200 µL DPBS to collect any adherent EVs, and this was added to the sample tube.

The filtered sample (~500 µL) was layered onto the SEC column and eluted with sterile, degassed DPBS. Following the void volume, 27 fractions of 250 µL were collected. Protein analysis was performed on the fractions using a NanoDrop 8000 spectrophotometer (Thermo Scientific, Waltham, MA). Following analysis, fractions were pooled, divided into 1 mL aliquots in polypropylene microcentrifuge tubes, and stored at -80°C until EV characterization.

Lyophilization of EVs for Transmission Electron Microscopy and Dot Blots

EVs were lyophilized similar to Charoenviriyakul et al. with modifications [343]. Briefly, to freeze-dry samples, frozen 1 mL aliquots were removed from the -80°C. Immediately a small hole was made in the top of the microcentrifuge tube using a sterile 20G x 1-inch needle (Becton Dickinson, Cat. No. 305175) and the lip of the lid was trimmed using scissors so that it could fit inside of a sterile 15 mL polypropylene centrifuge tube (Nunc, Cat. No. 339650). This was done so that the samples could be freeze-dried at a 45-60° angle and to catch any particles that spilled over from the hole in the tube. The lids of the 15 mL centrifuge tube were replaced with lids that had 5 holes previously made using a 20g needle. The samples were loaded into a TF-10A 1.2-liter vacuum freeze dryer (TEFIC BIOTECH CO., LIMITED, Xi`an, China), which has a condenser capable of reaching ≤56°C and a vacuum of <10 Pa. Samples were lyophilized in batches of 5-6 samples overnight for 16-18 hours. Following lyophilization, samples were stored at room temperature in the 15 mL centrifuge tube with original lids and sealed with parafilm to protect from moisture. Immediately prior to use, an aliquot of lyophilized EVs was rehydrated with sterile UltraPure distilled water (Invitrogen, Cat. No. 10977) to 20% of their original volume and

vortexed. Following lyophilization and rehydration, the protein concentration was measured. Lyophilized/reconstituted EV samples were used for transmission electron microscopy (TEM) and dot blot analysis.

Nanoparticle Tracking Analysis

Nanoparticle tracking analysis (NTA) was used to assess the EV population size distribution and concentration using a NanoSight LM-10 (Malvern Pananalytical Ltd., Malvern, UK). To ensure consistent viscosity of the samples, measurements were made at a constant temperature of 25°C ± 1. Acquisition settings were held constant for all samples and were as follows: blue 405 nm laser, camera type scientific CMOS, camera level 13, and detection threshold 3. NanoSight software (NTA 3.3) was used to analyze 60-second videos with 5 repetitions per sample. Five independent samples from each storage temperature were analyzed. The measurement was made from 5 technical replicates and averaged for comparison via repeated measures analysis of variance (ANOVA). The instrument was calibrated using 50 nm and 100 nm standards (Malvern Pananalytical Ltd., Cat. Nos., NTA4087 and NTA4088, respectively). Sterile DPBS was used as the negative control. The sample dilutions ranged from undiluted to 1:100 in sterile DPBS to ensure that sample measurements fell in the NTA optimal range of $1x10^8$ to $1x10^9$ particles/mL (30-50 particles/frame).

Using NTA concentration data, EVs released per cell was calculated. Population doubling time (PDT) in hours was calculated for each cell line using the previous passage data according to the equation given in Chapter 2. An estimate of the number of MSCs was calculated using the PDT and the number of hours that the cells have been in culture (data shown in Table 3). The assumption was made that when cell culture media was replaced with serum-free medium, expansion stopped.

The EVs released per cell was calculated as the total particles in the sample divided by the estimate of cells in culture. Five independent samples from each storage temperature were analyzed. The five independent measurements for particles per cell were averaged by both storage condition and by individual cell line and compared using one-way repeated measures ANOVA. The effect of MSC expansion (e.g., passage number and population doubling time) on EVs released per cell was evaluated. These results were plotted and a simple linear model derived using regression.

Table 3: Calculation of Viable Cell Number

Cell Line	*Passage*	*Previous Passage PDT (hours)*	*Time in Culture (hours)*	*Cells Seeded*	*Population Doublings*	*Estimated Viable Cell Number*
HUC 284	P5	58.7	72	150,000	1.23	$3.34x10^6$
HUC 293	P5	59.0	72	150,000	1.22	$3.33x10^6$
HUC 297	P6	38.4	96	150,000	2.50	$5.25x10^6$
HUC 298	P4	46.2	96	150,000	2.08	$4.62x10^6$
HUC 301	P6	51.6	72	150,000	1.39	$3.59x10^6$

Dynamic Light Scattering

Dynamic light scattering (DLS), zeta potential, and polydispersity index (PDI) were used to assess the hydrodynamic size distribution, surface charge properties, integrity, and stability of the EVs. Measurements were made using the Zetasizer Nano ZS (Malvern Pananalytical., Malvern, United Kingdom) as previously published [117]. Instrument settings were 10 runs of 10

seconds with 3 repetitions per sample. Five independent samples from each storage temperature were analyzed. Measurements were made with technical triplicates and averaged for comparison via one-way repeated measures ANOVA.

Transmission Electron Microscopy

TEM was used to visualize EV morphology and to generate a size estimate of the population. Lyophilized samples were rehydrated using sterile water. The samples were prepared, experimental conditions were masked, and the samples were blindly analyzed by the University of Kansas Medical Center. An area of approximately 69 μm^2 was sampled and a minimum of 20 micrographs were collected. Size of EVs was estimated by measuring data from two MSC lines that were chosen at random in all storage conditions. A minimum of 20 micrographs were captured per storage temperature and all EVs depicted were measured. From this data, sizes were averaged by storage condition to generate a size measurement to be compared using Kruskal-Wallis one-way ANOVA on ranks.

Determination of Protein Concentration

The protein concentration of the individual fractions from the SEC was determined using the absorbance at 280 nm on a NanoDrop 8000 spectrophotometer immediately following elution from the column. DPBS was used as the blank for background subtraction. This was done to detect any protein contamination in the samples and ensure proper separation.

Once the fractions were combined, the protein concentration of the EV sample was determined using a Pierce micro BCA protein assay kit (Thermo Scientific, Cat. No. 23235) according to the manufacturer's instructions. Samples were plated in technical triplicates in a 96

well plate (Corning, Cat. No. 3370). The absorbance was read at 562 nm using a SpectraMax i3x plate reader (Molecular Devices, San Jose, CA). A protein standard curve was generated using BSA standards supplied with the kit and by averaging technical triplicates. DPBS was used as a blank for background subtraction. Samples were plated in triplicate and the average was used to determine the protein content of the EVs.

Samples were reconstituted in 200 µL distilled water after lyophilization for dot blots. The protein content in the samples was determined using the absorbance at 280 nm on the NanoDrop spectrophotometer with distilled water as the blank for background subtraction. The protein content for each sample was calculated as the average of three technical replicates.

Characterization by Dot Blot

To perform dot blots, 0.75 µg of protein was loaded onto an activated polyvinylidene fluoride (PVDF) membrane (Merck Millipore Ltd., Cat. No. IPVH0010). After protein dots were completely dried, the membrane was blocked with 5% non-fat dried milk solution. The membrane was probed with mouse primary antibodies: anti-human CD9 (1:1000, Ts9, Invitrogen, Cat. No. 10626D), anti-human CD63 (1:500, Ts63, Invitrogen, Cat. No. 10628D), anti-human CD81 (1:500, M38, Invitrogen, Cat. No. 10630D), anti-human Hsp70 (1:200, 3A3, Santa Cruz Biotechnology, Cat. No. sc-32239), and anti-human beta-actin (β-actin, 1:2000, AC-74, Sigma Aldrich, Cat. No. A2228) overnight at 4°C with gentle rocking. Water and lysed MSCs (i.e., whole cell lysate) served as negative and positive controls, respectively. Following incubation with primary antibodies, membranes were washed three times using 1% tris-buffered saline with 0.1% Tween-20 detergent and blotted with secondary antibody HRP-conjugated goat anti-mouse IgG (1:2000, Poly4053, BioLegend, Cat. No. 405306) for 1 hour at room temperature with gentle

rocking. After washing, chemiluminescence detection reactions were performed using SuperSignal West Femto substrate (Thermo Scientific, Cat. No. 34095) according to the manufacturer's instructions. Images were captured using a Kodak Image Station 4000 after 2 minutes of exposure.

To score dot blot staining, 3 independent scorers were provided numbered dot blot strips, such that the experimental conditions were masked as to protein blotted and experimental group information, and a scoring standard (shown in Figure 16a). Scorers were instructed to judge the intensity of the dot only, not the size of the dot itself. Dots were scored on an ordinal (linear) integer scale as strong (2 points), weak (1 point), or negative (0 points). Expression of β-actin was not scored since it was used for a positive control. For each blotted protein, the score was averaged from three scorers. Averaged scores were summed for the four markers per MSC line and storage condition giving a total score for comparison. The maximum score possible was 8.0 (strong positive expression for all four markers). The total score for each storage condition and cell line from the five independent lines was analyzed using repeated measured ANOVA on ranks and pairwise comparisons were made using Dunn's method.

MicroRNA Isolation and Reverse Transcriptase-Polymerase Chain Reaction

MicroRNA (miRNA) was isolated and reverse transcribed (RT) into a cDNA template using RNAzol RT (Sigma Aldrich, Cat. No. R4533) according to manufacturer's instructions. Briefly, RNAzol RT was added to EV samples. Samples were covered, shaken vigorously, and then left at room temperature for 5-15 minutes. The mixture was centrifuged at 12,000 g for 15 minutes at 4-28°C. Supernatant was carefully removed and transferred to a clean microcentrifuge tube, leaving a small layer above the pellet of DNA and proteins. To precipitate mRNA, 75%

ethanol v/v was added to supernatant and let stand at room temperature for 10 minutes. The sample was centrifuged to pellet mRNA. The supernatant was transferred to a clean microcentrifuge tube. To pellet miRNA, 100% isopropanol v/v was added to supernatant, let stand at 4°C for 30 minutes, and then centrifuged. Both mRNA and miRNA were washed using 75% ethanol followed by 70% isopropanol and centrifuged at 15000 g for 1-3 minutes at room temperature. Alcohol was discarded and RNA pellets were reconstituted in RNase-free water. To check for protein contamination, a 260/280 ratio was obtained for each sample using a NanoDrop 8000 spectrophotometer.

The Poly(A) tail reaction and cDNA synthesis was performed using the MystiCq microRNA cDNA Synthesis Mix (Sigma Aldrich, Cat. No. MIRRT) according to manufacturer's instructions. Briefly, the miRNA sample was combined with Poly(A) polymerase, buffer, and water. The sample was sealed, vortexed, centrifuged, and incubated at 37°C for 60 minutes. The resulting reaction mixture was combined with ReadyScript Reverse Transcriptase and MystiCq microRNA cDNA reaction mix then sealed, vortexed, centrifuged, and incubated for 20 minutes at 42°C. Polymerase chain reaction (PCR) was performed using a BioRad iCycler: the initial denaturation at 98°C for 30 sec, 35 cycles of [98°C for 15 sec, 51°C for 30 sec, and 72°C for 5 sec], and the final extension at 72°C for 10 min. After PCR, the products were resolved on a 2% agarose gel with a 25 bp DNA ladder and imaged using ethidium bromide. The RNAs and the MystiCq Universal PCR primer (Sigma Aldrich, Cat. No., MIRUP) are provided in Table 4. miRNAs for analysis were chosen from the EV miRNA database [344]. Using the database, MSCs were selected and the database returned 9 miRNAs known to be expressed in EVs from MSCs [http://bioinfo.life.hust.edu.cn/EVmiRNA, filter = mesenchymal stem cell, accessed 6/3/2020].

Primers were designed using NCBI database and the sequences, along with accession number, are listed in Table 4.

Table 4: RT-PCR Primers

miRNA Primer	*Sequence (5' to 3')*	*Tm (ºC)*	*Accession Number*
HU.MIR7641	GCAGTTGATCTCGGAAGCT GTCCAGTTTTTTTTTTTTTTTGCTTAG	54.9 51.6	MIMAT0029782
HU.MIR6089	ACAGGAGGCCGGGGTGGG TCCAGTTTTTTTTTTTTTTTCCGC	65.7 52.2	MIMAT0023714
HU.MIR4792	ACAGCGGTGAGCGCTCG GTCCAGTTTTTTTTTTTTTTTGCCAG	61.3 53.4	MIMAT0019964
HU.MIR4466	ACAGGGGTGCGGGCCGG TCCAGTTTTTTTTTTTTTTTCCCCG	67.4 53.8	MIMAT0018993
HU.MIR3665	CAGAGCAGGTGCGGGGC TCCAGTTTTTTTTTTTTTTTCGCC	62.5 52.2	MIMAT0018087
HU.MIR1273e	CAGTTGCTTGAACCCAGGAA GTCCAGTTTTTTTTTTTTTTTCCAC	55.5 51.0	MIMAT0018079
HU.MIR1246	GCAGAATGGATTTTTGGAG GTCCAGTTTTTTTTTTTTTTTCCTG	49.2 50.8	MIMAT0005898
HU.MIR658	GGCGGAGGGAAGTAGGTC GTCCAGTTTTTTTTTTTTTTTACCAAC	57.4 51.6	MIMAT0003336
HU.MIR127	AGTCGGATCCGTCTGAGCTT GTCCAGTTTTTTTTTTTTTTTAGCC	58.0 50.9	MIMAT0000446
MystiCq Universal PCR Primer	Complimentary to adapter sequence added during cDNA synthesis		Cat. No. MIRUP

Samples were scored based on the presence or absence of a band of correct size (as determined by the primer length and addition of PolyA tail. A sample was scored a 1 for positive signal and a 0 for negative signal. Scores were added for each independent cell line per storage condition for a maximum score of 5 and a minimum score of 1. Scores were compared by storage condition using one-way ANOVA.

Statistics

ANOVA was used to evaluate main effects and interactions. Data was first checked to verify that the ANOVA assumptions were met before testing. For significant ANOVA terms, post hoc testing of planned comparisons was performed using either Bonferroni correction or Dunn's method. Data from these tests are presented as mean ± one standard deviation. For pairwise comparisons, statistical assumptions were confirmed and then data was analyzed using Student's t-test. If ANOVA assumptions were not met, Kruskal-Wallis analysis of variance on ranks was used. Data from these tests are presented using a box and whisker plot depicting the median, 25th, and 75th percentile in the box and whiskers showing the 10th and 90th percentile. Any potential outliers are depicted as open circles. As discussed in the text, data are presented as mean ± one standard deviation except where otherwise specified. Hypothesis testing was two-tailed and a $P<0.05$ was considered "significant." In some cases, a power analysis was conducted to determine the sample size needed to detect significant differences using a desired power of 0.8 and an alpha of 0.05. For the data analysis, the entire dataset, including potential outliers, was used for all analyses. Linear models were also constructed using SigmaPlot as describe above. All statistical analyses and graph generation was conducted using SigmaPlot (version 12.5, Systat Software,

Inc.). Graphs were exported as EMF files to be edited. Labels and edits were performed using Canvas X (version 15.5, build 1770, ACD Systems of America) and saved in TIFF format.

Results

EV Analysis by Nanoparticle Tracking Analysis

Nanoparticle tracking analysis (NTA) of the size of the EV population for each storage condition is shown in Table 5. No differences were detected in the size data between EVs isolated immediately or from the experimental storage conditions (P = 0.45). NTA sizes ranged from 85 nm to 106 nm, with immediate isolation condition tending to be the smallest size (85.1 ± 21.7 nm) and frozen -20°C tending to be the largest (105.4 ± 18.6 nm). Based upon the effect size observed here, power analysis revealed that for a power of 0.8 and an alpha of 0.05, a sample size of 20 would be required to detect significant differences between storage conditions assuming normal and unimodal distributions via two-tailed analysis.

Table 5: NTA Size Estimate of EVs by CM Storage Condition

CM Storage Condition	*NTA Size Mode (nm) ± SD*
Immediate	85.1 ± 21.7
Room Temperature	96.2 ± 19.7
4ºC	88.5 ± 8.1
-20 ºC	105.4 ± 18.6
-80 ºC	100.4 ± 21.9

The EV particle counts by CM storage temperature as measured by NTA are shown in Figure 12. No significant differences in EV total particle count were detected among samples isolated immediately or from experimental storage conditions. Total particle counts ranged between $6.99x10^{10} \pm 3.12x10^{10}$ – $1.28x10^{11} \pm 8.30x10^{10}$. This data indicates that storage temperature of CM did not significantly impact the number of EVs isolated from the sample. Based upon the effect size observed here, power analysis revealed that for a power of 0.8 and an alpha of 0.05, a sample size of 36 would be required to detect significant differences.

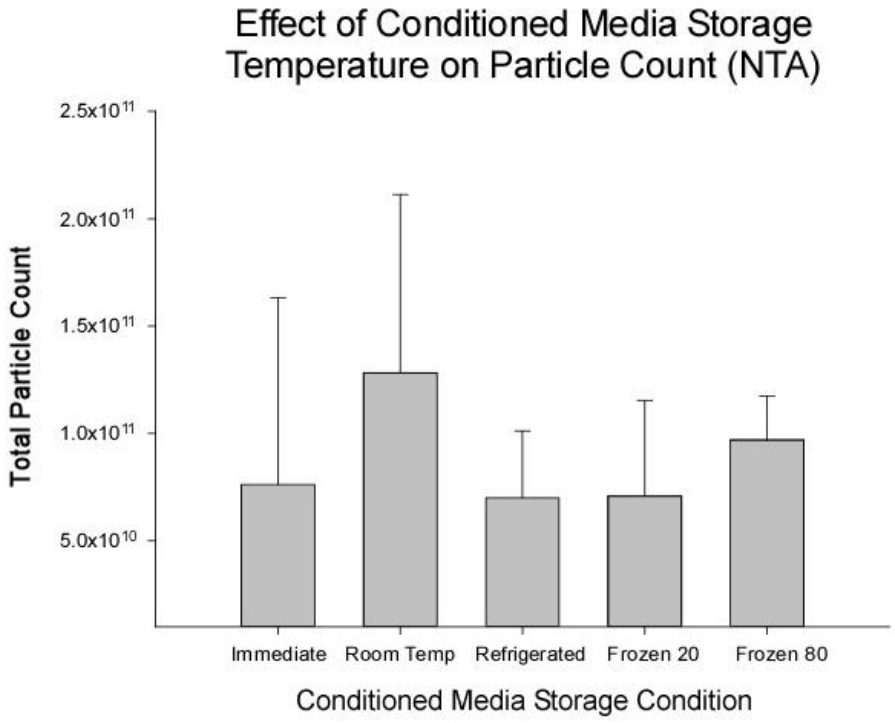

Figure 12: Effect of CM Storage Temperature on Particle Count

The storage temperature of conditioned media (CM) did not affect particle count measured by Nanoparticle Tracking Analysis (NTA). Particle counts ranged from $6.99x10^{10} \pm 3.12x10^{10}$ to $1.28x10^{11} \pm 8.30x10^{10}$. No significant differences in particle count were detected ($P = 0.332$) indicating that CM storage temperature prior to isolation did not significantly impact the number of particles isolated from the sample. Data are presented as mean ± standard deviation (n=5).

Using NTA particle count, EVs released per cell was estimated by averaging all storage temperatures per cell line (Table 6). No significant differences were detected between individual cell lines ($P = 0.08$) indicating that the five cell lines used here produced a similar number of EVs in the 24-hour conditioning period.

Table 6: EVs Released per MSC by Cell Line

MSC Line	*EVs Released per Cell (mean ± SD)*
HUC 284	$1.2x10^4 \pm 1.1x10^4$
HUC 293	$2.3x10^4 \pm 9.6x10^3$
HUC 297	$1.5x10^4 \pm 3.3x10^3$
HUC 298	$3.2x10^4 \pm 2.1x10^4$
HUC 301	$2.8x10^4 \pm 9.9x10^3$

The particles per cell was averaged by CM storage condition and is shown in Figure 13a. No significant differences were detected among experimental storage conditions ($P = 0.263$). Similar to the range observed by individual cell line, the range by CM storage condition was $1.7x10^4 \pm 7.7x10^3$ to $3.2x10^4 \pm 1.7x10^4$ particles/cell. Based upon the effect size observed here, power analysis predicted that a sample size of 18 would be required to detect significant differences among cell lines at a power level of 0.8 and alpha of 0.05. Regression analysis was performed with cell passage as the independent variable and particles per cell as the dependent variable (Figure 13b). No significant correlation was found but there was a trend for cell passage to be negatively correlated with EVs released per MSC. A second regression analysis was performed with PDT as the independent variable and particles per cell as the dependent variable

(Figure 13c). No significant correlation was found but there was a trend for MSCs with larger PDTs (i.e., slower growing cells) to release more EVs per MSC than faster growing cells.

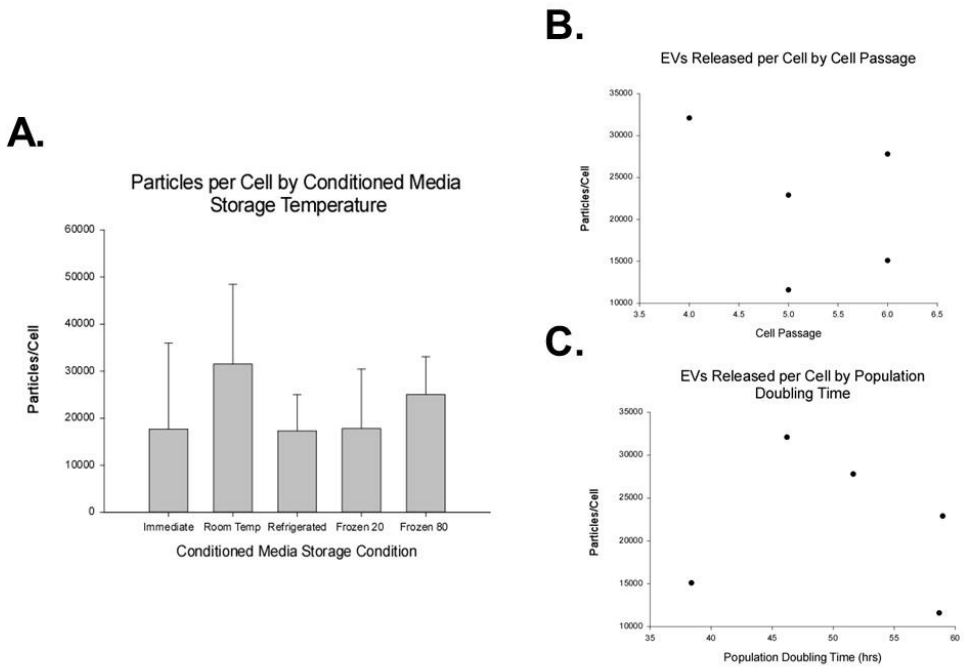

Figure 13: Particles per MSC by CM Storage Condition

Storage condition did not affect the number of particles recovered. (A) EVs released per human umbilical cord-derived mesenchymal stromal cell (MSC) by conditioned media (CM) storage temperature (immediate, room temperature, 4°C, -20°C, and -80°C). Total particles released per MSC ranged from $1.7x10^4 \pm 7.7x10^3$ to $3.2x10^4 \pm 1.7x10^4$. No significant differences were detected indicating that CM storage had no significant impact on number of vesicles released per cell. Data are presented as mean ± standard deviation and is representative of five independent cell line measurements. (B) Regression analysis of EVs released per MSC versus cell passage. No significant correlation was found. There was a trend for cell passage to be negatively correlated with EVs released per cell, n=5 (C) Regression analysis of EVs released per cell by population doubling time. No significant correlation was found. There was a trend for cells with larger population doubling times (i.e., slower growing cells) to release more EVs per MSC than faster growing cells, n=5.

EV Characterization by Dynamic Light Scattering

EVs were characterized using dynamic light scattering (DLS) to determine the polydispersity index (PDI), zeta surface potential, and hydrodynamic size. EVs isolated from CM stored at -80°C was different than the immediate group for PDI (Figure 14a, P = 0.012). EVs isolated immediately had a mean PDI of 0.64 compared to 0.34 for EVs from CM stored at -80°C. As shown in Figure 14b, the zeta potential of EVs was found to range from -7.7 ± 3.8 mV to -12.4 ± 2.5 mV. No significant differences were detected between experimental groups (P = 0.143) although there was a trend for EVs from CM stored at all experimental conditions to be lower than EVs isolated immediately. This indicates that CM storage temperature prior to isolation does not significantly impact the zeta potential of EVs. Based upon the observed effect size, power analysis revealed that a sample size of 12 would be required to detect significant differences at a power of 0.8 and an alpha of 0.05. As shown in Figure 14c, EVs displayed a hydrodynamic size of 165.6 ± 42.7 nm to 410.7 ± 262.9 nm. No significant differences were detected (P = 0.052) but there was a trend for EVs in the immediate group to be different than those in the -80°C and room temperature groups (see Figure 14c). Both room temperature and -80°C tended to display a smaller range among samples than other groups. The wide range of sizes in the immediate group compared to -80°C. Taken together the DLS data suggests that -80°C storage may produce a more homogenous population of EVs and smaller EVs compared to immediate processing.

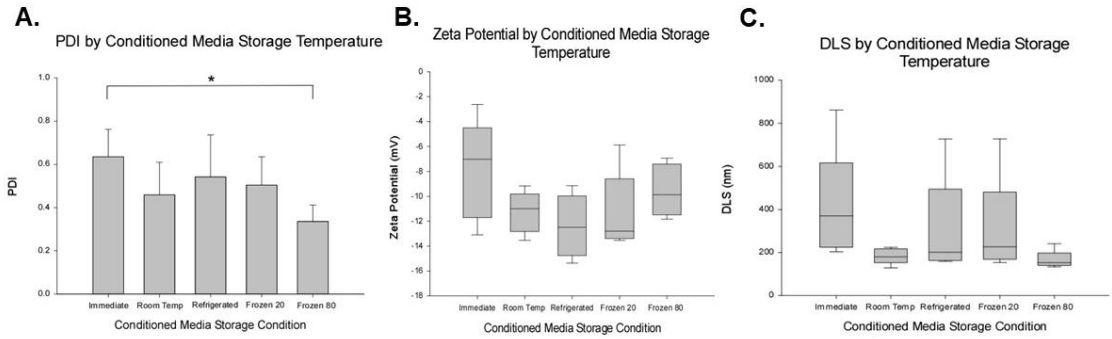

Figure 14: Dynamic Light Scattering Analysis of EVs

Dynamic light scattering (DLS) characterization of extracellular vesicles (EVs). (A) Polydispersity index (PDI) of EVs isolated immediately from human mesenchymal stromal cell (MSC) conditioned media (CM) and EVs from CM stored at either room temperature, 4°C, -20°C, and -80°C. A significant difference (P = 0.012) was noted in EVs isolated immediately and those from the -80°C experimental group, indicating that storage of CM at -80°C may produce a more homogeneous EV population. (B) Zeta potential of EVs. No significant differences noted (P = 0.143) although there was a trend for EVs from CM stored at all experimental conditions to be lower than those isolated immediately. (C) Hydrodynamic size of EVs by DLS ranged from of 165.6 ± 42.7 nm to 410.7 ± 262.9 nm. No significant differences noted (P = 0.052) but there was a trend for EVs in the immediate group to be different than those from CM stored at -80°C and room temperature. Room temperature and -80°C display a smaller size range, indicative of a more homogenous population in terms of size, similar to PDI data. Data are presented as mean ± standard deviation with an asterisk indicating significance, defined as P<0.05.

EV Analysis by TEM

Using TEM, EVs were detected in all CM storage conditions. For each storage condition, 10 to 29 (average 22.3 ± 5.77) EVs were measured per independent sample (Figure 15a). In all conditions, EVs appear to be roughly spherical and ranged in diameter from 67.9 to 95.0 nm. The morphology of EVs in the immediately processed and -80°C storage condition displayed a

prominent black ring indicating a bilayer structure whereas the other groups do not have as distinctive of a black ring (also described as a doughnut shape in the EV literature) [345, 346]. As shown in Figure 15b, significant size differences were noted between EVs isolated immediately and those isolated after storage at -20°C as well as between room temperature storage and -20°C storage condition groups. Similar to DLS data, EVs in the immediately processed group display a broader size range compared to other experimental groups. The TEM data suggests that storage of CM at -80°C may produce a more homogenous population of particle size compared to immediate processing.

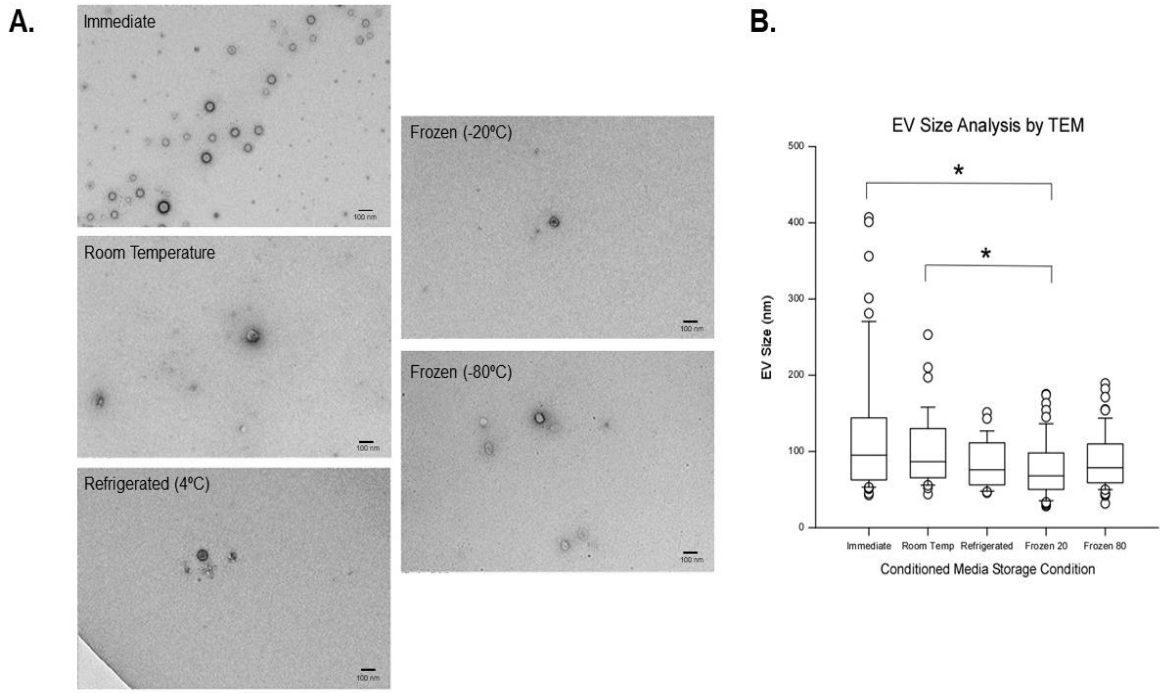

Figure 15: TEM Analysis of EVs

Transmission electron microscopy (TEM) analysis of extracellular vesicles (EVs) isolated immediately from human mesenchymal stromal cell (MSC) conditioned media (CM) and EVs from CM stored at either room temperature, 4°C, -20°C, and -80°C. (A) TEM micrographs depicting EVs from all experimental groups that are roughly spherical ranging in diameter from 67.9 – 95.0 nm. Note that the morphology of EVs in the immediate group are similar to those in the -80°C group with the distinct black ring (doughnut shape) indicating a bilayer structure. Calibration bar in micrographs is 100 nm. (B) TEM estimate of EV size. Significant differences were observed between EVs in the immediate group and -20°C ($P = 0.002$) and between EVs in the room temperature group and -20°C ($P = 0.045$). Data are presented as the median, 25th, and the 75th percentile in the box and whiskers show the 10th and 90th percentile. Potential outliers are depicted as open circles. Asterisk depicts significance (P-value < 0.05).

EV Characterization by Dot Blots

To assess protein staining, scorers rated the intensity of dot blots according to the scoring standard provided in Figure 16a. Following reconstitution of lyophilized samples, EVs were probed for expression of tetraspanins CD9, CD63, and CD81, as well as heat shock protein 70 (Hsp70) (Figure 16b). β-actin was used as a protein loading control and its expression was not scored. All storage conditions produced EV samples that had positive (defined as weak or strong staining) staining for at least three of the four characteristic markers but tended to vary in intensity. As shown in Figure 16c, significant differences were observed in dot blot score of EVs from the immediate group compared EVs isolated from CM stored at -80°C ($P = 0.005$). The median score for the immediate isolation group was 3.7 while the median score for the -80°C storage condition was 7.7. This result suggests that EVs isolated from CM stored at -80°C had higher intensity of staining for characteristic EV markers compared to EVs isolated immediately from CM. Specifically, the biggest expression difference was seen for Hsp70, as represented in Figure 16b. EVs isolated from CM stored at -80°C had a significantly higher average score for expression of Hsp70 compared to EVs isolated immediately from CM (1.4 vs. 0.467, respectively; $P = 0.023$).

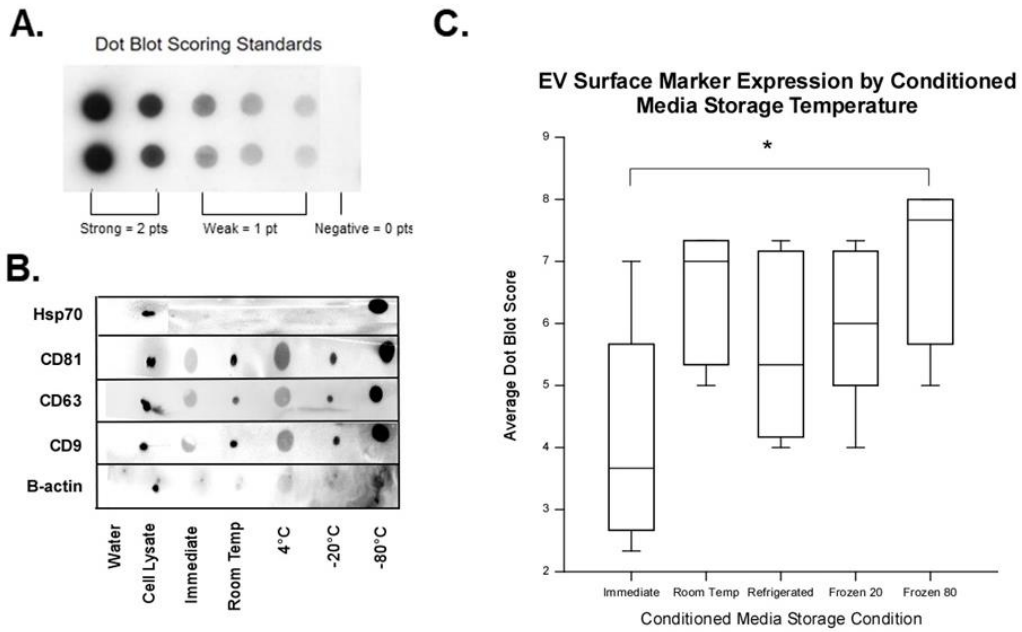

Figure 16: Effect of CM Storage Condition on EV Dot Blot Staining

(A) Dot blot scoring standard provided to independent, blinded scorers to assess the intensity of EV characterization marker staining. Strong positive staining was assigned 2 points, weak positive staining was assigned 1 point, and negative staining 0 points. (B) Representative dot blots showing the expression of tetraspanins: clusters of differentiation (CD)9, CD63, and CD81; heat shock protein (Hsp) 70; and protein loading control beta-actin (β-actin) by (left to right): water (negative control), whole MSC lysate (positive control), EVs isolated from CM of MSCs at storage conditions (immediate, room temperature, 4°C, -20°C, and -80°C). Note that while equal amounts of protein were blotted on the membrane, the -80°C storage condition had the strongest apparent staining. (C) Dot blot intensity scores were averaged from three blinded, independent scorers and summed for each MSC line in all experimental conditions for analysis. Dots were scored on an ordinal integer scale depicted in (A). Maximum score (strong positive for all markers) was 8.0. Expression of β-actin was not scored as it was a positive control marker. Significant differences were detected in dot blot scores of EVs from the immediate group compared to -80°C group ($P = 0.005$). This indicates that EVs from CM stored at -80°C has stronger expression of characteristic EV surface markers than EVs isolated immediately from CM. Data are presented as the median, 25th, and the 75th percentile in the box and whiskers show the 10th and 90th percentile. Potential outliers are depicted as open circles. Asterisk depicts significance (P-value < 0.05), n=5.

Analysis of EV-Associated miRNAs

To assess whether CM storage temperature has an effect on miRNA yield from EVs, we analyzed the yield of miRNA for five independent samples per storage condition. As shown in Figure 17, no significant differences were found (P = 0.07) but there was a trend for RNA from CM refrigerated at 4°C (18.3 µg/mL) to be different, or less than, other storage conditions. Yields from immediate (30.5 µg/mL), room temperature (25.7 µg/mL), -20°C (28.1 µg/mL), and -80°C (24.8 µg/mL) were consistent.

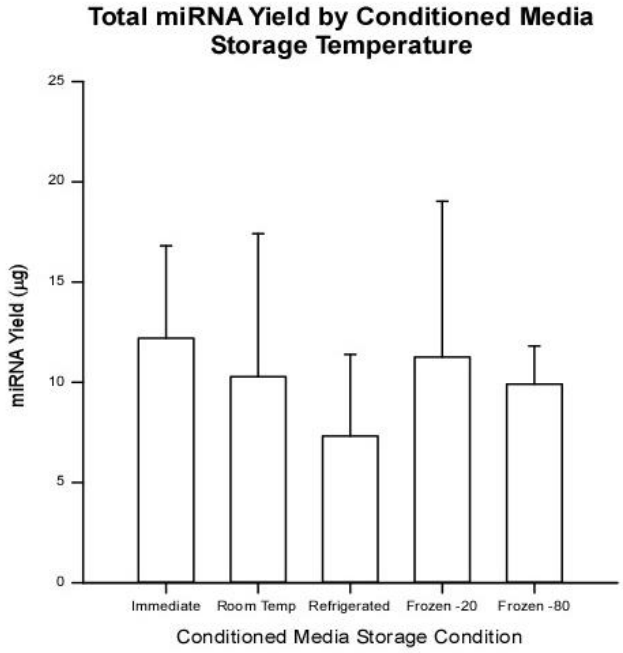

Figure 17: Total miRNA Yield from EVs

Total microRNA yield (µg/mL) from extracellular vesicles isolated from human umbilical cord-derived mesenchymal stromal cell conditioned media immediately or stored at room temperature, 4°C, -20°C, or -80°C. The trend was for RNA from CM stored at 4°C to have the smallest yield (18.3 µg/mL). Yields from immediate (30.5 µg/mL), room temperature (25.7 µg/mL), -20°C (28.1 µg/mL), and -80°C (24.8 µg/mL) were consistent. No significant differences were noted (p = 0.07). Data are presented as mean ± standard deviation, n = 5.

RT-PCR was performed and the results of four representative miRNAs are shown in Figure 18a (the remaining PCR results can be found in Appendix B, Supplementary Figure S8). Based on the PCR results, EVs contain miRNA for all miRNAs tested (miR-4466, miR-1273e, miR-4792, and miR-127, miR-658, miR-1246, miR-3665, miR-6089, and miR-7641). Figure 18b shows a heat map of miRNA results by storage condition with 5 being the maximum value and 0 being the minimum. Results for miR-1273e were consistent across all storage conditions. All samples except two had a positive result for miR-127. EVs from CM stored at -20°C displayed maximum scores (i.e., expression by all samples) for miR-127, miR-1246, and miR-3665 indicating that storage at -20°C did not affect expression of these miRs. EVs from CM stored at -80°C displayed maximum scores for miR-127 and miR-1246 indicating that storage at -80°C did not affect expression of these miRs. Results for miR-4792, miR-6089, and miR-7641 were the most inconsistent among all EV samples. In Figure 8c, mean scores were compared by storage condition for all miRNAs tested. No significant differences were found ($P = 0.846$). There was a trend for immediately-isolated EVs to score lower (5.2) compared to room temperature (6.0), 4°C (6.2), -20°C (7.0), and -80°C (6.4).

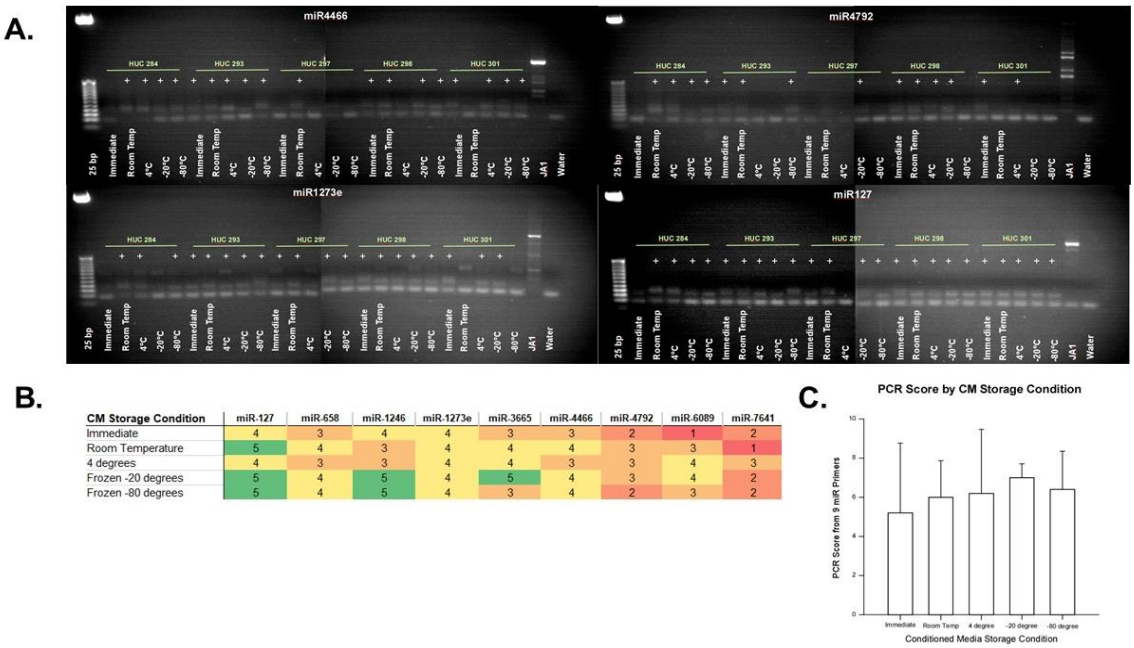

CM Storage Condition	miR-127	miR-658	miR-1246	miR-1273e	miR-3665	miR-4466	miR-4792	miR-6089	miR-7641
Immediate	4	3	4	4	3	3	2	1	2
Room Temperature	5	4	3	4	4	4	3	3	1
4 degrees	4	3	3	4	4	3	3	4	3
Frozen -20 degrees	5	4	5	4	5	4	3	4	2
Frozen -80 degrees	5	4	5	4	3	4	2	3	2

Figure 18: Effect of CM Storage Condition on miRNA Expression

Effect of storage condition on miRNA expression. No significant differences were detected (P = 0.846) between storage conditions. Analysis of extracellular vesicle (EV)-associated microRNAs (miRNAs) by real-time polymerase chain reaction (RT-PCR) for EVs isolated from human umbilical cord-derived mesenchymal stromal cells (UC-MSCs) conditioned media (CM) immediately or stored at room temperature, 4°C, -20°C, or -80°C. (A) RT-PCR analysis of MSC-associated EV miRNA. miR primers were designed using the NCBI GenBank data for human miR-127, miR-658, miR-1246, miR-1273e, miR-3665, miR-4466, miR-4792, miR-6089, and miR-7641 (see Table 4). There is evidence that EVs contain miRNA for all primers tested. Other PCR gels can be found in supplemental data (Appendix B, Supplementary Figure S8) (B) Heat map of PCR scores by CM storage condition. Individual samples were scored a 1 for positive expression or 0 for negative expression. Scores were added per miR for each storage condition for a maximum score of 5. Scores can range from 0 to 5 with green representing high scores and red depicting low scores. EVs in the -20°C had the most maximum scores followed by -80°C and then room temperature. Neither immediate nor 4°C had a maximum score. miR-1273e was consistent among all storage conditions. (C) Mean PCR scores for EVs by CM storage condition. There was a trend for immediately-isolated EVs to have a lower score (5.2) compared to room temperature (6.0), 4°C (6.2), -20°C (7.0), and -80°C (6.4). Data are presented as mean ± standard deviation, n = 5.

Discussion

Here, the effect of the storage of CM prior to EV isolation was analyzed. Four new findings encapsulate this work. First, CM storage conditions did not affect the number of EVs that were isolated from the five conditions tested. The five human MSC lines used in this work produced quite consistent numbers of EVs in the range of $1.0 – 3.0x10^4$ particles per cell over the 24-hour conditioning period. As expected with a small sample size, regression analysis did not detect any significant correlations between EV yield per MSC and a cell's passage or population doubling time. Second, PDI results revealed that storage of CM at -80°C produced in a more homogenous population of particles compared to immediate isolation, but did not affect the zeta potential or the hydrodynamic size. Third, TEM revealed that EVs isolated from CM stored at -80°C exhibited similar doughnut shape morphology to immediately isolated EVs. In contrast, the EVs detected in samples from CM stored at room temperature, 4°C, and -20°C did not show a clear doughnut shape, alluding to possible damage or degradation. Fourth, EVs from CM stored at -80°C displayed enhanced staining for CD9, CD63, CD81, and Hsp70 in protein blots compared to the other storage conditions. Again, suggesting preservation of the particles by the ultralow storage temperature prior to EV isolation. These findings were used to estimate an appropriate sample size required to answer related research questions in follow-up work. They suggest that as many as 30 samples are needed to find significant differences between storage conditions based upon the effect sizes reported here. Taken together, this work suggests that storage of CM prior to EV isolation may be important moving forward into scale up and clinical testing. For this initial work, storage of MSC-CM at -80°C for up to one month was optimal. These findings may apply to CMs from other cell

types or for biological fluids, and may be true for storage periods beyond one month, but further work will be needed to confirm.

In EV literature, there is no standard method for isolation, but ultracentrifugation and SEC are two common methods [347]. When selecting an isolation method available equipment, sample volume, and intended downstream use must be considered. Here, a combination of ultrafiltration and SEC was selected. SEC is advantageous compared to other methods, like ultracentrifugation, because it reduces protein contamination [135, 176, 208, 348]. In addition, it can be scaled up to accommodate large sample volumes (e.g., CM) and requires no special equipment aside from a standard benchtop centrifuge. Ultrafiltration allows for large volume samples to be concentrated and filtered, making downstream SEC separation more reasonable. In this work, ultrafiltration reduced CM sample volume by ~100x.

Little is known about the effects of storage temperature of CM and other biological fluids prior to EV isolation. Immediate isolation is the most common and was used as the standard for comparison here. Storage conditions of room temperature, 4°C, -20°C, and -80°C were selected based on a review of the existing literature. The goal was to test what we assumed to be common storage conditions. For example, in previous work by Zhou et al. and Romanov et al., CM storage temperatures 4°C, -20°C, and -80°C were tested [128, 338]. Romanov et al. also tested storage at -196°C but, with large CM volumes, this storage temperature was not feasible and thus it was not included in the experimental design [128]. We assumed that room temperature storage of CM would result in the degradation of EVs and thus this condition would serve as a negative control. In an unexpected result, storage of CM at room temperature for one week did not cause degradation of EVs. This finding was confirmed by NTA, DLS, TEM, PCR, and dot blot analysis.

NTA was used to estimate the concentration of particles and size distribution of the EV population. Sizes ranged from 85 nm to 106 nm among CM storage conditions, similar to previous reports of EVs from BM-MSCs [322]. The NTA estimates of the size of the EV population were in the desired range (30-150 nm) for EVs of interest (i.e., exosomes) for each storage condition [118, 120, 127, 130, 131, 133]. The results indicate that CM storage does not impact the size of the EV population isolated. Although a balanced experimental design was used to control for cell line-to-cell line variation, some experimental groups did show a high variance (e.g., immediate group was 25.5% of the sample mean) indicating that the data were more dispersed relative to the mean. Other experimental groups had a much lower standard deviation (e.g., 4°C standard deviation was 9.2% of the sample mean), indicating that the data was more clustered around the mean. Based upon the effect size seen here, a sample size of 20 would be required to detect significant differences.

Total particle counts ranged from $7.0x10^{10} \pm 3.1x10^{10}$ – $1.3x10^{11} \pm 8.3x10^{10}$ particles per sample. Similar particle counts were found among experimental groups, indicating that CM storage prior to EV isolation did not cause significant degradation. Likewise, Zhou et al. also found that storage of urine at -80°C allowed for a comparable number of exosomes to be recovered compared to fresh urine [338]. In addition, Romanov et al., also found that storage at 4°C for 1 week did not cause degradation of MVs isolated from CM [128]. In contrast, Romanov et al., reported that any freeze/thaw cycle, regardless of temperature, did cause significant degradation to MVs [128]. One explanation for this finding may be that because exosomes are the smallest of the extracellular vesicles, and thus, contain a smaller amount of liquid inside, their membrane is less susceptible to damage from freeze/thaw cycles. Taken together, our work and work by Zhou et al. supports this hypothesis [338]. MVs and ABs are much larger and, as a consequence, contain

more liquid. More liquid may possibly make the membranes more susceptible to damage from freeze/thaw regardless of the temperature, as demonstrated by Romanov et al. [128].

The largest source of experimental variability in both size and particle count estimates came from the NTA measurements themselves. High experimental variability makes it more difficult to detect a true difference when there is one. Here, samples were analyzed using 5 x 60 second videos to produce an average measurement, similar to previously reported [117]. Parsons et al., reported that increasing video replicates to 25 x 60 seconds reduced overall variance and increased precision of concentration estimates for particles between 50-120 nm from biological fluids [349]. Increasing the number of replicate videos captured used to calculate the sample concentration estimate may provide a more representative mean for samples and reduce experimental variation, thus making it easier to detect true differences in experimental groups without the need for large sample sizes.

EVs released per MSC was estimated using the previous PDT, time in culture prior to removal of serum-containing medium, and the NTA concentration data. For this calculation two assumptions were made. First, MSCs would continue to grow at the same rate exhibited in their prior passage. Second, expansion would stop after the removal of serum-containing medium. These assumptions are based upon experience and published work with these particular cell lines. First, human UC-MSCs isolation and culture conditions have been optimized so that they display consistent growth patterns [23, 279]. Lu et al. reported constant PDT for UC-MSCs from passage 1 to passage 10, which covers the range of passages studied in this work (P4 to P6) [30]. Second, serum or serum alternatives are required for expansion [350, 351]. Particles per cell was compared by both storage condition and individual line. No significant differences were noted. MSCs released an average of $2.2x10^4 \pm 8.5x10^3$ EVs per cell which is similar to previous reports from

BM-MSCs [322, 352]. In contrast, Crain et al. reported an average of $5.8x10^3 \pm 3.3x10^3$ EVs per MSC from canine UC-MSCs isolated via density gradient UC [197]. This disparity is likely due to species differences but may also be due to differences in EV isolation protocol. Our protocol utilized SEC isolation, Crain et al utilized density gradient UC [197]. Applying our EV isolation protocol to canine MSCs discussed in Chapter 2 would help elucidate if this disparity is largely from species differences or EV isolation protocol differences. Although line-to-line variation was accounted for in our experimental design, there was a trend for particles released per cell to be different among cell lines. MSCs used here were healthy (>95% viability), of similar passage (P4-P6), and grown in the same culture conditions. We offer no explanation for this other than biological variability. Differences among cell lines may be investigated in future work.

Regression analysis did not detect any significant correlations between EV yield per MSC and a cell's passage or population doubling time. This result is due in large part to the small sample size (n=5) in this work and also the small number of passages observed here (P4-P6). However, there was a trend for cell passage to be negatively correlated with EVs released per MSC. Thus, as a cell ages in culture less EVs are released. More work will need to be done with larger sample sizes and a broader passage range to confirm this finding. However, this is probable since aging cells are associated with cell senescence [322, 353-356]. Thus, senescent cells may release less EVs than healthy, proliferating cells. A second trend was noted when comparing EV yield per MSC by a cell's PDT. Cell's with a larger PDT (i.e., cells growing more slowly) tended to release more EVs per cell. Again, a larger sample size will be required to confirm this finding.

DLS was used to characterize the PDI, zeta surface potential, and hydrodynamic size of the EVs. In general, there was a trend for EVs isolated immediately to be different than EVs in the -80°C group in most DLS measurements. This was significant in the case of PDI. Mean PDI values

ranged from 0.34 to 0.64, similar to previously reported values [117]. PDI describes the non-uniformity of the size distribution in a given sample [357]. As discussed by Danaei et al., PDI is a dimensionless measure and values greater than 0.7 indicate that the sample has a wide size distribution, and is not considered to be ideal for analysis by DLS [357]. Although all storage conditions yielded EVs with PDIs less than 0.7, the immediate group had a PDI of 0.64 compared to EVs from the -80°C group (0.34). This indicates that storage of CM at -80°C produces a more uniformly-sized EV sample. This may occur as the freeze/thaw cycle damages larger vesicles in the population, thus supporting our previously discussed hypothesis. In addition, samples with a PDI larger than 0.7 are considered not ideal for DLS analysis. Immediately-isolated samples exhibited the highest PDI value (0.64) which is nearing the threshold. This presents a problem as DLS is regarded as a standard for EV characterization. A reduction in PDI values via storage of CM or other biological fluids may be necessary to achieve the size heterogeneity needed for DLS analysis.

Zeta potential is used as a measure of surface charge, colloidal stability, and integrity [352, 358]. EVs should carry a net negative surface charge under physiological conditions [358]. EVs in all experimental groups displayed a negative magnitude zeta potential similar to previous reports [117, 352, 359, 360]. Zeta potentials ranged from -7.73 ± 3.76 to -12.40 ± 2.50 mV. Although no significant differences were detected, the least negative zeta potential was exhibited in the immediate group (-7.73 ± 3.76 mV). This value could be due to the presence of charged molecules that increase the ionic strength and may lead to low dispersion stability and compromised biological function [193, 352]. Zeta potential values were similar to previously reported values [322, 352]. However, the zeta potential of EV samples were not as negative as others have reported [117, 358]. As discussed by Midekessa et al., zeta potential can be significantly impacted by the

buffer used for suspension, presence salts and detergents, and the pH of the sample [358]. Here, EVs were suspended in degassed, DPBS without calcium and magnesium. No detergent or additional salts were added. The pH of the samples was not recorded. All buffers used were held constant to allow for comparison of zeta potential as a result of CM storage condition. From this data, the trend was for EVs isolated immediately to be less stable than EVs from stored CM at all tested conditions.

Hydrodynamic size estimates measured via DLS were larger than sizes reported by NTA and TEM. Median size of EVs ranged between 165.6 ± 42.7 nm and 410.7 ± 262.9 nm, with no significant differences detected among storage groups. The largest median value was observed in the immediate group (410.7 nm), suggesting the presence of larger EVs (i.e., MVs and ABs). In contrast, the smallest median was observed in the -80°C experimental group (165.6 nm) suggesting minimal presence of larger EVs. This finding supports PDI differences previously discussed alluding to the reduction of large EVs from storage of CM at -80°C. EVs from room temperature and -80°C displayed a narrow size range compared to immediate, 4°C, and -20°C. The large size range noted in the immediate group and the narrow range in the -80°C group supports with the pattern in PDI values noted. Taken together, this data indicates that storage of CM at -80°C produces a more homogeneous sample by reducing larger EVs.

Using TEM analysis, EVs were detected in all experimental conditions. EVs have a roughly spherical appearance and ranged in diameter from 67.9 to 95.0 nm. TEM size estimates were similar to both NTA size estimates and previously reported values [117]. In TEM micrographs, only EVs in the immediate and -80°C experimental groups display a prominent black ring (doughnut shape) around the white center of the EV, indicative of a bilayer structure, similar to morphology reported by others [345, 346]. Despite the absence of the prominent doughnut shape,

EVs were detected in CM stored at room temperature, 4°C, and -20°C demonstrating that none of the CM storage conditions tested here caused significant degradation of EVs. Similar to DLS data, a broad size range was observed in the immediate group. This finding supports the presence of larger EVs in the immediate population. EVs from CM stored at 4°C, -20°C, and -80°C exhibited a narrow size range, suggesting less larger vesicles in the population. These findings further support our hypothesis that larger vesicles are destroyed via freeze/thaw due to the susceptibility of their membranes. Taken together, because of the narrow size range and morphology most similar to the immediate group, storage at -80°C is the optimal CM storage temperature.

Protein staining was assessed using dot blots for tetraspanins (CD9, CD63, and CD81) as well as Hsp70. EV samples had low protein concentrations (average 5.84 μg/mL) and this required a large volume to be loaded onto the PVDF membrane for probing. This led to issues with the sample drying on the membrane, samples bleeding into one another, and a lack of distinct dots for a signal. To avoid this, EV samples were lyophilized prior to probing similar to previously reported methods [343]. Lyophilization involves the removal of water from frozen samples by sublimation and desorption under a vacuum and is considered to be the most reliable method to preserve EVs [343, 361-364]. Using lyophilization, EV samples were concentrated 5x. This allowed for dots to be in the desired range of 5-20 μL per dot.

All storage conditions were capable of producing EVs that that stained for at least three of the four markers tested here, but varied in intensity of expression. After quantifying protein expression intensity, significant differences were observed in EVs isolated immediately compared to those from CM stored -80°C. On a scale of 0-8, EVs isolated immediately had a median score of 3.67 compared to a median of 7.67 for EVs in the -80°C experimental group. The difference in scores is due in large part to the difference in Hsp70 expression between the two groups. EVs in

the -80°C experimental group had an average Hsp70 score of 1.4 (a score of 1.0 denotes weak, positive expression) while EVs in the immediate group had a mean score of 0.47. This indicates that storage of CM at -80°C allows EVs isolated to retain expression of Hsp70. In contrast, Lee et al., found that storage of isolated EVs from HEK 293 CM at room temperature caused the loss of Hsp70 expression [183]. Taken together, overall higher protein expression of EV markers, specifically Hsp70, indicates that storage of CM at -80°C is the ideal storage condition.

The current recommendation by ISEV is that EVs should be stored in phosphate-buffered saline at -80°C in siliconized vessels but no recommendation is made concerning the use of cryoprotectants [137, 232, 233]. In the literature, EVs are commonly stored at -80°C with varying use of cryoprotectants [336, 337, 343]. Several cryoprotectants have been reported and disaccharides (e.g., trehalose) have been shown to be safe and effective for EVs, cells, and proteins [336, 343, 364-368]. Cryoprotectants were not added to samples prior to freezing the EV aliquots at -80ºC [362, 365]. Although the focus of this study was to examine the effects of CM storage on EV isolation, the lack of cryoprotectants is a limitation of this work and should be considered for future studies. Collectively, our results indicate that EVs were stable and did not suffer significant degradation after being stored at -80ºC for up to six months. Others have also reported similar stability or do not disclose the use of cryoprotectants [183, 233, 337]. In contrast, some studies have reported changes in morphology, biological activity, and RNA concentration [339, 343, 369, 370]. For future studies, specifically where the downstream use of EVs is greater than six months, use of a cryoprotectant will be considered.

In summary, this work investigates the method of CM storage for downstream EV isolation based upon the hypothesis that CM used for isolation of EVs, like other cells and cell-derived products, may be impacted by storage condition and temperature. This report found that although

all experimental storage conditions produced EVs, storage at -80°C is the ideal storage temperature for human UC-MSC CM. A comparable number of EVs were recovered from CM stored at -80°C compared to fresh CM. In addition, compared to fresh CM EVs, -80°C EVs were of comparable size, had a more homogeneous population, comparable surface potential, shared a similar morphology with a distinctive bilayer structure, and had an overall higher protein expression of characteristic EV markers (CD9, CD63, CD81, and Hsp70). While significant findings are reported here, further work remains to test whether these similar characteristics translate to functionality of EVs. The knowledge gap in the storage of CM and other biological fluids prior to EV isolation should be closed in order to maximize utility for clinical and diagnostic translation.

Chapter 4 - Procoagulant Activity of Canine MSC-EVs

Introduction

Mesenchymal stromal cells (MSCs) have been implicated as a potential therapeutic modality in ailments such as Crohn's and Graft versus Host disease, because of their ability to regenerate and create a variable, localized anti-inflammatory effect [44-49]. Although once believed to act through engraftment and differentiation post-implantation, it is now known that MSCs exert their therapeutic benefit in large part via paracrine effect, i.e., the production and secretion of soluble factors and extracellular vesicles (EVs) [119-121, 132].

EVs are nanoparticles with a phospholipid bilayer membrane released by many cell types, including MSCs [117, 123, 124, 131, 333]. EVs are grouped by their size and mechanism of cellular release into three subpopulations: microvesicles, apoptotic bodies, and exosomes [120, 126]. Exosomes, the particular EV of interest here, range in diameter from 30 to 150 nm and are released from the fusion of multivesicular bodies with the plasma membrane [131]. EVs have been shown to have a role in intercellular communication and signaling as well as antigen presentation, cell adhesion, inflammation, tissue remodeling, and function as biological disease markers [117, 323-328]. In addition, EVs have been shown to retain artifacts of the parental cell type, such as cargo and surface marker expression [129, 135].

Tissue factor (TF), also known as CD142 or coagulation factor III, can be found expressed by many extravascular cells and circulating in the blood in a non-cell associated soluble form [253-256]. TF functions in the body to provide supplementary protection to organs that are susceptible to mechanical injury, as well as to activate the extrinsic arm of the coagulation cascade

through binding of its extracellular domain to factor VII and factor VIIa, creating a TF-FVIIa covalent complex [253, 254]. Once the TF-FVIIa complex forms, it triggers the extrinsic pathway of the coagulation cascade, factors IX and X of the intrinsic and common pathways are activated, and this leads to the generation of a clot via thrombin, platelet activation, and fibrin deposition [253, 254, 257].

MSCs from various tissue sources have been shown to highly express TF on their surfaces and to exhibit procoagulant activity [53, 58, 247, 260-262]. Oeller et al. demonstrated that MSCs derived from both the umbilical cord (UC-MSCs) and adipose tissue (AT-MSCs) exhibit higher TF expression when compared to MSCs derived from bone marrow (BM-MSCs) and that TF expression could be altered through cell culture medium supplementation [260]. Similarly, Christy et al. reported that AT-MSCs expressed higher levels of TF than BM-MSCs and that the percentage of TF-positive AT-MSCs declined over time in culture starting at approximately 20 population doublings while the percentage of TF-positive BM-MSCs had no clear expansion-related pattern [53].

In addition to exhibiting TF expression, MSCs have also been shown to be functionally procoagulant when exposed to blood or plasma and that activity is due to TF expression [53, 244, 260, 261]. Christy et al. demonstrated that the percentage of TF-positive MSCs in a given population roughly correlates with the functional procoagulant activity [53]. Work by George et al. demonstrated that the procoagulant activity is at least partially dependent on TF expression since incubation with a TF neutralizing antibody (clone TF8-5G9) caused loss of functional procoagulant activity [261]. In mice, Tatsumi et al. showed that intravenous administration of AT-MSCs resulted in ~85% mortality within 24 hours due to the formation of a pulmonary embolism

[244]. In addition, procoagulant activity of mouse MSCs could be inhibited using an anti-TF antibody or using factor VII-deficient plasma [244].

As a therapeutic, MSCs have limitations such as limited in vivo survival and risk of thrombosis or embolism once infused intravenously. Because of this, EVs isolated from MSC conditioned medium (CM) represent an attractive cell-free alternative as some researchers consider EVs to be immunologically inert [135, 264, 265]. However, TF-exposing EVs have been noted in the blood, urine, and saliva [266]. Several cell types have been shown to release TF-exposing EVs including activated monocytes, endothelial, and many cancer types [266-268]. Increased numbers of EVs, and particularly TF-positive EVs, have been noted in patients with cancer, endotoxemia, and atrial fibrillation [269, 270]. In addition, EVs derived from multiple tumor types have been shown to also have procoagulant activity [271-275]. However, nothing is known regarding EVs derived from MSCs.

Because of the gaps in our understanding of MSC therapy, questions remain centered around the overall safety of MSCs, and this includes MSC-based products like EVs. Additionally, as EVs gain popularity as a potential therapeutic agent, the effects of manufacturing on their properties and characteristics, like procoagulant activity, must be elucidated. Given that EVs share many cell surface proteins with that of their parental cells and that MSCs highly express TF, we hypothesized that EVs derived from MSCs also express TF and harbor procoagulant activity as a result of TF expression. Our hypothesis was further supported by the fact that TF-positive EVs have been found secreted by other cell types and those EVs have been shown to be functionally procoagulant. This is particularly concerning as both MSCs and MSC-derived EVs are currently being explored as an experimental therapeutic modality in coronavirus (COVID-19) [47, 371-374].

Here, we outline the effects of both cell passage and isolation method on EVs derived from canine MSCs. Our data suggests that both parameters are important considerations for EV manufacturing scale-up and clinical translation. In addition, we demonstrate that EVs derived from MSCs express TF and possess TF-mediated procoagulant activity. Because of this work, we believe that EV administration is a safety concern and poses a risk of thromboembolism. We suggest that the procoagulant activity of EVs may serve as a screening tool in clinical settings and may be targeted for reduction to increase patient safety.

Materials and Methods

Experimental Design

Design of experiments (DOE) was utilized to plan experimental setup prior to beginning research. As shown in Figure 19, the experimental design was organized as an 8x2 factorial with factor A being passage with 8 levels (P2, P3, P4, P5, P9, P10, P11, P12) and factor B being EV isolation method with 2 levels (ultracentrifugation, UC; size-exclusion chromatography, SEC). The experimental design was balanced to ensure that there were an equal number of observations for all combinations. This was done to minimize the impact of line-to-line variation on the interpretation of results. Three independent replicate lines were randomly assigned to each isolation method. Passages 2-5 were grouped and considered as early passage. Passages 9-12 were grouped and considered as late passage. Middle passages (P6-P8) were collected and stored but excluded from testing.

ISOLATION	CELL PASSAGE							
	EARLY P2	*EARLY P3*	*EARLY P4*	*EARLY P5*	*LATE P9*	*LATE P10*	*LATE P11*	*LATE P12*
UC	CUC 23 CUC 28 CUC 30	CUC 23 CUC 28 CUC 30	CUC 23 CUC 28 CUC 30	CUC 23 CUC 28 CUC 30	CUC 23 CUC 28 CUC 30	CUC 23 CUC 28 CUC 30	CUC 23 CUC 28 CUC 30	CUC 23 CUC 28 CUC 30
SEC	CUC 20 CUC 21 CUC 27	CUC 20 CUC 21 CUC 27	CUC 20 CUC 21 CUC 27	CUC 20 CUC 21 CUC 27	CUC 20 CUC 21 CUC 27	CUC 20 CUC 21 CUC 27	CUC 20 CUC 21 CUC 27	CUC 20 CUC 21 CUC 27

Figure 19: Experimental Design

Experimental design of 8x2 factorial. Factor A was passage with 8 levels: P2, P3, P4, P5, P9, P10, P11, and P12. Factor B was isolation method with 2 levels: ultracentrifugation (UC) and size-exclusion chromatography (SEC). Six canine umbilical cord-derived mesenchymal stromal cell (CUC) lines were randomly selected and randomly assigned an isolation method. Individual lines are listed for reference. Conditioned medium (CM) was collected at each passage so that three replicates were collected at each combination of factors. CM from passages 6-8 were collected and stored but excluded from this analysis.

Preparation of Conditioned Media from Canine UC-MSCs

This research used canine umbilical cords and the research protocol was reviewed and approved by the Kansas State University Institutional Animal Care and Use Committee (IACUC). The protocol was deemed an "exempt animal use activity" under guideline #21 exemption policy 2.3 stating, "… studies that do not use live animal provided that tissue is obtained from an IACUC-approved source and is discarded in accordance with all relevant state laws and institutional policies governing disposal of hazardous waste."

Canine umbilical cord-derived mesenchymal stromal cells (UC-MSCs) were isolated, culture-expanded, characterized, and cryopreserved using the protocol described in Chapter 2 [12]. As shown in the experimental schematic in Figure 20, cryopreserved canine UC-MSCs (P1) were

thawed and seeded at a density of $2x10^4$ cells/cm^2 on gelatin-coated tissue culture vessels. Canine UC-MSCs were allowed to recover from cryopreservation for one passage prior to use. Canine UC-MSCs were maintained in culture according to previously described methods using ACB cell culture medium and incubated at 37°C, 90% humidity, 5% CO2 in a HeraCell 150i incubator [12]. Once cells reached ~80-90% confluency, cells were lifted using 1.75% nattokinase for 30 minutes at 37°C [12]. A live/dead cell count was performed at passage using acridine orange/propidium iodide (AOPI) staining solution (Nexcelom Bioscience, Cat. No., CS2-0106-5ML) on a Nexcelom Auto 2000 Cellometer (immune cells, low RBC program, Nexcelom Biosciences, Lawrence, MA). MSCs were seeded at a density of $2x10^4$ cells/cm^2 on two gelatin-coated flasks (i.e., one flask to maintain the cell line and one flask for production of CM). Canine UC-MSCs were maintained in culture through P12 and CM was collected at each passage from P2-P12. To collect CM, the standard cell culture medium was replaced with 30 mL of high glucose Dulbecco's Modified Eagle Medium (DMEM, 0.33 mL/cm^2, Gibco, Cat. No., 11965092) without fetal bovine serum (FBS) or other supplements when cells reached 60-70% confluence. After 24 hours, medium was collected and stored at -80ºC until thawing for isolation of EVs. To control the consistency of EVs, cell lines must have viability ≥95% at every passage.

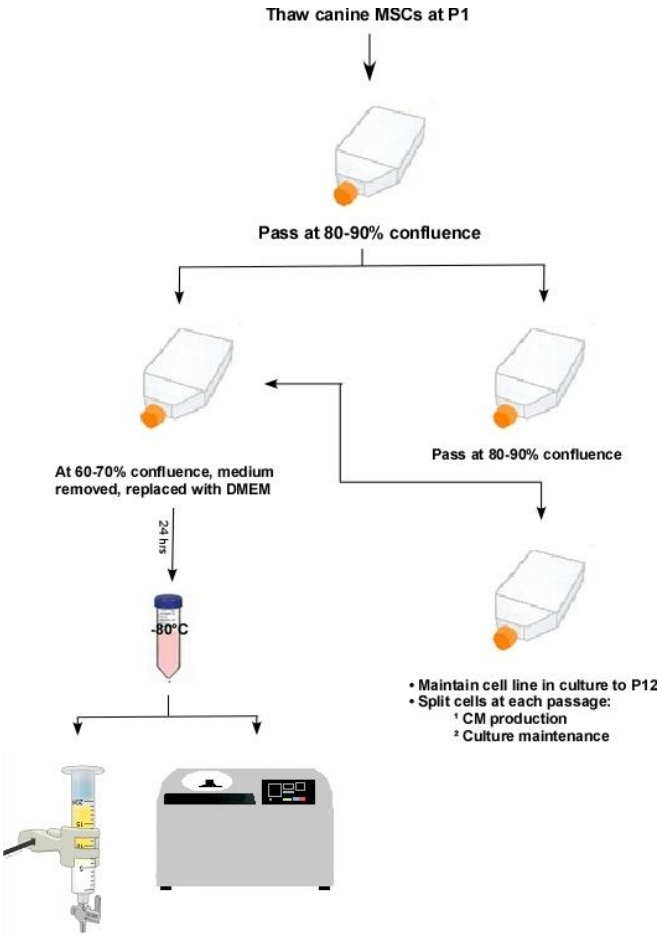

Figure 20: Experimental Schematic

Experimental schematic demonstrating production of extracellular vesicles (EVs). Canine umbilical cord-derived mesenchymal stromal cells (MSCs) were thawed at passage 1 (P1) and plated at a density of $2x10^4$ cells/cm^2 on gelatin-coated T-150 flasks and maintained in culture at 37°C, 90% humidity, 5% CO2 as previously described [12]. Once cells reached 80-90% confluence, MSCs were lifted with 1.75% nattokinase and plated in two T-150 flasks. Flask (1) was used for production of conditioned medium (CM) (left side). Once MSCs reached 60-70% confluence, cell culture medium was removed and replaced with warm DMEM. After 24 hours, the medium was considered conditioned and collected in a 50mL centrifuge tube. The CM was stored at -80°C until isolation via size-exclusion chromatography (SEC) or ultracentrifugation (UC). Flask (2) was used to maintain MSC line in culture (right side). Once MSCs reached 80-90% confluence, cells were passed and split into two flasks as previously done. Cells were maintained in culture from P2 to P12. CM was collected at every passage.

Preparation of Size-Exclusion Chromatography Column

A size-exclusion chromatography (SEC) column was prepared as previously described in Chapter 3 using Sepharose CL-2B (GE Healthcare, Cat. No. 65099-79-8) [200]. Briefly, the tip of a 20 mL sterile syringe (EXELINT, Cat. No. 26280) was stuffed with cotton wool and 20mL of Sepharose CL-2B slurry was poured into the syringe. The column was allowed to settle overnight at 4°C. After settling, the dimensions were 7.5 cm (length) x 2.21 cm (diameter). Next, the column was packed by passing three volumes of sterile, degassed Dulbecco's phosphate-buffered saline (DPBS, Gibco, Cat. No. 14-190-250) through at a rate controlled by gravity. The void volume and column packing and separation efficiency were determined by passing a solution containing 0.25 mL of both blue dextran solution (Sigma Aldrich, Cat. No. D5751) and bovine serum albumin (BSA, Sigma Aldrich, Cat. No. A3912-500G) through the column. Fractions of 0.25 mL were collected following the void volume up until those containing BSA (identified by protein concentration).

EV Isolation by a Combination of Ultrafiltration and SEC

EVs were isolated from CM using a combination of ultrafiltration (UF) and SEC as previously described in Chapter 3. Briefly, CM was thawed from -80°C at room temperature and centrifuged at 3200 g for 30 minutes at 4°C (Eppendorf 5810R centrifuge, swing bucket rotor A-4-62, Cat. No., FL08517291) to pellet cells and cell debris. Supernatant was filtered through a 0.22 µm syringe filter (Fisherbrand, Cat. No. 09-720-004) and then concentrated by approximately 100x using an Amicon Ultra-15 filter unit with an Ultracel-100 membrane (MWCO = 100 kDa, Merck Millipore, Cat. No. UFC910024). The sample was centrifuged at 3200 g at 4°C until the sample volume was ≤ 300 µL, and that sample was collected in a separate microcentrifuge tube.

The membrane was jetted with 200 µL DPBS and any adherent EVs were collected from the membrane and added to the sample tube.

The concentrated sample was layered onto the SEC column and was eluted with sterile, degassed DPBS. Following the void volume, 27 fractions of 250 µL were collected. Aliquots were sampled to estimate protein concentration using a NanoDrop 8000 spectrophotometer (1.5 µL per reading, samples measured in technical triplicates, Thermo Scientific, Waltham, MA). The EV-containing fractions were pooled, divided into 1 mL aliquots in polypropylene microcentrifuge tubes, and stored at -80°C until analysis.

EV Isolation by Ultracentrifugation

EVs were isolated from CM by ultracentrifugation using a previously described method with slight modifications [117, 375]. Briefly, CM was thawed from -80°C at room temperature and centrifuged at 3200 g for 30 minutes at 4°C to pellet cells and cell debris. Supernatant was collected, filtered through a 0.22 µm syringe filter, and transferred to a 38.5 mL open-top polypropylene tube (Beckman Coulter, Cat. No., 326823). CM was centrifuged at 20,000 *g* for 30 minutes at 4°C (SorvallTM wX+ Ultra Series Centrifuge, Thermo Fisher Scientific) with a SureSpin 630/36 rotor (Thermo Scientific, Cat. No., 79368). Following the first spin, CM was transferred to a new polypropylene tube and centrifuged at 120,000 *g* for 90 minutes at 4°C. The resulting pellet was suspended in 6 mL of DPBS, vortexed, divided into 1 mL aliquots, and stored at -80°C until analysis.

Lyophilization of EVs

EV Samples were freeze-dried as previously described in Chapter 3. Briefly, equal aliquots of samples were removed from -80°C and loaded into a TF-10A 1.2-liter vacuum freeze dryer (TEFIC BIOTECH CO., LIMITED, Xi`an, China). Samples were lyophilized in batches of six overnight for 16-18 hours. Following lyophilization, samples were stored at room temperature with parafilm to protect from moisture. Immediately before use, aliquots were rehydrated with sterile UltraPure distilled water (Invitrogen, Cat. No., 10977) to 10% of their original volume and briefly vortexed. Protein concentration of the reconstituted samples was measured using absorbance at 280 nm with a spectrophotometer and samples were analyzed via transmission electron microscopy and dot blots.

Nanoparticle Tracking Analysis

Nanoparticle tracking analysis (NTA) was used to estimate the EV population size distribution and concentration using a NanoSight LM-10 (Malvern Pananalytical Ltd., Malvern, UK) as previously described in Chapter 3. Briefly, the machine was calibrated using 50 nm and 100 nm size calibrated standards (Malvern Pananalytical Ltd., Cat. Nos., NTA4087 and NTA4088, respectively). Measurements were made at a constant temperature of 25°C ± 1°C to ensure constant viscosity of samples. Sterile DPBS was used as a negative control. Samples were unfiltered. Sample dilutions ranged from 1:5 to 1:100 in NanoPure water (Barnstead/Thermolyne Nanopure lab water system) so that samples were in the desired ranged of 30-50 particles/frame. Acquisition settings were held constant and were as follows blue 405 nm laser, camera type scientific CMOS, camera level 13, and detection threshold 3. Nanosight software (NTA 3.3) was used to analyze 60-second videos with 5 repetitions per sample. The concentration measurement reported was made

from the 5 technical replicates and averaged for comparison via two-way repeated measures analysis of variance (ANOVA) with factors being passage (P2-P5; P9-P12) and isolation (UC and SEC). Following significant ANOVA main effects or interactions, planned pairwise comparisons were made using Holm-Sidak method. Six independent cell lines were analyzed. To compare passage group as a whole, cell passages were grouped by early (P2-P5) and late (P9-P12) for comparison via Mann-Whitney rank sum test with Yates continuity. The size measurement was made from the 5 technical replicates and averaged for comparison via Mann-Whitney rank sum test.

Using NTA concentration data, EVs released per cell was calculated as previously described in Chapter 3. Briefly, population doubling time (PDT) was calculated for each cell line at each passage. An estimate of the number of adherent cells was calculated using the PDT and the number of hours that the cells have been in culture prior to removal of serum-containing media. The average expansion data for each of the six cell lines is shown in Table 7. The assumption was made that when cell culture media was removed, cell proliferation ceased. The EVs released per cell was estimated as the total particles in the sample divided by the estimate of cells in culture at the time of media removal. EVs released per cell was averaged by passage for six independent lines and compared using repeated measures ANOVA on ranks. To assess correlation, linear regression analysis was performed with particles per cell as the dependent variable and cumulative population doublings as the independent variable. A second linear regression analysis was performed with particles per cell as the dependent variable and population doubling time as the independent variable.

Table 7: Calculation of Viable Cell Number for Canine MSCs

Passage	*Mean Previous Passage PDT (hours)*	*Mean Time in Culture (hours)*	*Cells Seeded*	*Mean Population Doublings*	*Mean Estimated Cell Count*
2	94.9	115.7	300,000	2.06	$4.59x10^6$
3	74.7	124.3	300,000	2.19	$4.79x10^6$
4	70.5	120.7	300,000	1.98	$4.47x10^6$
5	50.7	110.2	300,000	2.09	$4.64x10^6$
9	46.4	102.7	300,000	2.26	$4.89x10^6$
10	39.7	77.0	300,000	2.07	$4.61x10^6$
11	46.9	82.2	300,000	1.94	$4.41x10^6$
12	71.7	79.3	300,000	1.66	$3.99x10^6$

Dynamic Light Scattering

DLS, zeta surface potential, and polydispersity index (PDI) were used to analyze the hydrodynamic size distribution, surface charge properties, membrane integrity, and overall stability of the EVs as previously described in Chapter 3 [117]. Measurements were made using the Zetasizer Nano ZS (Malvern Pananalytical., Malvern, United Kingdom). Instrument settings were 10 runs of 10 seconds with 3 repetitions per sample. Six independent samples from each passage were analyzed. Measurements were made in technical triplicates and averaged for comparison. PDI and zeta surface potential were compared using two-way repeated measures ANOVA with factors being isolation and passage. After significant ANOVA main or interaction

terms were found, pre-planned pairwise comparisons were performed using Holm-Sidak method. DLS size was compared using Mann-Whitney rank sum test.

Transmission Electron Microscopy

Transmission electron microscopy (TEM) was performed to visualize EV morphology and to generate an estimate of EV size as previously described in Chapter 3. Lyophilized samples were rehydrated using sterile, distilled water. Masked samples were prepared and analyzed by the University of Kansas Medical Center. An approximate area of 62.1 μm^2 was sampled and a minimum of 18 micrographs were collected per sample. EV size was estimated by measuring data from two independent lines chosen at random at each isolation x passage group (i.e., early and late). Extreme ends of the passage groups were selected (P2 and P12) since we assumed those to show the greatest differences. From this data, sizes were averaged by both isolation method and passage group to generate size measurements to be compared using Mann-Whitney rank sum test.

Determination of Protein Concentration

The protein concentration of samples isolated by UC was determined using a Pierce BCA protein assay kit (Thermo Scientific, Cat. No. 23225) according to the manufacturer's instructions. The protein concentration of samples isolated by SEC was determined using a Pierce micro BCA protein assay kit (Thermo Scientific, Cat. No. 23235) as previously described in Chapter 3. Samples were plated in triplicate in a 96-well plate (Corning, Cat. No. 3370). Protein standard curves were generated using albumin standards provided with each respective kit and by averaging the technical triplicate wells. The absorbance was read at 562 nm using a SpectraMax i3x plate reader (Molecular Devices, San Jose, CA) according to manufacturer's instructions. DPBS was

used as a blank for background subtraction. Individual sample protein measurements were made from the average of triplicate readings. Protein concentration was averaged among isolation methods and compared using Mann-Whitney rank sum test.

Protein content was measured post-lyophilization by measuring the absorbance at 280 nm on a NanoDrop 8000 spectrophotometer with distilled water as the blank for background subtraction. Post-lyophilization content for each individual sample was calculated as the average of triplicate readings.

As an estimate of purity of the samples, EV particle count per µg of sample protein was calculated as previously described [347]. Briefly, the particle count per mL of sample as determined by NTA was divided by the protein concentration (µg/mL) as determined by BCA assay to give a particle number isolated per µg of protein. Measurements from six independent lines at eight passages were averaged by isolation method and compared using Mann-Whitney rank sum test with Yates continuity correction.

Immunocytochemistry

To detect surface expression of tissue factor (CD142), human and canine UC-MSCs were grown in culture until 80-90% confluent. Once confluent, cell culture medium was removed and cells were washed with sterile DPBS with calcium and magnesium (Gibco, Cat. No., 14040-133). The cells were fixed with freshly prepared 4% paraformaldehyde in 10 mM phosphate buffer (pH 7.4) for 30 minutes at room temperature. Following the incubation period, cells were washed three times with DPBS. MSCs were blocked with DPBS plus 0.2% gelatin, 1% horse serum, and 1% goat serum. MSCs were incubated with primary antibody CD142 (Table 8, 1:200 dilution) overnight at 4°C. The following morning, cells were triple washed with DPBS and stained with

secondary antibody goat anti-rabbit IgG Alexa Fluor 488 (1:200 dilution, Life Technologies, Cat. No., A-11008) for three hours at 4°C protected from light. Cells were triple washed and DNA was stained with 4',6-diamidino-2-phenylindole (DAPI, 1 µg/mL, Sigma Aldrich, Cat. No., D9542) for 15 minutes at room temperature and rinsed with DPBS. Detergents were not used to minimize any positive cytoplasm signal. Human UC-MSCs served as the positive control. Human and canine MSCs incubated with secondary antibody only served as negative controls. Following incubation, fluorescent images were captured using an EVOS FL Auto imaging system (Life Technologies).

Protein Expression by Dot Blots

A polyvinylidene fluoride (PVDF) membrane (Merck Millipore Ltd., Cat. No. IPVH0010) was activated by submerging in methanol for 30 minutes. Lyophilized EV samples were rehydrated using 100 µL sterile water. Post-lyophilization protein content was measured as described above, and 0.75 µg of protein was loaded onto the membrane and air-dried. Water and canine MSC whole cell lysate were used as negative and positive controls, respectively. The membrane was blocked with 5% non-fat dried milk solution for 30 minutes at room temperature with gentle rocking. The membrane was probed with primary antibodies anti-CD9, anti-CD63, anti-CD81, anti-ALIX, anti-CD142, and anti-β-actin (Table 7) overnight at 4°C with gentle rocking. The following morning, membranes were washed three times using TBST buffer (tris-buffered saline with 0.1% Tween-20 detergent) and incubated with secondary antibodies (see Table 7) for one hour at room temperature with gentle rocking. Post-incubation, strips were washed three times with TBST buffer. Chemiluminescence detection reactions were performed using SuperSignal West Femto substrate (Thermo Scientific, Cat. No., 34095) according to manufacturer's directions. Images were captured using a Kodak Image Station 4000 after 2

minutes of exposure. Each sample was blotted for 5 proteins: CD9, CD63, CD81, ALIX, and TF. For each sample, a positive result was given a score of 1 and negative expression was assigned a score of 0. Total scores and scores for individual markers were analyzed using Mann-Whitney rank sum test.

Table 8: Antibodies Used for Dot Blots

Antibody	*Clone*	*Manufacturer*	*Catalog Number*	*Dilution*
CD9	HI9a	BioLegend	312102	1:400
CD63	H5C6	Novus Biologicals	NBP2-42225	1:500
CD81	1D6	Novus Biologicals	NB100-65805	1:500
ALIX	3A9	Santa Cruz Biotechnology	Sc-53538	1:200
CD142	Polyclonal	Bioss Antibodies	BS-4690R	1:300
B-actin	2F1-1	BioLegend	643801	1:500
HRP donkey anti-rabbit IgG	Polyclonal	BioLegend	406401	1:1000
HRP goat anti-mouse IgG	Polyclonal	BioLegend	405306	1:2000

Procoagulant Assay

The procoagulant activity of EVs isolated from canine UC-MSCs CM was assessed using a protocol proposed by Che et al. with modifications [274]. $5x10^7$ EVs per well were diluted in HEPES buffer (10 mM HEPES, 137 mM sodium chloride, 5 mM calcium chloride, 4 mM

potassium chloride, 10 mM glucose, 0.5% bovine serum albumin, pH 7.4) to a final volume of 50 µL. Diluted EVs were incubated with 1 nM FVIIa (Haematologic Technologies, Cat. No., HCVIIA-0031) and 10 µg/mL FX (Haematologic Technologies, Cat. No., HCX-0050) for 15 minutes at 37°C. Following incubation, a chromogenic substrate for FXa activity (40 µM, Chromogenix S-2765, Diapharma, Cat. No., S821413) was added and the color change was measured at 405 nm every minute for 20 minutes using a SpectraMax i3x plate reader. The amount of FXa generated was calculated based on a standard curve of purified FXa (Haematologic Technologies, Cat. No., HCXA-0060). All samples were loaded into a 96-well plate in technical triplicates and the absorbance readings were averaged. HEPES buffer served as a blank for background subtraction. To account for TF-independent FXa generation, control wells (EVs and FX only) were subtracted. MSC whole cell lysate and FX with FVIIa only served as positive and negative controls, respectively. To test TF-mediated FXa generation, EVs were incubated with anti-CD142 (Invitrogen clone HTF-1, functional grade, Cat. No., 16-1429-82 or Bioss polyclonal, Cat. No., BS-4690R) for 1 hour at 4°C prior to incubation with FVIIa and FX. Six independent cell lines were analyzed at both early (P2) and late (P12) passage.

To calculate procoagulant activity, the amount of FXa generated as determined from the standard curve was divided by the reaction volume in the well according to the formula below:

$$Procoagulant\ FXa\ Activity = \frac{FXa\ generated\ (ng)}{Volume\ in\ each\ well\ (mL)}$$

From the procoagulant activity calculation, the concentration of FXa (in nM) was reported by dividing the activity by the molecular weight (46 kDa) of FXa. FXa generation per $1x10^6$ EVs was calculated as the FXa generation (in nM) divided by millions of EVs present in the reaction well.

From the activity data, readings were averaged by passage and isolation method for comparison by Student's t test.

Statistics

ANOVA was used to evaluate main effects and/or interactions after first checking whether the ANOVA assumptions were met. After finding significant ANOVA term(s), post hoc testing of pre-planned comparisons was conducted using either the Bonferroni or Holm-Sidak method. Those data are presented as mean ± one standard deviation. If ANOVA assumptions were not met, Kruskal-Wallis ANOVA on ranks was used. Data from these tests are presented as a box and whisker plot. The box represents the median, 25th, and 75th percentile while the whiskers show the 10th and 90th percentile. Any potential outliers are shown as open circles. For pairwise comparisons, statistical assumptions were confirmed, and data was analyzed using Student's t test. Hypothesis testing was performed as two-tailed and a $P < 0.05$ was considered "significant." A power analysis was conducted to determine the sample size needed to detect significant differences at a desired power of 0.8 and an alpha of 0.05. Data discussed in the text is presented as mean ± one standard deviation unless otherwise specified. Regression analysis was conducted, and significant relationships were reported (regression line is plotted in cases of significant relationships). For the data analysis of this work, the entire dataset including potential outliers was used for statistical testing. The original dataset is available upon request. All statistical analysis and graph generation was conducted using SigmaPlot (version 12.5, Systat Software, Inc.). Graphs were exported from SigmaPlot as EMF files to be edited. Labels and edits for clarity were carried out in Canvas X (version 19, build 333, ACD Systems of America) and saved in TIFF format.

Results

Isolation of EVs

EVs were isolated from CM using either a combination of UF and SEC or UC similar to previously described methods in Chapter 3 [117, 375]. CM was stored at -80°C until isolation. The experimental schematic is shown in Figure 20.

EV Analysis by NTA

NTA analysis was used to estimate the particle concentration and size of the EV population. In Figure 21, particle counts per milliliter of sample are compared. In Figure 21a, the effect of cell passage on EV particle count is shown. No significant differences were found between individual passages ($P = 0.478$). Note the trend of particle numbers increasing by passage for early passage cells (P2-P5) and decreasing for each passage in the late group (P9-P12). In Figure 21b, the particle counts were grouped by early and late passage. Regardless of isolation method, particle numbers for early passage cells ($1.1x10^{10}$ EV particles/mL) was significantly higher than particle numbers for late passage cells ($7.7x10^{9}$ EV particles/mL, $P = 0.013$). In Figure 21c, the effect of EV isolation method on particle count is shown. Particle counts were significantly different between UC isolation and SEC isolation ($P = 0.023$), as expected since UC co-isolates extracellular proteins. Isolation via UC produced an average particle count of $1.5x10^{10}$ particles/mL compared to $9.6x10^{9}$ particles/mL for SEC isolation method.

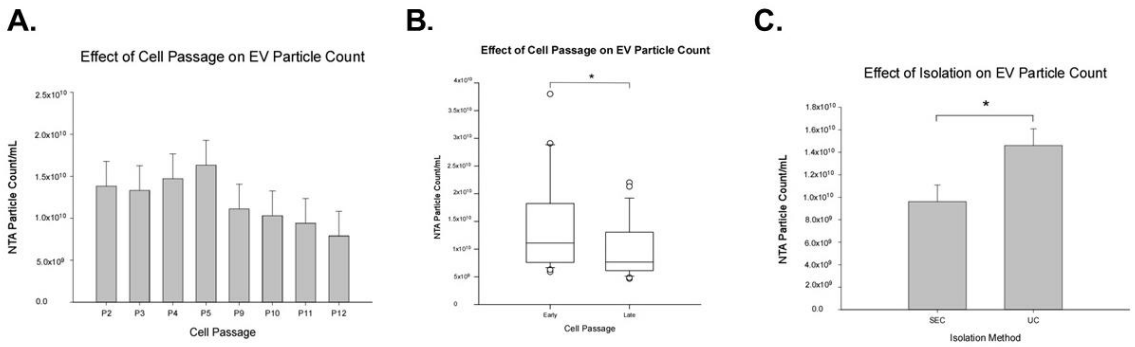

Figure 21: Nanoparticle Tracking Analysis Particle Counts

(A) NTA particle count of extracellular vesicles (EVs) isolate from canine umbilical cord-derived mesenchymal stromal cells (UC-MSCs) from passage 2 to passage 12 (P2 – P12). No significant differences were detected in particle counts by passage but there was a trend for early passage particle counts to be higher than later passage particle counts (P = 0.478). (B) The effect of passage group on EV particle count. Early passage (defined P2-P5) had a significantly higher median EV particle count ($1.1x10^{10}$ particles/mL) compared to late passage (defined as P9-P12) cells ($7.7x10^{9}$ particles/mL, P = 0.013). Data are presented as the median, 25th, and the 75th percentile in the box and the whiskers show the 10th and 90th percentile. Potential outliers are depicted as open circles. Asterisks depict significance as is defined as a P-value < 0.05, n=24 (C) EV isolation using ultracentrifugation (UC) yielded a significantly higher number of particles per mL of sample ($1.5x10^{10}$ particles/mL) compared to size-exclusion chromatography (SEC) isolation ($9.6x10^{9}$ particles/mL, P = 0.023). Data are presented as mean ± standard deviation with an asterisk indicating significance, defined as P < 0.05.

As shown in Figure 22, the size of the EVs was analyzed using NTA. In Figure 22a, EV size was compared across passage. The difference in EV size by passage was not significant (P = 0.270). EVs isolated from early passage CM had a median diameter of 93.0 nm compared to 88.0 nm for late passage EVs. The difference EV diameter by passage was not significant (P = 0.270). Using a power analysis, for a power of 0.8 and an alpha of 0.05, a sample size of 98 would be required to detect significant differences between early and late passage EVs. In contrast, the

diameter of EVs isolated from SEC and UC were significantly different (Figure 22b, $P < 0.001$). EVs isolated from SEC were larger with a median diameter of 95.0 nm compared to UC at 83.0 nm.

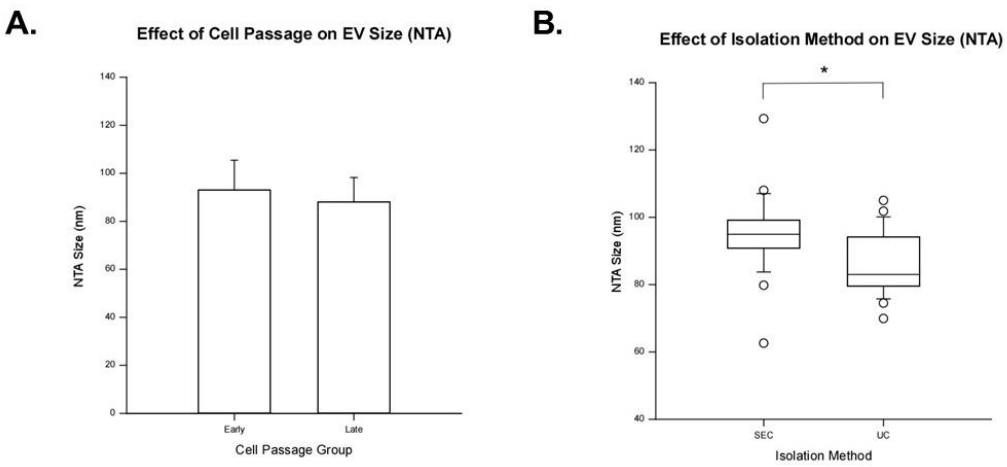

Figure 22: Nanoparticle Tracking Analysis of the Size of Canine MSC-EVs

(A) NTA-based size measurements comparing EVs from canine umbilical cord-derived mesenchymal stromal cells (UC-MSCs) from early passage (P2-P5) versus late passage (P9-P12). No significant size differences were observed over passage. Data are presented as mean ± standard deviation with an asterisk indicating significance, defined as $P < 0.05$ (B) The effect of EV isolation method on EV size (nm). EVs isolated by size-exclusion chromatography (SEC) were significantly larger than EVs isolated by ultracentrifugation (UC). Data are presented as the median, 25th, and the 75th percentile in the box and the whiskers show the 10th and 90th percentile. Potential outliers are depicted as open circles. Asterisks depict significance as is defined as a P-value < 0.05.

Using NTA concentration data, EVs released per cell was estimated and averaged by passage (Figure 23a). EVs from early passage cells (P2-P5) released an average of $2.6x10^4$ EVs per cell while late passage cells (P9-P12) released an average of $1.5x10^4$ EVs per cell. This finding

was not significant (P = 0.219). There was a trend for EVs from early passage cells to release more EVs per cell than late passage cells. Based upon the effect size observed here, power analysis revealed that for a power of 0.8 and an alpha of 0.05, a sample size of 55 would be required to detect significant differences between storage conditions assuming normal and unimodal distributions via two-tailed analysis. Regression analysis was performed with cumulative population doublings achieved by the cells as the independent variable and particles per cell as the dependent variable (Figure 23b). The findings showed that cumulative population doublings (i.e., passage) was negatively correlated with particles released per cell (r = -0.352). Taken together these findings indicate that as cells increase in passage, the number of EVs produced by each cell decreases. It also suggests that in early passage, there is much greater variability in the number of EVs released than later passage. Regression analysis was performed with population doubling time (hours) as the independent variable and particles per cell as the dependent variable (Figure 23c). The findings showed that population doubling time is positively correlated with particles released per MSC (r = 0.326). This finding indicates that cells with a larger PDT (i.e., growing more slowly) release more EVs per cell.

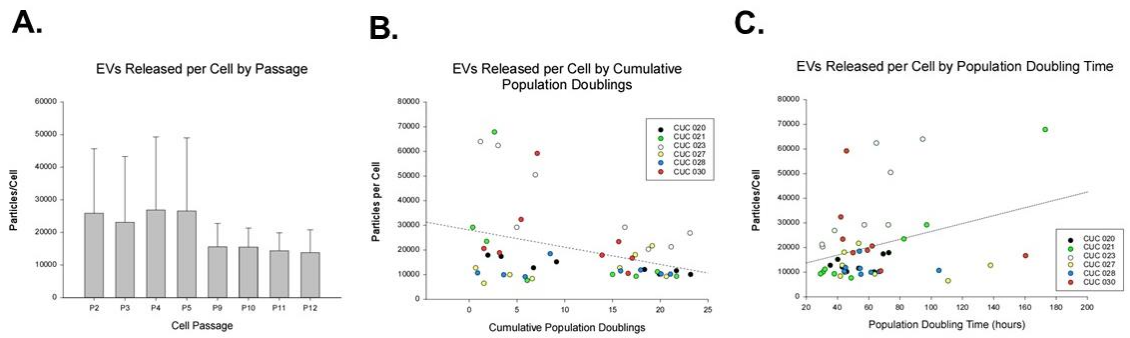

Figure 23: Effect of Cell Passage on the Number of EVs Released per Canine UC-MSC

(A) Average number of EVs released per canine UC-MSC over passage for passages 2 to 12. No significant differences were noted over passage (P = 0.219) but there was a trend for more particles to be released in early passages (P2-P5) compared to late passages (P9-P12) and early passage had much larger variation than later passage. The average EVs released per MSC for early passage cells was $2.6x10^4 \pm 2.1x10^4$ compared to the average for late passage cells $1.5x10^4 \pm 6.4x10^3$, which is approximately 43% fewer particles for late passage cells. Data are presented as mean ± standard deviation, n=6. (B) Regression analysis of EVs released per MSC versus cumulative population doublings achieved by the cells. Cumulative population doublings achieved was negatively correlated to EVs released per MSC (P = 0.014) with r = -0.352, n=48. Individual cell lines are color-coded. (C) Regression analysis of EVs released per MSC vs population doubling time (hours). Population doubling time was positively correlated with EVs released per MSC (P = 0.024) with r = 0.326, n=48. Individual cell lines are color-coded.

EV Characterization by Dynamic Light Scattering

EVs were characterized using DLS to determine the polydispersity index (PDI), zeta surface potential, and hydrodynamic size. EVs isolated using SEC differed from those isolated via UC in all measures. In contrast, early and late passage EVs tended to be the same in most measures. As shown in Figure 24a, the PDI was not different statistically as a result of passage. There was a trend for EVs from late passage cells to have a higher PDI than earlier passage cells (0.48 vs 0.46, respectively). PDI values differed significantly between EVs isolated by UC and SEC (Figure

24b). EVs isolated via UC had a lower PDI value at 0.38 compared to 0.55 for SEC-isolated samples. This indicates that UC-isolated EVs are more homogeneous-sized population of compared to those isolated via SEC.

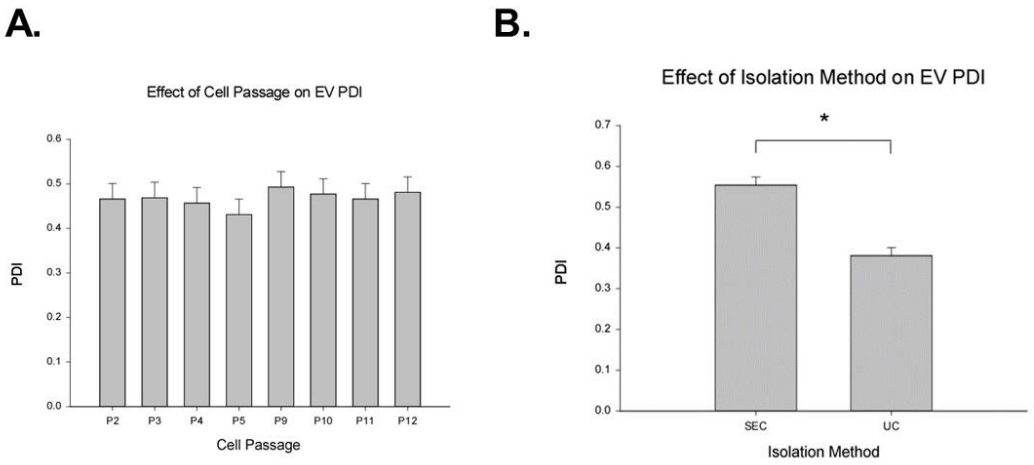

Figure 24: Dynamic Light Scattering Polydispersity Index of Canine EVs

Dynamic light scattering (DLS) data of polydispersity index (PDI) of extracellular vesicles (EVs) isolated from canine umbilical cord-derived mesenchymal stromal cells (UC-MSCs). (A) There was no significant effect of passage on PDI (P = 0.952). Early passage EVs (P2-P5) displayed an average PDI of 0.46, which is similar to late passage EVs (P9-P12) at 0.48. (B) EV samples isolated by size-exclusion chromatography (SEC) had a more heterogeneous-sized population than EVs isolated via ultracentrifugation (UC, P = 0.004). EVs isolated by SEC had a PDI of 0.55 compared to 0.38 demonstrated by UC-isolated EVs. Data are presented as mean ± standard deviation with an asterisk indicating significance, defined as P-value < 0.05.

ANOVA results indicate significant main effects and interactions of cell passage and isolation method on the zeta potential of EVs. As shown in Figure 25, zeta potential was significantly different between the two isolation methods at every passage except for P3 (significant differences denoted with an a). In general, SEC isolation produced EVs with a lower

(more negative) zeta potential than UC. The zeta potential did not change among SEC-isolated samples over passage. In contrast, EVs isolated by UC increased (became less negative) as passage increased. This was significant in the case of P9 compared to P3 and P5 (denoted in Figure 25 as b). Late passage EVs (P9-P12) isolated by UC were not different.

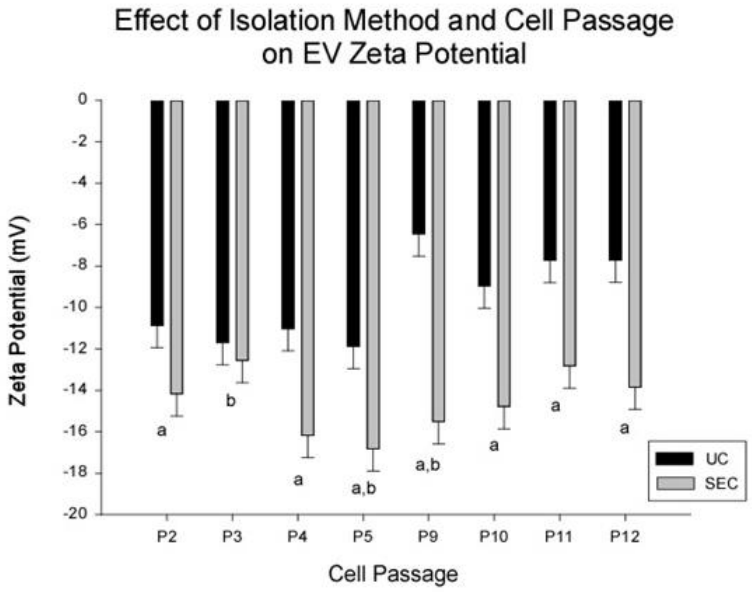

Figure 25: The Effect of Passage and Isolation Method on Canine EVs Zeta Potential

EVs isolated from the CM of canine umbilical cord-derived mesenchymal stromal cells (UC-MSCs) from passage 2 to passage 12 (P2 – P12). (**a**) indicates the significant difference between isolation method within passage. Thus, EVs isolated by ultracentrifugation (UC, black bars) had a less negative zeta potential than EVs isolated by size-exclusion chromatography (SEC, gray bars) at every passage. This was significant at every passage except for P3. The second observation was that SEC isolation did not reveal changes in zeta potential over passage, but UC showed a difference between early passage (P2-P5) and late passage (P9-P12). This was significant in the case of P9 compared to P3 and P5. (**b**) indicates a significant difference for passage within UC isolation method. In contrast to UC isolation, zeta potential did not change among the SEC isolation method over passage. Data are presented as mean ± standard deviation with an a or b indicating significance, defined as P-value < 0.05.

The hydrodynamic size of EVs was compared between passage group and isolation method using Mann-Whitney rank sum test. As shown In Figure 26a, the size of EVs isolated from early passage CM was not different than EVs isolated from late passage CM. Early passage EVs had a median diameter of 155.1 nm compared to 147.6 nm for late passage EVs. In contrast, as shown in Figure 26b, EVs isolated via SEC were significantly larger in size compared to those isolated using UC (151.2 nm and 128.4 nm, respectively).

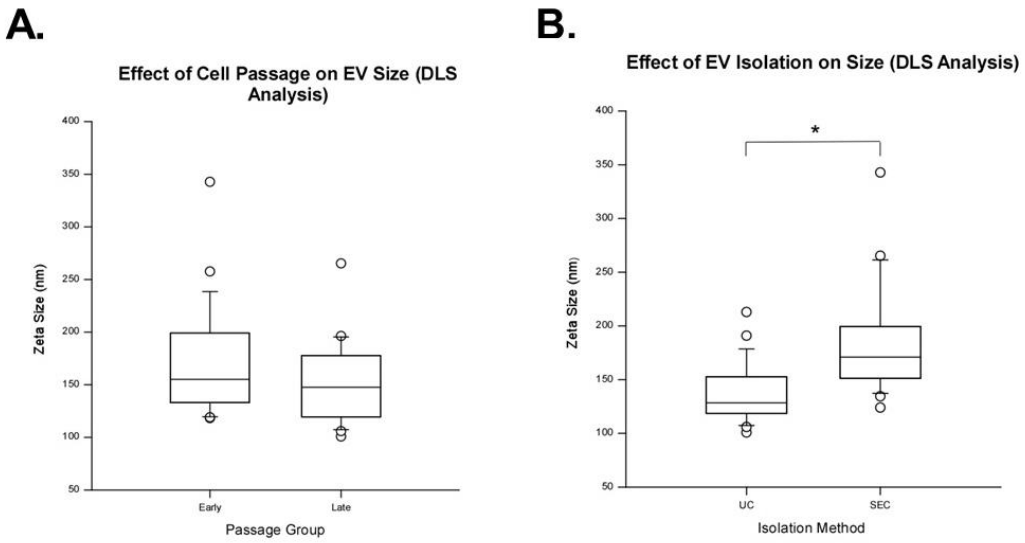

Figure 26: Hydrodynamic Size of Canine EVs

Hydrodynamic size of extracellular vesicles (EVs) isolated from canine umbilical cord-derived mesenchymal stromal cells (UC-MSCs) measured by dynamic light scattering (DLS). (A) The size of EVs isolated from early passage (P2-P5) conditioned media was not significantly different ($P = 0.228$) from EVs isolated from late passage (P9-P12). (B) EVs isolated using ultracentrifugation (UC) were smaller than those isolated via size-exclusion chromatography (SEC, $P < 0.001$). Data are presented as the median, 25th, and the 75th percentile in the box and the whiskers show the 10th and 90th percentile. Potential outliers are depicted as open circles. Asterisks depict significance as is defined as a P-value < 0.05.

EV Analysis by Transmission Electron Microscopy

EVs were analyzed via TEM and 31 to 40 (35.5 ± 4.2) EVs were measured per experimental group. As depicted in Figure 27a, EVs appeared roughly spherical and ranged in diameter from 38 nm to 218 nm. In all groups there appears to be a distinct black ring (i.e., doughnut shape) indicative of a bilayer structure. Note that when EVs isolated via UC more debris was observed than when SEC was used for EV isolation. As shown in Figure 27b, significant size differences were observed when comparing early passage (P2) to late passage (P12) EVs ($P = 0.018$). EVs isolated from early passage MSCs had a smaller median diameter (74.0 nm) than those isolated from late passage MSCs (98.8 nm). In Figure 27c, EVs isolated via SEC (85.4 nm) and those isolated by UC (84.0 nm) were not significantly different in size ($P = 0.695$).

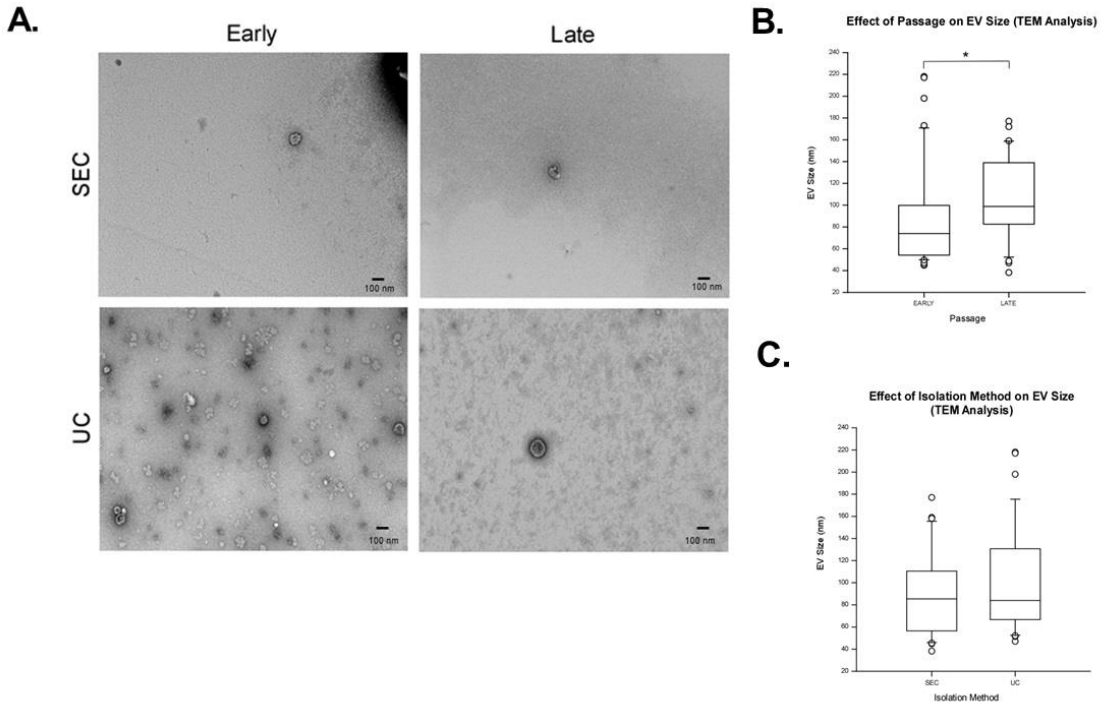

Figure 27: Transmission Electron Microscopy Analysis of Canine EVs

(A) Representative transmission electron microscopy (TEM) micrographs depicting EVs from size-exclusion chromatography (SEC, top) and ultracentrifugation (UC, bottom) as well as early passage (P2-P5, left) and late passage (P9-P12, right). EVs were roughly spherical, doughnut-shaped and their diameters range from 38 to 218 nm. Note that more debris was observed in UC samples compared to SEC samples. Calibration bar represents 100 nm. (B) Early passage EVs (74.0 nm) were significantly smaller than late passage EVs (98.8 nm, P = 0.018). (C) No significant differences were found between the size of EVs isolation via SEC (85.4 nm) and UC (84.0 nm, P = 0.695). Data are presented as the median, 25th, and the 75th percentile in the box and the whiskers show the 10th and 90th percentile. Potential outliers are depicted as open circles. Asterisks depict significance as is defined as a P-value < 0.05.

Comparison of Protein Content in EV Samples

Protein content was measured in EV samples isolated from both SEC and UC using a micro BCA or a BCA assay, respectively. As shown in Figure 28a, EV samples isolated by UC had more than 10x higher protein concentration than samples isolated via SEC. EV samples isolated by UC

had a mean protein concentration of 38.0 µg/mL but displayed a wide range of values (15-52 µg/mL). EV samples isolated via SEC had a median protein concentration of 3.3 µg/mL and displayed a smaller range of values (1-8 µg/mL). To determine the relationship between EVs and soluble protein, particle number per µg of protein is reported for UC and SEC samples (Figure 28b). Isolation by SEC yielded significantly more particles per µg of protein than UC (~ 10x, $P < 0.001$). SEC isolation yielded a median of $2.9x10^9$ particles/µg protein compared to $3.3x10^8$ particles/µg protein by UC isolation.

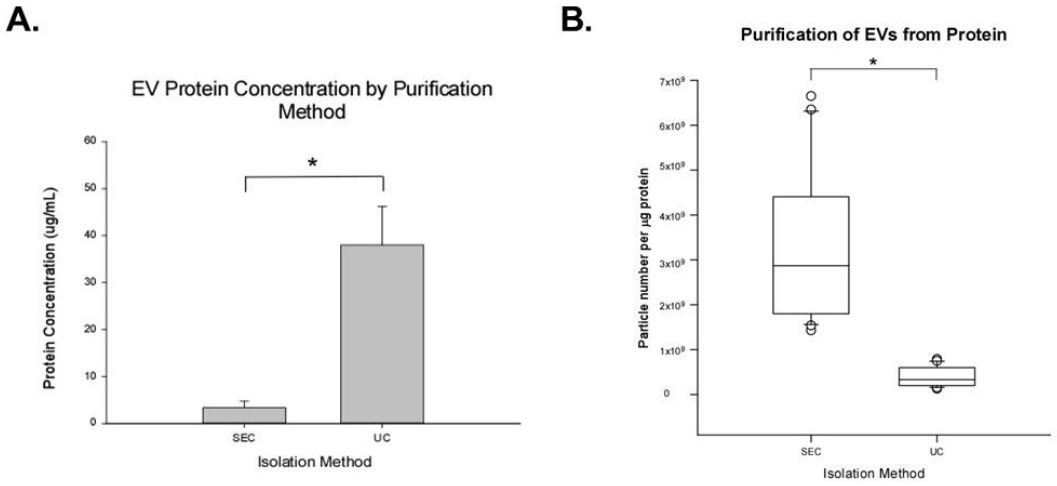

Figure 28: Relationship Between Soluble Protein Concentration and EVs by Isolation Method

(A) EVs isolated by ultracentrifugation (UC) method had more than 10x higher protein concentration (38.0 µg/mL) than EV samples isolated via size-exclusion chromatography (SEC, 3.3 µg/mL, $P < 0.001$). Data are presented as the mean ± one standard deviation, n=24. (B) Relationship between soluble protein concentration and EV number. Isolation by SEC yielded approximately 10x more particles per µg of protein compared to UC isolation method. SEC isolation yields significantly more particles per µg of soluble protein compared to isolation by UC ($P< 0.001$). Data are presented as median, 25th, and the 75th percentile in the box and the whiskers show the 10th and 90th percentile. Potential outliers are depicted as open circles. Asterisk depicts significance as is defined as a P-value < 0.05.

Expression of Tissue Factor by MSCs

Both human and canine MSCs had positive surface expression of TF as evidenced by the strong fluorescence (shown in Figure 29) via polyclonal anti-TF staining. Canine MSCs were not cross-reactive the human anti-mouse CD142 (functional clone HTF-1) and this was confirmed via flow cytometry (Appendix C, Supplementary Figure S9).

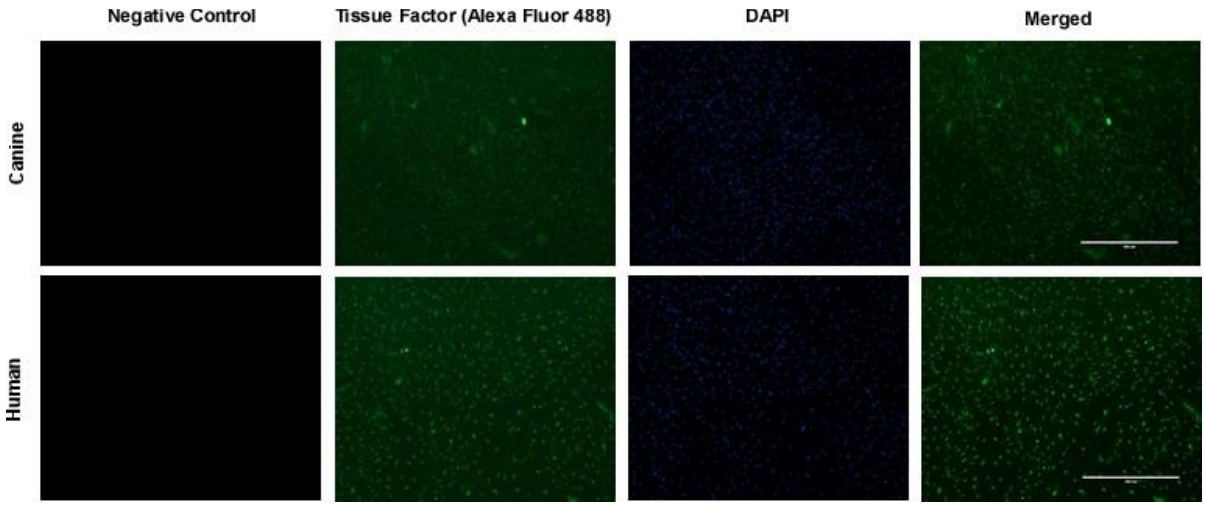

Figure 29: Tissue Factor Expression by Human and Canine MSCs
Tissue factor (TF) expression by human and canine umbilical cord-derived mesenchymal stromal cells (MSCs). Human and canine MSCs express TF as indicated by positive staining on the cell surface. Note that the staining intensity of human MSCs appears to be much higher than canine MSCs. Calibration bar represents 400 μM.

Tissue Factor Expression by EVs

EVs, specifically exosomes, express not only the characteristic exosome-associated surface markers (i.e., CD9, CD63, CD81, and ALIX) but also protein markers of the parental cells [117, 129, 376, 377]. Here, we observed that all EV samples had TF expression, regardless of isolation method or passage. In contrast, we observed changed in tetraspanin staining associated with

passage, as shown in Figure 30. Tetraspanins CD9, CD63, and CD81, as well as the protein ALIX, were expressed on EVs after both UC and SEC isolation at early passage (early is defined as P2-P5). The data is shown for three independent lines per isolation at two passages (P2 and P3). The blots for P4 and P5 were similar. In contrast, at late passage (late passage is defined as P9-P12, P11 and P12 are shown), EVs from both UC and SEC isolation methods express CD9, CD81, and ALIX, but expression of CD63 was not observed, regardless of isolation method. Specifically, CD63 expression was significantly different ($P = 0.023$) between early and late passage, but not different for isolation method ($P = 0.257$). At P2, 100% of EVs displayed expression of CD63. At P5, only 33% of EVs displayed expression of CD63 and at P12 0% of EV samples displayed CD63 expression.

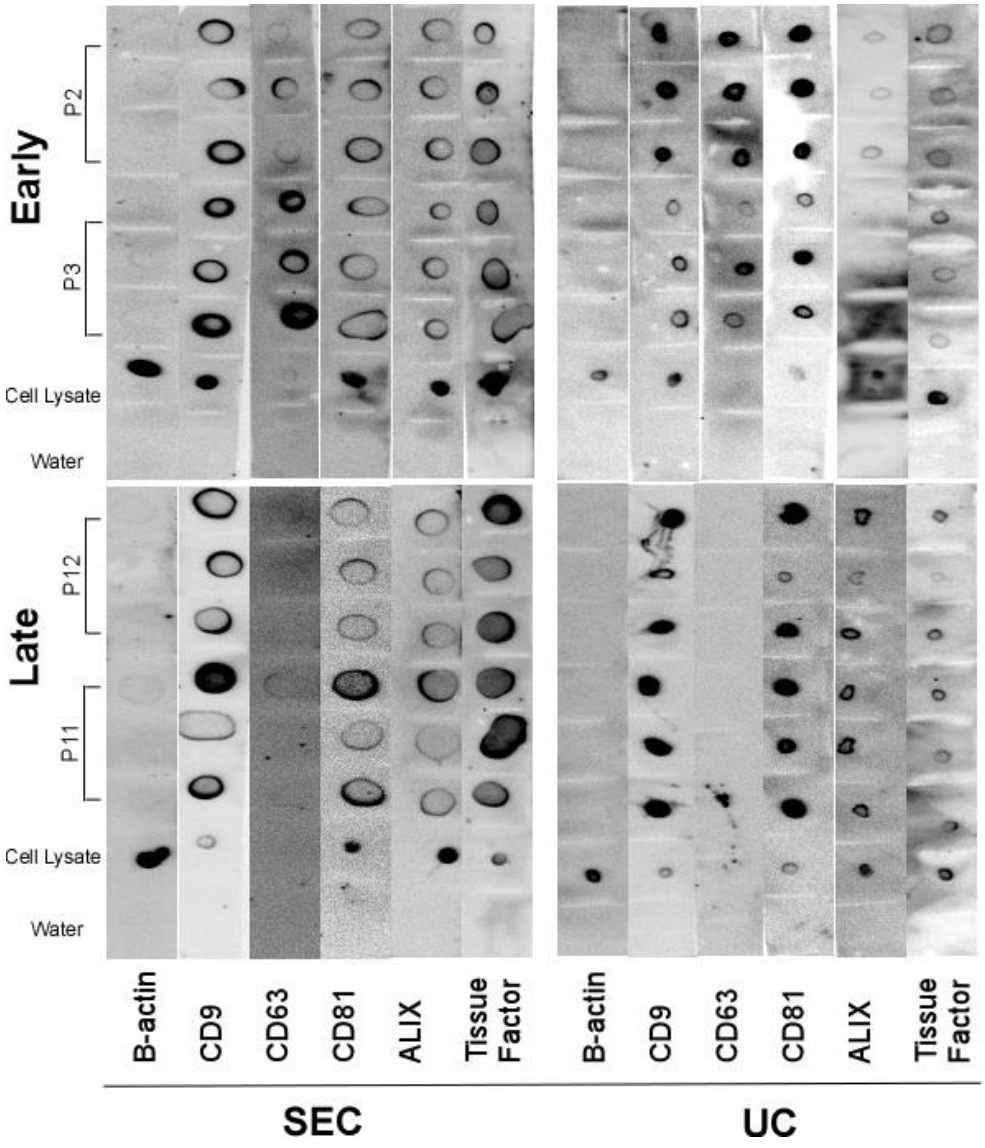

Figure 30: Dot Blot Analysis for Canine MSC-EVs

Extracellular vesicles (EVs) isolated from canine umbilical cord-derived mesenchymal stromal cells (MSCs) express tissue factor (TF) and differ in expression of CD63 over passage. Both early (P2 and P3 shown) and late passages (P11 and P12 shown) EVs expressed TF regardless of the EV isolation method (size-exclusion chromatography, SEC, or ultracentrifugation, UC). The expression of clusters of differentiation (CD) 9, CD63, CD81; ALIX; TF; and protein-loading control, β-actin, by negative control (water), whole MSC cell lysate (positive control) at both early (top) and late (bottom) passages as well as EVs isolated via SEC (left) and UC (right). Note that EVs express CD9, CD81, and ALIX regardless of passage or isolation, however CD63 expression was not observed in late passage EVs regardless of isolation method.

EVs Possess Procoagulant Activity

As shown in Figure 31, canine EVs had mean procoagulant activity levels of 72.1 ± 6.1 ng/mL. Similarly, human EVs had mean procoagulant activity levels of 79.8 ± 7.9 ng/mL. Human MSCs served as the positive control and had activity levels of 80.1 ± 13.7 ng/mL. No statistical difference was observed between the groups (P = 0.56). This finding indicates that canine and human EVs and MSCs have similar procoagulant activity levels.

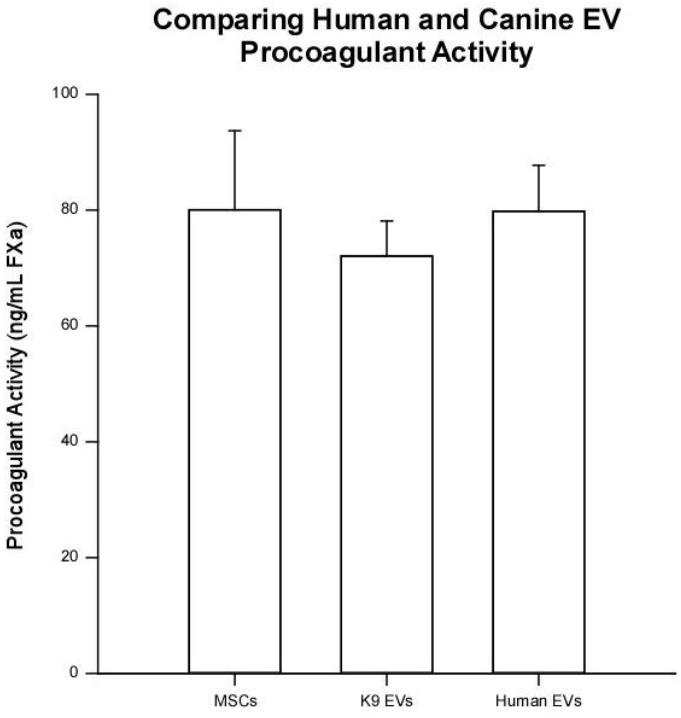

Figure 31: Comparing the Procoagulant Activity of Human and Canine EVs

The procoagulant activity (FXa generation) of human and canine extracellular vesicles (EVs) isolated from umbilical cord-derived mesenchymal stromal cells (MSCs). Similar procoagulant activity levels were exhibited by canine EVs (72.1 ± 6.1 ng/mL) and human EVs (79.8 ± 7.9 ng/mL). Human MSCs served as the positive control (80.1 ± 13.7 ng/mL). No difference was found between the groups (P = 0.56). Human data are from three independent human MSC lines and three independent EV samples at passages 4 to 6. Canine data is from three independent samples at passages 2 to 4. Data are presented as mean ± standard deviation, n=3.

To assess the procoagulant activity of canine MSC-EVs, FXa generation was measured for early passage (P2) and late passage (P12) EVs generated using both isolation methods. Regardless of passage or isolation method, EVs demonstrated procoagulant activity via generation of TF-specific FXa. As shown in Figure 32a, early passage EVs generated an average of 41.9 ± 34.3 ng/mL FXa while late passage EVs generated 66.2 ± 43.2 ng/mL of FXa. No difference was found between passage groups ($P = 0.305$). Based on the effect size observed here, power analysis revealed that for a power of 0.8 and an alpha of 0.05, a sample size of 51 would be required to detect significant differences between early and late passage EVs. As shown in Figure 32b, EVs isolated via SEC generated an average of 39.4 ± 39.6 ng/mL FXa compared to UC-isolated EVs at 68.7 ± 36.2 ng/mL. No significant difference was observed between isolation methods ($P = 0.21$). Based on the effect size observed here, a sample size of 30 would be required to detect significant differences between EVs isolated using the two methods. Taken together, this data indicates that canine MSC EVs are procoagulant due to expression of TF and this is not influenced by passage (i.e., time in culture) or isolation method.

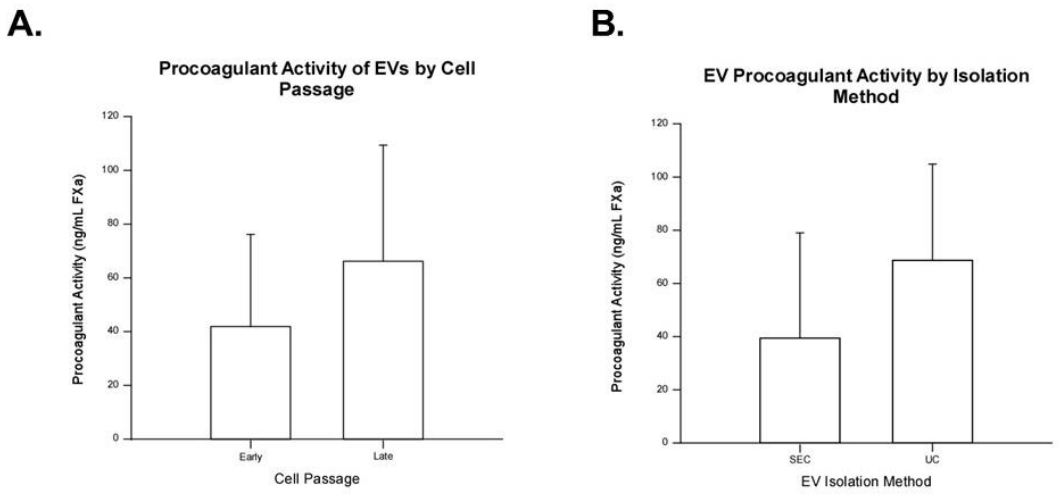

Figure 32: Procoagulant Activity of MSC-EVs

Procoagulant activity (ng/mL of FXa generated) of EVs isolated from canine umbilical cord-derived mesenchymal stromal cells (MSCs) by cell passage (early vs. late) and EV isolation method (size-exclusion chromatography (SEC) vs. ultracentrifugation (UC)). (A) Procoagulant activity of EVs by early (P2) versus late (P12) passage. No statistical differences were found (P = 0.305) but the trend was for late passage EVs to have higher levels of procoagulant activity. (B) No significant difference was found between isolation methods (P = 0.210). There was a trend for EVs isolated via UC to have a higher procoagulant activity level than those EVs isolated via SEC. Data are presented as mean ± standard deviation. Data from EVs derived from six independent canine MSC lines.

The procoagulant activity was calculated as FXa generated (in nM) per million EVs and per million cells and is shown in Table 9. The EV samples generated a range of 0.002 to 0.048 nM FXa per $1x10^6$ EVs. The average was 0.023 ± 0.02 nM FXa per $1x10^6$ EVs. When normalized to the cells producing the EVs, the range was 0.026 to 0.854 nM FXa per $1x10^6$ cells. The average was 0.329 ± 0.28 nM FXa per $1x10^6$ cells. Therapeutic doses of MSCs typically range from 3 – $5x10^6$ MSCs per kg of body weight, meaning that a MSC dose would have an associated average procoagulant activity range of 0.987 – 1.645 nM FXa per kg body weight. Using the assumption

that MSCs release an average of 20,000 EVs/MSC and the low end of an MSC therapeutic dose ($3x10^6$ MSCs/kg), an equivalent therapeutic dose of EVs would have an associated average procoagulant activity of 1405±1024 nM FXa per kg body weight. When looking at the patterns of the individual cell lines with the FXa generated normalized to cells, four of the six lines tested display higher values of FXa generated by late passage EVs than early passage. In contrast, two of the six lines display higher FXa generation by early passage compared to late passage.

Table 9: Procoagulant Activity per Million Cells and EVs

Line	*Passage*	*Isolation*	*EV Number (per well)*	*FXa Generated (ng/mL)*	*FXa Generated (nM) per $1x10^6$ EVs*	*FXa Generated (nM) per $1x10^6$ MSCs*	*FXa Generated (nM) by dose of EVs per kg*
CUC020	Early	SEC	$5x10^7$	37.7	0.016	0.236	960
CUC020	Late	SEC	$5x10^7$	111.4	0.048	0.651	2880
CUC021	Early	SEC	$5x10^7$	52.8	0.023	0.342	1380
CUC021	Late	SEC	$5x10^7$	5.20	0.002	0.026	120
CUC023	Early	UC	$5x10^7$	103.4	0.045	0.854	2700
CUC023	Late	UC	$5x10^7$	95.7	0.042	0.467	2520
CUC027	Early	SEC	$5x10^7$	8.20	0.004	0.029	240
CUC027	Late	SEC	$5x10^7$	20.8	0.009	0.094	540
CUC028	Early	UC	$5x10^7$	35.4	0.015	0.107	900

CUC028	Late	UC	$5x10^7$	89.9	0.039	0.588	2340
CUC030	Early	UC	$5x10^7$	13.8	0.006	0.063	360
CUC030	Late	UC	$5x10^7$	74.2	0.032	0.492	1920
Mean ± Standard Deviation					0.023 ± 0.02	0.329 ± 0.28	1405 ± 1024

To confirm that procoagulant activity demonstrated EVs was due to expression of TF, EVs were incubated with anti-TF (blocking) antibody prior to incubation with FVIIa and FX. As shown in Figure 33a, when canine EVs were incubated with anti-TF antibody (polyclonal), FXa generation was not inhibited. Similarly, when human EVs were incubated with the anti-TF antibody (polyclonal) FXa generation was not inhibited (Figure 33b). In contrast, when human EVs were incubated with a TF antibody described as inhibitory (clone HTF-1), that was previously shown to not be reactive with canine TF, FXa generation was inhibited. Human EVs alone generated 35.8 ± 7.2 ng/mL of FXa while human EVs with the HTF-1 clone of TF antibody generated -6.06 ± 24.3 ng/mL FXa and human EVs incubated with the polyclonal antibody generated 27.0 ± 7.5 ng/mL of FXa. In this case, the negative value indicates that the average FXa generation was less than the respective control wells (human EVs with FX only) that were subtracted out. Thus, this antibody did inhibit TF-mediated FXa generation by human EVs. Taken together, these results indicate that FXa generation is mediated by TF expression on EVs, but more work should be done to conclusively demonstrate inhibition of TF-mediated FXa generation in canine EVs.

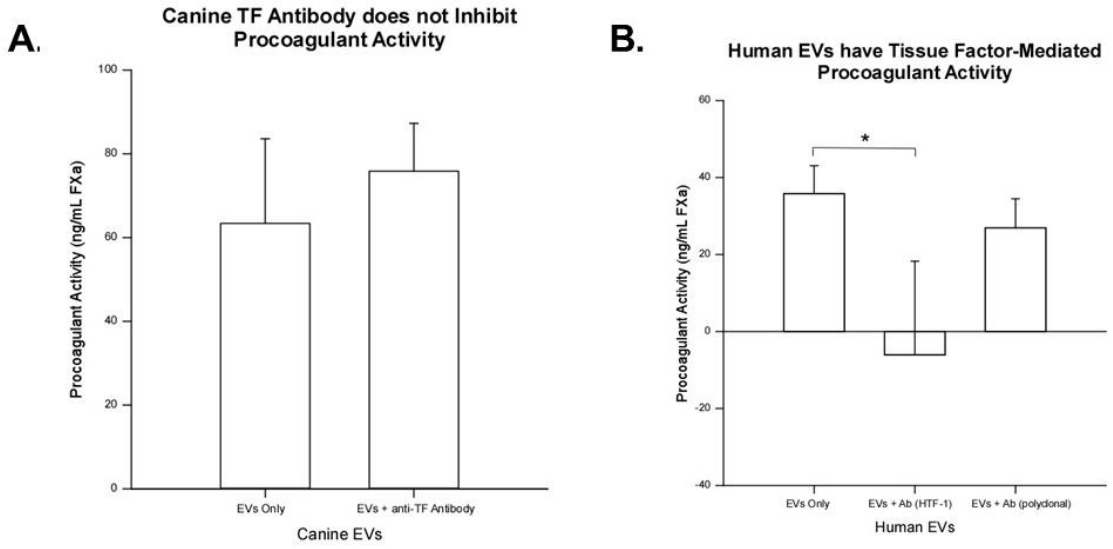

Figure 33: Inhibition of Procoagulant Activity of EVs

Inhibition of tissue factor (TF)-mediated FXa generation by extracellular vesicles (EVs) isolated umbilical cord-derived mesenchymal stromal cells (MSCs). (A) FXa generation was not inhibited in canine EVs incubated with polyclonal anti-tissue factor antibody. (B) In contrast, the procoagulant activity of human EVs was inhibited by a known blocking anti-TF antibody (clone HTF-1). Similar to canine, FXa generation was not inhibited with the polyclonal TF antibody. Data are presented as mean ± standard deviation with an asterisk indicating significance, defined as P-value < 0.05.

Discussion

Here, EVs from canine umbilical cord-derived MSCs were characterized based on two factors—cell passage and isolation method. To my knowledge, this is the first exploration of these factors simultaneously. Eight new findings encapsulate my work. First, EV yield (particle count) was affected by both the passage of the cells producing the EVs and the EV isolation method. Early passage cells (P2-P5) yielded more EVs than late passage cells (P9-P12). EV isolation via UC yielded more EVs than SEC. Second, the size of EVs was affected by isolation method but not

cell passage. EVs isolated via SEC were larger than UC when analyzed by both NTA and DLS. However, both isolation methods produced EVs within the size range associated with exosomes [118, 120, 127, 130, 131, 133]. When examining EV size over passage, EVs remained a consistent size. Third, a cell's cumulative population doublings achieved is negatively correlated to EV yield per cell. Fourth, the isolation method affected PDI but not cell passage. Unexpectedly, EVs isolated via SEC had a higher PDI (i.e., a more heterogeneous-sized population) than EVs isolated via UC. Fifth, cell passage and EV isolation method affected zeta potential. At seven of the eight passages analyzed, isolation methods produced EVs with different zeta potentials. Overall, SEC isolation method produced EVs with lower (more negative) zeta potential than UC, indicating an increased stability in SEC-isolated EVs compared to UC-isolated EVs. In addition, the zeta potential of SEC-isolated EVs remained consistent over passage while, in contrast, the zeta potential of UC-isolated EVs increased (i.e., became less negative) with passage. Sixth, passage affects the expression of some, but not all, exosome-associated surface proteins, specifically, CD63. Expression of CD63 was not observed in EVs isolated from late passage cells. Seventh, both human and canine MSCs express TF and TF expression was found on their EVs, too. Lastly, both human and canine EVs possess procoagulant activity due to TF expression. These data suggest important considerations for EV manufacturing scale-up and clinical translation.

In EV literature, there is no single standardized method for their isolation from biological fluids or CM, but UC and SEC are quite common [135, 347]. We previously reported the isolation of EVs from human umbilical cord-derived MSC CM using both UC [117] and SEC [Chapter 3]. To permit broader comparisons to previous work, both UC and SEC isolation methods were used for this work. In Chapter 2, I described the optimization of canine umbilical cord-derived MSC culture that demonstrated differences in the culture conditions of human and canine UC-MSCs

[12]. Due to these differences, we wanted to determine if the human EV isolation protocols also isolate canine EVs. EVs were successfully isolated from canine MSC CM using both SEC and UC methods. Based on NTA particle counts, canine MSCs yielded an average of $1.21x10^{10}$ EV particles/mL. This result is similar to the human MSCs average of $1.26x10^{10}$ EV particles/mL (see Chapter 3). Thus, the protocols presented here efficiently isolate EVs from both canine and human MSC CM with similar yield. There are opportunities for protocol optimization such as, evaluating the sex of the MSC donor, extending the conditioning period or the serum-starvation period, altering other culture conditions (e.g., 2D vs 3D culture, seeding density, media components, incubation parameters, hypoxic conditions), or perhaps pharmacological manipulations (e.g., N-methyldopamine and norepinephrine), which are targets for future work [378].

Based on the findings from Chapter 3, we assumed that CM storage at -80ºC prior to EV isolation would be optimal for this work. CM was collected from six canine umbilical cord-derived MSC lines from passages P2 to P12 and isolated via either SEC or UC. Because of the design, multiple CM samples were collected daily and there was insufficient time for them to be isolated within 24 hours. In addition, to make efficient use of the UC shared equipment, the maximum number of samples for the particular rotor (i.e., six samples) were processed at one time. Thus, our CM storage work summarized in Chapter 3 made this experimental design feasible.

EV particle counts were estimated using NTA. In early passages (P2-P5) as cell passage increased, the average EV particle counts increased. In contrast, in late passages (P9-P12) as passage increased, the average EV particle count decreased. When grouped by early and late passage, early passage cells produced a significantly higher number of EVs compared to late passage. Similarly, Patel et al. reported no differences in EV yield concentration between early passage cells (tested P2-P5) but later passages were not evaluated [322]. Our findings suggests

that it is more efficient to use early passage cells to produce large numbers of EVs for clinical research.

EV particle count differed between both isolation methods tested. EV isolation by UC yielded significantly more EVs than SEC. In contrast, previous work reported that SEC methods yield more EVs [203, 379]. Others have reported no significant differences between the EV yield of UC and SEC [191]. These inconsistencies in yield could be attributed to variations in isolation protocols and the biological fluid serving as the source of EVs. There is the concern, too, that UC isolation yields are less pure and may be contaminated by debris or other proteins compared to SEC. So, we should qualify that NTA data indicates that UC isolation yields more canine EVs than SEC with no regards to EV sample purity. As discussed below, the protein concentration in UC isolation supports the contention that UC isolation yields a less pure EV preparation.

EV size was estimated three ways: NTA, DLS, and TEM. NTA and DLS agreed that EV size was affected by isolation method but not passage. Size estimates provided by both methods were within the desired exosome range (30-150 nm) [118, 120, 127, 130, 131, 133]. The DLS size estimate of SEC-isolated EVs extended beyond the exosome range at 170.9 nm however this is similar to values reported for other MSC-EVs [117, 197]. EVs isolated via SEC were significantly larger than those isolated via UC. Similar to data from Chapter 3, DLS size estimates for EVs from human MSC (-80ºC storage group) isolated via SEC were 165 nm. This result indicates the presence of larger vesicles in the SEC population, or it may suggest that the UC isolation method yields a population containing smaller particles (as suggested by TEM, see Figure 27).

No size differences were detected between early and late passage EVs by either DLS or NTA indicating that the population of EVs isolated does not contain larger vesicles (e.g., apoptotic bodies) with the increased time in culture, similar to previous reports [353, 354]. Similarly, Patel

et al. did not detect any changes in size of EVs from MSCs over passage (P2-P5 tested, late passages not examined) [322]. Taken together with the particle number, this data shows that although less EVs can be isolated from late passage CM, the EV population isolated is similar in size. In contrast, TEM data alluded to larger size EVs isolated from late passage CM with no difference between isolation method (but there was more small material we call cell debris in TEM). NTA and DLS data was obtained and averaged from every sample. TEM data was performed on two independent, randomly-chosen lines at each passage group and isolation method. Furthermore, the TEM data was collected by samples which had been lyophilized and reconstituted. It is possible that lyophilization shifted EV size due to osmotic or surface charge-related effects. Plus, the sample size for TEM data is smaller. Therefore, the size estimates by TEM are derived from a smaller sampling than DLS or NTA estimates. However, the TEM size estimates generally agree with size estimates provided by NTA. In the future, a larger sampling by TEM would provide better size estimates and may resolve questions raised by other observations (i.e., CD63 staining).

EVs released per cell was estimated using the same assumptions discussed in Chapter 3. Canine MSCs released an average of $2.02x10^4 \pm 1.55x10^4$ EVs per cell. This is similar to the average of $2.19x10^4 \pm 8.5x10^3$ EVs per cell demonstrated by human MSCs in Chapter 3 and by Patel et al. [322, 352]. In contrast, Crain et al. reported an average of $5.78x10^3 \pm 3.3x10^3$ EVs per cell from canine WJ-MSCs [197]. This disparity is likely due to differences in canine MSC isolation and culture, and/or EV isolation protocol, which involved the addition of a density gradient UC step [197]. Taken together, our protocols produce more EVs per cell than previously reported, and produce them in a consistent manner from early and late passage MSCs. In addition,

when comparing results from Chapter 3, our protocols produce EVs in a consistent manner from both human and canine MSCs.

Regression analysis revealed that particles per cell is negatively correlated to a cell's cumulative population doublings (i.e., passage). This same relationship was seen by plotting yield versus passage number (data not shown) and agrees with the human data reported in Chapter 3. Cumulative population doublings achieved by the cells was used here instead of cell passage because it is the consensus in the literature that a cell's cumulative population doublings is more comparable across laboratories [380]. The population doublings a cell acquires in a passage can vary from laboratory to laboratory due to seeding density, cell confluence at the time of passage, or efficiency or lifting and counting cells. As a cell accumulates population doublings, the number of EVs released by that cell decreases. This data suggests that early passage cells are more efficient for production of EVs. This finding has important implications, specifically when considering translation to clinical applications where large numbers of EVs will be required.

It is well known that "aging" MSCs display increased senescence, decreased differentiation potential, genetic mutations, morphological changes, and phenotypic changes [381-384]. Aging MSCs can refer to both aging in culture or from older donors. Considering that UC-MSCs come from consistently aged donors, here, aging refers to aging in culture. Zhuang et al. reported that late passage UC-MSCs (P15) display stronger immunosuppressive properties than early passage MSCs (P3) [384]. Since EVs share many properties with their parental cells, the immunoregulatory properties of EVs from early and late passage MSCs still needs to be evaluated.

Regression analysis revealed that EV yield (i.e., particles per cell) is positively correlated to a cell's population doubling time. This finding agreed with human data discussed in Chapter 3. Since the cells are serum-starved to produce EVs and not passed, a PDT for that passage cannot

be determined. Rather, the previous passage PDT is used as an estimate under the assumption that the cells will continue to grow at the same rate. Although Lu et al. demonstrated that human UC-MSCs maintain a constant PDT from passage 1 to passage 10, our work here involved canine UC-MSCs and extended beyond passage 10 [30]. Because of this, this estimate does not perfectly fit our experimental design and with our findings in this work—i.e., early passage or cells with a low CPD produce more EVs. In future work involving canine UC-MSCs and/or of late passage, this estimate may be reconsidered. Here we see that the longer it takes for the cell's population to double, more EVs are released per cell. An explanation for this finding may be that the cells are in culture longer and thus have more time to generate EVs. Another explanation may be that perhaps cells undergoing rapid replications cannot afford to put energy into production of EVs. This finding suggests that perhaps optimizing culture conditions to decrease a cell's PDT may be counterproductive when it comes to production of CM for EV isolation.

PDI describes the heterogeneity of the size distribution of a given particle population [357]. As discussed in Chapter 3, samples with a PDI value greater than 0.7 indicate a wide size range and thus are not ideal for analysis by DLS [357]. All samples here were below the 0.7 threshold and were similar to those reported in Chapter 3. PDI did not differ between early and late passage EVs (0.46 vs. 0.48, respectively). This data, taken together with the NTA and DLS size estimates, confirms that EVs derived from late passage EVs are not co-isolated with other larger sized vesicles. PDI did differ between UC and SEC isolation. Unexpectedly, UC samples displayed a PDI value of 0.38 compared to 0.55 for SEC-isolated EVs. This was unexpected because sample purity is a concern when isolating EVs using UC methods, also as indicated by our TEM results [135, 176, 208, 348]. We hypothesized these impurities would be reflected in a higher PDI value in UC. In contrast, our data indicates that the EVs isolated via UC are more homogeneous than

those isolated via SEC. Another suggestion is that perhaps the PDI reflects UC-related damage through smaller particles and debris.

As discussed in Chapter 3, zeta potential is used as a measure of EV surface charge, colloidal stability, and membrane integrity [352, 358, 366, 385]. Similar to human MSC-EVs from Chapter 3 and other previous reports, canine MSC-EVs displayed a negative zeta potential [117, 352, 359, 385, 386]. Here, significant ANOVA main effects (both passage and isolation) were observed as well as a significant interaction term. We will discuss the interaction term and not the main effects. For passage within isolation method, there were opposite trends. For SEC-isolated EVs, as passage increased, the zeta potential of EVs remained constant. For UC-isolated EVs, as passage increased, the zeta potential of EVs decreased (this was significant at P9 vs. P3 and P5). This suggests that the combination of later passage and UC dramatically impacts the stability and integrity of EVs, suggested UC-related damage [387-390]. For isolation within passage, the zeta potential of EVs isolated from UC and SEC differ at almost every passage. At only one passage was this not different (P3). At most passages, SEC-isolated EVs had a larger (more negative) zeta potential alluding to a higher membrane stability and integrity of EVs. Again, this data suggests that UC may reduce EV membrane stability. In addition, EVs with a higher charger (i.e., more negative) are less likely to aggregate and are more stable when dispersed in a solution [385, 391]. This finding is important because the effects on the EVs from being sedimented against a solid surface for lengths of time are unknown, but it is thought to damage EVs or compromise their contents [135, 176, 387-390].

One of the disadvantages of using UC alone to isolate EVs is the potential contamination of proteins and lipoproteins [135, 191, 208, 348, 390]. Here, EVs isolated via UC had a 12x higher protein concentration than samples isolated using SEC, similar to previous reports [203, 224]. This

suggests significant co-isolation of proteins and lipoproteins with the UC protocol, and points out how the addition of density gradient UC might improve the purity of EVs [215-217, 392]. SEC-isolated samples had lower protein concentrations similar to what we reported in Chapter 3 and that of Nordin et al. [203]. As reported by Brennen et al., purification of EVs from soluble proteins was calculated as the particle number divided by the amount of protein in the sample [347]. Here, SEC samples produced a median of $2.9x10^9$ particles per µg of protein compared to $3.3x10^8$ particles per µg of protein for UC samples (approximately 10x more EVs with SEC). This is similar to previous reports for EVs isolated from human serum and CM of iPSC cells [203, 347]. This makes a case that SEC EV yields are of higher purity than UC samples. Since density gradient UC may further purify UC EV isolation, addition of this further step might increase UC EV purity [214-217, 348, 392]. I did not examine this question here.

Dot blots for exosome proteins including tetraspanins (CD9, CD63, and CD81), as well as ALIX, were used to characterize EVs. Since EV samples isolated via SEC had low protein concentration, EV samples were lyophilized and reconstituted which increased protein concentrations 10x [343, 361, 364, 393]. This allowed us to load less volume onto the membrane, producing more appealing blots. All EV samples stained positively for CD9, CD81, and ALIX similar to Chapter 3 and other previous reports [117, 394]. This data demonstrates enrichments of EVs using both isolation methods. Expression of exosome marker CD63 was not detected in EVs derived from late passage MSCs, regardless of the isolation method. It appeared that EVs started to lose expression of CD63 by P5 and it was undetectable by P12. Similarly, Patel et al. reported decreased levels of CD63 on MSC-EVs after five serial passages of MSCs [323, 352]. Interestingly, Moravcikova et al. reported that MSC CD63 surface expression initially increased with passage and then started to decrease at passage 5 [395].

It was previously reported that human MSCs express TF on their surface and possess procoagulant activity [53, 244, 260-262]. Thus, thromboembolism is a risk and safety concern for clinical application of allogeneic MSCs, particularly because the MSCs get trapped in the lungs and other capillary organs after intravenous injection [58, 61, 234, 235, 238, 242, 243, 252]. The risk of thromboembolism is more concerning since MSCs are being explored as a therapeutic in the respiratory complications of coronavirus-induced disease (COVID-19) [47, 48, 371, 373, 396].

Some reports claim that EVs, particularly exosomes, may offer the same therapeutic benefits (e.g., anti-inflammatory properties) as their parent cells, MSCs, without the risks and complications associated with the use of a cellular product [371, 373, 397-402]. The fact that EVs share many traits with their parental cells makes them a double-edged sword. On one hand, there is the potential for EVs to exert therapeutic benefit similar to MSCs. On the other hand, if EVs share TF expression with their parental cells, it is reasonable to assume that they may also share procoagulant activity and thus potential for thrombosis and formation of microemboli. Given that the procoagulant activity of tumor-derived EVs is well known, the assumption that MSC-EVs may also possess procoagulant activity is sensible [266-274].

Thus, we hypothesized that MSC EVs would express TF, like the parental cells do. To test this, first we confirmed that human MSCs express TF on the surface using immunocytochemistry. As discussed in Chapters 2 and 5, canine and human MSCs differ in their surface marker expression profile. For example, human MSCs are negative for hematopoietic marker CD34. In Chapter 2, we showed that canine MSCs express CD34 protein on their surface and make CD34 mRNA. Thus, surface TF expression by canine MSCs needed confirmation. Little previous work has been done regarding canine TF expression, but Gruber et al. reported that canine mammary cancer cells highly express TF [403]. As discussed in Chapter 2 and Chapter 5, canine antibody

selection is more sparse than human and mouse. We tested antibodies, including the one known to functionally block human TF (HTF-1), to see whether they would recognize the canine TF epitope. The anti-TF antibody clone HTF-1 was compatible with human MSCs but not canine. Expression of TF on canine MSCs was demonstrated using a polyclonal anti-TF antibody. The manufacturer revealed that the sequence of the protein that the antibody recognizes is 100% similar to the canine sequence. Due to COVID-19 restrictions, many core facilities were not available for use during this work, including confocal microscopy. Ideally, we would want to use confocal microscopy to obtain high-resolution images confirming the surface expression of TF on the MSCs. However, this was simply not an option for the timeframe of these experiments. As a substitute, we imaged the cells using immunocytochemistry. Detergents were not used to exclude signal from intracellular TF. Ideally, we would want to utilize confocal microscopy to confirm our findings of immunocytochemistry and to obtain better images for publication. Taken together, the results of the immunocytochemistry suggest that canine MSCs may also possess procoagulant activity as human MSCs do.

Next, we determined whether express TF using dot blots. Here, all canine MSC-EV samples express TF, regardless of isolation method or passage. Previous reports have speculated that TF expression by MSCs may be a product of cell culture [260]. In our study, EVs have a strong signal for TF starting at P2 and this signal did not change over passage up to P12 (the last passage evaluated). Efforts were made to quantify the TF expression using a TF standard protein curve but were not successful. Future work may explore assay troubleshooting and optimization or perhaps another quantification method such as a Western blot. Quantification by Western blot was not chosen pursued here due to the low protein content of the SEC-isolated samples.

Procoagulant activity was assessed using an assay that measured TF-specific FXa generation. For this assay we could not find a commercial source of canine FVIIa and FX. Options included human, rodent, and bovine. Others have demonstrated canine-human cross-species computability [404]. Knudsen et al. reported findings that human FVIIa binds to canine TF similarly to human [404]. To confirm this and test the assay with MSC-EVs, we compared the FXa generation using human MSCs, human MSC-EVs, and canine MSC-EVs. We found similar procoagulant activity levels among all groups. This observation confirms cross-species compatibility and feasibility of this modified assay for MSC-EVs.

Once procoagulant activity of canine MSC-EVs was confirmed, TF-specific FXa generation was compared for early (P2) and late (P12) passage EVs isolated via SEC and UC. Any non-specific signal (from samples minus FVIIa) was subtracted out prior to analysis. Since Oeller et al. reported an increase in TF expression with MSCs over passage, we expected to see a difference in TF between early and late passage MSC-EVs [260]. Interestingly, we did not see any passage-related changed and similar procoagulant activity levels were observed in early and late passage EVs. There was a trend for late passage EVs to have higher activity levels than early passage EVs (66.2 ng/mL versus 41.9 ng/mL, respectively), but this was not significant. There was also a trend for EVs isolated via UC to have higher procoagulant activity levels than SEC-isolated EVs, too (68.7 ng/mL versus 39.4 ng/mL, respectively). This assay had a large amount of variation despite performing technical triplicates and using six independent lines at two passages (P2 and P12). This could be due to biological variability (i.e., line-to-line variation), the sample size, or other sources of experimental variation. Based on the effect size demonstrated here, it was calculated that sample sizes of 30 – 51 would be required to detect significant differences between

passage and isolation method. This is the first report of canine MSC-EV procoagulant activity and the effect size observations should assist with the design of future work.

The assay used here was modified from previously reported EV assays and sufficiently measured the procoagulant activity of MSC-EVs [267, 274]. As noted by others, this assay is time-consuming, labor-intensive, expensive, and has high inter-assay variability [267, 274]. Although the reaction wells were performed with consistent number of EVs, high variability from particle count estimates provided by the NTA, as discussed in Chapter 3, could be a factor here as well. These limitations make this assay not ideal to screen EVs for clinical use as a safety measure. To apply this assay to a clinical setting, optimization would have to be done to decrease variability, time, labor, and cost.

Hisada et al. reported TF-specific procoagulant activity in EVs from human plasma samples [267]. Based on their work and previous studies, they proposed four response categories of EV TF activity: zero (0 to <0.5 pg/mL), weak (0.5 to <1 pg/mL), moderate (1 to <2 pg/mL), and strong (>2 pg/mL) [267, 269]. Based on their proposed classification for EVs from platelet-free plasma, MSC-EVs fall well above the strong category displaying an average procoagulant activity of 54.04 ng/mL (54,040 pg/mL). The much larger value exhibited by MSC-EVs compared to EVs from platelet-free plasma could be due to minor differences in the assay or differences in the activity of the specific EVs themselves. This comparison is concerning due to the fact that the MSC-EVs are displaying a much higher TF-activity level than even what is considered “strong” by others. This supports the procoagulant activity of EVs and alludes to possible safety concerns when used as a therapeutic.

In contrast, Che et al. reported TF-specific activity in EVs from the breast cancer cell line MDA-MB-231 [274]. From their work, they normalized FXa generated per million of tumor cells

producing EVs and reported values between 1 and 2 nM per million cells [274]. In contrast, when our activity levels were normalized per million MSCs, we reported between 0.026 and 0.854 (average 0.329 ± 0.28) nM per $1x10^6$ MSCs. Taken together, this indicates that the procoagulant activity of MSCs falls somewhere in between EVs from plasma and EVs derived from tumor cells.

A drawback of the two EV procoagulant assays previously discussed is that a set volume of EVs is used per reaction well. This creates difficulties when comparing the values across laboratories because the amount of EVs generating FXa varies. Here, we used a set number of EVs ($5x10^7$) per reaction well and balanced volume with buffer. This enabled consistency in the assay so that values exhibited were from differences in cell line, passage, or isolation and not from the amount of EVs in the reaction well.

Here, for the first time, we report a procoagulant activity (FXa generation) per million EVs. Samples ranged from 0.002 to 0.045 (0.023 ± 0.02) nM FXa per $1x10^6$ EVs. This value would better serve for comparison among studies, biological starting material, parental cell type, and other factors. This value also provides an estimate of procoagulant activity that can be calculated for a "dose" of EVs used in a clinical setting.

When comparing the procoagulant activity of $1x10^6$ EVs and $1x10^6$ MSCs, the data suggests that EVs may be less of a procoagulant risk when comparing equal numbers. However, when comparing dose-to-dose, EVs may have higher procoagulant activity levels. A therapeutic dose of MSCs ranges from $3\text{-}5x10^6$ MSCs per kg of body weight. The associated average procoagulant activity of a dose of MSCs ranges from 0.987 – 1.65 nM FXa per kg body weight. However, data indicated that an average of $2.02x10^4$ EVs are released per MSC. Using the low dose of MSCs ($3x10^6$ MSCs/kg), assuming that EVs are the active ingredient of an MSC dose, and that each MSC releases 20,000 EVs, an equivalent dose of EVs would be $6x10^{10}$ EVs. Under these

assumptions, an equivalent dose of EVs may carry an average procoagulant risk of 1405 nM FXa per kg body weight. This data would suggest that when compared dose-to-dose, EVs may have a higher procoagulant risk than MSCs. Conversely, when administering MSCs intravenously, EVs may be released before MSCs are cleared by the immune system. In that case, the procoagulant activity of an MSC dose would have to account for both the cells as well as secreted EVs. However, more work would need to be done to clarify this. Taken together, this data suggests that although EVs carry less procoagulant activity compared to an equal number of MSCs, when compared dose-to-dose, EVs exhibit higher procoagulant activity levels and thus may be considered more of a safety risk.

When data is normalized per million cells or per million EVs, two-thirds of the lines exhibit higher FXa generation by EVs from late passage compared to early passage. In contrast, one-third of the lines exhibit higher FXa generation by EVs from early passage compared to late passage. We can offer no explanation for this other than biological variability. This data indicates that a pattern may exist but a larger sample size with more passages might be needed to clarify. In addition, other biological characteristics such as, sex of donor or breed of donor may impact these results and this may not be resolved without more studies.

Lastly, to confirm that the procoagulant activity exhibited here by MSC-EVs is due to surface TF expression, EVs were incubated with a TF antibody. TF antibody clone HTF-1 is the antibody known to functionally inhibit human TF activity [274, 405-407]. We found that this clone appears to not be compatible with the canine TF epitope. Inhibition of FXa generation was tested using the canine-reactive polyclonal antibody used in dot blots. The antibody was not capable of inhibiting FXa generation by canine or human EVs. From this data, it was clarified whether the canine EV FXa generation was due to TF expression. Since we knew that human MSCs were

reactive with the HTF-1 clone antibody, and that their EVs exhibited similar levels of procoagulant activity to canine, we incubated human MSC EVs with the antibody clone HTF-1, and observed that this antibody inhibited FXa generation. Taken together, we suggest that the procoagulant activity exhibited by MSC-EVs is due to TF expression in canine MSC-EVs, similar to what is observed in human MSC-EVs.

MSCs have been investigated as a potential therapeutic in many modalities due to their ability to regenerate and create a variable, localized anti-inflammatory effect. MSCs exert their therapeutic effects largely through the production and secretion of soluble factors and EVs. EVs have a role in intercellular communication and signaling, antigen presentation, cell adhesion, inflammation, and tissue remodeling. In addition, EVs also share traits with their parental cell type, such as protein expression and cargo. Thus, MSC-EVs represent a potential cell-free therapeutic. Here, we outline the effects of passage and isolation method on canine MSC-EVs. Our data suggests that both parameters are important considerations for EV manufacturing scale-up and clinical translation. In addition, we demonstrate that MSC-EVs, like their parental cells, express TF and this translates to procoagulant activity. Consequently, EV administration is a safety concern and poses a risk of thromboembolism. This is concerning since MSCs, and possibly MSC-EVs, are being explored as a therapeutic in the respiratory complications of COVID-19. Thus, we suggest that the procoagulant activity of EVs may serve as a screening tool in clinical settings.

Chapter 5 - Therapeutic Use of Mesenchymal Stromal Cells: The Need for Inclusive Characterization Guidelines to Accommodate All Tissue Sources and Species

I contributed to all figures and tables. A modified version of Chapter 5 is published in Frontiers in Cell and Developmental Biology | Stem Cell Research [13].

Wright, A., M.L. Arthaud-Day, and M.L. Weiss, Therapeutic Use of Mesenchymal Stromal Cells: The Need for Inclusive Characterization Guidelines to Accommodate All Tissue Sources and Species. Frontiers in Cell and Developmental Biology, 2021. 9(66).

Introduction

Multipotent mesenchymal stromal cells (MSCs) are a heterogeneous population that when expanded in vitro includes stem, progenitor, and differentiated cells. MSCs have been implicated as a therapeutic modality in tissue injuries, chronic degenerative disorders, and inflammatory diseases on account of their regenerative potential and anti-inflammatory properties [1, 3, 44]. Although therapeutic use in humans is the end goal, preclinical research relies on animal models for proof of concept and technique development, and thus animal applications cannot be overlooked. The first isolation and culture of MSCs were performed using bone marrow from guinea pigs (the 1970s) and then extended to rats in the 1980s [8, 408]. Isolation and culture of human MSCs did not begin until the early 1990s [7, 409, 410]. Since then, MSCs have become a

widely studied experimental therapeutic product tested in over 1300 registered clinical trials (clinicaltrials.gov “mesenchymal” 6/5/20) [44]. In human clinical trials, allogeneic MSCs have been consistently shown to be safe but have not been able to replicate the large effect sizes predicted from preclinical research. For this reason, small and large trials have failed to meet efficacy endpoints [44, 411].

A vast preclinical dataset, from both in vitro and in vivo animal studies, supports the notion that MSCs are a potent cellular therapeutic agent. Here, we will review the in vitro preclinical data, but reviews of the in vivo preclinical data can be found here [412-415]. Why is there such a gap between the expectations set by preclinical data and human MSC trials? The inconsistent results could be due to product irregularities, transferability across species, or poor estimation of effect size from preclinical data leading to insignificant findings. Our thesis here is that to move forward strategically, the MSC field needs to recognize and address shortcomings that have been given little consideration in the rush toward clinical development. Preclinical data needs to be strengthened in regards to its ability to be translated. Instead of continuing to produce inconsistent preclinical in vitro and in vivo data that poorly translates, effort should be placed on determining the root of the transferability issues so that consistent, reliable data can be generated allowing for replication across research laboratories. In addition, although the potential of MSCs remains undisputed, questions remain concerning the mechanisms-of-action (MOAs), how in vitro testing correlates to in vivo activity, the number of cells in a dose, the route of administration, and how all of this relates to the therapeutic effects for the various indications [416].

To do this, we believe that first, characterization guidelines need to be updated to accommodate different MSC populations. This includes addressing variations in the literature that may obscure rather than explain MSC's physiological effects that impact therapeutic response.

These inconsistencies include, but are not limited to, MSC tissue source and species-to-species differences. Second, along with updated characterization guidelines, improved standardization in the field would help to eliminate product and lot-to-lot variation as well as address the concern of purity vs. potency. Lastly, to properly address these concerns, more research funding is required. With federal funding on research and development (R&D) declining, and businesses spending over three times the amount of the federal government on R&D, it is clear that industry-sponsored research is critical. Businesses are more prone to fund research that has commercial applicability rather than research that simply addresses a question [417]. By focusing research efforts on areas with commercial potential, not only could this increase research funding but also could decrease time to market.

Challenges for Clinical Translation of Mesenchymal Stromal Cells

Outdated Characterization Guidelines

In the early 1990s, Arnold Caplan was the first to use the term "mesenchymal stem cell" to describe the cells involved in embryonic bone and cartilage formation as well as repair and maintenance in the adult [6]. Following this discovery, many researchers argued that there was no feasible way to prove whether the in vitro cultured MSCs contained stem cells and, because of this, suggested alternative terms to label these cells. Although we still see the term "mesenchymal stem cells" used in literature more than 25 years later, the ISCT released a position piece in 2005 stating that the proper designation for these cells should be a multipotent mesenchymal stromal cell, seeing as they are a heterogeneous population in which not all cells have stem-like properties [10].

Following the nomenclature article, the ISCT's MSC working group released “minimal criteria” that should be demonstrated before a cell can be considered or referred to as an MSC [11]. These simplified guidelines include (1) Tissue culture plastic adherent; (2) Positive (≥95%) for surface antigen markers CD105, CD90, and CD73 while also negative (≤2%) for CD45 (pan-leukocyte), CD34 (hematopoietic and endothelial cells), CD14 or CD11b (monocytes and macrophages), CD79α or CD19 (B cells), and HLA-DR; and (3) Capable of differentiation to adipocytes, chondroblasts, and osteoblasts [11]. This definition is 14 years old and yet still widely used today. Although many researchers do go beyond this minimal definition, many also DO NOT meet this minimum.

The lack of uniformity has contributed to inconsistencies within the field. As noted by Mendicino et al., the current MSC guidelines used for characterization are not distinctive and therefore may not adequately define the cells and their biological function [416]. Furthermore, this simplified definition does not consider species differences, tissue source, and passage of cells at the time of characterization, pointing to the need for refinement or updating of the “minimal criteria.” In 2013, the ISCT amended the MSC definition to include a bioassay of immunosuppressive properties, but it did not refine the original definition. In 2019, ISCT updated their MSC definition to suggest (1) including the tissue origin of cells, (2) use of stromal cell nomenclature unless rigorous evidence for stemness is shown, and (3) including functional assays to define therapeutic mechanism of action, but no tissue-specific guidelines were addressed [418]. Although the ISCT suggestions exist, there has been no enforcement of the issue by academic journals. We suggest that the ISCT follow the International Society for Extracellular Vesicles (ISEV) and the Functional Genomics Data Society (FGED) and establish their own unique set of minimally accepted publication criteria [233, 419].

Biological Variability Translates to MSC Inconsistencies

To simply focus research on commercial use is only part of the picture. Science, either basic science or translational research, depends upon the ability to replicate published work, and hopefully, to extend that work. This includes observational research and hypothesis-driven research. As such, science depends upon the control of experimental variables, and minimizing experimental error. One issue in biology is that certain variables are inherently "variable" due to the complexity of the system, and this adds intricacy to the metrology (the science of measurement).

Historically, problems associated with cell culture have had a significant impact on the field of biology. Issues such as misidentification, the use of contaminated cell cultures (e.g., mycoplasmas), or the effects of phenotypic drift have led to the creation of guidelines that not only highlight the problems, but also provide guidance on how to avoid or eliminate the issues. In some countries, legislation or codes of practice govern research since it interacts with both ethical and scientific boundaries. For example, in stem cell research, the production of new human embryonic cell lines was restricted in the US, forcing science institutions, many which were federally-funded, to use only existing embryonic lines. The result of these sanctions was that researchers were only able to use a handful of preexisting lines that were easy to propagate and make available, thus forcing standardization of the industry. Although this means of standardization was extreme, it still allowed the field to conform thereby inducing reproducible research. Although standardization is not required by the FDA for clinical use, MSC stakeholders should support standardization efforts as it would benefit the field by allowing for more meaningful comparisons among studies,

thus allowing for a smoother clinical translation [416]. Further, replication as a result of standardization would allow for more efficient research, consequently transferring to cost savings.

Regulatory Gaps in MSC Therapy

Currently, there are ten approved MSC therapies worldwide (Table 10) on the market for various indications, yet not a single FDA-approved product for use in the United States [48, 420, 421]. Differences in regulatory approvals around the globe have left gaps where some countries have approved products that have been on the market for over 10 years and other countries still have yet to grant approval to an MSC product. All countries with approved MSC products have a governing body, similar to the FDA, that has regulatory oversight of cell therapy products. Although similar, each country governs their own unique set of regulations and approval processes. These processes are reviewed in depth here [422-428]. To alleviate gaps, some have suggested that the World Health Organization (WHO), an agency within the United Nations (UN), is a logical choice to develop guidelines and recommendations for the Member States [429]. Although not a regulatory authority, WHO has a mandate to advance and advocate for international standards involving biological and pharmaceutical products, and many countries look to WHO for guidance in developing guidelines [429].

Table 10: MSC Products with Regulatory Approval

MSC Product (company)	*Approval Granted (Year)*	*Indication*	*Product Type*
Queencell (Anterogen Co. Ltd.)	South Korea (2010)	Subcutaneous tissue defects	Autologous human AT-MSC
Cellgram-AMI (Pharmicell Co. Ltd.)	South Korea (2011)	Acute myocardial infarction	Autologous human BM-MSC
Cartistem (Medipost Co. Ltd.)	South Korea (2012)	Knee articular cartilage defects	Allogeneic human UC-MSC
Cupistem (Anterogen Co. Ltd.)	South Korea (2012)	Crohn's fistula	Autologous human BM-MSC
Prochymal remestemcel-L (Osiris Therapeutics, Inc. Mesoblast Ltd.)	Canada (2012) New Zealand (2012)	GvHD	Allogeneic human BM-MSC
Neuronata-R (Corestem Inc.)	South Korea (2014)	Amyotrophic lateral sclerosis	Autologous human BM-MSC
Temcell HS (JCR Pharmaceuticals)	Japan (2015)	GvHD	Allogeneic human BM-MSC
Stempeucel (Stempeutics Research PVT)	India (2016)	Critical limb ischemia	Allogeneic human BM-MSC
Alofisel (TiGenix NV/Takeda)	Europe (2018)	Complex perianal fistulas in Crohn's disease	Allogeneic human AT-MSC
Stemirac (Nipro Corp)	Japan (2018	Spinal cord injury	Autologous human BM-MSC

Table data derived from [48, 420].

In the US, culture-expanded MSC-like cells are considered to be a more-than-minimally-manipulated cellular and gene therapy (CGT) product regulated by section 351 of the Public Health Service (PHS) Act 42 U.S.C.262 [278]. Due to this designation, MSC-like cells require an Investigational New Drug (IND) application and approval from the FDA to be used in a clinical trial [278]. Under this regulation, a test to measure potency as part of the release criteria is required although standardization among the field and ISCT minimal criteria are not required [278, 430]. The FDA has released guidelines for CGT products, regulated under the Code of Federal Regulations (CFR) 210, 211 that outline release testing. The guidance released by the FDA includes: demonstration of biological activity (potency); quantitative data; pre-defined acceptance and/or rejection criteria; employment of appropriate standards, controls, and reference materials; documentation of accuracy, sensitivity, specificity, and reproducibility of test methods; ingredient strength and identity; dating periods; and labeling requirements [278, 431].

Similarly, in Europe, clinical MSCs are considered an advanced therapy medicinal product (ATMP) in accordance with the European Medicines Agency (EMA) regulation 1394/2007 of the European commission (EC) [422, 432, 433]. Under the ATMP, the identity and impurities of the MSCs must be described using the ISCT minimal criteria or a modification to the criteria [10, 11, 432-434]. In addition, release criteria, which vary by type of clinical trial and requirements from other national competent authorities, are also governed under the ATMP and include contamination screening (microbial, endotoxin, and mycoplasma), viability, clonogenicity, identity, purity, and functional tests [422, 432, 433]. Europe's regulatory approval process for cell therapy products is reviewed more thoroughly here [422, 435]. Although, the ISCT made a point to clarify that their 2006 proposed guidelines should not be confused with final product release

criteria, the ATMP regulations, along with the literature and FDA regulation submissions point to the fact that they may be seen as synonymous by some [416].

Although the FDA has released recommendations for developing tests to measure potency of the MSC product, the FDA does not provide recommendations regarding which specific assay should be used. Currently, each IND application is reviewed based on individual product attributes and is not compared to other MSC products [44, 278]. Due to the biological nature and limited amount of the MSC product, hurdles exist that make development of assays and standardization difficult. Galipeau and Senséb review these challenges thoroughly and they list a number of problems such as variability of raw materials, limited product for testing, absence of appropriate standards, and in vivo fate of the product [44]. For "biologics" (i.e., biologically-derived therapeutics) such as MSC-based therapeutics to be successfully manufactured at large scale, they must meet four criteria: (1) a stable and well-defined cell line; (2) a good manufacturing practice (GMP)-grade supply chain with a process control plan that has set variability values that produce a product with the desired therapeutic effect; (3) a standardized procedure that allows for process changes while maintaining product consistency; and (4) integrated redundancy and flexibility to allow for adaptation without sacrificing product consistency [436]. Even with these criteria met, biologics are still produced from living organisms and this variability causes product changes (e.g., quality, behavior, safety) that in turn affect the clinical use [436].

An analysis of FDA IND applications by Mendicino et al. revealed variability in MSC tissue sources, manufacturing methods, and MSC characterization [416]. Interestingly, it was noted that only 7 of the 9 ISCT-recommended MSC markers were ranked in the top 20 markers used by applicants to characterize human MSCs [416]. In addition, they discovered that applications were submitted with MSC-characterization markers reported well below the 95%

proposed by the ISCT, e.g., submissions with CD105 reported at only ~80%, although it is unclear whether this impacts MSC function or not [416]. This data brings the ISCT guidelines into question. If the end goal is clinical use as an FDA-approved therapeutic, yet the FDA does not require the proposed criteria, and they are not consistently demonstrated by applicants, what purpose are they serving related to that goal? If applicants are struggling to meet these guidelines, how well are the guidelines serving the human MSC product? Further, how can it be expected that nonhuman MSCs will adhere to these standards? To combat MSC product inconsistencies and ensure successful clinical translation, variability in the process and product must be realized, described, and managed.

Additionally, as noted in a review from the FDA, MSC manufacturing reflects a broadening of MSC characterization release criteria that are associated with phased clinical testing [416]. This is the opposite of what the FDA expects and is a double-edged sword—allowing cells which fail to meet MSC criteria in the released MSC product may have secondary consequences of reduced potency and increased lot-to-lot variation. It should be noted that although MSC characterization is not required by the FDA, generating a consensus MSC definition would benefit all MSC shareholders as it would enable comparison across studies and enable therapeutic use by producing more consistent effect sizes [416].

MSC-Based Products Also Suffer from Lack of Standardization

MSCs being a product-by-process has implications that challenge the field, and it is a barrier to the idea that an MSC is a defined cell type. First, it implies that a process is necessary to generate or enrich cells of interest. Note that a similar notion is applied to pluripotent stem cells (PSCs), where the cells of interest are unnatural artifacts of the culture process and the culture

conditions required to maintain them as immortal cells are known. In contrast, MSCs are mortal cells since the culture conditions needed to render MSCs as immortal cells are unknown. The product-by-process, together with the mortality of MSCs, implies that different MSC products are obtained at different times. Further, measures may reflect processes, and thus parse rather than unify.

The product-by-process assumption implies that prospective identification of MSCs is irrelevant since the product requires processing to be revealed. It also implies that different products are produced by altering the process. For example, “priming” MSCs by exposure to inflammatory cytokines can cause significant changes to MSCs such as inducing expression of MHC II [437, 438]. Moreover, the product-by-process focuses on in vitro and not the in vivo functionality of MSCs, and this is a key shortcoming to clinical translation.

If we embrace the product-by-process notion for MSCs, like we do PSCs, we can perhaps refocus efforts on what we can control and measure. For example, of the methods used to define MSCs, flow cytometry is the best method of cellular-level measurement that lends itself to metrology, i.e., a reference measurement system with traceability to the SI or other internationally agreed-upon units. In contrast, tri-lineage differentiation assays cannot be considered metrology as they lack defined measurands and reference materials. Therefore, we suggest that the MSC field develop and require measurable differentiation assays for publication.

It was once believed that the primary mechanisms of action for MSCs was contact-dependent signaling and engraftment into tissues, based on their potential for differentiation [63]. In the past few years, it has become more widely accepted that MSCs' primary mechanism of action is through a paracrine effect. Through the paracrine effect, MSCs can secrete biologically active molecules, such as cytokines, chemokines, growth factors, extracellular matrix, and

extracellular vesicles (EVs) [439]. These molecules act therapeutically to stimulate tissue regeneration and angiogenesis as well as to modify inflammation, apoptosis, and fibrosis [440-443]. Due to their regenerative potential, EVs derived from MSCs (MSC-EVs) have become a target for therapeutic use. Preclinical data indicates that MSC-EVs may possess therapeutic behaviors similar to their parent cell of origin but with the additional benefit of using a cell-free product [444-446]. Although promising, the issue at hand is that without a consensus on the guidelines for characterizing an MSC, how can we logically move forward with MSC-based products? EVs isolated from conditioned media come with their own unique inconsistencies that can be due to parent cell of origin, the health of the cell donor, isolation and separation method, and storage condition [209, 323]. Taken together with MSCs, the inconsistencies between the two products can only multiply when MSCs are used to manufacture EVs. Establishing guidelines for MSCs would further benefit EV research by allowing scientists to focus efforts on EVs rather than attempting to parse out inconsistencies from both sources.

Tissue Source Differences

MSC-like cells have been found in many tissues but due to the fact that MSCs were first described in the bone marrow (BM), BM-MSCs have dominated the field and are the focus for the defining criteria. BM harvest is a painful and invasive procedure. BM-MSCs isolated from elderly donors have been shown to be less “stemmy,” and difficult, or sometimes impossible, to expand since they rapidly senesce [7, 25]. Here, “stemmy” is referring to cells within the MSC population with stem cell-like properties. Other adult tissue-derived MSCs such as adipose tissue (AT); dental pulp; muscle; and extra-embryonic tissues, such as the umbilical cord stroma, umbilical cord blood, and placenta, are also rich sources of MSCs [12]. Some of these tissues, such as AT and

extra-embryonic tissues, can be harvested rather easily secondary to routine or elective procedures. Furthermore, extra-embryonic tissues represent a painlessly-collected, virtually inexhaustible resource for MSC isolations. Consequently, they may represent an ideal source for MSCs because they are easily and painlessly obtained from donors of a consistent young age, hence minimizing the potential effects of aging or prior health conditions on the MSC pool.

Research groups may have a strong preference regarding which MSC tissue source they study and strong beliefs lead to claims of perceived superiority of a particular tissue source. Although there is consensus that MSCs derived from various tissues are not identical, the differences regarding characterization, and other behaviors, are often overlooked or perhaps exaggerated. The strongest evidence for this fact comes from the joint statement put out from the International Federation for Adipose Therapeutics (IFATS) and the ISCT in 2013 establishing an amended set of minimal guidelines for characterization of the uncultured stromal vascular fraction (SVF) and cultured stromal cells both derived from adipose tissue [14]. Importantly, these guidelines acknowledge that SVF can be CD34+ and adds CD44 (positive) and CD31 (negative) to the panel for cultured adipose-derived MSCs [14]. Interestingly, tissue-specific guidelines do not exist for other sources.

The literature highlighting tissue-specific MSC differences is vast but can often be conflicting and difficult to interpret. For example, umbilical cord-derived (UC-MSCs) and adipose-derived (AT) MSCs have been shown to have a higher proliferative capacity when compared to BM-MSCs [19, 30, 440, 447-450]. Lu et al. reported a constant population doubling time (PDT) for human UC-MSCs passage 1−10 of ~24 h compared to a PDT of ~40 h for BM-MSCs, which increased significantly after passage 6 [30]. Peng et al. not only reported different PDTs of rat AT-MSCs compared to BM (45.2 h compared to 61.2 h, respectively) but also noted

that BM-MSCs are morphologically larger than AT-MSCs [451]. In regards to differentiation potential, BM-MSCs have been shown to have increased osteogenic potential and decreased adipogenic potential compared to AT-MSCs [452, 453]. Chen et al. demonstrated that although human BM- and UC-MSCs have similar adipogenic, chondrogenic, and osteogenic potential, UC-MSCs have a higher endothelial differentiation potential making them ideal for neovascularization of engineered tissues [440]. Work reported from gene expression pathway analysis suggests that MSCs derived from human UC and amniotic membrane may possess an increased immunomodulatory capacity compared to BM-MSCs, while BM-MSCs have a higher potential for neuronal differentiation and development [34]. Interestingly, in human placenta-, UC-, and amniotic membrane-derived MSCs, CD105 and CD29 expression was found to be negatively correlated to maternal age [454, 455]. In equines, gene expression data found significant differences in CD44, CD90, CD29, and CD34 between BM and AT-MSCs [456].

Species Differences

The ISCT's MSC definitions were based upon human BM-MSCs yet a large portion of MSC preclinical work is done in other species. Similar to pluripotent stem cells (PSCs), human MSCs are likely to have different characteristics than MSCs derived from other animals. To further complicate the matter, human MSCs also share some defining characteristics with animal MSCs, as shown in the case of human PSCs compared to rat and mouse PSCs [457]. These similarities and differences between MSCs across species should be embraced to gain consensus and uniformity in the field [458-460]. Additionally, availability and reliability of many antibodies against key surface markers are disparate across species, making it difficult to find reliable

information for MSC characterization [12]. Hence, it can be difficult to determine whether characterization differences are true differences or an artifact of antibody selection/performance.

Further, the tri-lineage differentiation potential of MSCs derived from nonhuman species is similar but not identical [460, 461]. Scuteri et al. showed that BM-derived rat MSCs vary in their differentiation potential compared to BM-derived human MSCs in standard culture conditions [462]. In terms of osteogenic and chondrogenic differentiation, the time required for differentiation was different between rat and human MSCs, while in adipogenic differentiation, human MSCs had a greater capacity than rat MSCs [462]. In the canine MSC literature, it has been proposed that differentiation to two lineages is sufficient for characterization rather than three [46, 297, 316, 461, 463]. In our review of 46 canine MSC papers, 22 (48%) demonstrated differentiation to three lineages. Of the remaining papers, 11 (24%) demonstrated differentiation to 2 of the lineages, and 10 (22%) papers did not address differentiation of the MSCs in any capacity [12]. Of those, the most common lineage not shown, or not successful, was chondrogenic, which can be difficult [464].

One similarity that all species seem to share is that differentiation potential decreases as cumulative population doublings increase. This attribute appears to be consistent among all lineages, species, and tissue sources [465-468]. This evidence indicates that a true property of MSCs perhaps is a loss of potency, or "stemness," with time in culture. Despite this common feature, no priority has been placed on developing a standardized quantitative assay to measure differentiation or setting a standard number of cumulative population doublings at which differentiation potential should be assessed. In many cases, that information is not provided in MSC literature.

Mouse BM-derived MSCs have been shown to vary notably from human MSCs in their surface marker expression, specifically in the instance of CD34 [461]. Hu et al. demonstrated that BM-MSCs from C57BL/6 mice expressed high levels of CD34 but lacked CD90 as well as noted slight strain differences in surface marker expression [459]. In our laboratory, canine MSCs derived from the UC require different culture conditions with regard to attachment factors, media formulation, and lifting agents compared to human UC-derived MSCs [12, 23]. Further, we have demonstrated that canine UC-MSCs express CD34 and CD90, albeit CD90 expression is not as high as human UC-MSCs [12]. While others have also shown that canine MSCs express CD34, this finding raises concerns about the similarities of MSCs from different species [104, 311, 314]. AT-derived MSCs from rhesus monkeys and horses were shown to have related biological properties to human MSCs but differ in expression of surface markers and proliferation rates [456, 460, 469]. AT-derived MSCs from rats and mice have also been shown to exhibit similar yet different surface marker expression compared to human AT-MSCs [460, 470, 471].

As shown in Figure 34, in the canine MSC literature, there is a problem with demonstrating surface marker expression of all 3 classic MSC markers designated by the ISCT (CD73, CD90, and CD105). Some researchers believe that positive expression of CD44 and CD90 along with the negative expression of CD34, CD45, CD80, CD86, or MHC II is sufficient to characterize canine MSCs [46, 297, 316, 461, 463]. Of the 46 papers reviewed, 41 (89%) either had negative results or did not report results for CD73, while only 4 (9%) had positive results (generously defined as >50% surface marker expression), and 1 (2%) had moderate expression (as defined as ≥5%—<50%). Note here the discrepancy in "positive" expression. The ISCT definition dictates that the MSCs should have ≥95% surface marker expression to be deemed positive yet instances exist of researchers stating positive results in populations with <50% expression. While CD90 expression

was most consistently reported, only 27 (57%) of papers reviewed had positive expression. For CD105 expression, 37 (79%) of the papers reviewed had negative or unreported results. Bearden et al. (2017) reported that not only was CD105 expression more variable in canine MSCs than seen in humans, but it was also variable among canine MSC tissue sources. In the flow cytometric analysis of canine MSCs isolated from adipose, bone marrow, and synovium at the same passage, CD105 expression in MSCs derived from adipose (~60%) and synovium (~46%) was significantly higher than from bone marrow (~17%) [310].

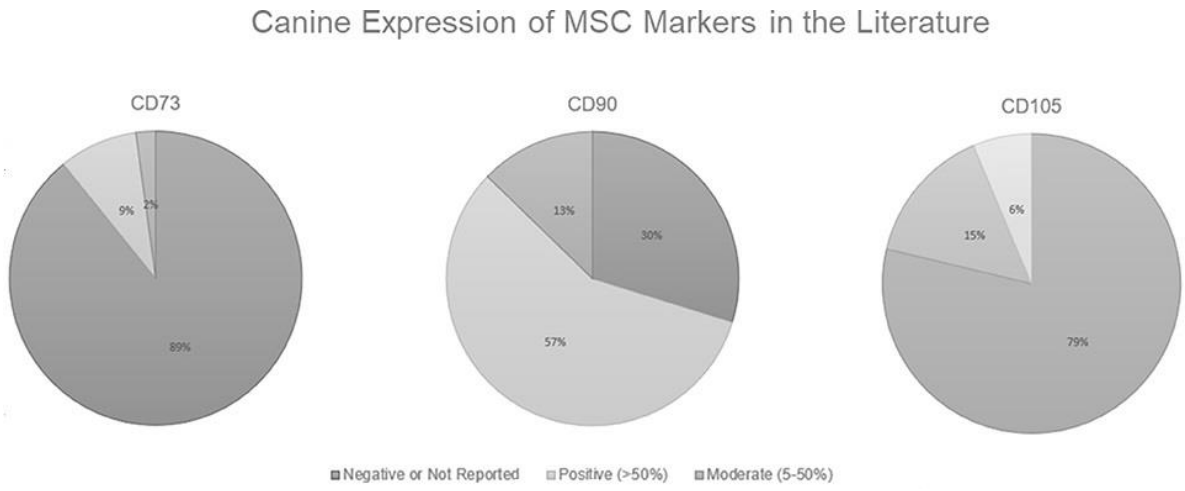

Figure 34: Canine Expression of MSC Markers in the Literature
Canine Expression of MSC Markers in the Literature. Positive expression is defined here as >50% surface marker expression, moderate is defined as ≥5%— <50%, and anything <5% is considered to be a negative result. Data derived from [12].

Although some researchers report that MSCs are positive for a certain surface marker, what designates a positive expression is not clear and can be seen as subjective. The ISCT standards state that MSCs should be ≥95% expression for humans and other species are often held to this same standard [11]. We, and others, have only been able to demonstrate positive expression by

approximately half, or even less, of the population [12, 105, 292, 298, 299, 472-476]. In the canine literature, this seems to be an issue with CD90 in particular [12, 102, 105, 298, 299, 472, 473]. Further, in earlier published work, we demonstrated that there was no difference in expression between an antibody raised specifically to canine for CD90 and a human antibody with canine cross-reactivity [12]. Either there is lower expression of CD90 in canine MSCs or there are issues with antibody specificity.

In a review of MSCs derived from other species, all species noted some difficulties exhibiting expression of the 3 classic MSC markers. In the equine literature, CD73 and CD105 are most often unreported or negative [42, 43, 456, 474, 477-482]. In mouse literature, there are several examples of researchers being able to demonstrate one marker and not the other two, but no clear pattern as to which marker is shown to have positive expression [483-488]. In rat literature, there are also several examples of researchers being able to demonstrate one marker and not the other two, with all of the examples including CD105 as one of the two surface markers missing or negatively expressed [489-493]. Porcine [494-498], ovine [499-501], rabbit [476, 502-504], bovine [239, 505-507], buffalo [508], and chickens [509] also demonstrate negative or missing classic MSC surface marker expression with no clear pattern or rationale. Interestingly, Kamm et al. noted significantly higher CD90 cell surface expression in MSCs derived from universal blood donor Standardbred equines compared to non-blood donor Standardbreds [480].

There is no way to know for certain if the negative results are true negatives, alluding to the fact that surface marker expression of MSCs varies by species, or if the antibody availability is limited for other species causing false negatives. There is evidence for both claims leading us to believe that it is a combination of the two. Researchers have demonstrated that these markers are present at the mRNA level, even if the protein expression is negative or not strongly positive [12,

197, 465]. Although not equal to showing surface marker protein expression, the fact that researchers feel compelled to demonstrate classic MSC markers at the mRNA level, yet cannot produce ISCT-standard flow cytometric data, brings the surface marker panel for MSC characterization into question. By holding MSCs from nonhuman species accountable for human characterization criteria, are we excluding valuable data from the field? Instead, we should be working toward a new consensus that makes accommodations for non-human MSCs.

MSC Heterogeneity

When considered jointly, the definition of an MSC and the ISCT minimal defining criteria contradict one another. On one hand, there is the definition of MSCs—a heterogeneous population that includes stem, progenitor, and differentiated cells. On the other hand, there are the guidelines for demonstrating that these cells are indeed MSCs, which includes plastic-adherence, tri-lineage differentiation, and a panel of positive and negative surface markers in which the positive should be expressed in ≥95% of the population [11]. Where did 95% come from? It may be unrealistic to assume that a heterogeneous population of cells, derived by different methods, from different tissues and species, may be able to demonstrate such high expression of a single marker, let alone an entire panel. Perhaps in the journey to reach a consensus on what an MSC is, the actual intent has been lost.

In addition, the definition of an MSC includes those cells from all tissues, yet the guidelines were established for human BM-MSCs. Researchers have been liberal with applying these guidelines to MSCs from many tissue sources and species. This act alone implies that MSCs isolated from different tissues and species are phenotypically and functionally similar. MSCs are not uniform and to insist that they are is unnecessarily forcing a round peg into a square hole.

There is considerable evidence pointing to differences in MSCs derived from different culture conditions, different tissue sources, different aged donors, and different species. These differences are exhibited in MSC surface marker expression, their culture requirements, their longevity in culture, their transcriptome, their response to stimulation, and their growth rate. Taken together, this alludes to the fact that a simple definition might not properly serve all MSCs.

Purity vs. Potency

The issue remains that the characterization guidelines are nonspecific and, as discussed above, MSCs are a heterogenous population of cells with different gene expression profiles, differentiation and proliferation potential, and phenotype, which are all influenced by donor age, tissue source, species of origin, isolation procedure, and culture conditions [510]. It is still unclear whether surface marker characterization, which is meant to assess the purity of the population, is correlated to functional activity, or potency of the MSCs. To combat this, most researchers use a functional assay to demonstrate potency of the cells. The assay should relate to the intended therapeutic MOA, but assays are left to the discretion of the researcher. At this time, it is still unclear whether in vitro functional assays correlate to in vivo activity, and that assumption is a major flaw with potency measures.

Need for an Expanded Surface Marker Characterization Panel

Even with the species variations considered, there are surface markers that are more uniformly expressed on MSCs of all species that are often included in flow cytometric panels (even in commercially available kits), and are thought of as “standard” MSC markers– yet they are not included in the ISCT characterization guidelines. Expression of CD44 and CD29 should be

considered as logical additions to the MSC surface marker panel and adding them may give researchers working with nonhuman species additional options for MSC characterization.

CD44 is a hyaluronic acid receptor and a critical adhesion molecule. CD44 has been found to be highly expressed on MSCs derived from human [23, 65, 511-524], canine [12, 102, 294, 473, 525-527], equine [42, 43, 467, 474, 477, 478, 480-482], mouse [331, 483, 486, 488, 528, 529], rat [489-492, 530, 531], rabbit [476, 502-504], buffalo [508, 532], bovine [239, 505-507], porcine [494, 496-498], ovine [499, 500, 533], and chickens [509]. CD44 expression is often associated with cell proliferation and migration [530, 534, 535]. It has been reported that CD44 expression in MSCs, both human and mice, is a product of in vitro culture as freshly isolated MSCs do not express CD44 until after cultured [536]. On the contrary, some have demonstrated that CD44+ primary isolates are present [331, 468, 474, 537]. Many researchers have documented increased CD44 expression on MSCs of multiple species with time in culture [468, 474, 519, 536] with only minimal evidence of CD44 expression decreasing as time in culture increases [467]. Since flow cytometry assesses cell surface markers, the dissociation of MSCs using trypsin is also problematic due to cleavage or disruption of antigens. For example, trypsin dissociation significantly reduces CD44 expression, as well as other MSC surface markers, on human MSCs compared to other dissociation agents such as TrypLE [538]. Further, CD44 expression may also affect the chondrogenic differentiation of human MSCs via the Smad 2/3 and ERK ½ signaling pathway [539]. In UC blood-derived MSCs, Kwon et al. demonstrated that CD44 has an immunoregulatory role as evidenced by the induction of macrophage polarization via CD44 expression by the proteoglycan, decorin [540].

CD29, integrin beta-1, is a cell surface receptor that is involved in cell adhesion. CD29 has been found to be “highly” expressed (≥95%) on MSCs derived from human [18, 65, 455, 511-516,

519, 522-524, 541, 542], rat [449, 493, 543-545], equine [43, 456, 477, 479, 482, 546], canine [294, 525, 526], mouse [483, 488], porcine [495, 497, 498], buffalo [532], rabbit [476, 502], bovine [505, 506], and chickens [509]. Evidence suggests that CD29 expression may be involved with MSC migration along with CD73 [547]. CD29 and CD105 expression has been found to be negatively correlated with maternal age on human placenta- and UC-derived MSCs and was proposed as a marker for quality control [454, 455]. Both CD29 and CD44 expression were found to be involved with MSC adhesion, migration, and engraftment in the diseased liver [512].

A total of 72% of canine papers demonstrated either a single alternative MSC marker (CD29 or CD44) or both, which is more consistent than any of the classic MSC markers (Figure 34). This remains true with all other species examined here. All species noted here were able to demonstrate expression of either CD29, CD44, or both as a positive surface marker and at levels >50% of the population. Because of this, we believe that both CD29 and CD44 are logical additions to the MSC markers for all species, due to their demonstrated high expression levels and inclusion within all species. Although both CD29 and CD44 are expressed on epithelial cells, epithelial cells do not express the classic MSC markers CD105, CD90, and CD73, hence CD31 could be added as a negative marker for MSC characterization [522, 548]. The addition of CD44 and CD31 has already been done in the IFATS guidelines for cultured adipose-derived MSCs [14].

Other markers, such as Stro-1, CD271, CD362, and ABCB5, are also considered as MSC markers by some researchers and even used for MSC flow sorting [549-552]. However, in our review we did not find these antibodies to be as available for other species or as well-demonstrated in the literature as CD29 and CD44. For those reasons we suggest CD29 and CD44 as the next logical additions to the MSC panel. Perhaps attempting to make generalized criteria to define MSCs from any tissue source, any species, and any culture conditions is too simplistic. Rather, an

updated species- and tissue-specific set of criteria could better serve the field of MSC research given that they are specific and reproducible [553]. Further, MSCs may represent different products, and treating them as homogeneous may impede new work in the field.

Metrology Standards

It is recognized that the MSC definition casts a "wide net" as it does not rely upon a single cell surface marker or activity assay that can prospectively identify the stemmy population within the mixed population. In lieu of a single surface marker, a surface marker analysis panel, consisting of both positive and negative markers, is one key element to defining MSCs. There is a vast amount of literature that addresses the flow cytometric analysis of MSCs, and it is quite challenging to compare the results between laboratories [460].

In response to this issue, some experts have proposed that MSC lines be generated and highly characterized to serve as "gold standard" lines for calibration [289, 554]. Others have suggested the use of dedicated laboratories to serve as characterization centers for MSCs to enable standardized characterization in the field, as has been done with certain diagnostic tests. We find that both of these proposals come with their own advantages and disadvantages. A third, and perhaps more realistic consideration might be to forgo the simplified definition of an MSC in favor of guidelines that are specific to the species and tissue used to generate the MSCs. Generating a consensus sponsored by the ISCT around authentication methods and materials, e.g., specific monoclonal antibody clones, protocols, and criteria regarding positive and negative staining, as well as a consistent presentation of results, would enable reproducibility and comparison across laboratories.

Since the National Institutes of Health (NIH) and National Science Foundation (SF) require authentication of biological reagents, we suggest that cellular metrology standards be set, just as they have been for other biologicals such as microbiology strains, bacteria, and cancer cell lines. Standards set by the community should provide guidance for publication, reproducibility requirements, and authentication standards. It is our belief that the ISCT should establish MSC metrology guidelines by species and tissue source; generate a consensus-gathering list of available and acceptable resources for characterization by species and tissue source; and enumerate guidelines that dictate the minimal information required for published MSC studies that includes characterization, methodology, and reproducibility requirements.

Research Driven by Commercial Applicability

Despite the nuances, a shared trait among all MSCs is that they possess unique and tissue-specific differences in immunomodulatory properties and regenerative potential. To simply take advantage of these unique features and push MSCs to market for therapeutic use is not feasible. Questions remain concerning the mechanism of action, how in vitro testing correlates to in vivo activity, the number of cells in a dose, the route of administration, and how all of this relates to the therapeutic effects for the various indications [416]. To properly address these concerns, more research funding is required.

In the United States, R&D is primarily funded through the federal government, state governments, businesses, academia, and nonprofit organizations. From historical data dating back to 1953, businesses and the federal government combined have accounted for over 90% of the R&D expenditures [417]. While the federal government suffered 7 consecutive years of declines

in funding (2009-2016), businesses have increased funding since 1953 [417]. In the most recent data for the fiscal year 2018 released this year, the federal government spent $127.3 billion on R&D while businesses spent $404.2 billion and state governments, academia, and nonprofit organizations spent a combined $48.5 billion [417]. Although it cannot be parsed out exactly where these funds were distributed, the point can be made that businesses are spending 2-4x more money on R&D than the US government. In a search of sponsored clinical trials in the United States (clinicaltrials.gov, search MSC, all trials, US, 7/29/20), other sponsors (individuals, universities, and organizations) accounted for almost half of the 1,195 total registered clinical trials (578), while industries sponsored 368, and NIH and other federal agencies accounted for 279, the smallest pool.

Research supported by federally-funded grants is fundamentally different from industry-sponsored research. While both are critical to moving science forward, federally-funded research addresses questions aiming to fill a void of knowledge. Industry-sponsored research is more focused on topics with a clear commercial application and an established large market share [555]. For example, work examining biomedical research funding in the United States from the early 2000s found that industries were more likely to sponsor research centered around diseases projected to afflict areas of higher income as opposed to NIH funding targeting diseases with a global burden [555, 556]. MSCs represent an attractive research topic because they have applicability for numerous indications with widespread prevalence, an established market share, and the potential to outperform many standard of care therapies. Research focused on the big picture, i.e., commercial use of MSCs, could attract more industries looking to enter the MSC market, thus leading to increased research funds from industry sponsors. Here, we will compare the market of allogeneic and autologous MSC therapy. We should note that there are many other

factors to take into consideration such as shipping logistics, cryopreservation, culture conditions, and manipulations to alter therapeutic effect (e.g., priming) that are not addressed here.

Allogeneic MSC Therapy Represents a Viable Business Model

MSCs can be used therapeutically in either an autologous or allogeneic manner and both have their own unique set of benefits and limitations. Autologous MSC therapies are considered a lower risk than allogeneic therapies for humans with intact immune systems. The two types of therapies are not synonymous and the results cannot be compared across clinical trials. Further, within allogeneic and autologous therapies, other factors such as preparative regimen, administration method, disease models, the dosage of MSCs administered, and the use of either culture-expanded or cryopreserved cells should also be carefully considered before comparing results, as they possibly impact therapeutic effectiveness of MSCs and the cells' ability to meet primary endpoints.

Autologous MSCs are a form of personalized medicine and are of less risk immunologically since they are one's cells. However, autologous MSCs typically require in vitro culture-expansion to produce enough cells to constitute a therapeutic dose. Hence, they are limited to situations in which time is not a critical factor and collection is feasible. Turnaround times from harvest to patient administration can vary widely due to the variable proliferation rates among patients and the number of cells required for a therapeutic dose. Further, MSCs have been shown to be less efficacious when harvested from elderly donors, thus limiting the potential patient pool [285, 286]. The high cost of autologous MSC therapy coupled with the lack of insurance coverage makes it unattainable for the majority of possible recipients. Despite causing heavy criticism and providing risky services that claim to provide unproven results, unregulated “stem” cell clinics

around the world demonstrate that the market demand for cell therapy exists. In fact, the global market demand for MSCs is expected to reach $7.5 billion USD by 2022, with the US expected to have the largest market share (34.3%) despite the fact that the US has yet to grant approval to an MSC product [420]. It should be noted that unregulated stem cell clinics operate using a "minimally-manipulated" product or a homologous lipoaspirate [21 CFR 1271.10(a)(1) and 21 CFR 1271.10(a)(2), respectively]. It is unclear whether or not this will continue to be an exempt product in the future. It should be noted that MSCs are not considered minimally manipulated since they require in vitro expansion and thus are not exempt.

Industry sponsors have funded the majority of advanced phase clinical trials [44, 442]. Without industry support, getting MSC products approved for use is cost prohibitive. To gain industry backing, a clear path to profitability must be established in a manufacturing market that is driven by margins. To explore potential markets, let us apply a standard business model used to analyze industry profitability (Figure 35). Michael Porter's "five forces" approach to industry analysis examines the broader industry structure to determine the overall attractiveness of an industry for investment [557]. In addition to interfirm rivalry, profit potential is determined by the threat of new entrants, the availability of attractive substitutes, and the power of suppliers and buyers, respectively.

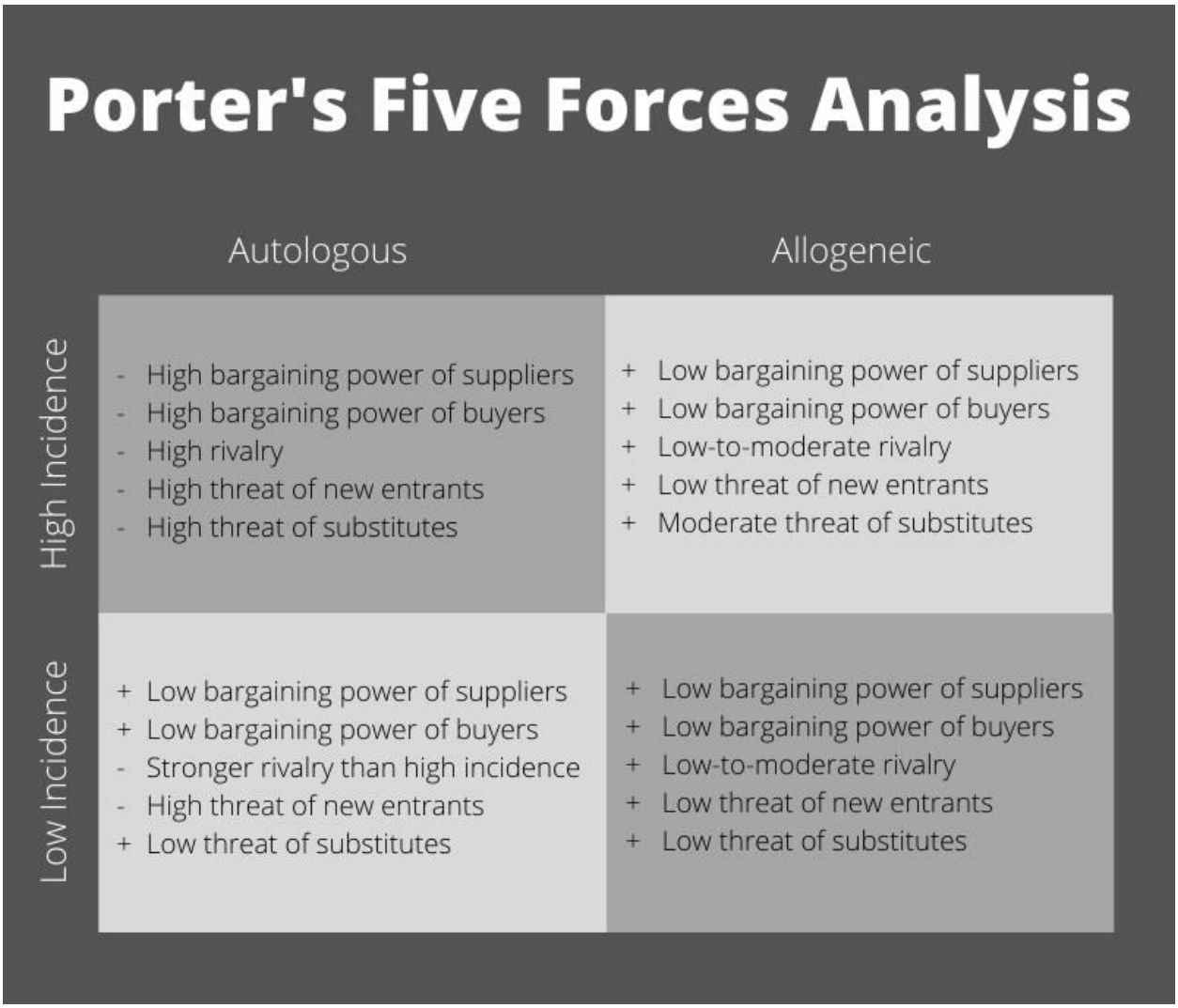

Figure 35: Porter's Five Forces Analysis

Porter's five forces analysis of the competitive environment within MSC clinical use.

The most logical pathway to commercialization is to target a sizable indication with a high incidence rate (Figure 35). Applying Porter's five forces model, autologous cell therapy does not appear to have the ability to produce an adequate profit pool. The industry is fully reliant on donors' willingness and suitability to provide the key input (autologous cells) as well as their desire and ability to pay (e.g., high buyer and supplier power). Due to the nature of the manufacturing process for autologous cells, production processes are not scalable. Large batch manufacturing is not cost

effective; as a result, production remains dominated by small, local laboratories. Without economies of scale to serve as an entry barrier, autologous MSC therapy has a high risk of new entrants, making for a highly competitive environment. Further, it is worth clarifying that there are two patent pathways: cell line and production/differentiation techniques. With autologous MSC therapy, cell lines, although more easily patentable and marketable, are moot and this leaves process patents. As evidenced in iPSC technology, process patents come with unique challenges such as a low number of approvals compared to applications (e.g., only 11% of applications approved by the European Patent Office with 89% waiting to be reviewed), differences in international intellectual property laws, and small patent portfolios distributed among several entities [558, 559]. Particularly, patents are an issue in Europe where exemptions to patentability exist that may affect stem cell therapeutics, specifically the "use of human embryos for industrial or commercial purposes" [558]. Additionally, patents can be seen as risky since the regulatory approval process to get cell therapies to market is quite long; patents may expire before the technology can be utilized commercially [559]. Because of this, many companies rely on trade secrets, which allow for processes to be improved and protected from common knowledge, but alleviate the concern of expired patents, making trade secrets a more viable alternative to intellectual property [559]. So, in the case of autologous cell therapy, you're left with a splintered landscape of patents and trade secrets where companies are forced to "brand" their technology to convince the market that they have any sort of strategic competitive advantage. This leaves a perfectly competitive market of a wide range of technological advances where it is difficult for brands to build brand recognition and demand a premium price compared to other competitors. Autologous MSC therapy also has a high risk of substitution. A majority of high incidence indications already have an existing standard of care produced using efficient manufacturing

processes that have been refined over the years. To even be considered, autologous MSCs would have to demonstrate therapeutic benefits and safety beyond currently approved modalities to justify the higher cost. In this context, multiple, small firms would be forced to compete based on price alone (i.e., perfect competition), narrowing profit margins even further and making autologous cell therapy an unattractive industry to enter.

In contrast, allogeneic MSCs have the potential to be a readily-available product that can serve in instances of acute disorders where time to culture-expand cells is not feasible, or as an option for patients who are not able to serve as their own donor. Because allogeneic MSCs may be produced from a wider pool of "qualified" donors, producers have much greater control over their supply chain. Meanwhile, manufacturing processes for allogeneic cell therapies are more closely related to other noncellular pharmaceuticals and biologics. Based on these similarities, protocols for culture-expansion of cells in smaller batches could easily be scaled up using existing technologies and equipment. Particularly if automated, large-scale manufacturing of allogeneic cell therapies would spread the cost of goods, labor, and quality control across more samples, thus lowering the cost of production per sample, making this option ideal to treat large numbers of patients. Due to economies of scale, allogeneic MSCs would face a lower risk of new entrants and fewer overall competitors. As an off-the-shelf product, allogeneic MSCs must be licensed and approved for treatment by the FDA. The time and costs associated with regulatory licensing as well as the high costs of capital (e.g., equipment, facilities, and trained staff) needed to manufacture allogeneic MSCs at a large scale represent additional barriers to market entry. Allogeneic cell therapy has a substitution risk but due to the lower cost, it may be able to compete effectively with existing standard of care therapies, especially if it can demonstrate superior safety and efficacy. Marketing these cells under a brand name, utilizing the pharmaceutical industry's sophisticated

marketing capabilities, could help allogeneic MSCs to build brand recognition, thus commanding a price premium. The ability to differentiate based on quality combined with cheaper costs of production would increase firms' power over "buyers," who be more willing to pay a price premium for an approved therapy. From this standpoint, allogeneic MSCs represent a viable business venture.

An alternative "industry" to consider is an indication with a low incidence in which a standard of care may not exist or one with nonresponsive patients (Figure 35, bottom half). Autologous MSCs could be an option for treatment, if not time-constrained, due to the lack of available substitutes. Without the ability to scale, manufacturing costs would still be high, but buyers would be less price-sensitive and willing to pay a premium for a product with demonstrated efficacy, especially given the lack of a standard treatment option. By definition, an indication with a low incidence would have a small market size. Because of the low entry barriers, new laboratories could still join the industry, but the lack of growth potential would result in an increased level of rivalry. While this scenario is modestly improved compared to the high incidence quadrant, allogeneic MSCs again represent the more commercially viable option. With their broader pool of donors (suppliers), allogeneic MSCs can increase production to meet demand, thus benefiting from economies of scale. Due to the lack of substitutes and decreased price-sensitivity of buyers, firms could demand a premium price for a product with demonstrated efficacy, increasing profits. Again, with an allogeneic product, higher market entry barriers exist due to licensing and the costs of startup at scale. The ability to differentiate products decreases both the intensity of rivalry and the threat posed by new entrants. Although the overall market size is notably smaller, allogeneic MSCs still represent an attractive industry in terms of profitability.

Biologics have been successful on the market—over 250 products are available and they account for seven of the top 10 selling drugs globally—and several companies have already taken advantage of the allogeneic MSC model to produce clinical therapeutics [560]. There are well-established companies such as, JCR Pharmaceuticals [Japan], Mesoblast [Australia], and Osiris Therapeutics [United States], with new biotechnology companies opening worldwide regularly. Prochymal from Osiris Therapeutics was granted conditional licensing approval to treat children suffering from acute graft vs. host disease (GvHD) in Canada in 2012 [44, 561]. It was revealed in 2016 that Prochymal had not been utilized because it could not get reimbursed [44, 562]. On the other hand, JCR Pharmaceuticals has had financial success with its product, TEMCELL®, which was approved for use in acute GvHD in 2015 [44]. From JCR Pharmaceuticals' financial reports, they have reported revenue of ¥86.6 billion (~817,400,000 USD) from fiscal years 2016–2019, with revenue increasing annually, and an operating income of ¥14.4 billion (~135,919,000 USD) [563-566]. Collectively, these data indicate that allogeneic MSC therapy represents the clearest path to profitability. By focusing research efforts on this modality, industry-sponsored funding may increase.

Conclusion

The cell therapy market is expected to grow to $61 billion by 2022 [420]. MSCs are an attractive cellular therapeutic product backed by promising preclinical data in animal models. There are currently ten MSC therapeutics with regulatory approval worldwide. Despite the positive preclinical data, in the US clinical trials have failed to meet efficacy endpoints, pointing to issues with translation from preclinical studies to clinical trials. Because of this, an FDA-approved MSC therapeutic product still does not exist. Unified under the common goal of widespread therapeutic

use of MSCs, stakeholders should focus efforts on strengthening preclinical data so that it can be translated into safe and effective therapies, replicated among researchers, and compared across laboratories. To accomplish this, characterization guidelines should be updated to accommodate MSC populations from all tissue sources and species. Second, improved standardization that has both general characteristics and specific characteristics for each MSC population should be generated to decrease product variability. To accomplish this, research with commercial applicability should be prioritized to attract industry research funds. Without established consistency among MSCs, both MSCs and MSC-based products, such as EVs, will suffer from a lack of standardization, increasing the time to market as a licensed therapeutic.

Chapter 6 - Conclusion

Mesenchymal stromal cells (MSCs) are of therapeutic interest due to their regenerative potential and immunomodulatory properties. As a therapeutic, allogeneic MSCs have limitations such as a low rate of engraftment and risk of thrombosis or embolism once intravenously administered. Extracellular vesicles (EVs) share many properties with their parental cells including surface marker expression and cargo. MSC-EVs have been shown to be involved with physiological cell signaling and paracrine communication. Thus, MSC-EVs represent a potential cellular-free therapeutic.

In Chapter 2, I optimized the isolation, culture, and cryopreservation of canine umbilical cord-derived MSCs. My review of the field shows that culturing canine MSCs is problematic in that the cells cannot be maintained past passage 7 (P7) without senescing, and the surface marker characterization of canine MSCs is inconsistent. My work demonstrated that the addition of a gelatin-coating to cell culture surfaces increased colony-forming units-fibroblast efficiency and decreased population doubling times for canine MSCs. In addition, my isolation and culture protocol enabled the superior expansion of canine MSCs by increasing the passage reached before senescence and by allowing more lines to reach passage 15. My work revealed that canine MSCs have different culture requirements than human umbilical cord-derived MSCs. The addition of basic fibroblast growth factor (bFGF) to the medium decreased the population doubling time and enabled more canine MSC lines to be maintained in culture past P11. My improved cryopreservation method resulted in canine MSCs with >90% viability when thawed after being cryopreserved for up to two years. My work provides a framework that would enable commercialization via master-bank and working-bank plans for allogeneic MSC testing in naturally occurring canine diseases. For the future, additional optimization steps may be performed

to make improvements to population doubling time and canine MSC survival time prior to senescence. It is still unresolved whether canine breed impacts culture potential. In addition, efforts may be directed at improving the flow cytometry methods and creating a standardized surface marker panel like what is available for human MSCs to characterize canine MSCs.

In Chapter 3, I examined the effect of cell-conditioned medium (CM) storage conditions prior to the isolation of human MSC-derived EVs. Proper cryostorage of cells and other cell-derived products is crucial for maintaining their function. Little is known about the impact of the storage condition of CM and other biological fluids on EVs prior to isolation. Previous work has focused heavily on the storage of EVs once isolated. My work demonstrates that although all CM storage conditions yielded EVs, storage of CM at -80°C is the optimum condition for downstream EV isolation. Similar numbers of EVs were isolated from CM stored at room temperature, 4°C - 20°C, and -80°C for at least one week compared to EVs isolated immediately following CM collection. Storage at -80°C resulted in a more homogeneous population of EVs with similar surface potential and hydrodynamic size compared to immediately isolated EVs. Only EVs from CM stored at -80°C displayed similar morphology and size via transmission electron microscopy to immediately isolated EVs. Finally, my work showed enhanced protein blotting for clusters of differentiation (CD)9, CD63, CD81, and heat shock protein 70 (Hsp70) -- markers that are important for characterizing EVs. My work indicates that storage of CM at -80°C prior to EV isolation may enable scale-up and clinical testing of EVs. My work provides estimates of appropriate sample sizes required to answer related research questions and indicates that groups of 30 are appropriate, in comparison to the two to ten commonly used in the industry. For future work, the scope might be expanded to determine whether my findings apply to other biological fluids and CM from other cell types. Furthermore, my work addresses many properties of EVs but

did not address their function. In the future, the function of EVs following CM storage needs to be addressed to meet the characterization criteria established by the International Society for Extracellular Vesicles (ISEV).

In Chapter 4, I examined the impact of MSC culture conditions on EV production. For this work, I prepared EV samples using two methods: size-exclusion chromatography (SEC) and ultracentrifugation (UC) and over passage (P2-P12). My work showed that more EVs were obtained from early passage MSCs (defined as passages two through five) than late passage MSCs (defined as passages nine through twelve) and that UC isolation produced more particles than SEC isolation. This observation was supported by regression analysis of cell cumulative population doublings versus the number of particles released per cell showing a negative correlation. Other EV characteristics, such as size and heterogeneity of the population, were affected only by isolation method and not passage. My findings show that late passage MSCs produce comparable EV populations with no increase in larger vesicles, such as apoptotic bodies. My data showed that although late passage cells produce EVs, CD63 expression is lost on EVs from late passage cells. The implications of this observation remain to be found. In the final project, I examined the procoagulant activity of MSCs and their EVs. My work demonstrated that human and canine MSCs and their EVs express tissue factor (TF) on their surface. In addition, EVs retain the expression of TF independent of both passage and isolation method. I showed that expression of TF resulted in TF-mediated procoagulant activity via generation of FXa and that it can be inhibited using a functional antibody. These findings may impact the scale-up and clinical testing of EVs and suggest that, although EVs are a cell-free product, they possess TF-mediated procoagulant activity and thus may pose a safety risk for clinical use. To pursue this inquiry in the future, it would be beneficial to streamline the FXa generation assay to increase commercial applicability.

In Chapter 5, I highlight the need for tissue- and species-specific characterization guidelines for MSCs. The common goal of researchers in the MSC field is to move toward therapeutic use of MSCs. Preclinical data in animal models supports the therapeutic effects of MSCs yet this has not translated effectively into human clinical trials. My review identified the barriers that impede the therapeutic use of MSCs and offers strategies to accomplish this goal.

References

1. Friedenstein, A.J., et al., *Heterotopic of bone marrow. Analysis of precursor cells for osteogenic and hematopoietic tissues.* Transplantation, 1968. **6**(2): p. 230-47.
2. Bianco, P., P.G. Robey, and P.J. Simmons, *Mesenchymal stem cells: revisiting history, concepts, and assays.* Cell Stem Cell, 2008. **2**(4): p. 313-9.
3. Friedenstein, A.J., R.K. Chailakhjan, and K.S. Lalykina, *The development of fibroblast colonies in monolayer cultures of guinea-pig bone marrow and spleen cells.* Cell Tissue Kinet, 1970. **3**(4): p. 393-403.
4. Charbord, P., *Bone marrow mesenchymal stem cells: historical overview and concepts.* Hum Gene Ther, 2010. **21**(9): p. 1045-56.
5. Prockop, D.J., *Marrow stromal cells as stem cells for nonhematopoietic tissues.* Science, 1997. **276**(5309): p. 71-4.
6. Caplan, A.I., *Mesenchymal stem cells.* J Orthop Res, 1991. **9**(5): p. 641-50.
7. Pittenger, M.F., et al., *Multilineage potential of adult human mesenchymal stem cells.* Science, 1999. **284**(5411): p. 143-7.
8. Owen, M. and A.J. Friedenstein, *Stromal stem cells: marrow-derived osteogenic precursors.* Ciba Found Symp, 1988. **136**: p. 42-60.
9. Dennis, J.E., et al., *A quadripotential mesenchymal progenitor cell isolated from the marrow of an adult mouse.* J Bone Miner Res, 1999. **14**(5): p. 700-9.
10. Horwitz, E.M., et al., *Clarification of the nomenclature for MSC: The International Society for Cellular Therapy position statement.* Cytotherapy, 2005. **7**(5): p. 393-5.
11. Dominici, M., et al., *Minimal criteria for defining multipotent mesenchymal stromal cells. The International Society for Cellular Therapy position statement.* Cytotherapy, 2006. **8**(4): p. 315-7.
12. Wright, A., et al., *A Protocol for the Isolation, Culture, and Cryopreservation of Umbilical Cord-Derived Canine Mesenchymal Stromal Cells: Role of Cell Attachment in Long-Term Maintenance.* Stem Cells Dev, 2020. **29**(11): p. 695-713.
13. Wright, A., M.L. Arthaud-Day, and M.L. Weiss, *Therapeutic Use of Mesenchymal Stromal Cells: The Need for Inclusive Characterization Guidelines to Accommodate All Tissue Sources and Species.* Frontiers in Cell and Developmental Biology, 2021. **9**(66).
14. Bourin, P., et al., *Stromal cells from the adipose tissue-derived stromal vascular fraction and culture expanded adipose tissue-derived stromal/stem cells: a joint statement of the International Federation for Adipose Therapeutics and Science (IFATS) and the International Society for Cellular Therapy (ISCT).* Cytotherapy, 2013. **15**(6): p. 641-8.
15. Seshareddy, K., D. Troyer, and M.L. Weiss, *Method to isolate mesenchymal-like cells from Wharton's Jelly of umbilical cord.* Methods Cell Biol, 2008. **86**: p. 101-19.
16. Faramarzi, H., et al., *The Potential of Menstrual Blood-Derived Stem Cells in Differentiation to Epidermal Lineage: A Preliminary Report.* World journal of plastic surgery, 2016. **5**(1): p. 26-31.
17. Wu, M., et al., *Comparison of the Biological Characteristics of Mesenchymal Stem Cells Derived from the Human Placenta and Umbilical Cord.* Scientific Reports, 2018. **8**(1): p. 5014.
18. Al-Nbaheen, M., et al., *Human stromal (mesenchymal) stem cells from bone marrow, adipose tissue and skin exhibit differences in molecular phenotype and differentiation potential.* Stem Cell Rev Rep, 2013. **9**(1): p. 32-43.

19. Hass, R., et al., *Different populations and sources of human mesenchymal stem cells (MSC): A comparison of adult and neonatal tissue-derived MSC.* Cell Commun Signal, 2011. **9**: p. 12.
20. Sibov, T.T., et al., *Mesenchymal stem cells from umbilical cord blood: parameters for isolation, characterization and adipogenic differentiation.* Cytotechnology, 2012. **64**(5): p. 511-521.
21. Čamernik, K., et al., *Skeletal-muscle-derived mesenchymal stem/stromal cells from patients with osteoarthritis show superior biological properties compared to bone-derived cells.* Stem Cell Res, 2019. **38**: p. 101465.
22. Ledesma-Martínez, E., V.M. Mendoza-Núñez, and E. Santiago-Osorio, *Mesenchymal Stem Cells Derived from Dental Pulp: A Review.* Stem Cells International, 2016. **2016**: p. 4709572.
23. Smith, J.R., A. Cromer, and M.L. Weiss, *Human Umbilical Cord Mesenchymal Stromal Cell Isolation, Expansion, Cryopreservation, and Characterization.* Curr Protoc Stem Cell Biol, 2017. **41**: p. 1f.18.1-1f.18.23.
24. Troyer, D.L. and M.L. Weiss, *Wharton's jelly-derived cells are a primitive stromal cell population.* Stem Cells, 2008. **26**(3): p. 591-9.
25. Stolzing, A., et al., *Age-related changes in human bone marrow-derived mesenchymal stem cells: consequences for cell therapies.* Mech Ageing Dev, 2008. **129**(3): p. 163-73.
26. Gupta, A., et al., *Umbilical cord-derived Wharton's jelly for regenerative medicine applications.* J Orthop Surg Res, 2020. **15**(1): p. 49.
27. Mitchell, K.E., et al., *Matrix cells from Wharton's jelly form neurons and glia.* Stem Cells, 2003. **21**(1): p. 50-60.
28. Sobolewski, K., et al., *Wharton's jelly as a reservoir of peptide growth factors.* Placenta, 2005. **26**(10): p. 747-752.
29. Karahuseyinoglu, S., et al., *Biology of stem cells in human umbilical cord stroma: in situ and in vitro surveys.* Stem Cells, 2007. **25**(2): p. 319-31.
30. Lu, L.L., et al., *Isolation and characterization of human umbilical cord mesenchymal stem cells with hematopoiesis-supportive function and other potentials.* Haematologica, 2006. **91**(8): p. 1017-26.
31. Weiss, M.L. and D.L. Troyer, *Stem cells in the umbilical cord.* Stem Cell Rev, 2006. **2**(2): p. 155-62.
32. Fu, Y.S., et al., *Transformation of human umbilical mesenchymal cells into neurons in vitro.* J Biomed Sci, 2004. **11**(5): p. 652-60.
33. Wang, H.S., et al., *Mesenchymal stem cells in the Wharton's jelly of the human umbilical cord.* Stem Cells, 2004. **22**(7): p. 1330-7.
34. Wegmeyer, H., et al., *Mesenchymal stromal cell characteristics vary depending on their origin.* Stem Cells Dev, 2013. **22**(19): p. 2606-18.
35. Seo, M.S., S.B. Park, and K.S. Kang, *Isolation and characterization of canine Wharton's jelly-derived mesenchymal stem cells.* Cell Transplant, 2012. **21**(7): p. 1493-502.
36. Ryu, H.H., et al., *Comparison of mesenchymal stem cells derived from fat, bone marrow, Wharton's jelly, and umbilical cord blood for treating spinal cord injuries in dogs.* J Vet Med Sci, 2012. **74**(12): p. 1617-30.
37. Groza, I., et al., *Canine Wharton's Jelly Derived Mesenchymal Stem Cells Isolation.* Agriculture and Agricultural Science Procedia, 2016. **10**: p. 408-411.

38. Carlin, R., et al., *Expression of early transcription factors Oct-4, Sox-2 and Nanog by porcine umbilical cord (PUC) matrix cells.* Reprod Biol Endocrinol, 2006. **4**: p. 8.
39. Raoufi, M.F., et al., *Isolation and differentiation of mesenchymal stem cells from bovine umbilical cord blood.* Reprod Domest Anim, 2011. **46**(1): p. 95-9.
40. Kumar, K., et al., *Isolation and characterization of mesenchymal stem cells from caprine umbilical cord tissue matrix.* Tissue Cell, 2016. **48**(6): p. 653-658.
41. Cremonesi, F., et al., *Isolation, in vitro culture and characterization of foal umbilical cord stem cells at birth.* Vet Res Commun, 2008. **32 Suppl 1**: p. S139-42.
42. Barberini, D.J., et al., *Equine mesenchymal stem cells from bone marrow, adipose tissue and umbilical cord: immunophenotypic characterization and differentiation potential.* Stem Cell Research & Therapy, 2014. **5**(1): p. 25.
43. Lepage, S.I.M., O.J. Lee, and T.G. Koch, *Equine Cord Blood Mesenchymal Stromal Cells Have Greater Differentiation and Similar Immunosuppressive Potential to Cord Tissue Mesenchymal Stromal Cells.* Stem Cells Dev, 2019. **28**(3): p. 227-237.
44. Galipeau, J. and L. Sensébé, *Mesenchymal Stromal Cells: Clinical Challenges and Therapeutic Opportunities.* Cell Stem Cell, 2018. **22**(6): p. 824-833.
45. Chu, D.T., et al., *Adipose Tissue Stem Cells for Therapy: An Update on the Progress of Isolation, Culture, Storage, and Clinical Application.* J Clin Med, 2019. **8**(7).
46. Djouad, F., et al., *Mesenchymal stem cells: innovative therapeutic tools for rheumatic diseases.* Nat Rev Rheumatol, 2009. **5**(7): p. 392-9.
47. Durand, N., J. Mallea, and A.C. Zubair, *Insights into the use of mesenchymal stem cells in COVID-19 mediated acute respiratory failure.* npj Regenerative Medicine, 2020. **5**(1): p. 17.
48. Levy, O., et al., *Shattering barriers toward clinically meaningful MSC therapies.* Science Advances, 2020. **6**(30): p. eaba6884.
49. Pittenger, M.F., et al., *Mesenchymal stem cell perspective: cell biology to clinical progress.* npj Regenerative Medicine, 2019. **4**(1): p. 22.
50. Phinney, D.G. and J. Galipeau, *Manufacturing mesenchymal stromal cells for clinical applications: A survey of Good Manufacturing Practices at U.S. academic centers.* Cytotherapy, 2019. **21**(7): p. 782-792.
51. Luk, F., et al., *Efficacy of immunotherapy with mesenchymal stem cells in man: a systematic review.* Expert Rev Clin Immunol, 2015. **11**(5): p. 617-36.
52. Galipeau, J., *The mesenchymal stromal cells dilemma--does a negative phase III trial of random donor mesenchymal stromal cells in steroid-resistant graft-versus-host disease represent a death knell or a bump in the road?* Cytotherapy, 2013. **15**(1): p. 2-8.
53. Christy, B.A., et al., *Procoagulant activity of human mesenchymal stem cells.* J Trauma Acute Care Surg, 2017. **83**(1 Suppl 1): p. S164-s169.
54. Lalu, M.M., et al., *Safety of cell therapy with mesenchymal stromal cells (SafeCell): a systematic review and meta-analysis of clinical trials.* PLoS One, 2012. **7**(10): p. e47559.
55. Thompson, M., et al., *Cell therapy with intravascular administration of mesenchymal stromal cells continues to appear safe: An updated systematic review and meta-analysis.* EClinicalMedicine, 2020. **19**.
56. Wang, H., et al., *Autologous Mesenchymal Stem Cell and Islet Cotransplantation: Safety and Efficacy.* STEM CELLS Translational Medicine, 2018. **7**(1): p. 11-19.

57. Moll, G., et al., *Intravascular Mesenchymal Stromal/Stem Cell Therapy Product Diversification: Time for New Clinical Guidelines.* Trends Mol Med, 2019. **25**(2): p. 149-163.
58. Moll, G., et al., *Are therapeutic human mesenchymal stromal cells compatible with human blood?* Stem Cells, 2012. **30**(7): p. 1565-74.
59. Vulliet, P.R., et al., *Intra-coronary arterial injection of mesenchymal stromal cells and microinfarction in dogs.* Lancet, 2004. **363**(9411): p. 783-4.
60. Cyranoski, D., *Korean deaths spark inquiry.* Nature, 2010. **468**(7323): p. 485.
61. Jung, J.W., et al., *Familial occurrence of pulmonary embolism after intravenous, adipose tissue-derived stem cell therapy.* Yonsei Med J, 2013. **54**(5): p. 1293-6.
62. Zhao, R., et al., *Serious adverse events of cell therapy for respiratory diseases: a systematic review and meta-analysis.* Oncotarget, 2017. **8**(18): p. 30511-30523.
63. Ankrum, J.A., J.F. Ong, and J.M. Karp, *Mesenchymal stem cells: immune evasive, not immune privileged.* Nat Biotechnol, 2014. **32**(3): p. 252-60.
64. De Becker, A. and I.V. Riet, *Homing and migration of mesenchymal stromal cells: How to improve the efficacy of cell therapy?* World journal of stem cells, 2016. **8**(3): p. 73-87.
65. Le Blanc, K., et al., *Mesenchymal stem cells inhibit and stimulate mixed lymphocyte cultures and mitogenic responses independently of the major histocompatibility complex.* Scand J Immunol, 2003. **57**(1): p. 11-20.
66. Chinnadurai, R., et al., *Cryopreserved Mesenchymal Stromal Cells Are Susceptible to T-Cell Mediated Apoptosis Which Is Partly Rescued by IFNγ Licensing.* Stem cells (Dayton, Ohio), 2016. **34**(9): p. 2429-2442.
67. François, M., et al., *Cryopreserved mesenchymal stromal cells display impaired immunosuppressive properties as a result of heat-shock response and impaired interferon-γ licensing.* Cytotherapy, 2012. **14**(2): p. 147-52.
68. Le Blanc, K. and O. Ringdén, *Immunomodulation by mesenchymal stem cells and clinical experience.* Journal of Internal Medicine, 2007. **262**(5): p. 509-525.
69. Isakova, I.A., et al., *Allo-Reactivity of Mesenchymal Stem Cells in Rhesus Macaques Is Dose and Haplotype Dependent and Limits Durable Cell Engraftment In Vivo.* PLOS ONE, 2014. **9**(1): p. e87238.
70. Nauta, A.J., et al., *Donor-derived mesenchymal stem cells are immunogenic in an allogeneic host and stimulate donor graft rejection in a nonmyeloablative setting.* Blood, 2006. **108**(6): p. 2114-20.
71. Eliopoulos, N., et al., *Allogeneic marrow stromal cells are immune rejected by MHC class I- and class II-mismatched recipient mice.* Blood, 2005. **106**(13): p. 4057-65.
72. Poncelet, A.J., et al., *Although pig allogeneic mesenchymal stem cells are not immunogenic in vitro, intracardiac injection elicits an immune response in vivo.* Transplantation, 2007. **83**(6): p. 783-90.
73. Lohan, P., et al., *Anti-Donor Immune Responses Elicited by Allogeneic Mesenchymal Stem Cells and Their Extracellular Vesicles: Are We Still Learning?* Front Immunol, 2017. **8**: p. 1626.
74. Reinders, M.E.J., et al., *Safety of allogeneic bone marrow derived mesenchymal stromal cell therapy in renal transplant recipients: the neptune study.* Journal of translational medicine, 2015. **13**: p. 344-344.

75. von Bahr, L., et al., *Long-term complications, immunologic effects, and role of passage for outcome in mesenchymal stromal cell therapy.* Biol Blood Marrow Transplant, 2012. **18**(4): p. 557-64.
76. Hwang, J.W., et al., *A Comparison of Immune Responses Exerted Following Syngeneic, Allogeneic, and Xenogeneic Transplantation of Mesenchymal Stem Cells into the Mouse Brain.* International journal of molecular sciences, 2020. **21**(9): p. 3052.
77. Shearin, A.L. and E.A. Ostrander, *Leading the way: canine models of genomics and disease.* Dis Model Mech, 2010. **3**(1-2): p. 27-34.
78. Ostrander, E.A., F. Galibert, and D.F. Patterson, *Canine genetics comes of age.* Trends Genet, 2000. **16**(3): p. 117-24.
79. Patterson, D.F., *Companion animal medicine in the age of medical genetics.* J Vet Intern Med, 2000. **14**(1): p. 1-9.
80. Parker, H.G. and E.A. Ostrander, *Canine genomics and genetics: running with the pack.* PLoS Genet, 2005. **1**(5): p. e58.
81. Wayne, R.K. and E.A. Ostrander, *Lessons learned from the dog genome.* Trends Genet, 2007. **23**(11): p. 557-67.
82. Hytönen, M.K. and H. Lohi, *Canine models of human rare disorders.* Rare diseases (Austin, Tex.), 2016. **4**(1): p. e1241362-e1241362.
83. Hytönen, M.K., et al., *Canine models of human amelogenesis imperfecta: identification of novel recessive ENAM and ACP4 variants.* Hum Genet, 2019. **138**(5): p. 525-533.
84. Hoffman, J.M., et al., *The companion dog as a model for human aging and mortality.* Aging Cell, 2018. **17**(3): p. e12737.
85. Cotman, C.W. and E. Head, *The Canine (Dog) Model of Human Aging and Disease: Dietary, Environmental and Immunotherapy Approaches.* Journal of Alzheimer's Disease, 2008. **15**: p. 685-707.
86. Rowell, J.L., D.O. McCarthy, and C.E. Alvarez, *Dog models of naturally occurring cancer.* Trends Mol Med, 2011. **17**(7): p. 380-8.
87. Shelton, G.D. and E. Engvall, *Canine and feline models of human inherited muscle diseases.* Neuromuscul Disord, 2005. **15**(2): p. 127-38.
88. Nardone, R., et al., *Canine degenerative myelopathy: a model of human amyotrophic lateral sclerosis.* Zoology (Jena), 2016. **119**(1): p. 64-73.
89. Poole, D.C., et al., *Guidelines for animal exercise and training protocols for cardiovascular studies.* Am J Physiol Heart Circ Physiol, 2020. **318**(5): p. H1100-h1138.
90. Petersen-Jones, S.M., *Animal models of human retinal dystrophies.* Eye (Lond), 1998. **12 (Pt 3b)**: p. 566-70.
91. Head, E., *A canine model of human aging and Alzheimer's disease.* Biochimica et biophysica acta, 2013. **1832**(9): p. 1384-1389.
92. Cummings, B.J., et al., *The canine as an animal model of human aging and dementia.* Neurobiol Aging, 1996. **17**(2): p. 259-68.
93. Cope, P.J., et al., *Models of osteoarthritis: the good, the bad and the promising.* Osteoarthritis and Cartilage, 2019. **27**(2): p. 230-239.
94. Kuyinu, E.L., et al., *Animal models of osteoarthritis: classification, update, and measurement of outcomes.* J Orthop Surg Res, 2016. **11**: p. 19.
95. Marijnissen, A.C., et al., *The canine 'groove' model, compared with the ACLT model of osteoarthritis.* Osteoarthritis Cartilage, 2002. **10**(2): p. 145-55.

96. de Bakker, E., et al., *Canine mesenchymal stem cells: state of the art, perspectives as therapy for dogs and as a model for man.* Vet Q, 2013. **33**(4): p. 225-33.
97. Black, L.L., et al., *Effect of adipose-derived mesenchymal stem and regenerative cells on lameness in dogs with chronic osteoarthritis of the coxofemoral joints: a randomized, double-blinded, multicenter, controlled trial.* Vet Ther, 2007. **8**(4): p. 272-84.
98. Guercio, A., et al., *Canine mesenchymal stem cells (MSCs): characterization in relation to donor age and adipose tissue-harvesting site.* Cell Biol Int, 2013. **37**(8): p. 789-98.
99. Vilar, J.M., et al., *Controlled, blinded force platform analysis of the effect of intraarticular injection of autologous adipose-derived mesenchymal stem cells associated to PRGF-Endoret in osteoarthritic dogs.* BMC Vet Res, 2013. **9**: p. 131.
100. Upchurch, D.A., et al., *Effects of administration of adipose-derived stromal vascular fraction and platelet-rich plasma to dogs with osteoarthritis of the hip joints.* Am J Vet Res, 2016. **77**(9): p. 940-51.
101. Cabon, Q., et al., *Long-Term Safety and Efficacy of Single or Repeated Intra-Articular Injection of Allogeneic Neonatal Mesenchymal Stromal Cells for Managing Pain and Lameness in Moderate to Severe Canine Osteoarthritis Without Anti-inflammatory Pharmacological Support: Pilot Clinical Study.* Front Vet Sci, 2019. **6**: p. 10.
102. Ayala-Cuellar, A.P., et al., *Characterization of canine adipose tissue-derived mesenchymal stem cells immortalized by SV40-T retrovirus for therapeutic use.* J Cell Physiol, 2019.
103. Gardin, C., et al., *Therapeutic Potential of Autologous Adipose-Derived Stem Cells for the Treatment of Liver Disease.* Int J Mol Sci, 2018. **19**(12).
104. Russell, K.A., et al., *Characterization and Immunomodulatory Effects of Canine Adipose Tissue- and Bone Marrow-Derived Mesenchymal Stromal Cells.* PLoS One, 2016. **11**(12): p. e0167442.
105. Liu, Z., et al., *Characterization of Canine Adipose-Derived Mesenchymal Stromal/Stem Cells in Serum-Free Medium.* Tissue Eng Part C Methods, 2018. **24**(7): p. 399-411.
106. Pérez-Merino, E.M., et al., *Safety and efficacy of allogeneic adipose tissue-derived mesenchymal stem cells for treatment of dogs with inflammatory bowel disease: Clinical and laboratory outcomes.* Vet J, 2015. **206**(3): p. 385-90.
107. Lee, K.S., et al., *Sequential sub-passage decreases the differentiation potential of canine adipose-derived mesenchymal stem cells.* Res Vet Sci, 2014. **96**(2): p. 267-75.
108. Chung, D.J., et al., *Osteogenic proliferation and differentiation of canine bone marrow and adipose tissue derived mesenchymal stromal cells and the influence of hypoxia.* Res Vet Sci, 2012. **92**(1): p. 66-75.
109. El-Zekrid, M.H., et al., *Healing Capacity of Autologous Bone Marrow-derived Mesenchymal Stem Cells on Partially Pulpotomized Dogs' Teeth.* J Endod, 2019. **45**(3): p. 287-294.
110. Eslaminejad, M.B. and L. Taghiyar, *Study of the structure of canine mesenchymal stem cell osteogenic culture.* Anat Histol Embryol, 2010. **39**(5): p. 446-55.
111. Sahoo, A.K., J.K. Das, and S. Nayak, *Isolation, culture, characterization, and osteogenic differentiation of canine endometrial mesenchymal stem cell.* Veterinary world, 2017. **10**(12): p. 1533-1541.
112. Zucconi, E., et al., *Mesenchymal stem cells derived from canine umbilical cord vein--a novel source for cell therapy studies.* Stem Cells Dev, 2010. **19**(3): p. 395-402.

113. Soleimani, M. and S. Nadri, *A protocol for isolation and culture of mesenchymal stem cells from mouse bone marrow.* Nat Protoc, 2009. **4**(1): p. 102-6.
114. Yu, Y., et al., *Characterization of long-term in vitro culture-related alterations of human tonsil-derived mesenchymal stem cells: role for CCN1 in replicative senescence-associated increase in osteogenic differentiation.* Journal of anatomy, 2014. **225**(5): p. 510-518.
115. Lee, K.S., et al., *Effects of serial passage on the characteristics and chondrogenic differentiation of canine umbilical cord matrix derived mesenchymal stem cells.* Asian-Australasian journal of animal sciences, 2013. **26**(4): p. 588-595.
116. Boxall, S.A. and E. Jones, *Markers for Characterization of Bone Marrow Multipotential Stromal Cells.* Stem Cells International, 2012. **2012**: p. 975871.
117. Abello, J., et al., *Biodistribution of gadolinium- and near infrared-labeled human umbilical cord mesenchymal stromal cell-derived exosomes in tumor bearing mice.* Theranostics, 2019. **9**(8): p. 2325-2345.
118. Assunção-Silva, R.C., et al., *Exploiting the impact of the secretome of MSCs isolated from different tissue sources on neuronal differentiation and axonal growth.* Biochimie, 2018. **155**: p. 83-91.
119. Damania, A., et al., *Mesenchymal stromal cell-derived exosome-rich fractionated secretome confers a hepatoprotective effect in liver injury.* Stem cell research & therapy, 2018. **9**(1): p. 31-31.
120. Barros, F.M., et al., *Exosomes and Immune Response in Cancer: Friends or Foes?* Front Immunol, 2018. **9**: p. 730.
121. Sarkar, P., et al., *Reduced neuroprotective potential of the mesenchymal stromal cell secretome with ex vivo expansion, age and progressive multiple sclerosis.* Cytotherapy, 2018. **20**(1): p. 21-28.
122. Sevivas, N., et al., *Mesenchymal Stem Cell Secretome Improves Tendon Cell Viability In Vitro and Tendon-Bone Healing In Vivo When a Tissue Engineering Strategy Is Used in a Rat Model of Chronic Massive Rotator Cuff Tear.* Am J Sports Med, 2018. **46**(2): p. 449-459.
123. Takov, K., et al., *Small extracellular vesicles secreted from human amniotic fluid mesenchymal stromal cells possess cardioprotective and promigratory potential.* Basic Res Cardiol, 2020. **115**(3): p. 26.
124. Kovács Á, F., et al., *The impact of circulating preeclampsia-associated extracellular vesicles on the migratory activity and phenotype of THP-1 monocytic cells.* Sci Rep, 2018. **8**(1): p. 5426.
125. L. Ramos, T., et al., *MSC surface markers (CD44, CD73, and CD90) can identify human MSC-derived extracellular vesicles by conventional flow cytometry.* Cell Communication and Signaling, 2016. **14**(1): p. 2.
126. György, B., et al., *Detection and isolation of cell-derived microparticles are compromised by protein complexes resulting from shared biophysical parameters.* Blood, 2011. **117**(4): p. e39-48.
127. Crescitelli, R., et al., *Distinct RNA profiles in subpopulations of extracellular vesicles: apoptotic bodies, microvesicles and exosomes.* J Extracell Vesicles, 2013. **2**.
128. Romanov, Y.A., et al., *Effect of Storage Conditions on the Integrity of Human Umbilical Cord Mesenchymal Stromal Cell-Derived Microvesicles.* Bull Exp Biol Med, 2019. **167**(1): p. 131-135.

129. Romanov, Y.A., et al., *Human Umbilical Cord Mesenchymal Stromal Cell-Derived Microvesicles Express Surface Markers Identical to the Phenotype of Parental Cells.* Bull Exp Biol Med, 2018. **166**(1): p. 124-129.
130. Colombo, M., G. Raposo, and C. Théry, *Biogenesis, secretion, and intercellular interactions of exosomes and other extracellular vesicles.* Annu Rev Cell Dev Biol, 2014. **30**: p. 255-89.
131. Hessvik, N.P. and A. Llorente, *Current knowledge on exosome biogenesis and release.* Cell Mol Life Sci, 2018. **75**(2): p. 193-208.
132. Silva, A.M., et al., *Dendritic Cell-derived Extracellular Vesicles mediate Mesenchymal Stem/Stromal Cell recruitment.* Scientific Reports, 2017. **7**(1): p. 1667.
133. Kalra, H., G.P.C. Drummen, and S. Mathivanan, *Focus on Extracellular Vesicles: Introducing the Next Small Big Thing.* International journal of molecular sciences, 2016. **17**(2): p. 170-170.
134. Théry, C., et al., *Isolation and characterization of exosomes from cell culture supernatants and biological fluids.* Curr Protoc Cell Biol, 2006. **Chapter 3**: p. Unit 3.22.
135. Konoshenko, M.Y., et al., *Isolation of Extracellular Vesicles: General Methodologies and Latest Trends.* BioMed Research International, 2018. **2018**: p. 8545347.
136. Jeppesen, D.K., et al., *Comparative analysis of discrete exosome fractions obtained by differential centrifugation.* Journal of extracellular vesicles, 2014. **3**: p. 25011-25011.
137. Witwer, K.W., et al., *Standardization of sample collection, isolation and analysis methods in extracellular vesicle research.* Journal of Extracellular Vesicles, 2013. **2**(1): p. 20360.
138. Akers, J.C., et al., *Biogenesis of extracellular vesicles (EV): exosomes, microvesicles, retrovirus-like vesicles, and apoptotic bodies.* J Neurooncol, 2013. **113**(1): p. 1-11.
139. Mathivanan, S., H. Ji, and R.J. Simpson, *Exosomes: extracellular organelles important in intercellular communication.* J Proteomics, 2010. **73**(10): p. 1907-20.
140. Boukouris, S. and S. Mathivanan, *Exosomes in bodily fluids are a highly stable resource of disease biomarkers.* PROTEOMICS – Clinical Applications, 2015. **9**(3-4): p. 358-367.
141. Borges, F.T., L.A. Reis, and N. Schor, *Extracellular vesicles: structure, function, and potential clinical uses in renal diseases.* Braz J Med Biol Res, 2013. **46**(10): p. 824-30.
142. Ciardiello, C., et al., *Focus on Extracellular Vesicles: New Frontiers of Cell-to-Cell Communication in Cancer.* Int J Mol Sci, 2016. **17**(2): p. 175.
143. Yokoi, A., Y. Yoshioka, and T. Ochiya, *Towards the realization of clinical extracellular vesicle diagnostics: challenges and opportunities.* Expert Rev Mol Diagn, 2015. **15**(12): p. 1555-66.
144. Tamkovich, S., et al., *Blood Circulating Exosomes Contain Distinguishable Fractions of Free and Cell-Surface-Associated Vesicles.* Curr Mol Med, 2019. **19**(4): p. 273-285.
145. Gould, S.J. and G. Raposo, *As we wait: coping with an imperfect nomenclature for extracellular vesicles.* J Extracell Vesicles, 2013. **2**.
146. Pisitkun, T., R.F. Shen, and M.A. Knepper, *Identification and proteomic profiling of exosomes in human urine.* Proc Natl Acad Sci U S A, 2004. **101**(36): p. 13368-73.
147. Caby, M.P., et al., *Exosomal-like vesicles are present in human blood plasma.* Int Immunol, 2005. **17**(7): p. 879-87.
148. Lässer, C., et al., *Human saliva, plasma and breast milk exosomes contain RNA: uptake by macrophages.* J Transl Med, 2011. **9**: p. 9.

149. Admyre, C., et al., *Exosomes with immune modulatory features are present in human breast milk.* J Immunol, 2007. **179**(3): p. 1969-78.
150. Vella, L.J., et al., *Enrichment of prion protein in exosomes derived from ovine cerebral spinal fluid.* Vet Immunol Immunopathol, 2008. **124**(3-4): p. 385-93.
151. Keller, S., et al., *CD24 is a marker of exosomes secreted into urine and amniotic fluid.* Kidney Int, 2007. **72**(9): p. 1095-102.
152. Peng, P., Y. Yan, and S. Keng, *Exosomes in the ascites of ovarian cancer patients: origin and effects on anti-tumor immunity.* Oncol Rep, 2011. **25**(3): p. 749-62.
153. Fornaciari, I., et al., *Gamma-glutamyltransferase fractions in human plasma and bile: characteristic and biogenesis.* PLoS One, 2014. **9**(2): p. e88532.
154. Madison, M.N., P.H. Jones, and C.M. Okeoma, *Exosomes in human semen restrict HIV-1 transmission by vaginal cells and block intravaginal replication of LP-BM5 murine AIDS virus complex.* Virology, 2015. **482**: p. 189-201.
155. Lama, V.N., *Peering into a Rejecting Lung: Can Bronchoalveolar Lavage Exosomes Provide Novel Insights?* Am J Respir Crit Care Med, 2015. **192**(12): p. 1413-4.
156. Dismuke, W.M., et al., *Human aqueous humor exosomes.* Exp Eye Res, 2015. **132**: p. 73-7.
157. Qazi, K.R., et al., *Proinflammatory exosomes in bronchoalveolar lavage fluid of patients with sarcoidosis.* Thorax, 2010. **65**(11): p. 1016-24.
158. Andre, F., et al., *Malignant effusions and immunogenic tumour-derived exosomes.* Lancet, 2002. **360**(9329): p. 295-305.
159. Abels, E.R. and X.O. Breakefield, *Introduction to Extracellular Vesicles: Biogenesis, RNA Cargo Selection, Content, Release, and Uptake.* Cell Mol Neurobiol, 2016. **36**(3): p. 301-12.
160. Lozano-Ramos, I., et al., *Size-exclusion chromatography-based enrichment of extracellular vesicles from urine samples.* J Extracell Vesicles, 2015. **4**: p. 27369.
161. Wahlgren, J., et al., *Plasma exosomes can deliver exogenous short interfering RNA to monocytes and lymphocytes.* Nucleic Acids Res, 2012. **40**(17): p. e130.
162. Guescini, M., et al., *Astrocytes and Glioblastoma cells release exosomes carrying mtDNA.* J Neural Transm (Vienna), 2010. **117**(1): p. 1-4.
163. Balaj, L., et al., *Tumour microvesicles contain retrotransposon elements and amplified oncogene sequences.* Nat Commun, 2011. **2**: p. 180.
164. Waldenström, A., et al., *Cardiomyocyte microvesicles contain DNA/RNA and convey biological messages to target cells.* PLoS One, 2012. **7**(4): p. e34653.
165. Iraci, N., et al., *Extracellular vesicles are independent metabolic units with asparaginase activity.* Nat Chem Biol, 2017. **13**(9): p. 951-955.
166. Meng, F., et al., *MicroRNA-193b-3p regulates chondrogenesis and chondrocyte metabolism by targeting HDAC3.* Theranostics, 2018. **8**(10): p. 2862-2883.
167. Kim, J., et al., *Exosome cargo reflects TGF-β1-mediated epithelial-to-mesenchymal transition (EMT) status in A549 human lung adenocarcinoma cells.* Biochem Biophys Res Commun, 2016. **478**(2): p. 643-8.
168. Sharma, A., *Transgenerational epigenetics: Integrating soma to germline communication with gametic inheritance.* Mech Ageing Dev, 2017. **163**: p. 15-22.
169. Yáñez-Mó, M., et al., *Biological properties of extracellular vesicles and their physiological functions.* Journal of Extracellular Vesicles, 2015. **4**(1): p. 27066.

170. Frühbeis, C., D. Fröhlich, and E.M. Krämer-Albers, *Emerging roles of exosomes in neuron-glia communication.* Front Physiol, 2012. **3**: p. 119.
171. Marcilla, A., et al., *Extracellular vesicles from parasitic helminths contain specific excretory/secretory proteins and are internalized in intestinal host cells.* PLoS One, 2012. **7**(9): p. e45974.
172. Luga, V., et al., *Exosomes mediate stromal mobilization of autocrine Wnt-PCP signaling in breast cancer cell migration.* Cell, 2012. **151**(7): p. 1542-56.
173. Regev-Rudzki, N., et al., *Cell-cell communication between malaria-infected red blood cells via exosome-like vesicles.* Cell, 2013. **153**(5): p. 1120-33.
174. Barteneva, N.S., N. Maltsev, and I.A. Vorobjev, *Microvesicles and intercellular communication in the context of parasitism.* Front Cell Infect Microbiol, 2013. **3**: p. 49.
175. Lin, Y., et al., *Exosomes in disease and regeneration: biological functions, diagnostics, and beneficial effects.* American Journal of Physiology-Heart and Circulatory Physiology, 2020. **319**(6): p. H1162-H1180.
176. Popovic, M., *Routine and novel methods for isolation of extracellular vesicles.* Biologica Serbica, 2019. **41**(2).
177. Shah, N., et al., *Extracellular vesicle-mediated long-range communication in stressed retinal pigment epithelial cell monolayers.* Biochim Biophys Acta Mol Basis Dis, 2018. **1864**(8): p. 2610-2622.
178. Smith, V.L., et al., *Exosomes function in antigen presentation during an in vivo Mycobacterium tuberculosis infection.* Sci Rep, 2017. **7**: p. 43578.
179. Zhang, B., et al., *Mesenchymal stromal cell exosome-enhanced regulatory T-cell production through an antigen-presenting cell-mediated pathway.* Cytotherapy, 2018. **20**(5): p. 687-696.
180. Sung, B.H., et al., *Directional cell movement through tissues is controlled by exosome secretion.* Nature Communications, 2015. **6**(1): p. 7164.
181. Huang, B., et al., *Exosomes derived from human adipose mesenchymal stem cells improve ovary function of premature ovarian insufficiency by targeting SMAD.* Stem Cell Research & Therapy, 2018. **9**(1): p. 216.
182. Yuan, F.-L., et al., *Osteoclast-Derived Extracellular Vesicles: Novel Regulators of Osteoclastogenesis and Osteoclast-Osteoblasts Communication in Bone Remodeling.* Frontiers in physiology, 2018. **9**: p. 628-628.
183. Lee, M., *Influence of storage condition on exosome recovery.* Biotechnology and bioprocess engineering, 2016. **v. 21**(no. 2): p. pp. 299-304-2016 v.21 no.2.
184. Tang, T.-T., et al., *Extracellular Vesicles: Opportunities and Challenges for the Treatment of Renal Diseases.* Frontiers in physiology, 2019. **10**: p. 226-226.
185. Garikipati, V.N.S., et al., *Extracellular Vesicles and the Application of System Biology and Computational Modeling in Cardiac Repair.* Circulation research, 2018. **123**(2): p. 188-204.
186. Wiklander, O.P.B., et al., *Advances in therapeutic applications of extracellular vesicles.* Science translational medicine, 2019. **11**(492): p. eaav8521.
187. Dickhout, A. and R.R. Koenen, *Extracellular Vesicles as Biomarkers in Cardiovascular Disease; Chances and Risks.* Frontiers in Cardiovascular Medicine, 2018. **5**(113).
188. Saenz-Pipaon, G., et al., *Functional and transcriptomic analysis of extracellular vesicles identifies calprotectin as a new prognostic marker in peripheral arterial disease (PAD).* J Extracell Vesicles, 2020. **9**(1): p. 1729646.

189. Gupta, S.K., C. Bang, and T. Thum, *Circulating microRNAs as biomarkers and potential paracrine mediators of cardiovascular disease.* Circ Cardiovasc Genet, 2010. **3**(5): p. 484-8.
190. Michael, A., et al., *Exosomes from human saliva as a source of microRNA biomarkers.* Oral Dis, 2010. **16**(1): p. 34-8.
191. Gheinani, A.H., et al., *Improved isolation strategies to increase the yield and purity of human urinary exosomes for biomarker discovery.* Scientific reports, 2018. **8**(1): p. 3945-3945.
192. Ohno, S., et al., *Systemically injected exosomes targeted to EGFR deliver antitumor microRNA to breast cancer cells.* Mol Ther, 2013. **21**(1): p. 185-91.
193. Bunggulawa, E.J., et al., *Recent advancements in the use of exosomes as drug delivery systems.* Journal of Nanobiotechnology, 2018. **16**(1): p. 81.
194. Luan, X., et al., *Engineering exosomes as refined biological nanoplatforms for drug delivery.* Acta Pharmacologica Sinica, 2017. **38**(6): p. 754-763.
195. Akers, J.C., et al., *Optimizing preservation of extracellular vesicular miRNAs derived from clinical cerebrospinal fluid.* Cancer biomarkers : section A of Disease markers, 2016. **17**(2): p. 125-132.
196. An, M., et al., *Comparison of an Optimized Ultracentrifugation Method versus Size-Exclusion Chromatography for Isolation of Exosomes from Human Serum.* Journal of proteome research, 2018. **17**(10): p. 3599-3605.
197. Crain, S.K., et al., *Extracellular Vesicles from Wharton's Jelly Mesenchymal Stem Cells Suppress CD4 Expressing T Cells Through Transforming Growth Factor Beta and Adenosine Signaling in a Canine Model.* Stem Cells Dev, 2019. **28**(3): p. 212-226.
198. Clayton, A., et al., *Adhesion and signaling by B cell-derived exosomes: the role of integrins.* Faseb j, 2004. **18**(9): p. 977-9.
199. Kumeda, N., et al., *Characterization of Membrane Integrity and Morphological Stability of Human Salivary Exosomes.* Biological and Pharmaceutical Bulletin, 2017. **40**(8): p. 1183-1191.
200. Böing, A.N., et al., *Single-step isolation of extracellular vesicles by size-exclusion chromatography.* J Extracell Vesicles, 2014. **3**.
201. Livshits, M.A., et al., *Isolation of exosomes by differential centrifugation: Theoretical analysis of a commonly used protocol.* Scientific Reports, 2015. **5**(1): p. 17319.
202. Benedikter, B.J., et al., *Ultrafiltration combined with size exclusion chromatography efficiently isolates extracellular vesicles from cell culture media for compositional and functional studies.* Scientific Reports, 2017. **7**(1): p. 15297.
203. Nordin, J.Z., et al., *Ultrafiltration with size-exclusion liquid chromatography for high yield isolation of extracellular vesicles preserving intact biophysical and functional properties.* Nanomedicine: Nanotechnology, Biology and Medicine, 2015. **11**(4): p. 879-883.
204. Guerreiro, E.M., et al., *Efficient extracellular vesicle isolation by combining cell media modifications, ultrafiltration, and size-exclusion chromatography.* PLOS ONE, 2018. **13**(9): p. e0204276.
205. Momen-Heravi, F., et al., *Impact of biofluid viscosity on size and sedimentation efficiency of the isolated microvesicles.* Front Physiol, 2012. **3**: p. 162.
206. Cvjetkovic, A., J. Lötvall, and C. Lässer, *The influence of rotor type and centrifugation time on the yield and purity of extracellular vesicles.* J Extracell Vesicles, 2014. **3**.

207. Abramowicz, A., P. Widlak, and M. Pietrowska, *Proteomic analysis of exosomal cargo: the challenge of high purity vesicle isolation.* Molecular BioSystems, 2016. **12**(5): p. 1407-1419.
208. Rikkert, L.G., et al., *Centrifugation affects the purity of liquid biopsy-based tumor biomarkers.* Cytometry Part A, 2018. **93**(12): p. 1207-1212.
209. Li, X., et al., *Challenges and opportunities in exosome research-Perspectives from biology, engineering, and cancer therapy.* APL Bioeng, 2019. **3**(1): p. 011503.
210. Yang, D., et al., *Progress, opportunity, and perspective on exosome isolation - efforts for efficient exosome-based theranostics.* Theranostics, 2020. **10**(8): p. 3684-3707.
211. Fernández-Llama, P., et al., *Tamm-Horsfall protein and urinary exosome isolation.* Kidney Int, 2010. **77**(8): p. 736-42.
212. Chen, C., et al., *Microfluidic isolation and transcriptome analysis of serum microvesicles.* Lab Chip, 2010. **10**(4): p. 505-11.
213. Hogan, M.C., et al., *Subfractionation, characterization, and in-depth proteomic analysis of glomerular membrane vesicles in human urine.* Kidney Int, 2014. **85**(5): p. 1225-37.
214. de Araújo, M.E., G. Lamberti, and L.A. Huber, *Isolation of Early and Late Endosomes by Density Gradient Centrifugation.* Cold Spring Harb Protoc, 2015. **2015**(11): p. 1013-6.
215. Onódi, Z., et al., *Isolation of High-Purity Extracellular Vesicles by the Combination of Iodixanol Density Gradient Ultracentrifugation and Bind-Elute Chromatography From Blood Plasma.* Frontiers in Physiology, 2018. **9**(1479).
216. Li, K., et al., *Cushioned-Density Gradient Ultracentrifugation (C-DGUC): A Refined and High Performance Method for the Isolation, Characterization, and Use of Exosomes.* Methods in molecular biology (Clifton, N.J.), 2018. **1740**: p. 69-83.
217. Duong, P., et al., *Cushioned-Density Gradient Ultracentrifugation (C-DGUC) improves the isolation efficiency of extracellular vesicles.* PloS one, 2019. **14**(4): p. e0215324-e0215324.
218. Vergauwen, G., et al., *Confounding factors of ultrafiltration and protein analysis in extracellular vesicle research.* Scientific Reports, 2017. **7**(1): p. 2704.
219. Quintana, J.F., et al., *Extracellular Onchocerca -derived small RNAs in host nodules and blood.* Parasites & Vectors, 2015. **8**(1): p. 58.
220. Li, P., et al., *Progress in Exosome Isolation Techniques.* Theranostics, 2017. **7**(3): p. 789-804.
221. Cutler, P., *Size-Exclusion Chromatography*, in *Methods in Molecular Biology: Protein Purification Protocols*, P. Cutler, Editor. 2004, Humana Press Inc.: Totowa, NJ. p. 239 - 252.
222. Gámez-Valero, A., et al., *Size-Exclusion Chromatography-based isolation minimally alters Extracellular Vesicles' characteristics compared to precipitating agents.* Sci Rep, 2016. **6**: p. 33641.
223. Mol, E.A., et al., *Higher functionality of extracellular vesicles isolated using size-exclusion chromatography compared to ultracentrifugation.* Nanomedicine: Nanotechnology, Biology and Medicine, 2017. **13**(6): p. 2061-2065.
224. An, M., et al., *Comparison of an Optimized Ultracentrifugation Method versus Size-Exclusion Chromatography for Isolation of Exosomes from Human Serum.* J Proteome Res, 2018. **17**(10): p. 3599-3605.

225. Sokolova, V., et al., *Characterisation of exosomes derived from human cells by nanoparticle tracking analysis and scanning electron microscopy.* Colloids Surf B Biointerfaces, 2011. **87**(1): p. 146-50.
226. Taylor, D.D., I.N. Chou, and P.H. Black, *Isolation of plasma membrane fragments from cultured murine melanoma cells.* Biochem Biophys Res Commun, 1983. **113**(2): p. 470-6.
227. Taylor, D.D., W. Zacharias, and C. Gercel-Taylor, *Exosome isolation for proteomic analyses and RNA profiling.* Methods Mol Biol, 2011. **728**: p. 235-46.
228. Ogawa, Y., et al., *Exosome-like vesicles with dipeptidyl peptidase IV in human saliva.* Biol Pharm Bull, 2008. **31**(6): p. 1059-62.
229. Hong, C.-S., et al., *Isolation of biologically active and morphologically intact exosomes from plasma of patients with cancer.* Journal of extracellular vesicles, 2016. **5**: p. 29289-29289.
230. Muller, L., et al., *Isolation of biologically-active exosomes from human plasma.* J Immunol Methods, 2014. **411**: p. 55-65.
231. Rood, I.M., et al., *Comparison of three methods for isolation of urinary microvesicles to identify biomarkers of nephrotic syndrome.* Kidney Int, 2010. **78**(8): p. 810-6.
232. Lötvall, J., et al., *Minimal experimental requirements for definition of extracellular vesicles and their functions: a position statement from the International Society for Extracellular Vesicles.* Journal of extracellular vesicles, 2014. **3**: p. 26913-26913.
233. Théry, C., et al., *Minimal information for studies of extracellular vesicles 2018 (MISEV2018): a position statement of the International Society for Extracellular Vesicles and update of the MISEV2014 guidelines.* J Extracell Vesicles, 2018. **7**(1): p. 1535750.
234. Eggenhofer, E., et al., *Mesenchymal stem cells are short-lived and do not migrate beyond the lungs after intravenous infusion.* Front Immunol, 2012. **3**: p. 297.
235. Gao, J., et al., *The dynamic in vivo distribution of bone marrow-derived mesenchymal stem cells after infusion.* Cells Tissues Organs, 2001. **169**(1): p. 12-20.
236. Toma, C., et al., *Fate of culture-expanded mesenchymal stem cells in the microvasculature: in vivo observations of cell kinetics.* Circ Res, 2009. **104**(3): p. 398-402.
237. Koç, O.N., et al., *Allogeneic mesenchymal stem cell infusion for treatment of metachromatic leukodystrophy (MLD) and Hurler syndrome (MPS-IH).* Bone Marrow Transplantation, 2002. **30**(4): p. 215-222.
238. Fischer, U.M., et al., *Pulmonary passage is a major obstacle for intravenous stem cell delivery: the pulmonary first-pass effect.* Stem Cells Dev, 2009. **18**(5): p. 683-92.
239. Gao, Y., et al., *Multilineage potential research of bovine amniotic fluid mesenchymal stem cells.* Int J Mol Sci, 2014. **15**(3): p. 3698-710.
240. Ge, J., et al., *The size of mesenchymal stem cells is a significant cause of vascular obstructions and stroke.* Stem Cell Rev Rep, 2014. **10**(2): p. 295-303.
241. Furlani, D., et al., *Is the intravascular administration of mesenchymal stem cells safe? Mesenchymal stem cells and intravital microscopy.* Microvasc Res, 2009. **77**(3): p. 370-6.
242. Schrepfer, S., et al., *Stem cell transplantation: the lung barrier.* Transplant Proc, 2007. **39**(2): p. 573-6.
243. Barbash, I.M., et al., *Systemic delivery of bone marrow-derived mesenchymal stem cells to the infarcted myocardium: feasibility, cell migration, and body distribution.* Circulation, 2003. **108**(7): p. 863-8.

244. Tatsumi, K., et al., *Tissue factor triggers procoagulation in transplanted mesenchymal stem cells leading to thromboembolism.* Biochem Biophys Res Commun, 2013. **431**(2): p. 203-9.
245. Karp, J.M. and G.S. Leng Teo, *Mesenchymal Stem Cell Homing: The Devil Is in the Details.* Cell Stem Cell, 2009. **4**(3): p. 206-216.
246. Qian, H., et al., *Contribution of alpha6 integrins to hematopoietic stem and progenitor cell homing to bone marrow and collaboration with alpha4 integrins.* Blood, 2006. **107**(9): p. 3503-10.
247. Liao, L., et al., *Heparin improves BMSC cell therapy: Anticoagulant treatment by heparin improves the safety and therapeutic effect of bone marrow-derived mesenchymal stem cell cytotherapy.* Theranostics, 2017. **7**(1): p. 106-116.
248. Bennet, W., et al., *Incompatibility between human blood and isolated islets of Langerhans: a finding with implications for clinical intraportal islet transplantation?* Diabetes, 1999. **48**(10): p. 1907-14.
249. Nilsson, B., et al., *Can cells and biomaterials in therapeutic medicine be shielded from innate immune recognition?* Trends Immunol, 2010. **31**(1): p. 32-8.
250. Goto, M., et al., *Dissecting the instant blood-mediated inflammatory reaction in islet xenotransplantation.* Xenotransplantation, 2008. **15**(4): p. 225-234.
251. Cheng, Y., et al., *Mechanism for the Instant Blood-Mediated Inflammatory Reaction in Rat Islet Transplantation.* Transplant Proc, 2017. **49**(6): p. 1440-1443.
252. Quimby, J.M., et al., *Safety and efficacy of intravenous infusion of allogeneic cryopreserved mesenchymal stem cells for treatment of chronic kidney disease in cats: results of three sequential pilot studies.* Stem cell research & therapy, 2013. **4**(2): p. 48-48.
253. Chu, A.J., *Tissue factor, blood coagulation, and beyond: an overview.* Int J Inflam, 2011. **2011**: p. 367284.
254. Mandal, S.K., U.R. Pendurthi, and L.V. Rao, *Cellular localization and trafficking of tissue factor.* Blood, 2006. **107**(12): p. 4746-53.
255. Okorie, U.M., et al., *Determination of surface tissue factor thresholds that trigger coagulation at venous and arterial shear rates: amplification of 100 fM circulating tissue factor requires flow.* Blood, 2008. **111**(7): p. 3507-3513.
256. Bogdanov, V.Y., et al., *Alternatively spliced human tissue factor: a circulating, soluble, thrombogenic protein.* Nat Med, 2003. **9**(4): p. 458-62.
257. Rapaport, S.I. and L.V. Rao, *The tissue factor pathway: how it has become a "prima ballerina".* Thromb Haemost, 1995. **74**(1): p. 7-17.
258. Bromberg, M.E., et al., *Role of tissue factor in metastasis: functions of the cytoplasmic and extracellular domains of the molecule.* Thromb Haemost, 1999. **82**(1): p. 88-92.
259. Carmeliet, P., et al., *Role of tissue factor in embryonic blood vessel development.* Nature, 1996. **383**(6595): p. 73-5.
260. Oeller, M., et al., *Selection of Tissue Factor-Deficient Cell Transplants as a Novel Strategy for Improving Hemocompatibility of Human Bone Marrow Stromal Cells.* Theranostics, 2018. **8**(5): p. 1421-1434.
261. George, M.J., et al., *Clinical Cellular Therapeutics Accelerate Clot Formation.* Stem cells translational medicine, 2018. **7**(10): p. 731-739.

262. Gleeson, B.M., et al., *Bone Marrow-Derived Mesenchymal Stem Cells Have Innate Procoagulant Activity and Cause Microvascular Obstruction Following Intracoronary Delivery: Amelioration by Antithrombin Therapy.* Stem Cells, 2015. **33**(9): p. 2726-37.
263. Krishnamurthy, M. and M.L. Freedman, *Complications of anticoagulation with heparin.* Virtual Mentor, 2005. **7**(4).
264. Ullah, M., et al., *Stem cell-derived extracellular vesicles: role in oncogenic processes, bioengineering potential, and technical challenges.* Stem cell research & therapy, 2019. **10**(1): p. 347-347.
265. Tannetta, D., et al., *Extracellular vesicles and reproduction–promotion of successful pregnancy.* Cellular & Molecular Immunology, 2014. **11**(6): p. 548-563.
266. Kleinjan, A., et al., *Microparticles in vascular disorders: how tissue factor-exposing vesicles contribute to pathology and physiology.* Thromb Res, 2012. **130 Suppl 1**: p. S71-3.
267. Hisada, Y. and N. Mackman, *Measurement of tissue factor activity in extracellular vesicles from human plasma samples.* Research and Practice in Thrombosis and Haemostasis, 2018. **3**.
268. Schmedes, C.M., et al., *Circulating Extracellular Vesicle Tissue Factor Activity During Orthohantavirus Infection Is Associated With Intravascular Coagulation.* The Journal of Infectious Diseases, 2019. **222**(8): p. 1392-1399.
269. Hisada, Y., et al., *Detection of tissue factor-positive extracellular vesicles by laser scanning confocal microscopy.* Thrombosis Research, 2017. **150**: p. 65-72.
270. Mørk, M., et al., *Elevated blood plasma levels of tissue factor-bearing extracellular vesicles in patients with atrial fibrillation.* Thromb Res, 2019. **173**: p. 141-150.
271. Nielsen, T., et al., *Extracellular vesicle-associated procoagulant phospholipid and tissue factor activity in multiple myeloma.* PLoS One, 2019. **14**(1): p. e0210835.
272. van Es, N., et al., *Extracellular vesicles exposing tissue factor for the prediction of venous thromboembolism in patients with cancer: A prospective cohort study.* Thromb Res, 2018. **166**: p. 54-59.
273. Gomes, F.G., et al., *Breast-cancer extracellular vesicles induce platelet activation and aggregation by tissue factor-independent and -dependent mechanisms.* Thromb Res, 2017. **159**: p. 24-32.
274. Che, S.P.Y., J.Y. Park, and T. Stokol, *Tissue Factor-Expressing Tumor-Derived Extracellular Vesicles Activate Quiescent Endothelial Cells via Protease-Activated Receptor-1.* Front Oncol, 2017. **7**: p. 261.
275. Wortzel, I., et al., *Exosome-Mediated Metastasis: Communication from a Distance.* Dev Cell, 2019. **49**(3): p. 347-360.
276. Moll, G., et al., *Mesenchymal stromal cells engage complement and complement receptor bearing innate effector cells to modulate immune responses.* PLoS One, 2011. **6**(7): p. e21703.
277. Li, Y. and F. Lin, *Mesenchymal stem cells are injured by complement after their contact with serum.* Blood, 2012. **120**(17): p. 3436-43.
278. Galipeau, J., et al., *International Society for Cellular Therapy perspective on immune functional assays for mesenchymal stromal cells as potency release criterion for advanced phase clinical trials.* Cytotherapy, 2016. **18**(2): p. 151-9.

279. Smith, J.R., et al., *Standardizing Umbilical Cord Mesenchymal Stromal Cells for Translation to Clinical Use: Selection of GMP-Compliant Medium and a Simplified Isolation Method.* Stem Cells Int, 2016. **2016**: p. 6810980.
280. Fazzina, R., et al., *A new standardized clinical-grade protocol for banking human umbilical cord tissue cells.* Transfusion, 2015. **55**(12): p. 2864-73.
281. Badowski, M., A. Muise, and D.T. Harris, *Mixed effects of long-term frozen storage on cord tissue stem cells.* Cytotherapy, 2014. **16**(9): p. 1313-21.
282. Chatzistamatiou, T.K., et al., *Optimizing isolation culture and freezing methods to preserve Wharton's jelly's mesenchymal stem cell (MSC) properties: an MSC banking protocol validation for the Hellenic Cord Blood Bank.* Transfusion, 2014. **54**(12): p. 3108-20.
283. Han, Z.C., *Umbilical cord mesenchymal stem cells (UC-MSC: biology, banking and clinical applications).* Bull Acad Natl Med, 2009. **193**(3): p. 545-7; discussion 547.
284. Ganguly, P., et al., *Age-related Changes in Bone Marrow Mesenchymal Stromal Cells: A Potential Impact on Osteoporosis and Osteoarthritis Development.* Cell Transplant, 2017. **26**(9): p. 1520-1529.
285. Lepperdinger, G., *Inflammation and mesenchymal stem cell aging.* Curr Opin Immunol, 2011. **23**(4): p. 518-24.
286. Alt, E.U., et al., *Aging alters tissue resident mesenchymal stem cell properties.* Stem Cell Res, 2012. **8**(2): p. 215-25.
287. Saulnier, N., et al., *Canine placenta: A promising potential source of highly proliferative and immunomodulatory mesenchymal stromal cells?* Vet Immunol Immunopathol, 2016. **171**: p. 47-55.
288. Clark, K.C., et al., *Canine and Equine Mesenchymal Stem Cells Grown in Serum Free Media Have Altered Immunophenotype.* Stem Cell Rev Rep, 2016. **12**(2): p. 245-56.
289. Viswanathan, S., et al., *Soliciting strategies for developing cell-based reference materials to advance mesenchymal stromal cell research and clinical translation.* Stem Cells Dev, 2014. **23**(11): p. 1157-67.
290. Weiss, M.L., et al., *Manufacturing Cells for Clinical Use.* Stem Cells International, 2016. **2016**: p. 1750697.
291. Bertolo, A., et al., *Canine Mesenchymal Stem Cell Potential and the Importance of Dog Breed: Implication for Cell-Based Therapies.* Cell Transplant, 2015. **24**(10): p. 1969-80.
292. Escalhão, C.C.M., et al., *Safety of Allogeneic Canine Adipose Tissue-Derived Mesenchymal Stem Cell Intraspinal Transplantation in Dogs with Chronic Spinal Cord Injury.* Stem Cells International, 2017. **2017**: p. 3053759.
293. Taroni, M., et al., *Evaluation of the Effect of a Single Intra-articular Injection of Allogeneic Neonatal Mesenchymal Stromal Cells Compared to Oral Non-Steroidal Anti-inflammatory Treatment on the Postoperative Musculoskeletal Status and Gait of Dogs over a 6-Month Period after Tibial Plateau Leveling Osteotomy: A Pilot Study.* Front Vet Sci, 2017. **4**: p. 83.
294. Choi, S.A., et al., *Isolation of canine mesenchymal stem cells from amniotic fluid and differentiation into hepatocyte-like cells.* In Vitro Cell Dev Biol Anim, 2013. **49**(1): p. 42-51.
295. Csaki, C., et al., *Chondrogenesis, osteogenesis and adipogenesis of canine mesenchymal stem cells: a biochemical, morphological and ultrastructural study.* Histochem Cell Biol, 2007. **128**(6): p. 507-20.

296. Whitworth, D.J., et al., *Derivation of mesenchymal stromal cells from canine induced pluripotent stem cells by inhibition of the TGFβ/activin signaling pathway.* Stem cells and development, 2014. **23**(24): p. 3021-3033.
297. Vieira, N.M., et al., *Isolation, characterization, and differentiation potential of canine adipose-derived stem cells.* Cell Transplant, 2010. **19**(3): p. 279-89.
298. Kisiel, A.H., et al., *Isolation, characterization, and in vitro proliferation of canine mesenchymal stem cells derived from bone marrow, adipose tissue, muscle, and periosteum.* Am J Vet Res, 2012. **73**(8): p. 1305-17.
299. Takemitsu, H., et al., *Comparison of bone marrow and adipose tissue-derived canine mesenchymal stem cells.* BMC Vet Res, 2012. **8**: p. 150.
300. Chow, L., et al., *Mechanisms of Immune Suppression Utilized by Canine Adipose and Bone Marrow-Derived Mesenchymal Stem Cells.* Stem Cells Dev, 2017. **26**(5): p. 374-389.
301. Heiden, T., et al., *Combined Analysis of DNA Ploidy, Proliferation, and Apoptosis in Paraffin-Embedded Cell Material by Flow Cytometry.* Laboratory Investigation, 2000. **80**(8): p. 1207-1213.
302. Darzynkiewicz, Z., H.D. Halicka, and H. Zhao, *Analysis of cellular DNA content by flow and laser scanning cytometry.* Advances in experimental medicine and biology, 2010. **676**: p. 137-147.
303. Hong, J., et al., *A Focused Microarray for Screening Rat Embryonic Stem Cell Lines.* Stem Cells and Development, 2013. **22**(3): p. 431-443.
304. Kobayashi, K., et al., *On-site fabrication of Bi-layered adhesive mesenchymal stromal cell-dressings for the treatment of heart failure.* Biomaterials, 2019. **209**: p. 41-53.
305. Carrion, B., et al., *A safe and efficient method to retrieve mesenchymal stem cells from three-dimensional fibrin gels.* Tissue engineering. Part C, Methods, 2014. **20**(3): p. 252-263.
306. Nawrocka, D., et al., *Basic Fibroblast Growth Factor Inhibits Apoptosis and Promotes Proliferation of Adipose-Derived Mesenchymal Stromal Cells Isolated from Patients with Type 2 Diabetes by Reducing Cellular Oxidative Stress.* Oxid Med Cell Longev, 2017. **2017**: p. 3027109.
307. Colenci, R., et al., *Bone marrow mesenchymal stem cells stimulated by bFGF up-regulated protein expression in comparison with periodontal fibroblasts in vitro.* Arch Oral Biol, 2014. **59**(3): p. 268-76.
308. Fierro, F.A., et al., *Effects on proliferation and differentiation of multipotent bone marrow stromal cells engineered to express growth factors for combined cell and gene therapy.* Stem Cells, 2011. **29**(11): p. 1727-37.
309. Devireddy, L.R., et al., *A serum-free medium formulation efficiently supports isolation and propagation of canine adipose-derived mesenchymal stem/stromal cells.* PLoS One, 2019. **14**(2): p. e0210250.
310. Bearden, R.N., et al., *In-vitro characterization of canine multipotent stromal cells isolated from synovium, bone marrow, and adipose tissue: a donor-matched comparative study.* Stem Cell Res Ther, 2017. **8**(1): p. 218.
311. Kang, J.W., et al., *Soluble factors-mediated immunomodulatory effects of canine adipose tissue-derived mesenchymal stem cells.* Stem Cells Dev, 2008. **17**(4): p. 681-93.

312. Mielcarek, M., et al., *Mesenchymal stromal cells fail to prevent acute graft-versus-host disease and graft rejection after dog leukocyte antigen-haploidentical bone marrow transplantation.* Biol Blood Marrow Transplant, 2011. **17**(2): p. 214-25.
313. Rodríguez Sánchez, D.N., et al., *Canine Adipose-Derived Mesenchymal Stromal Cells Enhance Neuroregeneration in a Rat Model of Sciatic Nerve Crush Injury.* Cell Transplant, 2019. **28**(1): p. 47-54.
314. Ryu, H.H., et al., *Functional recovery and neural differentiation after transplantation of allogenic adipose-derived stem cells in a canine model of acute spinal cord injury.* J Vet Sci, 2009. **10**(4): p. 273-84.
315. Sasaki, A., et al., *Canine mesenchymal stem cells from synovium have a higher chondrogenic potential than those from infrapatellar fat pad, adipose tissue, and bone marrow.* PLoS One, 2018. **13**(8): p. e0202922.
316. Wood, J.A., et al., *Periocular and intra-articular injection of canine adipose-derived mesenchymal stem cells: an in vivo imaging and migration study.* Journal of ocular pharmacology and therapeutics : the official journal of the Association for Ocular Pharmacology and Therapeutics, 2012. **28**(3): p. 307-317.
317. Alves, E.G., et al., *Comparison of the osteogenic potential of mesenchymal stem cells from the bone marrow and adipose tissue of young dogs.* BMC Vet Res, 2014. **10**: p. 190.
318. Wang, T., et al., *Osteoinduction and proliferation of bone-marrow stromal cells in three-dimensional poly (ε-caprolactone)/ hydroxyapatite/collagen scaffolds.* J Transl Med, 2015. **13**: p. 152.
319. Tan, G.K., et al., *Effects of biomimetic surfaces and oxygen tension on redifferentiation of passaged human fibrochondrocytes in 2D and 3D cultures.* Biomaterials, 2011. **32**(24): p. 5600-14.
320. Spencer, A.Y. and T.E. Lallier, *Mechanical tension alters semaphorin expression in the periodontium.* J Periodontol, 2009. **80**(10): p. 1665-73.
321. Olsen, T.R., et al., *Peak MSC-Are We There Yet?* Front Med (Lausanne), 2018. **5**: p. 178.
322. Patel, D.B., et al., *Effects of cell seeding density and passage number on mesenchymal stem cell exosome biogenesis and vascularization activity.* Bioengineering and Translational Medicine, 2017(2): p. 170-179.
323. Ludwig, N., T.L. Whiteside, and T.E. Reichert, *Challenges in Exosome Isolation and Analysis in Health and Disease.* Int J Mol Sci, 2019. **20**(19).
324. Oshima, K., et al., *Secretion of a peripheral membrane protein, MFG-E8, as a complex with membrane vesicles.* Eur J Biochem, 2002. **269**(4): p. 1209-18.
325. Fedele, C., et al., *The αvβ6 integrin is transferred intercellularly via exosomes.* J Biol Chem, 2015. **290**(8): p. 4545-51.
326. Cui, X., et al., *Exosomes From Adipose-derived Mesenchymal Stem Cells Protect the Myocardium Against Ischemia/Reperfusion Injury Through Wnt/β-Catenin Signaling Pathway.* Journal of cardiovascular pharmacology, 2017. **70**(4): p. 225-231.
327. Shimoda, A., et al., *Glycan profiling analysis using evanescent-field fluorescence-assisted lectin array: Importance of sugar recognition for cellular uptake of exosomes from mesenchymal stem cells.* Biochem Biophys Res Commun, 2017. **491**(3): p. 701-707.
328. McAtee, C.O., et al., *Prostate tumor cell exosomes containing hyaluronidase Hyal1 stimulate prostate stromal cell motility by engagement of FAK-mediated integrin signaling.* Matrix Biol, 2019. **78-79**: p. 165-179.

329. Karasu, E., et al., *Extracellular Vesicles: Packages Sent With Complement.* Frontiers in immunology, 2018. **9**: p. 721-721.
330. Robbins, P.D. and A.E. Morelli, *Regulation of immune responses by extracellular vesicles.* Nature reviews. Immunology, 2014. **14**(3): p. 195-208.
331. Fujita, R., et al., *Endogenous Mesenchymal Stromal Cells in Bone Marrow Are Required to Preserve Muscle Function in mdx Mice.* STEM CELLS, 2015. **33**(3): p. 962-975.
332. Yang, M. and S.Y. Wu, *The Advances and Challenges in Utilizing Exosomes for Delivering Cancer Therapeutics.* Frontiers in pharmacology, 2018. **9**: p. 735-735.
333. Ramirez, M.I., et al., *Technical challenges of working with extracellular vesicles.* Nanoscale, 2018. **10**(3): p. 881-906.
334. Mentkowski, K.I., et al., *Therapeutic Potential of Engineered Extracellular Vesicles.* The AAPS Journal, 2018. **20**(3): p. 50.
335. Pieters, B.C., et al., *Commercial cow milk contains physically stable extracellular vesicles expressing immunoregulatory TGF-β.* PLoS One, 2015. **10**(3): p. e0121123.
336. Bosch, S., et al., *Trehalose prevents aggregation of exosomes and cryodamage.* Scientific Reports, 2016. **6**(1): p. 36162.
337. Jeyaram, A. and S.M. Jay, *Preservation and Storage Stability of Extracellular Vesicles for Therapeutic Applications.* The AAPS journal, 2017. **20**(1): p. 1-1.
338. Zhou, H., et al., *Collection, storage, preservation, and normalization of human urinary exosomes for biomarker discovery.* Kidney Int, 2006. **69**(8): p. 1471-6.
339. Lőrincz, Á.M., et al., *Effect of storage on physical and functional properties of extracellular vesicles derived from neutrophilic granulocytes.* Journal of extracellular vesicles, 2014. **3**: p. 25465-25465.
340. Bæk, R., et al., *The impact of various preanalytical treatments on the phenotype of small extracellular vesicles in blood analyzed by protein microarray.* J Immunol Methods, 2016. **438**: p. 11-20.
341. Cheng, Y., et al., *Effect of pH, temperature and freezing-thawing on quantity changes and cellular uptake of exosomes.* Protein Cell, 2019. **10**(4): p. 295-299.
342. Kreke, M., et al., *Processes for producing stable exosome formulations*. 2015, CAPRICOR, Inc. : United States.
343. Charoenviriyakul, C., et al., *Preservation of exosomes at room temperature using lyophilization.* Int J Pharm, 2018. **553**(1-2): p. 1-7.
344. Liu, T., et al., *EVmiRNA: a database of miRNA profiling in extracellular vesicles.* Nucleic Acids Res, 2019. **47**(D1): p. D89-d93.
345. Vaswani, K., et al., *A Method for the Isolation of Exosomes from Human and Bovine Milk.* Journal of Nutrition and Metabolism, 2019. **2019**: p. 5764740.
346. Whiteside, T.L., *Exosomes and tumor-mediated immune suppression.* The Journal of Clinical Investigation, 2016. **126**(4): p. 1216-1223.
347. Brennan, K., et al., *A comparison of methods for the isolation and separation of extracellular vesicles from protein and lipid particles in human serum.* Scientific Reports, 2020. **10**(1): p. 1039.
348. Langevin, S.M., et al., *Balancing yield, purity and practicality: a modified differential ultracentrifugation protocol for efficient isolation of small extracellular vesicles from human serum.* RNA Biol, 2019. **16**(1): p. 5-12.

349. Parsons, M.E.M., et al., *A Protocol for Improved Precision and Increased Confidence in Nanoparticle Tracking Analysis Concentration Measurements between 50 and 120 nm in Biological Fluids.* Frontiers in cardiovascular medicine, 2017. **4**: p. 68-68.
350. Tekkatte, C., et al., *"Humanized" stem cell culture techniques: the animal serum controversy.* Stem cells international, 2011. **2011**: p. 504723-504723.
351. Dessels, C., M. Potgieter, and M.S. Pepper, *Making the Switch: Alternatives to Fetal Bovine Serum for Adipose-Derived Stromal Cell Expansion.* Frontiers in Cell and Developmental Biology, 2016. **4**(115).
352. Patel, G.K., et al., *Comparative analysis of exosome isolation methods using culture supernatant for optimum yield, purity and downstream applications.* Scientific Reports, 2019. **9**(1): p. 5335.
353. Takasugi, M., et al., *Small extracellular vesicles secreted from senescent cells promote cancer cell proliferation through EphA2.* Nature Communications, 2017. **8**(1): p. 15729.
354. Kadota, T., et al., *Emerging role of extracellular vesicles as a senescence-associated secretory phenotype: Insights into the pathophysiology of lung diseases.* Mol Aspects Med, 2018. **60**: p. 92-103.
355. Bonab, M.M., et al., *Aging of mesenchymal stem cell in vitro.* BMC Cell Biol, 2006. **7**: p. 14.
356. Izadpanah, R., et al., *Long-term in vitro expansion alters the biology of adult mesenchymal stem cells.* Cancer research, 2008. **68**(11): p. 4229-4238.
357. Danaei, M., et al., *Impact of Particle Size and Polydispersity Index on the Clinical Applications of Lipidic Nanocarrier Systems.* Pharmaceutics, 2018. **10**(2).
358. Midekessa, G., et al., *Zeta Potential of Extracellular Vesicles: Toward Understanding the Attributes that Determine Colloidal Stability.* ACS Omega, 2020. **5**(27): p. 16701-16710.
359. Chang, M., et al., *Exosome purification based on PEG-coated Fe3O4 nanoparticles.* PLOS ONE, 2018. **13**(6): p. e0199438.
360. Deregibus, M.C., et al., *Charge-based precipitation of extracellular vesicles.* International journal of molecular medicine, 2016. **38**(5): p. 1359-1366.
361. Chen, C., et al., *An overview of liposome lyophilization and its future potential.* J Control Release, 2010. **142**(3): p. 299-311.
362. Lee, M.K., et al., *Cryoprotectants for freeze drying of drug nano-suspensions: effect of freezing rate.* J Pharm Sci, 2009. **98**(12): p. 4808-17.
363. Abdelwahed, W., et al., *Freeze-drying of nanoparticles: formulation, process and storage considerations.* Adv Drug Deliv Rev, 2006. **58**(15): p. 1688-713.
364. Kusuma, G.D., et al., *To Protect and to Preserve: Novel Preservation Strategies for Extracellular Vesicles.* Frontiers in Pharmacology, 2018. **9**(1199).
365. Leslie, S.B., et al., *Trehalose and sucrose protect both membranes and proteins in intact bacteria during drying.* Applied and environmental microbiology, 1995. **61**(10): p. 3592-3597.
366. Hood, J.L., M.J. Scott, and S.A. Wickline, *Maximizing exosome colloidal stability following electroporation.* Anal Biochem, 2014. **448**: p. 41-9.
367. Buchanan, S.S., et al., *Cryopreservation of Human Hematopoietic Stem and Progenitor Cells Loaded with Trehalose: Transient Permeabilization via the Adenosine Triphosphate-Dependent P2Z Receptor Channel.* Cell Preservation Technology, 2005. **3**(4): p. 212-222.

368. Motta, J.P., et al., *Evaluation of intracellular and extracellular trehalose as a cryoprotectant of stem cells obtained from umbilical cord blood.* Cryobiology, 2014. **68**(3): p. 343-8.
369. Wu, Y., W. Deng, and D.J. Klinke, 2nd, *Exosomes: improved methods to characterize their morphology, RNA content, and surface protein biomarkers.* Analyst, 2015. **140**(19): p. 6631-42.
370. Maroto, R., et al., *Effects of storage temperature on airway exosome integrity for diagnostic and functional analyses.* Journal of extracellular vesicles, 2017. **6**(1): p. 1359478-1359478.
371. Gupta, A., et al., *Mesenchymal stem cells and exosome therapy for COVID-19: current status and future perspective.* Human cell, 2020. **33**(4): p. 907-918.
372. Moll, G., et al., *MSC Therapies for COVID-19: Importance of Patient Coagulopathy, Thromboprophylaxis, Cell Product Quality and Mode of Delivery for Treatment Safety and Efficacy.* Frontiers in Immunology, 2020. **11**(1091).
373. Rezakhani, L., et al., *Mesenchymal stem cell (MSC)-derived exosomes as a cell-free therapy for patients Infected with COVID-19: Real opportunities and range of promises.* Chemistry and physics of lipids, 2021. **234**: p. 105009-105009.
374. Sengupta, V., et al., *Exosomes Derived from Bone Marrow Mesenchymal Stem Cells as Treatment for Severe COVID-19.* Stem cells and development, 2020. **29**(12): p. 747-754.
375. Momen-Heravi, F., *Isolation of Extracellular Vesicles by Ultracentrifugation*, in *Extracellular Vesicles: Methods and Protocols*, W.P. Kuo and S. Jia, Editors. 2017, Springer New York: New York, NY. p. 25-32.
376. Kim, D.K., et al., *EVpedia: an integrated database of high-throughput data for systemic analyses of extracellular vesicles.* J Extracell Vesicles, 2013. **2**.
377. Keerthikumar, S., et al., *ExoCarta: A Web-Based Compendium of Exosomal Cargo.* Journal of molecular biology, 2016. **428**(4): p. 688-692.
378. Wang, J., et al., *Boosting the Biogenesis and Secretion of Mesenchymal Stem Cell-Derived Exosomes.* Cells, 2020. **9**(3).
379. Takov, K., D.M. Yellon, and S.M. Davidson, *Comparison of small extracellular vesicles isolated from plasma by ultracentrifugation or size-exclusion chromatography: yield, purity and functional potential.* Journal of extracellular vesicles, 2018. **8**(1): p. 1560809-1560809.
380. Greenwood, S.K., et al., *Population doubling: a simple and more accurate estimation of cell growth suppression in the in vitro assay for chromosomal aberrations that reduces irrelevant positive results.* Environ Mol Mutagen, 2004. **43**(1): p. 36-44.
381. Wang, Y., et al., *Long-term cultured mesenchymal stem cells frequently develop genomic mutations but do not undergo malignant transformation.* Cell Death & Disease, 2013. **4**(12): p. e950-e950.
382. Yang, Y.-H.K., et al., *Changes in phenotype and differentiation potential of human mesenchymal stem cells aging in vitro.* Stem Cell Research & Therapy, 2018. **9**(1): p. 131.
383. Wu, P.K., et al., *Early Passage Mesenchymal Stem Cells Display Decreased Radiosensitivity and Increased DNA Repair Activity.* Stem Cells Transl Med, 2017. **6**(6): p. 1504-1514.

384. Zhuang, Y., et al., *Comparison of biological properties of umbilical cord-derived mesenchymal stem cells from early and late passages: Immunomodulatory ability is enhanced in aged cells.* Mol Med Rep, 2015. **11**(1): p. 166-174.
385. Melzer, C., et al. *Taxol-Loaded MSC-Derived Exosomes Provide a Therapeutic Vehicle to Target Metastatic Breast Cancer and Other Carcinoma Cells*. Cancers, 2019. **11**, DOI: 10.3390/cancers11060798.
386. Kanchanapally, R., et al., *Drug-loaded exosomal preparations from different cell types exhibit distinctive loading capability, yield, and antitumor efficacies: a comparative analysis.* Int J Nanomedicine, 2019. **14**: p. 531-541.
387. Kırbaş, O.K., et al., *Optimized Isolation of Extracellular Vesicles From Various Organic Sources Using Aqueous Two-Phase System.* Scientific Reports, 2019. **9**(1): p. 19159.
388. Lobb, R.J., et al., *Optimized exosome isolation protocol for cell culture supernatant and human plasma.* J Extracell Vesicles, 2015. **4**: p. 27031.
389. Lamparski, H.G., et al., *Production and characterization of clinical grade exosomes derived from dendritic cells.* J Immunol Methods, 2002. **270**(2): p. 211-26.
390. Sidhom, K., P.O. Obi, and A. Saleem, *A Review of Exosomal Isolation Methods: Is Size Exclusion Chromatography the Best Option?* Int J Mol Sci, 2020. **21**(18).
391. Soares Martins, T., et al., *Exosome isolation from distinct biofluids using precipitation and column-based approaches.* PLoS One, 2018. **13**(6): p. e0198820.
392. Yu, L.-L., et al., *A Comparison of Traditional and Novel Methods for the Separation of Exosomes from Human Samples.* BioMed Research International, 2018. **2018**: p. 3634563.
393. El Baradie, K.B.Y., et al., *Freeze-Dried Extracellular Vesicles From Adipose-Derived Stem Cells Prevent Hypoxia-Induced Muscle Cell Injury.* Front Cell Dev Biol, 2020. **8**: p. 181.
394. Willms, E., et al., *Extracellular Vesicle Heterogeneity: Subpopulations, Isolation Techniques, and Diverse Functions in Cancer Progression.* Frontiers in Immunology, 2018. **9**(738).
395. Moravcikova, E., et al., *Proteomic Profiling of Native Unpassaged and Culture-Expanded Mesenchymal Stromal Cells (MSC).* Cytometry A, 2018. **93**(9): p. 894-904.
396. Moll, G., et al., *MSC Therapies for COVID-19: Importance of Patient Coagulopathy, Thromboprophylaxis, Cell Product Quality and Mode of Delivery for Treatment Safety and Efficacy.* Frontiers in immunology, 2020. **11**: p. 1091-1091.
397. Phinney, D.G. and M.F. Pittenger, *Concise Review: MSC-Derived Exosomes for Cell-Free Therapy.* Stem Cells, 2017. **35**(4): p. 851-858.
398. He, N., et al., *Exosomes: Cell-Free Therapy for Cardiovascular Diseases.* Journal of Cardiovascular Translational Research, 2020. **13**(5): p. 713-721.
399. Wu, P., et al., *MSC-exosome: A novel cell-free therapy for cutaneous regeneration.* Cytotherapy, 2018. **20**(3): p. 291-301.
400. Ma, Z.J., et al., *Mesenchymal stem cell-derived exosomes: Toward cell-free therapeutic strategies in regenerative medicine.* World J Stem Cells, 2020. **12**(8): p. 814-840.
401. Yin, K., S. Wang, and R.C. Zhao, *Exosomes from mesenchymal stem/stromal cells: a new therapeutic paradigm.* Biomarker Research, 2019. **7**(1): p. 8.
402. Hu, P., et al., *Mesenchymal stromal cells-exosomes: a promising cell-free therapeutic tool for wound healing and cutaneous regeneration.* Burns & Trauma, 2019. **7**.

403. Gruber, E.J., J.L. Catalfamo, and T. Stokol, *Role of tissue factor expression in thrombin generation by canine tumor cells.* Am J Vet Res, 2016. **77**(4): p. 404-12.
404. Knudsen, T., et al., *Characterization of canine coagulation factor VII and its complex formation with tissue factor: canine-human cross-species compatibility*. J Thromb Haemost, 2010. **8**(8): p. 1763-72.
405. Basavaraj, M.G., et al., *Differential ability of tissue factor antibody clones on detection of tissue factor in blood cells and microparticles.* Thromb Res, 2012. **130**(3): p. 538-46.
406. Tripisciano, C., et al., *Different Potential of Extracellular Vesicles to Support Thrombin Generation: Contributions of Phosphatidylserine, Tissue Factor, and Cellular Origin.* Scientific Reports, 2017. **7**(1): p. 6522.
407. Hu, Z., et al., *Tissue factor is an angiogenic-specific receptor for factor VII-targeted immunotherapy and photodynamic therapy.* Angiogenesis, 2017. **20**(1): p. 85-96.
408. Friedenstein, A.J., R.K. Chailakhyan, and U.V. Gerasimov, *Bone marrow osteogenic stem cells: in vitro cultivation and transplantation in diffusion chambers.* Cell Tissue Kinet, 1987. **20**(3): p. 263-72.
409. Haynesworth, S.E., et al., *Characterization of cells with osteogenic potential from human marrow*. Bone, 1992. **13**(1): p. 81-88.
410. Lazarus, H.M., et al., *Ex vivo expansion and subsequent infusion of human bone marrow-derived stromal progenitor cells (mesenchymal progenitor cells): implications for therapeutic use.* Bone Marrow Transplant, 1995. **16**(4): p. 557-64.
411. Li, Y., J. Fung, and F. Lin, *Local Inhibition of Complement Improves Mesenchymal Stem Cell Viability and Function After Administration.* Mol Ther, 2016. **24**(9): p. 1665-74.
412. Vu, Q., et al., *Meta-analysis of preclinical studies of mesenchymal stromal cells for ischemic stroke.* Neurology, 2014. **82**(14): p. 1277-1286.
413. Squillaro, T., G. Peluso, and U. Galderisi, *Clinical Trials With Mesenchymal Stem Cells: An Update.* Cell Transplant, 2016. **25**(5): p. 829-48.
414. Lukomska, B., et al., *Challenges and Controversies in Human Mesenchymal Stem Cell Therapy.* Stem Cells International, 2019. **2019**: p. 9628536.
415. Dave, C., et al., *Comparison of freshly cultured versus freshly thawed (cryopreserved) mesenchymal stem cells in preclinical in vivo models of inflammation: a protocol for a preclinical systematic review and meta-analysis.* Systematic Reviews, 2020. **9**(1): p. 188.
416. Mendicino, M., et al., *MSC-Based Product Characterization for Clinical Trials: An FDA Perspective.* Cell Stem Cell, 2014. **14**(2): p. 141-145.
417. Jr., J.F.S., *U.S. Research and Development Funding and Performance: Fact Sheet*, C.R. Service, Editor. 2020. p. 1-6.
418. Viswanathan, S., et al., *Mesenchymal stem versus stromal cells: International Society for Cell & Gene Therapy (ISCT®) Mesenchymal Stromal Cell committee position statement on nomenclature.* Cytotherapy, 2019. **21**(10): p. 1019-1024.
419. Brazma, A., et al., *Minimum information about a microarray experiment (MIAME)-toward standards for microarray data.* Nat Genet, 2001. **29**(4): p. 365-71.
420. Pereira Chilima, T.D., F. Moncaubeig, and S.S. Farid, *Impact of allogeneic stem cell manufacturing decisions on cost of goods, process robustness and reimbursement.* Biochemical Engineering Journal, 2018. **137**: p. 132-151.
421. Shammaa, R., et al., *Mesenchymal Stem Cells Beyond Regenerative Medicine.* Frontiers in cell and developmental biology, 2020. **8**: p. 72-72.

422. Ancans, J., *Cell therapy medicinal product regulatory framework in Europe and its application for MSC-based therapy development.* Frontiers in Immunology, 2012. **3**(253).
423. Choi, M., et al., *Regulatory Oversight of Gene Therapy and Cell Therapy Products in Korea.* Adv Exp Med Biol, 2015. **871**: p. 163-79.
424. Ridgway, A., et al., *Regulatory Oversight of Cell and Gene Therapy Products in Canada.* Adv Exp Med Biol, 2015. **871**: p. 49-71.
425. Nagai, S. and K. Ozawa, *New Japanese Regulatory Frameworks for Clinical Research and Marketing Authorization of Gene Therapy and Cellular Therapy Products.* Curr Gene Ther, 2017. **17**(1): p. 17-28.
426. Tiwari, S.S. and P.N. Desai, *Unproven Stem Cell Therapies in India: Regulatory Challenges and Proposed Paths Forward.* Cell Stem Cell, 2018. **23**(5): p. 649-652.
427. Mendicino, M., et al., *Current state of U.S. Food and Drug Administration regulation for cellular and gene therapy products: potential cures on the horizon.* Cytotherapy, 2019. **21**(7): p. 699-724.
428. O'Sullivan, G.M., et al., *Cell and gene therapy manufacturing capabilities in Australia and New Zealand.* Cytotherapy, 2019. **21**(12): p. 1258-1273.
429. Petricciani, J., et al., *Scientific considerations for the regulatory evaluation of cell therapy products.* Biologicals, 2017. **50**: p. 20-26.
430. Administration, F.a.D., *Guidance for Industry: Potency Tests for Cellular and Gene Therapy Products*, C.f.B.E.a. Research, Editor. 2011: https://www.fda.gov/regulatory-information/search-fda-guidance-documents/potency-tests-cellular-and-gene-therapy-products.
431. Administration, F.a.D., *Code of Federal Regulations Title 21: Current Good Manufacturing Practice (CGMP) Regulations* https://www.ecfr.gov/cgi-bin/text-idx?SID=1ac963b3ff39aabe6b482df921ab192f&mc=true&tpl=/ecfrbrowse/Title21/21cfrv4_02.tpl#0.
432. Commission, E., *Regulation (EC) No 1394/2007 of the European Parliament and of the Council of 13 November2007 on advanced therapy medicinal products and amending Directive 2001/ 83/EC and Regulation (EC) No 726/2004*, O.J.o.t.E. Union, Editor. 2007. p. 121-137.
433. Rojewski, M.T., et al., *Translation of a standardized manufacturing protocol for mesenchymal stromal cells: A systematic comparison of validation and manufacturing data.* Cytotherapy, 2019. **21**(4): p. 468-482.
434. Wuchter, P., et al., *Standardization of Good Manufacturing Practice-compliant production of bone marrow-derived human mesenchymal stromal cells for immunotherapeutic applications.* Cytotherapy, 2015. **17**(2): p. 128-39.
435. Blasimme, A. and E. Rial-Sebbag, *Regulation of cell-based therapies in Europe: current challenges and emerging issues.* Stem cells and development, 2013. **22 Suppl 1**(Suppl 1): p. 14-19.
436. Melsheimer, R., et al., *Ensuring Product Quality, Consistency and Patient Supply over Time for a Large-Volume Biologic: Experience with Remicade(®).* BioDrugs, 2018. **32**(5): p. 405-414.
437. Romieu-Mourez, R., et al., *Regulation of MHC Class II Expression and Antigen Processing in Murine and Human Mesenchymal Stromal Cells by IFN-γ, TGF-β, and Cell Density.* The Journal of Immunology, 2007. **179**(3): p. 1549-1558.

438. Tang, K.C., et al., *Down-Regulation of MHC II in Mesenchymal Stem Cells at High IFN-γ Can Be Partly Explained by Cytoplasmic Retention of CIITA.* The Journal of Immunology, 2008. **180**(3): p. 1826-1833.
439. Liang, X., et al., *Paracrine mechanisms of mesenchymal stem cell-based therapy: current status and perspectives.* Cell Transplant, 2014. **23**(9): p. 1045-59.
440. Chen, M.-Y., et al., *Endothelial differentiation of Wharton's jelly–derived mesenchymal stem cells in comparison with bone marrow–derived mesenchymal stem cells.* Experimental Hematology, 2009. **37**(5): p. 629-640.
441. Meirelles Lda, S., et al., *Mechanisms involved in the therapeutic properties of mesenchymal stem cells.* Cytokine Growth Factor Rev, 2009. **20**(5-6): p. 419-27.
442. Ankrum, J. and J.M. Karp, *Mesenchymal stem cell therapy: Two steps forward, one step back.* Trends Mol Med, 2010. **16**(5): p. 203-9.
443. Linero, I. and O. Chaparro, *Paracrine effect of mesenchymal stem cells derived from human adipose tissue in bone regeneration.* PLoS One, 2014. **9**(9): p. e107001.
444. Tögel, F., et al., *Vasculotropic, paracrine actions of infused mesenchymal stem cells are important to the recovery from acute kidney injury.* Am J Physiol Renal Physiol, 2007. **292**(5): p. F1626-35.
445. Yeo, R.W., et al., *Mesenchymal stem cell: an efficient mass producer of exosomes for drug delivery.* Adv Drug Deliv Rev, 2013. **65**(3): p. 336-41.
446. Park, K.S., et al., *Enhancement of therapeutic potential of mesenchymal stem cell-derived extracellular vesicles.* Stem Cell Res Ther, 2019. **10**(1): p. 288.
447. Kern, S., et al., *Comparative analysis of mesenchymal stem cells from bone marrow, umbilical cord blood, or adipose tissue.* Stem Cells, 2006. **24**(5): p. 1294-301.
448. Baksh, D., R. Yao, and R.S. Tuan, *Comparison of proliferative and multilineage differentiation potential of human mesenchymal stem cells derived from umbilical cord and bone marrow.* Stem Cells, 2007. **25**(6): p. 1384-92.
449. Wu, L.F., et al., *Differentiation of Wharton's jelly primitive stromal cells into insulin-producing cells in comparison with bone marrow mesenchymal stem cells.* Tissue Eng Part A, 2009. **15**(10): p. 2865-73.
450. Yu, Y.B., et al., *Differentiation of umbilical cord mesenchymal stem cells into hepatocytes in comparison with bone marrow mesenchymal stem cells.* Mol Med Rep, 2018. **18**(2): p. 2009-2016.
451. Peng, L., et al., *Comparative analysis of mesenchymal stem cells from bone marrow, cartilage, and adipose tissue.* Stem Cells Dev, 2008. **17**(4): p. 761-73.
452. Danisovic, L., et al., *Comparison of in vitro chondrogenic potential of human mesenchymal stem cells derived from bone marrow and adipose tissue.* Gen Physiol Biophys, 2009. **28**(1): p. 56-62.
453. Xu, L., et al., *Tissue source determines the differentiation potentials of mesenchymal stem cells: a comparative study of human mesenchymal stem cells from bone marrow and adipose tissue.* Stem Cell Research & Therapy, 2017. **8**(1): p. 275.
454. Alrefaei, G.I., S.A. Alkarim, and H.S. Abduljabbar, *Impact of Mothers' Age on Telomere Length and Human Telomerase Reverse Transcriptase Expression in Human Fetal Membrane-Derived Mesenchymal Stem Cells.* Stem Cells and Development, 2019. **28**(24): p. 1632-1645.

455. Alrefaei, G.I., et al., *Effects of maternal age on the expression of mesenchymal stem cell markers in the components of human umbilical cord.* Folia Histochem Cytobiol, 2015. **53**(3): p. 259-71.
456. Ranera, B., et al., *Immunophenotype and gene expression profiles of cell surface markers of mesenchymal stem cells derived from equine bone marrow and adipose tissue.* Vet Immunol Immunopathol, 2011. **144**(1-2): p. 147-54.
457. Schnerch, A., C. Cerdan, and M. Bhatia, *Distinguishing between mouse and human pluripotent stem cell regulation: the best laid plans of mice and men.* Stem Cells, 2010. **28**(3): p. 419-30.
458. Tropel, P., et al., *Isolation and characterisation of mesenchymal stem cells from adult mouse bone marrow.* Exp Cell Res, 2004. **295**(2): p. 395-406.
459. Hu, Y., et al., *Comparative Study on In Vitro Culture of Mouse Bone Marrow Mesenchymal Stem Cells.* Stem Cells Int, 2018. **2018**: p. 6704583.
460. Uder, C., et al., *Mammalian MSC from selected species: Features and applications.* Cytometry A, 2018. **93**(1): p. 32-49.
461. Chamberlain, G., et al., *Concise review: mesenchymal stem cells: their phenotype, differentiation capacity, immunological features, and potential for homing.* Stem Cells, 2007. **25**(11): p. 2739-49.
462. Scuteri, A., et al., *Mesengenic differentiation: comparison of human and rat bone marrow mesenchymal stem cells.* Int J Stem Cells, 2014. **7**(2): p. 127-34.
463. Neupane, M., et al., *Isolation and characterization of canine adipose-derived mesenchymal stem cells.* Tissue Eng Part A, 2008. **14**(6): p. 1007-15.
464. Zhang, X., et al., *Chondrogenic differentiation of bone marrow-derived stem cells cultured in the supernatant of elastic cartilage cells.* Mol Med Rep, 2015. **12**(4): p. 5355-5360.
465. Requicha, J.F., et al., *Effect of anatomical origin and cell passage number on the stemness and osteogenic differentiation potential of canine adipose-derived stem cells.* Stem Cell Rev Rep, 2012. **8**(4): p. 1211-22.
466. Volk, S.W., Y. Wang, and K.D. Hankenson, *Effects of donor characteristics and ex vivo expansion on canine mesenchymal stem cell properties: implications for MSC-based therapies.* Cell Transplant, 2012. **21**(10): p. 2189-200.
467. Sasao, T., et al., *Population doubling level-dependent change of secreted glycosaminoglycan in equine bone marrow-derived mesenchymal stem cells.* J Equine Sci, 2015. **26**(3): p. 73-80.
468. Marín-Llera, J.C. and J. Chimal-Monroy, *A small population of resident limb bud mesenchymal cells express few MSC-associated markers, but the expression of these markers is increased immediately after cell culture.* Cell Biol Int, 2018. **42**(5): p. 570-579.
469. Izadpanah, R., et al., *Biologic properties of mesenchymal stem cells derived from bone marrow and adipose tissue.* J Cell Biochem, 2006. **99**(5): p. 1285-97.
470. Taha, M.F. and V. Hedayati, *Isolation, identification and multipotential differentiation of mouse adipose tissue-derived stem cells.* Tissue Cell, 2010. **42**(4): p. 211-6.
471. Jeong, S.H., Y.H. Ji, and E.S. Yoon, *Immunosuppressive activity of adipose tissue-derived mesenchymal stem cells in a rat model of hind limb allotransplantation.* Transplant Proc, 2014. **46**(5): p. 1606-14.

472. Long, C., et al., *Isolation and characterization of canine placenta-derived mesenchymal stromal cells for the treatment of neurological disorders in dogs.* Cytometry Part A, 2018. **93**(1): p. 82-92.
473. Screven, R., et al., *Immunophenotype and gene expression profile of mesenchymal stem cells derived from canine adipose tissue and bone marrow.* Vet Immunol Immunopathol, 2014. **161**(1-2): p. 21-31.
474. Radcliffe, C.H., M.J. Flaminio, and L.A. Fortier, *Temporal analysis of equine bone marrow aspirate during establishment of putative mesenchymal progenitor cell populations.* Stem Cells Dev, 2010. **19**(2): p. 269-82.
475. Hermida-Gómez, T., et al., *Quantification of cells expressing mesenchymal stem cell markers in healthy and osteoarthritic synovial membranes.* J Rheumatol, 2011. **38**(2): p. 339-49.
476. Kovac, M., et al., *Different RNA and protein expression of surface markers in rabbit amniotic fluid-derived mesenchymal stem cells.* Biotechnology Progress, 2017. **33**(6): p. 1601-1613.
477. Alipour, F., et al., *Equine adipose-derived mesenchymal stem cells: phenotype and growth characteristics, gene expression profile and differentiation potentials.* Cell journal, 2015. **16**(4): p. 456-465.
478. de Mattos Carvalho, A., et al., *Isolation and immunophenotypic characterization of mesenchymal stem cells derived from equine species adipose tissue.* Vet Immunol Immunopathol, 2009. **132**(2-4): p. 303-6.
479. Gale, A.L., et al., *The effect of hypoxia on chondrogenesis of equine synovial membrane-derived and bone marrow-derived mesenchymal stem cells.* BMC Veterinary Research, 2019. **15**(1): p. 201.
480. Kamm, J.L., et al., *Blood type and breed-associated differences in cell marker expression on equine bone marrow-derived mesenchymal stem cells including major histocompatibility complex class II antigen expression.* PLoS One, 2019. **14**(11): p. e0225161.
481. Maia, L., et al., *Immunophenotypic, immunocytochemistry, ultrastructural, and cytogenetic characterization of mesenchymal stem cells from equine bone marrow.* Microscopy Research and Technique, 2013. **76**(6): p. 618-624.
482. Zahedi, M., et al., *Stemness Signature of Equine Marrow-derived Mesenchymal Stem Cells.* International journal of stem cells, 2017. **10**(1): p. 93-102.
483. Meirelles Lda, S. and N.B. Nardi, *Murine marrow-derived mesenchymal stem cell: isolation, in vitro expansion, and characterization.* Br J Haematol, 2003. **123**(4): p. 702-11.
484. Anderson, P., et al., *CD105 (Endoglin)-Negative Murine Mesenchymal Stromal Cells Define a New Multipotent Subpopulation with Distinct Differentiation and Immunomodulatory Capacities.* PLOS ONE, 2013. **8**(10): p. e76979.
485. Hosseinzadeh Shirzeily, M., et al., *Comparison of differentiation potential of male mouse adipose tissue and bone marrow derived-mesenchymal stem cells into germ cells.* Iran J Reprod Med, 2013. **11**(12): p. 965-76.
486. Deng, L., et al., *Adipose derived mesenchymal stem cells efficiently rescue carbon tetrachloride-induced acute liver failure in mouse.* ScientificWorldJournal, 2014. **2014**: p. 103643.

487. Li, F. and C. Niyibizi, *Engraftability of Murine Bone Marrow-Derived Multipotent Mesenchymal Stem Cell Subpopulations in the Tissues of Developing Mice following Systemic Transplantation.* Cells Tissues Organs, 2016. **201**(1): p. 14-25.
488. Ahmed, M., M. Ghabriel, and A. Amleh, *Enrichment, Propagation, and Characterization of Mouse Testis-Derived Mesenchymal Stromal Cells.* Cell Reprogram, 2017. **19**(1): p. 35-43.
489. Rui, Y.F., et al., *Isolation and characterization of multipotent rat tendon-derived stem cells.* Tissue Eng Part A, 2010. **16**(5): p. 1549-58.
490. Meric, A., et al., *Comparison of chondrocytes produced from adipose tissue-derived stem cells and cartilage tissue.* J Craniofac Surg, 2013. **24**(3): p. 830-3.
491. Sobh, M.A., *Adipogenesis of Sprague Dawely rats mesenchymal stem cells: a morphological, immunophenotyping and gene expression follow-up study.* Anat Cell Biol, 2014. **47**(2): p. 83-90.
492. Sarvandi, S.S., et al., *In vitro differentiation of rat mesenchymal stem cells to hepatocyte lineage.* Iran J Basic Med Sci, 2015. **18**(1): p. 89-97.
493. Suto, E.G., et al., *Prospectively isolated mesenchymal stem/stromal cells are enriched in the CD73(+) population and exhibit efficacy after transplantation.* Sci Rep, 2017. **7**(1): p. 4838.
494. Brückner, S., et al., *Isolation and hepatocyte differentiation of mesenchymal stem cells from porcine bone marrow--"surgical waste" as a novel MSC source.* Transplant Proc, 2013. **45**(5): p. 2056-8.
495. Ock, S.A., B.G. Jeon, and G.J. Rho, *Comparative characterization of porcine mesenchymal stem cells derived from bone marrow extract and skin tissues.* Tissue Eng Part C Methods, 2010. **16**(6): p. 1481-91.
496. Pérez-Serrano, R.M., et al., *PPAR Agonists Promote the Differentiation of Porcine Bone Marrow Mesenchymal Stem Cells into the Adipogenic and Myogenic Lineages.* Cells Tissues Organs, 2017. **203**(3): p. 153-172.
497. Wiater, J., et al., *Identification of perivascular and stromal mesenchymal stem/progenitor cells in porcine endometrium.* Reprod Domest Anim, 2018. **53**(2): p. 333-343.
498. Lee, A.Y., et al., *Comparative studies on proliferation, molecular markers and differentiation potential of mesenchymal stem cells from various tissues (adipose, bone marrow, ear skin, abdominal skin, and lung) and maintenance of multipotency during serial passages in miniature pig.* Res Vet Sci, 2015. **100**: p. 115-24.
499. Fadel, L., et al., *Protocols for obtainment and isolation of two mesenchymal stem cell sources in sheep.* Acta Cir Bras, 2011. **26**(4): p. 267-73.
500. Czernik, M., et al., *Differentiation potential and GFP labeling of sheep bone marrow-derived mesenchymal stem cells.* J Cell Biochem, 2013. **114**(1): p. 134-43.
501. Ji, M., et al., *Biological characterization of sheep kidney-derived mesenchymal stem cells.* Exp Ther Med, 2016. **12**(6): p. 3963-3971.
502. Lee, T.H., et al., *Characterization and spinal fusion effect of rabbit mesenchymal stem cells.* BMC Res Notes, 2013. **6**: p. 528.
503. Xia, C.S., et al., *Isolation of rabbit bone marrow mesenchymal stem cells using density gradient centrifugation and adherence screening methods.* Minerva Med, 2013. **104**(5): p. 519-25.

504. Xiao, F., et al., *[The effects of CD44 fucosylation on fluid adhesion force of rabbit bone marrow mesenchymal stem cells].* Zhongguo Xiu Fu Chong Jian Wai Ke Za Zhi, 2018. **32**(1): p. 99-103.
505. Corradetti, B., et al., *Mesenchymal stem cells from amnion and amniotic fluid in the bovine.* Reproduction, 2013. **145**(4): p. 391-400.
506. de Moraes, C.N., et al., *Bovine endometrial cells: a source of mesenchymal stem/progenitor cells.* Cell Biol Int, 2016. **40**(12): p. 1332-1339.
507. Yue, Y., et al., *De novo lipogenesis and desaturation of fatty acids during adipogenesis in bovine adipose-derived mesenchymal stem cells.* In Vitro Cell Dev Biol Anim, 2018. **54**(1): p. 23-31.
508. Ghosh, K., et al., *Buffalo (Bubalus bubalis) term amniotic-membrane-derived cells exhibited mesenchymal stem cells characteristics in vitro.* In Vitro Cell Dev Biol Anim, 2015. **51**(9): p. 915-21.
509. Bai, C., et al., *Biological characterization of chicken mesenchymal stem/progenitor cells from umbilical cord Wharton's jelly.* Mol Cell Biochem, 2013. **376**(1-2): p. 95-102.
510. de Wolf, C., M. van de Bovenkamp, and M. Hoefnagel, *Regulatory perspective on in vitro potency assays for human mesenchymal stromal cells used in immunotherapy.* Cytotherapy, 2017. **19**(7): p. 784-797.
511. Hu, Y., et al., *Isolation and identification of mesenchymal stem cells from human fetal pancreas.* J Lab Clin Med, 2003. **141**(5): p. 342-9.
512. Aldridge, V., et al., *Human mesenchymal stem cells are recruited to injured liver in a β1-integrin and CD44 dependent manner.* Hepatology, 2012. **56**(3): p. 1063-73.
513. Brooke, G., et al., *Molecular trafficking mechanisms of multipotent mesenchymal stem cells derived from human bone marrow and placenta.* Stem Cells Dev, 2008. **17**(5): p. 929-40.
514. Guan, X., et al., *Evaluation of CD24 as a marker to rapidly define the mesenchymal stem cell phenotype and its differentiation in human nucleus pulposus.* Chin Med J (Engl), 2014. **127**(8): p. 1474-81.
515. Katsiani, E., et al., *Chorionic villi derived mesenchymal like stem cells and expression of embryonic stem cells markers during long-term culturing.* Cell Tissue Bank, 2016. **17**(3): p. 517-29.
516. Kaviani, M., et al., *Comparison of Human Mesenchymal Stem Cells Derived from Various Compartments of Human Adipose Tissue and Tunica Adventitia Layer of the Arteries Subsequent to Organ Donation.* Int J Organ Transplant Med, 2019. **10**(2): p. 65-73.
517. Lee, D.H., et al., *Isolation and expansion of synovial CD34(-)CD44(+)CD90(+) mesenchymal stem cells: comparison of an enzymatic method and a direct explant technique.* Connect Tissue Res, 2011. **52**(3): p. 226-34.
518. Liu, T., et al., *CD44+/CD105+ human amniotic fluid mesenchymal stem cells survive and proliferate in the ovary long-term in a mouse model of chemotherapy-induced premature ovarian failure.* Int J Med Sci, 2012. **9**(7): p. 592-602.
519. Park, E. and A.N. Patel, *Changes in the expression pattern of mesenchymal and pluripotent markers in human adipose-derived stem cells.* Cell Biol Int, 2010. **34**(10): p. 979-84.

520. Qu, C., et al., *Extensive CD44-dependent hyaluronan coats on human bone marrow-derived mesenchymal stem cells produced by hyaluronan synthases HAS1, HAS2 and HAS3.* Int J Biochem Cell Biol, 2014. **48**: p. 45-54.
521. Secunda, R., et al., *Isolation, expansion and characterisation of mesenchymal stem cells from human bone marrow, adipose tissue, umbilical cord blood and matrix: a comparative study.* Cytotechnology, 2015. **67**(5): p. 793-807.
522. Togarrati, P.P., et al., *CD29 is highly expressed on epithelial, myoepithelial, and mesenchymal stromal cells of human salivary glands.* Oral Dis, 2018. **24**(4): p. 561-572.
523. Van Pham, P., et al., *Isolation and proliferation of umbilical cord tissue derived mesenchymal stem cells for clinical applications.* Cell Tissue Bank, 2016. **17**(2): p. 289-302.
524. Wexler, S.A., et al., *Adult bone marrow is a rich source of human mesenchymal 'stem' cells but umbilical cord and mobilized adult blood are not.* Br J Haematol, 2003. **121**(2): p. 368-74.
525. Filioli Uranio, M., et al., *Isolation, proliferation, cytogenetic, and molecular characterization and in vitro differentiation potency of canine stem cells from foetal adnexa: a comparative study of amniotic fluid, amnion, and umbilical cord matrix.* Mol Reprod Dev, 2011. **78**(5): p. 361-73.
526. Ivanovska, A., et al., *Immunophenotypical characterization of canine mesenchymal stem cells from perivisceral and subcutaneous adipose tissue by a species-specific panel of antibodies.* Res Vet Sci, 2017. **114**: p. 51-58.
527. Zhang, S., et al., *Characteristics and multi-lineage differentiation of bone marrow mesenchymal stem cells derived from the Tibetan mastiff.* Mol Med Rep, 2018. **18**(2): p. 2097-2109.
528. Valorani, M.G., et al., *Hypoxia increases Sca-1/CD44 co-expression in murine mesenchymal stem cells and enhances their adipogenic differentiation potential.* Cell Tissue Res, 2010. **341**(1): p. 111-20.
529. Naik, S.K., et al., *Mouse Bone Marrow Sca-1(+) CD44(+) Mesenchymal Stem Cells Kill Avirulent Mycobacteria but Not Mycobacterium tuberculosis through Modulation of Cathelicidin Expression via the p38 Mitogen-Activated Protein Kinase-Dependent Pathway.* Infect Immun, 2017. **85**(10).
530. Yang, M.C., et al., *The influence of rat mesenchymal stem cell CD44 surface markers on cell growth, fibronectin expression, and cardiomyogenic differentiation on silk fibroin - Hyaluronic acid cardiac patches.* Biomaterials, 2010. **31**(5): p. 854-62.
531. Li, Z., et al., *Comparison of different methods for the isolation and purification of rat nucleus pulposus-derived mesenchymal stem cells.* Connect Tissue Res, 2020. **61**(5): p. 426-434.
532. Deng, Y., et al., *Isolation and characterization of buffalo (bubalus bubalis) amniotic mesenchymal stem cells derived from amnion from the first trimester pregnancy.* J Vet Med Sci, 2018. **80**(4): p. 710-719.
533. Chen, F., et al., *The biological characteristics of sheep umbilical cord mesenchymal stem cells.* Can J Vet Res, 2018. **82**(3): p. 216-224.
534. Azghadi, S.M., et al., *Mesenchymal stromal cells support the viability and differentiation of thymocytes through direct contact in autologous co-cultures.* Histochem Cell Biol, 2016. **146**(2): p. 153-65.

535. Ouhtit, A., et al., *CD44 mediates stem cell mobilization to damaged lung via its novel transcriptional targets, Cortactin and Survivin.* Int J Med Sci, 2020. **17**(1): p. 103-111.
536. Qian, H., K. Le Blanc, and M. Sigvardsson, *Primary mesenchymal stem and progenitor cells from bone marrow lack expression of CD44 protein.* J Biol Chem, 2012. **287**(31): p. 25795-807.
537. Hachisuka, H., et al., *Flow cytometric discrimination of mesenchymal progenitor cells from bone marrow-adherent cell populations using CD34/44/45(-) and Sca-1(+) markers.* J Orthop Sci, 2007. **12**(2): p. 161-9.
538. Tsuji, K., et al., *Effects of Different Cell-Detaching Methods on the Viability and Cell Surface Antigen Expression of Synovial Mesenchymal Stem Cells.* Cell Transplant, 2017. **26**(6): p. 1089-1102.
539. Xu, Y., et al., *Effect of CD44 on differentiation of human amniotic mesenchymal stem cells into chondrocytes via Smad and ERK signaling pathways.* Mol Med Rep, 2020. **21**(6): p. 2357-2366.
540. Kwon, J.H., et al., *Decorin Secreted by Human Umbilical Cord Blood-Derived Mesenchymal Stem Cells Induces Macrophage Polarization via CD44 to Repair Hyperoxic Lung Injury.* Int J Mol Sci, 2019. **20**(19).
541. Pruszak, J., et al., *CD15, CD24, and CD29 define a surface biomarker code for neural lineage differentiation of stem cells.* Stem Cells, 2009. **27**(12): p. 2928-40.
542. Yang, Y., et al., *CD29 of human umbilical cord mesenchymal stem cells is required for expansion of CD34(+) cells.* Cell Prolif, 2014. **47**(6): p. 596-603.
543. Davies, O.G., et al., *Isolation of adipose and bone marrow mesenchymal stem cells using CD29 and CD90 modifies their capacity for osteogenic and adipogenic differentiation.* J Tissue Eng, 2015. **6**: p. 2041731415592356.
544. Walker, P.A., et al., *Effect of needle diameter and flow rate on rat and human mesenchymal stromal cell characterization and viability.* Tissue Eng Part C Methods, 2010. **16**(5): p. 989-97.
545. Song, K., et al., *Cultivation and identification of rat bone marrow-derived mesenchymal stem cells.* Mol Med Rep, 2014. **10**(2): p. 755-760.
546. Esteves, C.L., et al., *Equine Mesenchymal Stromal Cells Retain a Pericyte-Like Phenotype.* Stem Cells Dev, 2017. **26**(13): p. 964-972.
547. Ode, A., et al., *CD73 and CD29 concurrently mediate the mechanically induced decrease of migratory capacity of mesenchymal stromal cells.* Eur Cell Mater, 2011. **22**: p. 26-42.
548. Seeberger, K.L., et al., *Epithelial cells within the human pancreas do not coexpress mesenchymal antigens: epithelial-mesenchymal transition is an artifact of cell culture.* Lab Invest, 2009. **89**(2): p. 110-21.
549. Álvarez-Viejo, M., Y. Menéndez-Menéndez, and J. Otero-Hernández, *CD271 as a marker to identify mesenchymal stem cells from diverse sources before culture.* World journal of stem cells, 2015. **7**(2): p. 470-476.
550. Ballikaya, S., et al., *Process data of allogeneic ex vivo-expanded ABCB5(+) mesenchymal stromal cells for human use: off-the-shelf GMP-manufactured donor-independent ATMP.* Stem Cell Res Ther, 2020. **11**(1): p. 482.
551. Gonzalez, H., et al., *Umbilical Cord-Derived CD362(+) Mesenchymal Stromal Cells Attenuate Polymicrobial Sepsis Induced by Caecal Ligation and Puncture.* Int J Mol Sci, 2020. **21**(21).

552. Ning, H., et al., *Mesenchymal stem cell marker Stro-1 is a 75 kd endothelial antigen.* Biochemical and biophysical research communications, 2011. **413**(2): p. 353-357.
553. Keating, A., *Mesenchymal stromal cells: new directions.* Cell Stem Cell, 2012. **10**(6): p. 709-716.
554. Tanavde, V., et al., *Research using Mesenchymal Stem/Stromal Cells: quality metric towards developing a reference material.* Cytotherapy, 2015. **17**(9): p. 1169-77.
555. Fabbri, A., et al., *The Influence of Industry Sponsorship on the Research Agenda: A Scoping Review.* Am J Public Health, 2018. **108**(11): p. e9-e16.
556. Dorsey, E.R., et al., *Financing of U.S. biomedical research and new drug approvals across therapeutic areas.* PLoS One, 2009. **4**(9): p. e7015.
557. Porter, M., *The five competitive forces that shape strategy.* Harvard Business Review, 2008. **86**(1): p. 78-93.
558. Zachariades, N.A., *Stem cells: intellectual property issues in regenerative medicine.* Stem cells and development, 2013. **22 Suppl 1**(Suppl 1): p. 59-62.
559. Roberts, M., et al., *The global intellectual property landscape of induced pluripotent stem cell technologies.* Nat Biotechnol, 2014. **32**(8): p. 742-8.
560. Melsheimer, R., et al., *Ensuring Product Quality, Consistency and Patient Supply over Time for a Large-Volume Biologic: Experience with Remicade®.* BioDrugs, 2018. **32**(5): p. 405-414.
561. Chisholm, J., C. Ruff, and S. Viswanathan, *Current state of Health Canada regulation for cellular and gene therapy products: potential cures on the horizon.* Cytotherapy, 2019. **21**(7): p. 686-698.
562. David Gagnon, C., *HESA Committee Meetig Minutes of Proceedings*, S.C.o.H. (HESA), Editor. 2016.
563. JCR Pharmaceuticals Co., L., *Annual Report 2017*. 2017.
564. JCR Pharmaceuticals Co., L., *Annual Report 2018*. 2018.
565. JCR Pharmaceuticals Co., L., *Annual Report 2019*. 2019.
566. JCR Pharmaceuticals Co., L., *Annual Report 2020*. 2020.
567. Villatoro, A.J., et al., *Use of Adipose-Derived Mesenchymal Stem Cells in Keratoconjunctivitis Sicca in a Canine Model.* BioMed Research International, 2015. **2015**: p. 527926.
568. *Impact of Mothers' Age on Telomere Length and Human Telomerase Reverse Transcriptase Expression in Human Fetal Membrane-Derived Mesenchymal Stem Cells.* Stem Cells and Development, 2019. **28**(24): p. 1632-1645.
569. Han, Y.F., et al., *Optimization of human umbilical cord mesenchymal stem cell isolation and culture methods.* Cytotechnology, 2013. **65**(5): p. 819-27.
570. Marmotti, A., et al., *Minced Umbilical Cord Fragments as a Source of Cells for Orthopaedic Tissue Engineering: An In Vitro Study.* Stem Cells International, 2012. **2012**: p. 326813.
571. Petry, F., et al., *Manufacturing of Human Umbilical Cord Mesenchymal Stromal Cells on Microcarriers in a Dynamic System for Clinical Use.* Stem Cells International, 2016. **2016**: p. 4834616.
572. Crisan, M., et al., *A perivascular origin for mesenchymal stem cells in multiple human organs.* Cell Stem Cell, 2008. **3**(3): p. 301-13.
573. da Silva Meirelles, L., P.C. Chagastelles, and N.B. Nardi, *Mesenchymal stem cells reside in virtually all post-natal organs and tissues.* J Cell Sci, 2006. **119**(Pt 11): p. 2204-13.

574. Li, X., et al., *Comprehensive characterization of four different populations of human mesenchymal stem cells as regards their immune properties, proliferation and differentiation.* Int J Mol Med, 2014. **34**(3): p. 695-704.
575. Sensebé, L., M. Gadelorge, and S. Fleury-Cappellesso, *Production of mesenchymal stromal/stem cells according to good manufacturing practices: a review.* Stem cell research & therapy, 2013. **4**(3): p. 66-66.
576. Emnett, R.J., et al., *Evaluation of Tissue Homogenization to Support the Generation of GMP-Compliant Mesenchymal Stromal Cells from the Umbilical Cord.* Stem Cells Int, 2016. **2016**: p. 3274054.
577. Burnouf, T., et al., *Human platelet lysate: Replacing fetal bovine serum as a gold standard for human cell propagation?* Biomaterials, 2016. **76**: p. 371-87.
578. Walenda, G., et al., *Human platelet lysate gel provides a novel three dimensional-matrix for enhanced culture expansion of mesenchymal stromal cells.* Tissue Eng Part C Methods, 2012. **18**(12): p. 924-34.
579. Copland, I.B., et al., *The effect of platelet lysate fibrinogen on the functionality of MSCs in immunotherapy.* Biomaterials, 2013. **34**(32): p. 7840-50.
580. FDA, *FDA approves pathogen reduction system to treat platelets.*, U.S.F.a.D. Administration, Editor. 2014, U.S. Food and Drug Administration.
581. Guo, J., et al., *Xenogeneic immunosuppression of human umbilical cord mesenchymal stem cells in a major histocompatibility complex-mismatched allogeneic acute graft-versus-host disease murine model.* Eur J Haematol, 2011. **87**(3): p. 235-43.
582. López, Y., et al., *Wharton's jelly or bone marrow mesenchymal stromal cells improve cardiac function following myocardial infarction for more than 32 weeks in a rat model: a preliminary report.* Curr Stem Cell Res Ther, 2013. **8**(1): p. 46-59.
583. Weiss, M.L., et al., *Human umbilical cord matrix stem cells: preliminary characterization and effect of transplantation in a rodent model of Parkinson's disease.* Stem Cells, 2006. **24**(3): p. 781-92.
584. Sharma, A.K., et al., *Mesenchymal Stem Cells Attenuate NADPH Oxidase-Dependent High Mobility Group Box 1 Production and Inhibit Abdominal Aortic Aneurysms.* Arteriosclerosis, thrombosis, and vascular biology, 2016. **36**(5): p. 908-918.

Appendix A - Supplementary Data from Chapter 2

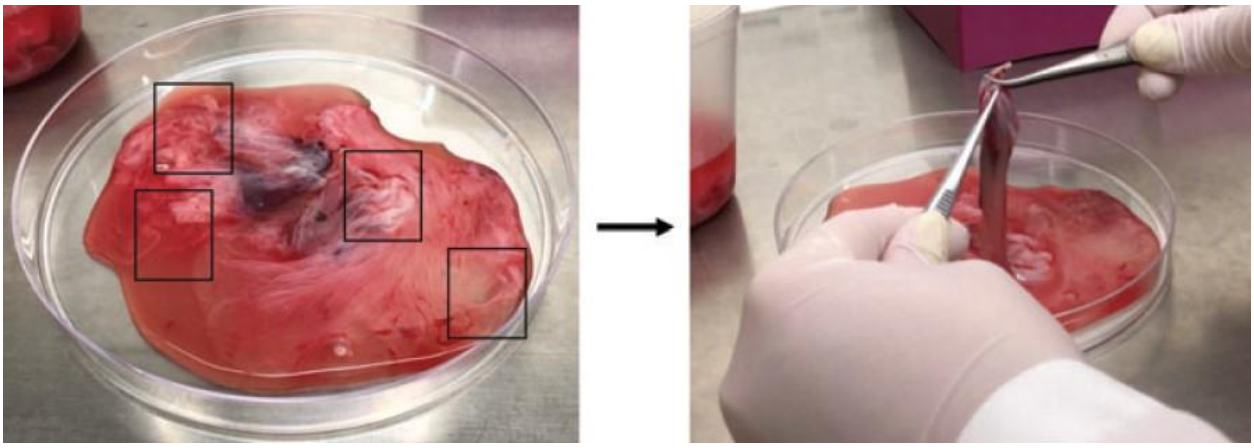

Figure 36: Supplementary Figure S1

Isolation of canine umbilical cords from fetal adnexa tissue. Canine umbilical cords from the litter are obtained from the veterinarian after caesarian-section delivery. Left: Umbilical cords are intertwined within the fetal adnexa tissue (see boxes). Right: Visible cord sections were dissected from the adnexa without stretching or ripping the umbilical cord. Sections are pooled and measured for desired amount per tube.

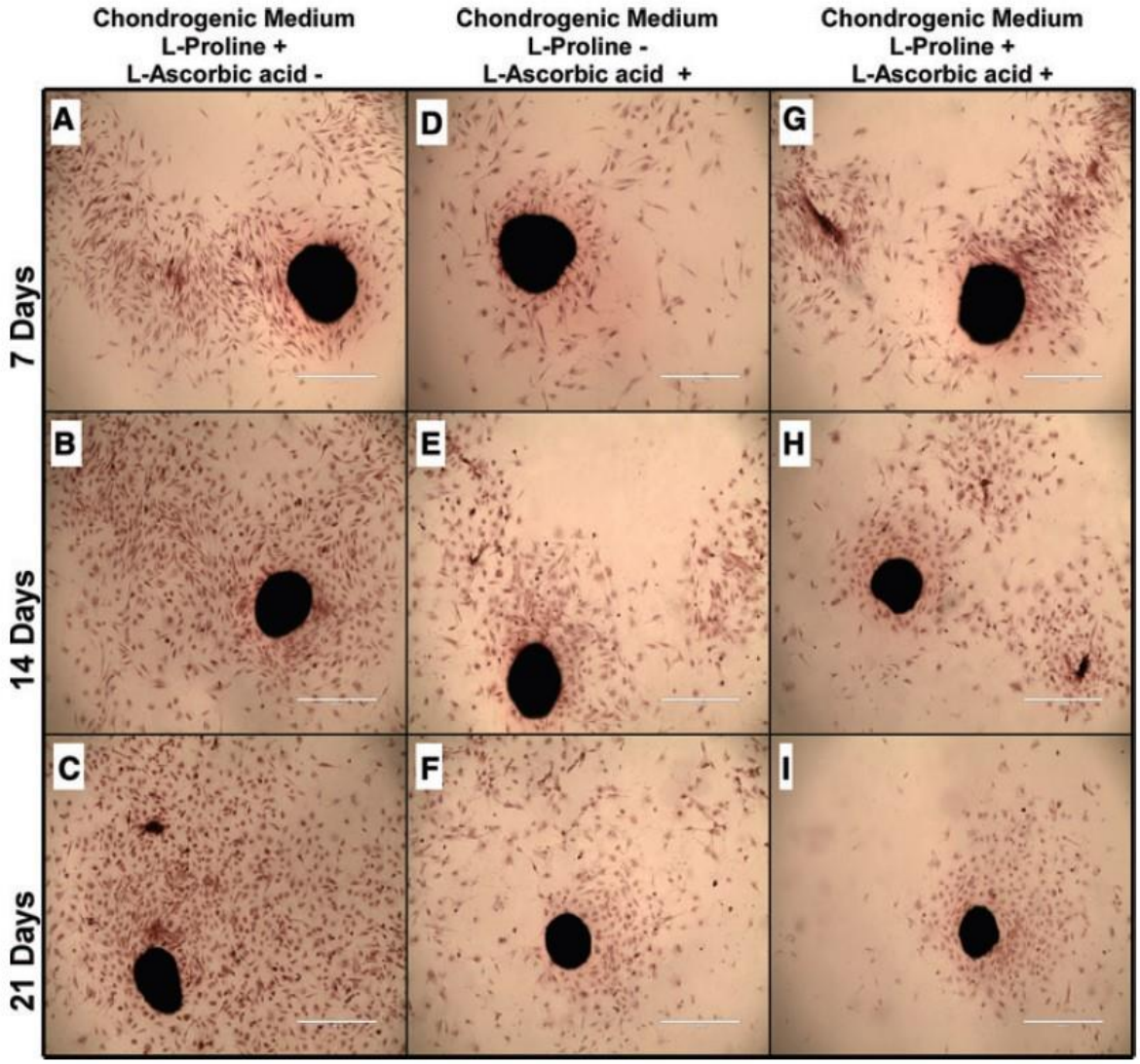

Figure 37: Supplementary Figure S2

Chondrogenic medium selection using canine MSCs (line 30 at passage 5). Three different media conditions compared after 7 (A, D, G), 14 (B, E, H), or 21 (C, F, I) days of differentiation. (A–C) Chondrogenic differentiation medium with 40 mg/mL l-proline and no l-ascorbic acid 2-phosphate (l-ascorbic acid). (D, E) Chondrogenic differentiation medium with 50mM l-ascorbic acid and no l-proline. (G–I) Chondrogenic differentiation medium with 40 mg/mL l-proline and 50mM l-ascorbic acid. Note that micromasses or aggregates of cells form and stain intensely. Note that prominent staining is seen in all media conditions tested, even after only 7 days of differentiation. Safranin O staining for acidic proteoglycans (cartilage) after fixation. Calibration bar equals 1,000 mm. Representative wells from technical duplicates.

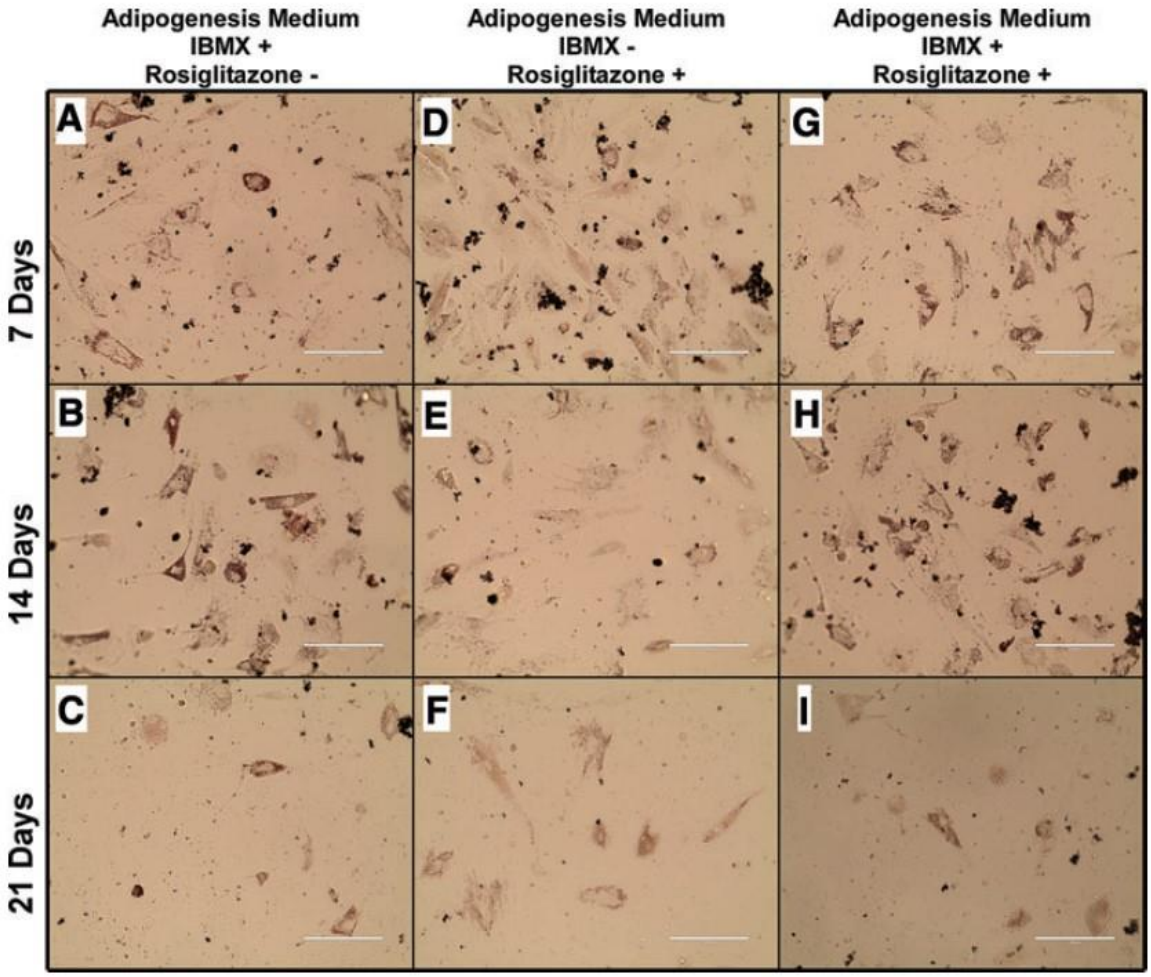

Figure 38: Supplementary Figure S3

Adipogenic differentiation media selection using canine MSCs (line 30 at passage 5). Three different media conditions compared after 7 (A, D, G), 14 (B, E, H), or 21 (C, F, I) days of differentiation. (A–C) Adipogenic differentiation medium with 0.5mM IBMX and no rosiglitazone. (D, E) Adipogenic differentiation medium with 5mM rosiglitazone and no IBMX. (G–I) Adipogenic differentiation media with 0.5mM IBMX and 5mM rosiglitazone. Note that MSC loss is seen in all three differentiation medias over time. The most prominent lipid staining is seen when using adipogenic medium containing 0.5mM IBMX and no rosiglitazone at 7 and 14 days of differentiation (A and B). Oil Red O staining for lipid droplets after fixation. Calibration bar equals 200 mm. Representative wells from technical duplicates. IBMX, 3-isobutyl-1-methylxanthine.

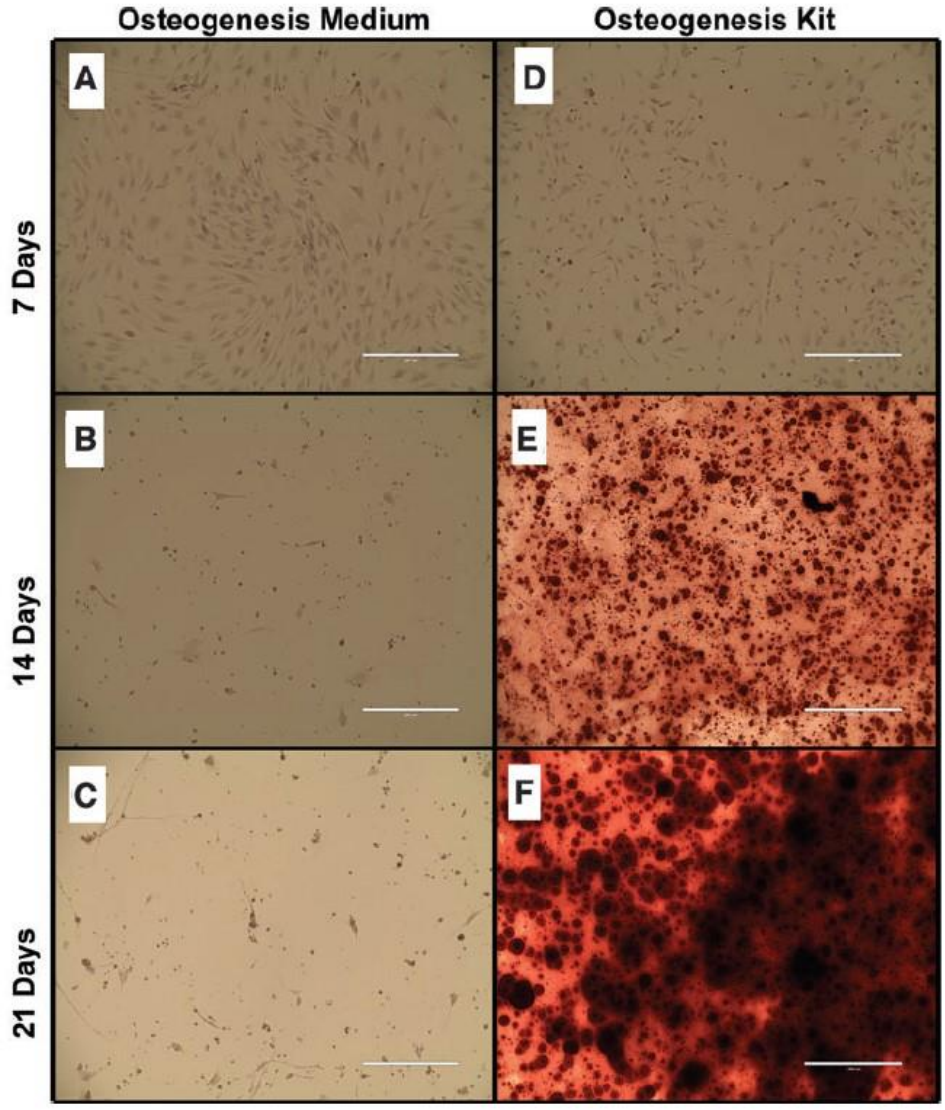

Figure 39: Supplementary Figure S4

Osteogenic differentiation medium selection using canine MSCs (line 30 at passage 5). Two different media conditions compared after 7 (A, D), 14 (B, E), or 21 (C, F) days of differentiation. (A–C) Osteogenic differentiation medium made in the laboratory (see text). (D–F) Osteogenic differentiation medium from the MSC differentiation kit. Note that using the osteogenic differentiation medium from the kit yields robust staining, and that matrix deposition was observed after 14 days and intensified over the next week. In contrast, the medium made up in the laboratory resulted in MSC loss and very poor deposition of matrix. Alizarin Red S staining for calcium deposition after fixation. Calibration bar equals 400 mm. Representative wells from technical duplicates.

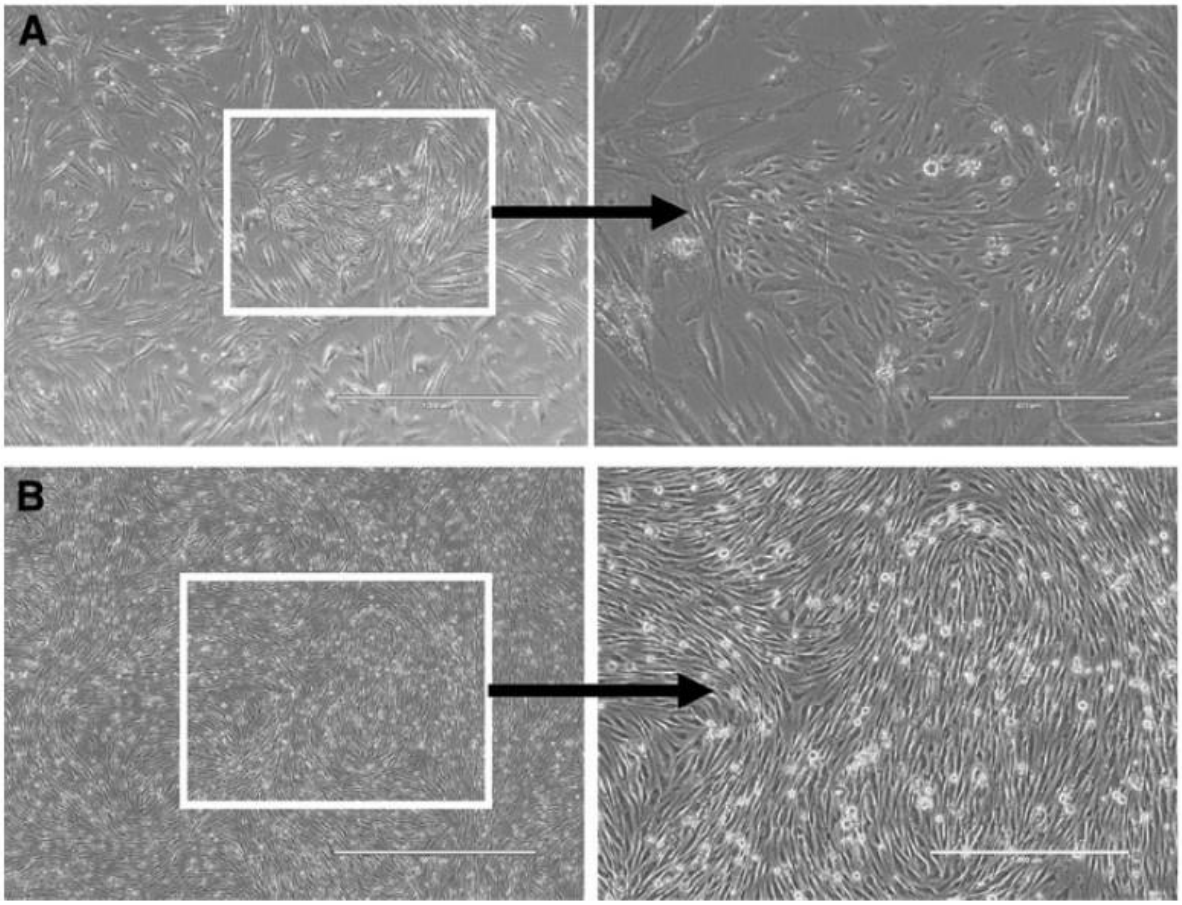

Figure 40: Supplementary Figure S5

Expansion of canine MSCs grown on gelatin-coated plates for 24 h. (A) Random field taken 4 days after plating canine MSCs. (B) The same field taken 24 h later. Note that the field is filled with MSCs of consistent size and shape. Note the swirling pattern of the MSCs. Micrograph in (B) was taken just before cell passage. Note the small round phase-bright MSCs indicating a healthy culture in log growth phase. In (A, B) inset field is shown at higher magnification in the right panel. Calibration bar in (A) and (B) is 1,000 µm; calibration bar in inset is 400 µm. MSC, mesenchymal stromal cell.

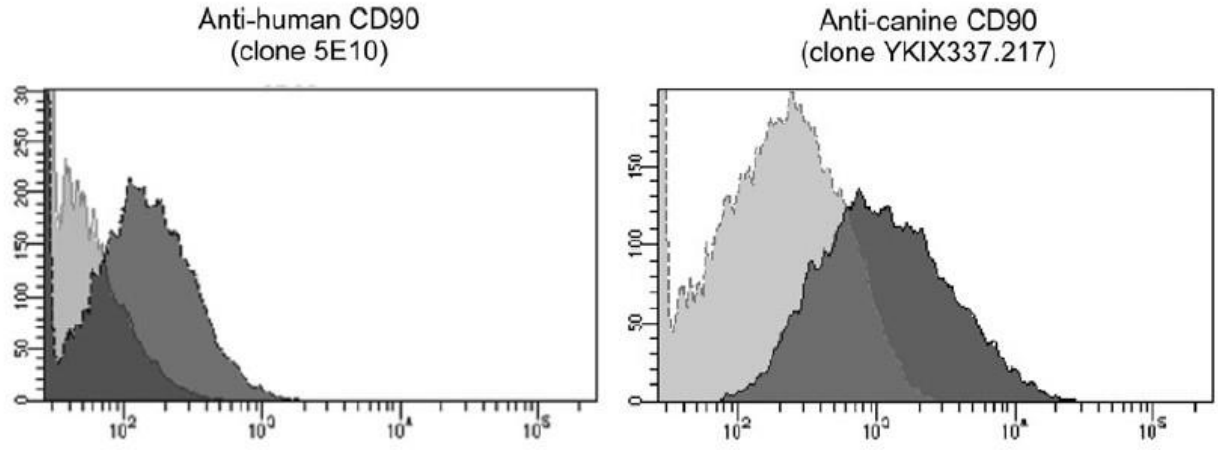

Figure 41: Supplementary Figure S6

Comparison of mouse anti-human CD90 (left panel) and rat anti-canine CD90 (right panel) flow cytometry results. By inspection, no frank differences in the positive staining shift were observed. We conclude that the mouse anti-human CD90 (5E10) and the rat anti-canine CD90 (YKIX337.217) work equally well to detect surface expression of Thy1 in canine UC-MSCs.

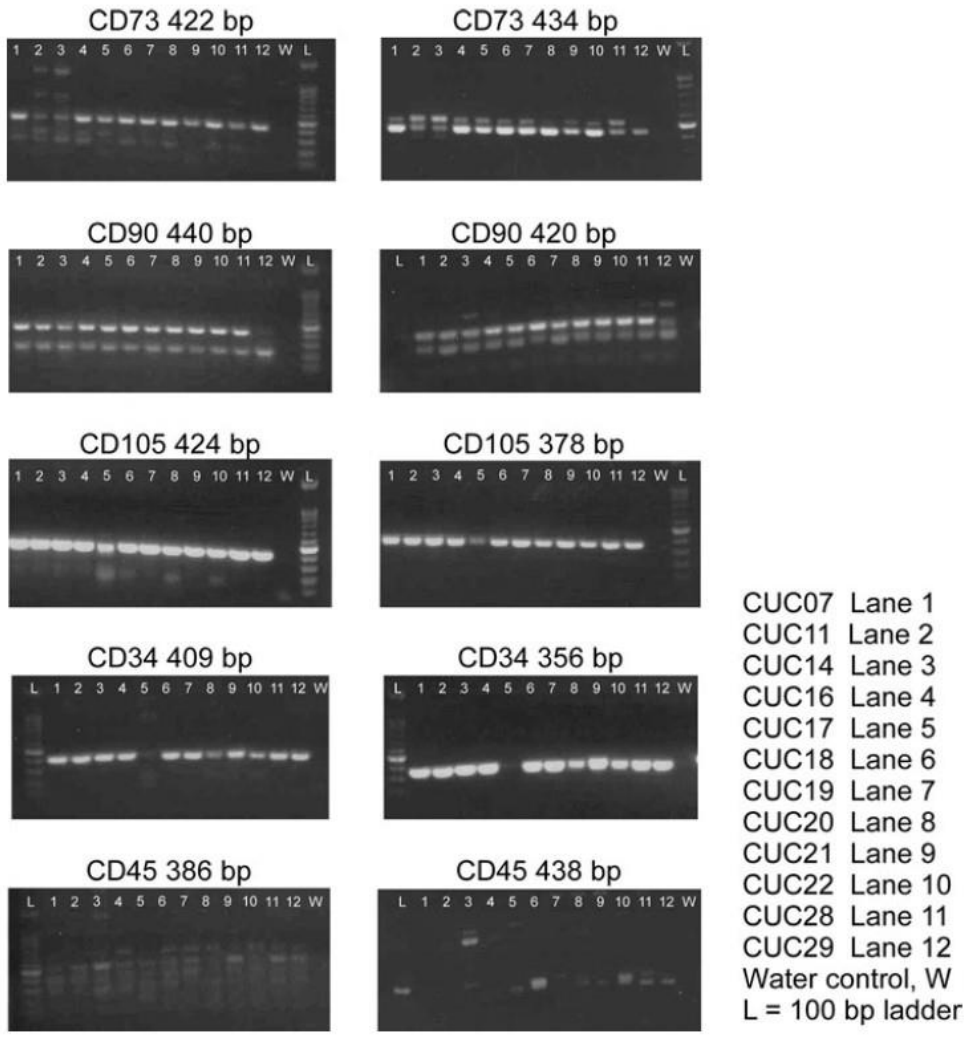

Figure 42: Supplementary Figure S7

RT-PCR analysis of MSC markers in 12 canine MSC lines. Two RT-PCR primer sets that span an intron were designed using the NCBI Genebank data for canine CD73, CD90, CD105, CD34, and CD45 (Table 2). Total RNA was collected from 12 canine MSC lines and processed for RT-PCR. The RT-PCR results indicate that canine MSC lines make mRNA for CD73, CD90, CD105, and CD34. There is no RT-PCR evidence that canine MSC lines make mRNA for CD45. For CD73 primer set 422 bp and 434, CD90 primer set 440 bp and 420, CD105 primer set 424 bp and 378, and CD34 primer set 409 bp and 356, DNA samples from three independent MSC lines (e.g., amplicons of the expected size) were cut from the agarose gel, purified and submitted for sequencing. DNA sequencing confirmed 99%–100% identity. mRNA, messenger RNA; RT-PCR, reverse transcriptase-polymerase chain reaction.

Table 11: Supplementary Table S1. Media Formulations Tested for Trilineage Differentiation

Chondrogenesis conditions *Seeding: 200,000 cells/well in 2D micromass* *Differentiation time: 7, 14, and 21 days*		
I.	*II.*	*III.*
DMEM, high glucose 1% Penicillin-streptomycin 10 ng TGF-β1 1% Fetal bovine serum 100 nM Dexamethasone 1 mM Sodium pyruvate 40 µg L-Proline	DMEM, high glucose 1% Penicillin-streptomycin 10 ng TGF-β1 1% Fetal bovine serum 100 nM Dexamethasone 1 mM Sodium pyruvate 50 mM Ascorbic acid 2-phosphate	DMEM, high glucose 1% Penicillin-streptomycin 10 ng TGF-β1 1% Fetal bovine serum 100 nM Dexamethasone 1 mM Sodium pyruvate 40 µg L-Proline 50 mM Ascorbic acid 2-phosphate
Adipogenesis conditions *Seeding: 50,000 cells/well* *Differentiation time: 7, 14, and 21 days*		
I.	*II.*	*III.*
DMEM, high glucose 1% Penicillin-streptomycin 5% Rabbit serum 100 nM Dexamethasone 200 µM Indomethacine 10 µM Insulin 0.5 mM 3-Isobutyl-1-methylxanthine	DMEM, high glucose 1% Penicillin-streptomycin 5% Rabbit serum 100 nM Dexamethasone 200 µM Indomethacine 10 µM Insulin 5 µM Rosiglitazone	DMEM, high glucose 1% Penicillin-streptomycin 5% Rabbit serum 100 nM Dexamethasone 200 µM Indomethacine 10 µM Insulin 0.5 mM 3-Isobutyl-1-methylxanthine 5 µM Rosiglitazone
Osteogenesis conditions *Seeding: 40,000 cells/well* *Differentiation time: 7, 14, and 21 days*		
I.	*II.*	
DMEM, high glucose 1% Penicillin-streptomycin 1% Fetal bovine serum 100 nM Dexamethasone 50 µM Ascorbic acid 2-phosphate 10 mM β-glycerophosphate	StemPro osteogenesis differentiation kit according to manufacturer's instructions	

Articles that demonstrated canine MSC trilineage differentiation were examined [105, 110, 287, 291, 292, 309, 567], and similarities between those methods led us to test three different chondrogenic differentiation conditions, three different adipogenic differentiation conditions, and

two different osteogenic differentiation conditions. The results of that testing are shown in Supplementary Figure S5 for chondrogenic differentiation, Supplementary Figure S6 for adipogenic differentiation, and Supplementary Figure S7 for osteogenic differentiation. 2D, two-dimensional; DMEM, Dulbecco's modified Eagle's medium; MSC, mesenchymal stromal cell; TGF-β1, transforming growth factor beta 1.

Table 12: Supplementary Table S2. Antibody Clone Discrepancies Noted

Marker	*Clone*	*Our Result*	*Articles SAME*	*Articles OPPOSITE*
CD105	OTI8A1	Positive	[300, 313]	
CD105	SN6	Negative	[101, 103]	[36, 103, 287]
CD105	P3D1	Negative		
CD73	D12	Negative		
CD73	AD2	Negative	[35, 103]	
CD73	7G2	Positive	[36, 104]	
CD34	1H6	Positive	[104, 311, 314]	[36, 101, 103-105, 287, 293, 299, 300, 309, 310, 312, 314, 316, 317]
CD44	IM7	Positive	[36, 101, 103, 287, 293, 299, 300, 313]	[315]
CD45	YKIX716.13	Negative	[101-104, 287, 293, 310, 313]	[315]
CD90	5E10	Positive	[299, 313]	
CD14	TUK4	Negative		[104]

Appendix B - Supplementary Data from Chapter 3

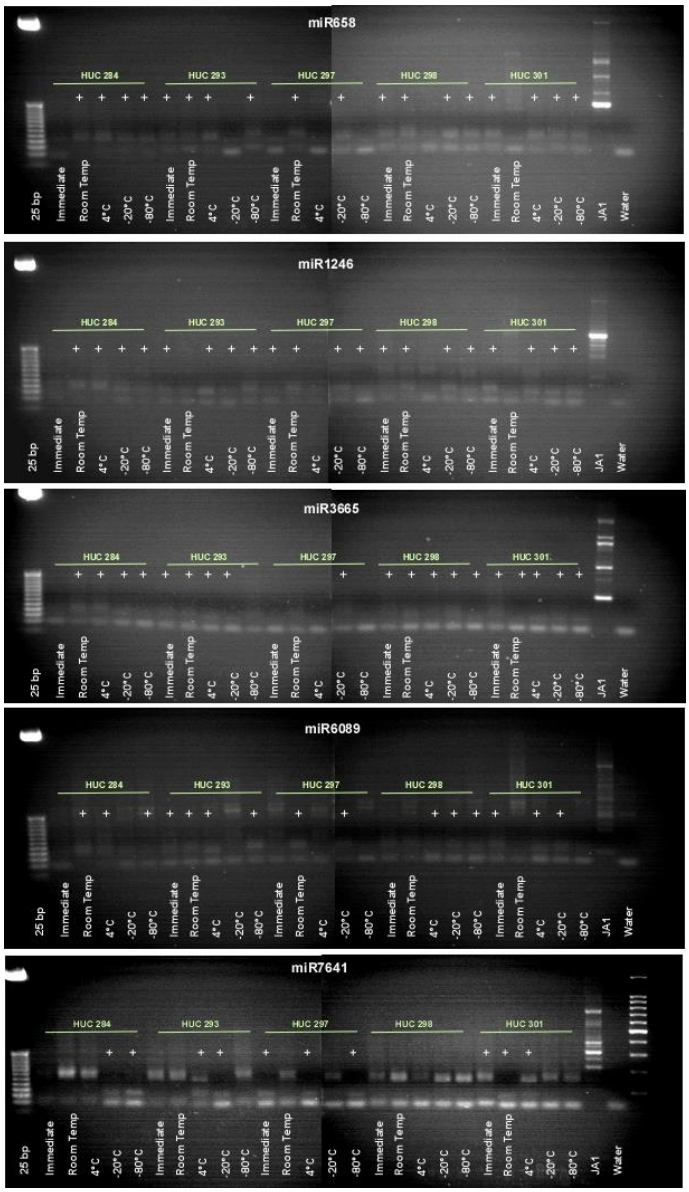

Figure 43: Supplementary Figure S8

Analysis of extracellular vesicle (EV)-associated microRNAs (miRNAs) by real-time polymerase chain reaction (RT-PCR) for EVs isolated from human umbilical cord-derived mesenchymal stromal cells (UC-MSCs) conditioned media (CM) immediately or stored at room temperature, 4°C, -20°C, or -80°C. miR primers were designed using the NCBI GenBank data for human miR-658, miR-1246, miR-3665, miR6089, and miR-7641 (see Table 4). There is evidence that EVs contain miRNA for all primers tested.

Appendix C - Supplementary Data from Chapter 4

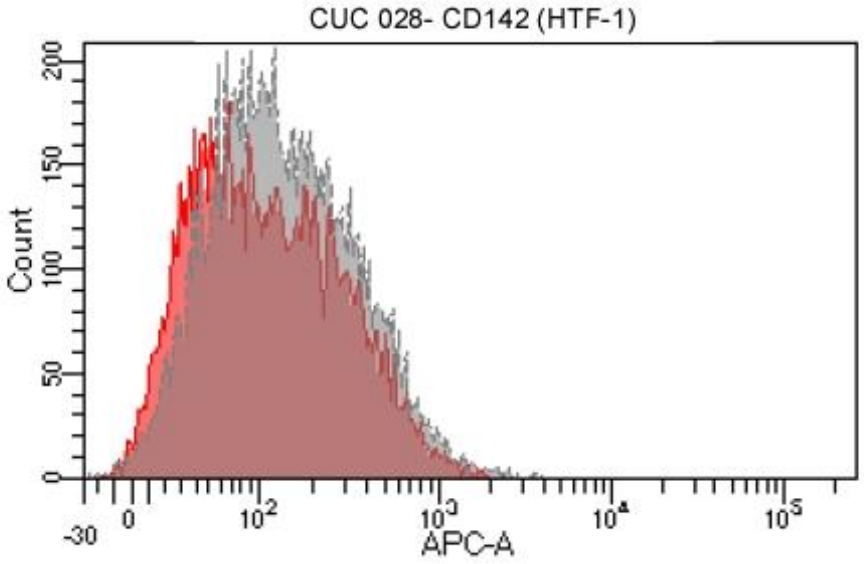

Figure 44: Supplementary Figure S9

Representative flow cytometry histogram with unstained cells (light gray) versus antibody-labeled sample (red) for three canine MSC cell lines. Canine MSCs were stained with primary antibody human anti-mouse CD142 and secondary antibody goat anti-mouse IgG APC (Invitrogen, Cat. No. A-865). There was no shift in fluorescence intensity indicating this particular antibody was not cross-reactive with canines.

Appendix D - Human Umbilical Cord Mesenchymal Stromal Cell Isolation, Expansion, Cryopreservation, and Characterization

A modified version of Appendix D is published in Frontiers in Current Protocols in Stem Cell Biology [23].

Smith, J.R., A. Cromer, and M.L. Weiss, Human Umbilical Cord Mesenchymal Stromal Cell Isolation, Expansion, Cryopreservation, and Characterization. Curr Protoc Stem Cell Biol, 2017. 41: p. 1f.18.1-1f.18.23.

Introduction

Several isolation techniques for umbilical cord-derived mesenchymal stromal cells (UC-MSCs) exist, however no method has emerged as a standard. For example, umbilical cord tissue explant method, or cell isolation following blood vessel dissection and enzymatic dissociation were described [568-570]. Previously, we described a method that required blood vessel removal followed by mechanical and enzymatic digestion to dissociate the cord matrix and isolate UC-MSCs [15, 24]. That method required dissection of vessels, used xenogeneic materials and could not scale-up for clinical production. Recently, we described a simplified and scalable method that uses a closed system for isolation. One objective of our revised method was to reduce or eliminate the use of animal products in our medium. Here we elaborate on methods for isolating, expanding and characterizing UC-MSCs with the intent to unify isolation and expansion methods across laboratories [279].

Basic Protocol 1 describes the isolation UC-MSCs using mechanical and enzymatic digestion (Figure 45). It does not require removing the blood vessels or mincing the cord since

these factors increase contamination risk and decrease yield. Instead, mechanical dissociation using the Miltenyi C-Tubes is used (Figure 45). Basic Protocol 2 describes the expansion UC-MSCs using a medium that eliminates animal-product components. MSCs rapidly attach and expand in this medium. The freezing and thawing process provided in Basic Protocol 3 yields >90% viability at thaw and supports cryostorage of up to 5 million MSCs per mL.

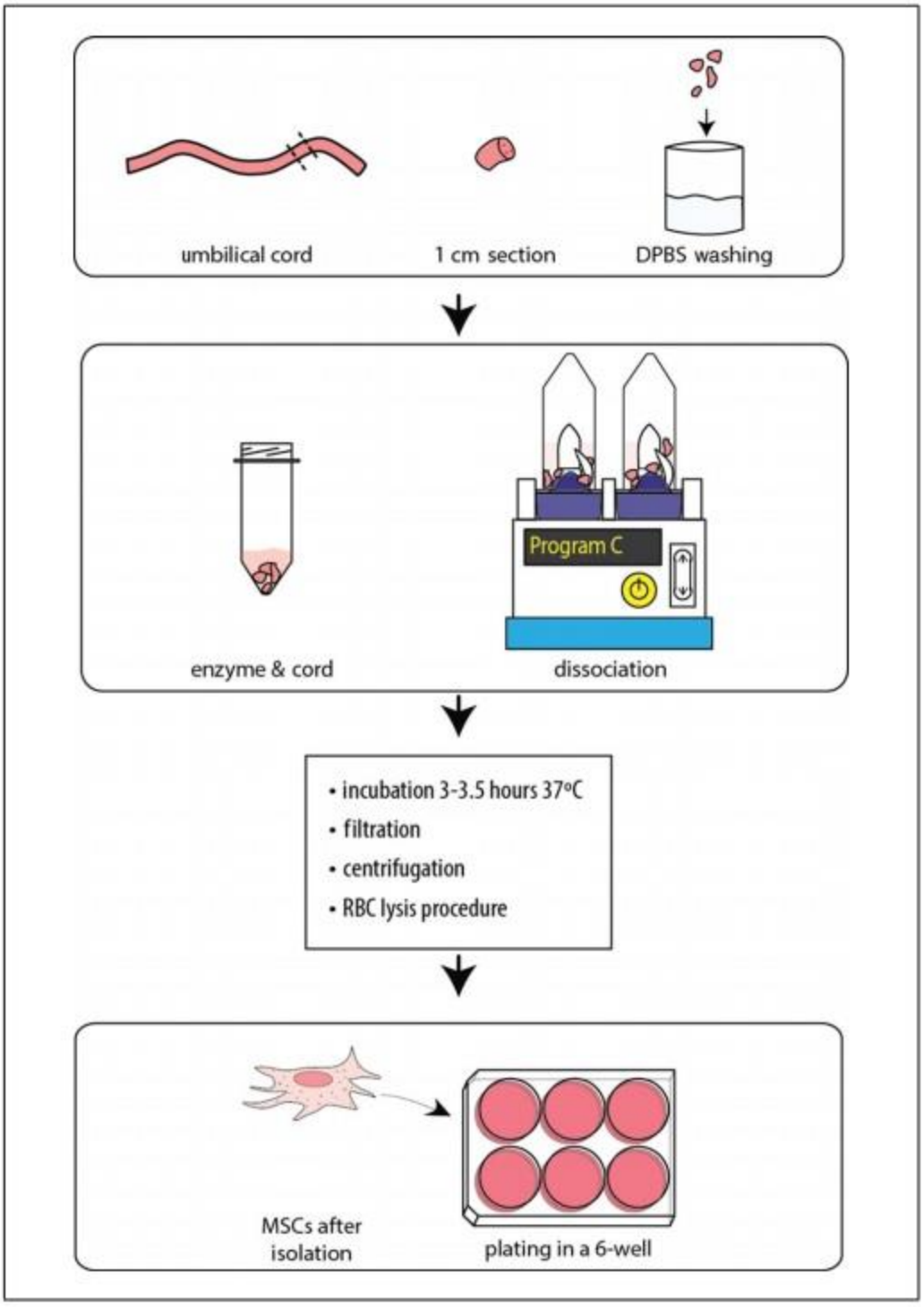

Figure 45: Isolation Flowchart

Flowchart for the isolation procedure showing the major steps involved for obtaining MSCs from the umbilical cord. This figure is an updated version of our previous figure [279].

Basic Protocols 4 to 7 describe characterization of MSCs per the International Society of Cell Therapy (ISCT) minimum definition. Basic Protocol 4 describes flow cytometry methods, Basic Protocols 5 and 6 delineate differentiation methodology and staining (see Figures 47 and 48). Assay of colony-forming unit (CFU) efficiency is described in Basic Protocol 7 (see Figure 49). In summary, the protocols described here generate UC-MSCs in an efficient and scalable manner. UC-MSCs meet the ISCT minimal definition criteria [11].

Strategic Planning

Human subjects committee and biosafety committee review is required for working with human materials. Workplace biohazards program enrollment, health monitoring, biohazardous waste mitigation, sharps and aerosols minimization, spill procedures and biosafety training are required. Depending upon research goals, umbilical cord collection may require enrolling donors and informed consent. If collection of anonymous, discarded human umbilical tissues is sufficient for your work, then your work may be deemed not "human subjects research" under exemption 45 CFR 46.101 (b)(4). In contrast, collection of umbilical cords from people with a particular medical condition, such as Down's syndrome or genetically screened individuals, will require enrollment from targeted populations and informed consent.

Basic Protocol 1: Isolation of Cells from Umbilical Cord

This method is adapted from our previous protocol to accommodate clinical manufacturing considerations such as contamination risk reduction, scaling factors, and reduction of xenogeneic products [15]. Here, Miltenyi C-tubes, human platelet lysate (HPL)-enriched medium, and automated cell counts are used (Figure 45). Each step was optimized to improve cell yield and

viability. UC-MSCs isolated by this method have been upscaled by the supporting protocols for clinical manufacturing (e.g., [571]. Average number of cells per isolation are 1.88×10^5 cells per gram ($\pm 1.27 \times 10^4$ SE, n = 35) (Table 13). This represents a ×150 improvement over our previous protocol [15, 279].

Table 13: Umbilical Cord Isolation Numbers Averaged per Variable

	# Cords	*Avg Cord Weight (g)*	*Avg Viability*	*Avg Total Cells*	*Avg Live Cells*	*Avg Tube Weight (g)*	*Avg Live Size (µm)*	*Avg Dead Size (µm)*	*Cells per gram*	*Live cells per cord*
Cesarean	27	62.2	64.6%	$4.0x10^5$	$2.6x10^5$	1.4	13.9	6.6	$1.8x10^5$	$1.1x10^7$
Std Error		± 4.4	±1.9%	$±3.6x10^4$	$±2.6x10^4$	±0.1	±0.4	±0.1	$±1.6x10^4$	$±1.3x10^6$
Vaginal	10	58.4	62.3%	$5.1x10^5$	$3.0x10^5$	1.4	13.8	6.5	$2.0x10^5$	$1.2x10^7$
Std Error		±4.9	±4.3%	$±7.9x10^4$	$±4.3x10^4$	±0.1	±0.3	±0.2	$±2.4x10^4$	$±1.9x10^6$
High Enzyme	14	64.3	67.5%	$4.7x10^5$	$3.2x10^5$	1.5	13.9	6.6	$2.0x10^5$	$1.4x10^7$
Std Error		±5.0	±2.6%	$±6.1x10^4$	$±4.4x10^4$	±0.1	±0.3	±0.1	$±2.4x10^4$	$±2.3x10^6$
Low Enzyme	23	59.2	61.9%	$4.1x10^5$	$2.4x10^5$	1.4	13.8	6.6	$1.8x10^5$	$9.9x10^6$
Std Error		±4.6	±2.3%	$±4.1x10^4$	$±2.3x10^4$	±0.1	±0.4	±0.2	$±1.6x10^4$	$±9.3x10^5$
Female	18	56.7	65.1%	$3.8x10^5$	$2.5x10^5$	1.3	13.6	6.5	$1.9x10^5$	$1.1x10^7$
Std Error		±5.6	±2.1%	$±5.3x10^4$	$±3.7x10^4$	±0.1	±0.5	±0.2	$±2.2x10^4$	$±2.0x10^6$
Male	19	65.3	62.9%	$4.8x10^5$	$2.9x10^5$	1.6	14.1	6.7	$1.9x10^5$	$1.2x10^7$
Std Error		±4.0	±2.9%	$±4.3x10^4$	$±2.6x10^4$	±0.1	±0.3	±0.1	$±1.7x10^4$	$±1.0x10^6$
All Cords	37	61.2	64.0%	$4.3x10^5$	$2.7x10^5$	1.4	13.8	6.6	$1.9x10^5$	$1.1x10^7$
Std Error		±3.3	±1.7%	$±3.3x10^4$	$±2.1x10^4$	±0.1	±0.3	±0.1	$±1.3x10^4$	$±1.0x10^6$

Materials

Human umbilical cord

Enzyme solution (see recipe)

DPBS-AA (see recipe)

Providone-Iodine solution (see recipe)

Human platelet lysate-enriched medium (HPLM; see recipe)

Red blood cell lysing buffer (Hybri-Max; Sigma, cat. no. R7757)

ViaStain live dead cell stain (Nexcelom, cat. no. C52-0106-5ML)

Personal protective equipment (PPE) including:

Cuffed laboratory coat

Closed-toe shoes

Nitrile gloves

Safety glasses

Surgical mask

Splash shield

Class II biological safety cabinet

Pre-enzyme materials:

C-Tubes (Miltenyi Biotec, cat. no. 130-096-534)

250-ml sterile specimen cups (Fisher, cat. no. 02-540-10)

Sterile forceps; 2, 8-cm straight, blunt end, serrated

Sterile no. 3 scalpel handle

Sterile no. 10 scalpel blade

Sterile 150 × 15–mm petri dishes

Sterile 100 × 15–mm petri dishes

Plastic ruler

37°C water bath

GentleMACS Dissociator (Miltenyi Biotec, cat. no. 130-093-235)

MACSmix Tube Rotator (Miltenyi Biotec, cat. no. 130-090-753)

Post-enzyme materials:

100-µm sterile cell strainer (Fisher, cat. no. 22-363-549)

50-ml, 60-µm Steriflip filters (Fisher, cat. no. SCNY00060)

50-ml sterile centrifuge tubes

1.5-ml microcentrifuge tubes

Counting chambers (Nexcelom, cat. no. CHT4-SD100-014)

Tissue culture treated plates (see materials list for Basic Protocol 2)

Centrifuge

Biohazardous waste container

Waste flask (Erlenmeyer flask containing 10% household bleach)

Sharps container

Auto2000 Cellometer (Nexcelom Bioscience)

37°C, 5% CO2 incubator (90% humidity)

NOTE: Procedures are performed inside a class II biosafety cabinet (BSC). Materials are wiped down with 70% ethanol prior to placing them in the BSC. Sterile packs are opened within the BSC. Universal precautions are used to prevent possible transmission

of human blood borne pathogens.

Umbilical Cord

1. For optimal viability, process the umbilical cord within 24 hr of birth.

   The cord is transported in a sterile specimen cup with double layers of sealed plastic bags from the hospital in normal isotonic saline. Store the samples up to 4 days at 4°C until it is processed.

Setup

2. Assemble pre-enzyme materials in BSC.
3. Add 9 ml enzyme solution to each C-tube and record weight.
4. Warm DPBS-AA and C-tubes with enzyme solution in the water bath for 15 min at 37°C.

Wash and Sanitize

5. Rinse the cord with 100 mL DPBS-AA in a sterile cup. Wash off as much blood as possible.
6. Immerse the cord (until covered, 100 to 200 mL) in Providone-Iodine solution for 5 min at room temperature. Swirl the cup periodically.
7. Remove the cord from Providone-Iodine solution and in a new sterile cup rinse with 100 mL of 37°C DPBS-AA.
8. Place the ruler under the 150 × 15–mm petri dish and measure the length of the cord, unwinding it in the process.

Cutting and Rinsing

9. Along the middle of its length, cut the umbilical cord into 1-cm sections with the scalpel. Rinse the 1-cm sections in a sterile cup with 37°C DPBS-AA (e.g., Figure 45).
10. Using a new sterile petri dish, scalpel and forceps, cut 1-cm cord sections into four equal pieces by making two cuts. Place the pieces into 100 × 15–mm petri dish filled with 37°C DPBS-AA to rinse.

    Repeat rinsing if necessary, to remove as much blood as possible.

Dissociation with Enzyme and Incubation

11. Transfer the pieces into C-tubes with warmed enzyme solution. Pieces from 1-cm section of cord per C-tube.
12. Weigh the C-tube and record the weight.
13. Put the C-tubes into a GentleMACS dissociator and run standard program “C” once.
14. Place the C-tubes into the MACsmixer, incubate with 12 rpm rotation for 3 to 3.5 hr at 37°C.

BSC Setup and After Incubation

15. Prior to the end of the enzymatic incubation, warm DPBS-AA and HPLM in a water bath 15 min at 37°C.
16. Assemble post-enzyme materials in the BSC.
17. Remove the C-tubes from the incubator and run standard program “B” once on the

GentleMACS dissociator.

Filtration

18. Filter the C-tubes contents using a sterile 100-µm cell strainer (or 60-µm Steriflip filter).
19. Rinse C-tubes with 5 mL of warm DPBS-AA and pour through the filter. (For Steriflip, add the 5 mL of DPBS-AA to the C-tube prior to attaching Steriflip).
20. Centrifuge for 5 min at 200 *g*, room temperature.
21. Discard the supernatant into biohazardous waste.

RBC Lysis

22. Suspend the pellet in 0.5 ml HPLM.
23. Add 0.5 mL RBC lysing buffer to each tube. Gently pipette mix each tube for 1 min.
24. Add 9 mL DPBS-AA, and then centrifuge for 5 min at 200 *g*, room temperature.
25. Discard the supernatant in biohazard waste.

Repeat RBC lysis, if necessary (if cell pellet is bright red that indicates blood cell contamination).

Cell Counting with ViaStain

26. Suspend the pellet in 1 mL HPLM.
27. Add 20 µL sample of cell solution into a 1.5-ml microcentrifuge tube. Add 20 µL of ViaStain and mix well by pipetting up and down 4 times.

28. Add 20 µl of 1:1 ViaStain-cell solution to a counting chamber and using the Nexcelom Auto2000 run Nexcelom standard program “Immune cells low RBC” to obtain live/dead count.

Plating Cells

29. Plate the cells on tissue culture treated plates or flasks at a density of 10,000 to 15,000 live cells/cm^2 in HPLM.

    See Table 14 for medium amount per plate or flask, and Figure 45 for example.

Table 14: Passaging and Culturing Component Volume for Plate Size

Culture Vessel	*DPBS (mL)*	*Trypsin (mL)*	*HPLM (mL)*
12-well plate	0.5	0.25	0.75 – 1.0
6-well plate	1	0.5	1.5 – 2.0
T-25 flask	3	1	5
T-75 flask	10	4	15
T-225 flask	25	12	45

30. Cells are passage 0 after the isolation. Culture cells at 37°C, 5% CO2 and 90% humidity until 70% to 80% confluent.
31. Every 3 days, remove half the medium and replace with fresh 37°C HPLM to feed the cells.

Debris will be present in initial isolation. Debris is reduced by passaging and feedings. Cells typically take 10 to 14 days to reach sufficient confluence to make first passage. For passaging, see Basic Protocol 2.

Basic Protocol 2: Culturing and Passaging UC-MSCs

This medium uses fewer components than our previous gold standard medium which reduces preparation time, work load and inventory requirements. Human platelet lysate (HPL) enrichment of the medium supports attachment and expansion. Cells typically appear as shown in Figure 46a when approaching confluence. The average cell yield after passaging is >50,000 cells/cm^2 typically for P0 and >75,000 cells/cm^2 typically for subsequent passages [15, 279].

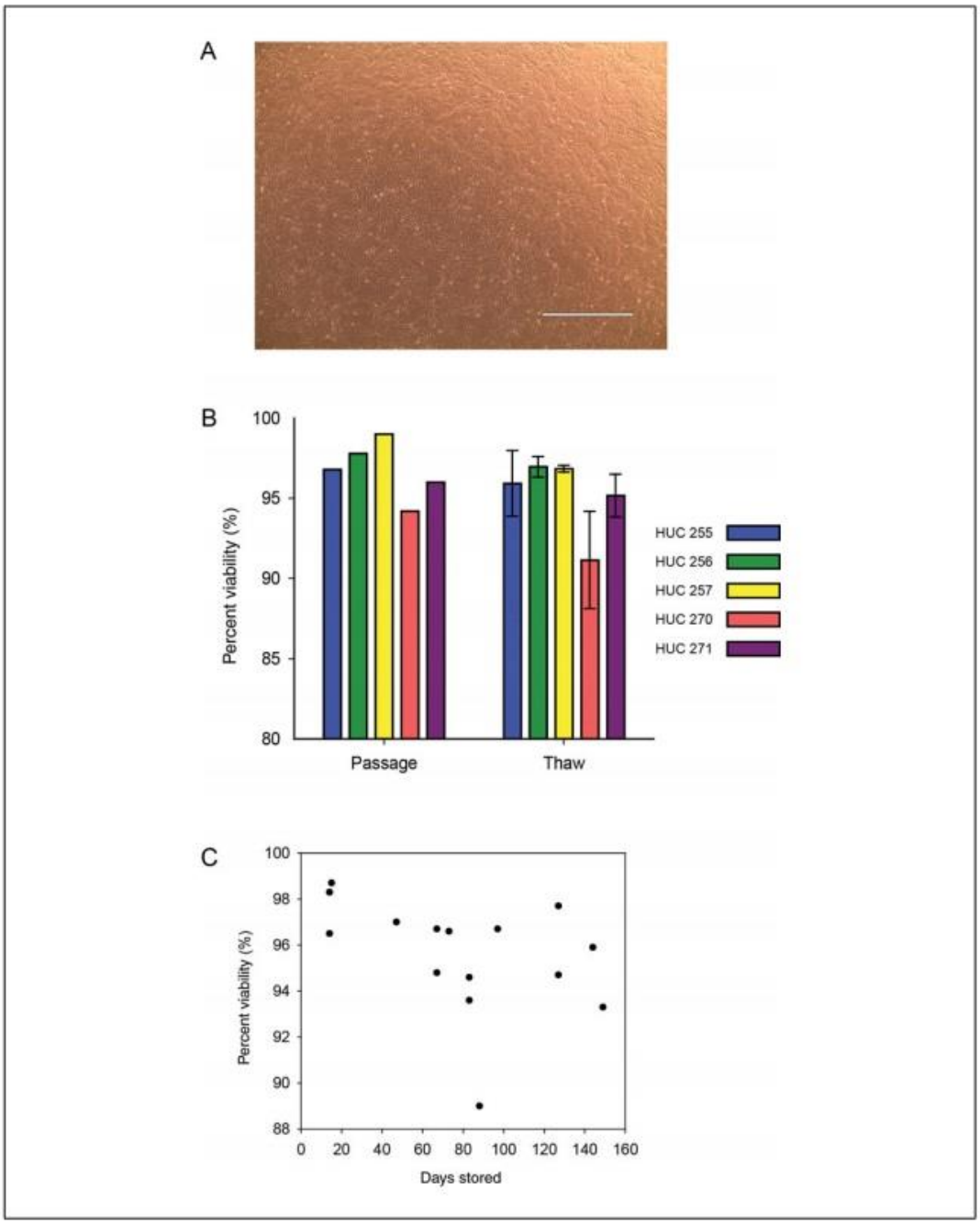

Figure 46: Cell Numbers for Isolation and Expansion

(A) Image of MSCs grown for 3 days before passaging, scale bar = 1000 µm. (B) Viability of 5 cell lines after passage before freezing and after thawing. Error bars represent ± standard deviation, no error bars for passage because n = 1, multiple samples were frozen from the passage for thawing analysis at least n = 2. (C) Percent viability of the thawed sample over time frozen at liquid nitrogen.

Materials

UC-MSCs at 70% to 90% confluence (see Basic Protocol 1 for obtaining cells)

Dulbecco's phosphate-buffered saline (without Ca or Mg, DPBS; Fisher, cat. no. 14190)

0.25% Trypsin-EDTA (Fisher, cat. no. 25200)

Human platelet lysate-enriched medium (HPLM; see recipe)

ViaStain live dead cell stain (Nexcelom, cat. no. C52-0106-5ML)

Tissue culture treated plates

12-well plate (CytoOne, USA Scientific, cat. no. CC7682-7512)

6-well plate (CytoOne, USA Scientific, cat. no. CC7682-7506)

25-cm2 flask (Corning, Fisher, cat. no. 10-126-28)

75-cm2 flask (Corning, Fisher, cat. no. 10-126-37)

225-cm2 flask (Corning, Fisher, cat. no. 10-126-63)

37°C, 5% CO2 incubator

Phase-contrast inverted microscope

50-ml sterile centrifuge tubes

15-ml sterile centrifuge tubes

Cell counting equipment and supplies (see Basic Protocol 1)

Passaging the Cells

Cells are passaged when they are 70% to 90% confluent.

1. Remove medium and rinse cells with volume of 37°C DPBS indicated in Table 14.
2. Dilute 37°C 0.25% Trypsin-EDTA with 37°C DPBS to make a 0.05% Trypsin solution (1:5 dilution) and add to the plate (see Table 14 for volume used).

Aliquots of 0.05% Trypsin-EDTA can be prepared ahead of time and stored up to 1 year at −20°C or it can be stored up to 1 week at 4°C.

3. Incubate 3 min at 37°C.
4. Gently tap side of the plate or flask to facilitate detachment. Evaluate detachment by visualizing with phase-contrast microscopy.

   Minimizing the contact time of cells with enzyme is important: Contact with Trypsin-EDTA for <5 min.
5. Stop enzyme action with 3 volumes of HPLM. Rinse the cells off the plate carefully and collect in a 15- or 50-mL centrifuge tube.

   Centrifuge tube size is dependent on volume of trypsin plus medium mixture. Sometimes more than one tube will be required.
6. Centrifuge for 5 min at 200 × *g*, room temperature.
7. Discard the supernatant. Suspend the pellet in 1 mL of 37°C HPLM.

   Suspend in 1 mL when harvesting up to 150 cm^2 (expected yield is <15 million cells). When harvesting >150 cm^2, suspend in 2 mL of medium.

Counting and Plating UC-MSCs

8. Count the live cells with ViaStain, as in Basic Protocol 1 (see steps 26 to 28).
9. Plate cells at 10,000 cells/cm^2 using 37°C HPLM.
10. Plate the cells by dropwise addition and rock back-and-forth 5 times for homogeneous distribution.

Culturing UC-MSCs

11. Incubate at 37°C, 5% CO_2, and 90% humidity.

    Typically, MSCs take 3 to 4 days to reach 70% to 90% confluence needed for passage.

12. Check confluence every day and feed every three days by removing half the volume of spent medium and replacing it with fresh 37°C HPLM (see Table 14 for volumes).

Basic Protocol 3: Cryopreservation and Thawing of UC-MSCs

Previously we reported that MSCs are sensitive to cryostorage with average viability at thaw of 70% to 80% [15]. Closely following the new freezing protocol is essential to obtain cell viability >90% after thawing. Freeze medium and Mr. Frosty should be kept in 4°C and on ice during cell preparation. This protocol averages 95.6% (±2.4% SD) viable cells after thawing vials that had been frozen from a week to 5 months (Figure 46b). Note, the length of cryostorage does not appear to affect viability of MSCs (Figure 46c).

Materials

UC-MSCs after passage (see Basic Protocol 2)

hES freeze medium (Globalstem, cat. no. GSM-4200)

Ice

Human platelet lysate-enriched medium (HPLM; see recipe)

Mr. Frosty freezing container (Fisher, cat. no. 15-350-50)

Cryogenic vials (2 ml; Fisher, cat. no. 03-337-7D)

−80°C freezer

Liquid nitrogen storage tank

37°C water bath

15-ml sterile centrifuge tubes

Centrifuge

Cell counting equipment and supplies (see Basic Protocol 1)

NOTE: Prior to freezing, MSCs should be in the log growth phase. The final density of MSCs should not exceed 5 million live cells per mL and final volume should not exceed 1.4 mL for a 2-mL cryovial.

Cryopreservation

1. Add cold freeze medium to the MSCs in HPLM at a 1:1 volume to volume dilution and place on ice.

   The freezing medium is at 2× concentration. Example: 500 µL of freeze medium is added to 500 µL HPLM containing 5 million cells for a final concentration of 2.5 million cells per mL.

2. Keep freeze medium on ice to thaw and keep it ice cold until use. Keep Mr. Frosty on ice while loading and after filling preparing vials.
3. Label cryogenic vials and add up to 1.4 mL of the MSCs in freeze medium to each 2-mL tube.
4. Place the vials into the ice-cold Mr. Frosty. When all vials are prepared, place the Mr. Frosty to the bottom of a −80°C freezer for controlled freezing (−1°C per minute.)

5. After 24 hr, transfer vials from Mr. Frosty to liquid nitrogen vapor phase for long-term storage.

Thawing Frozen Cells

6. Remove cryovial(s) from liquid nitrogen storage and place on ice.

   Follow proper safety precautions when working with liquid nitrogen. Warming cyrovials can lead to explosion from pressure build-up. Do not work with liquid nitrogen in an enclosed space.

7. Place cyrovial halfway into a 37°C water bath until frozen pellet is the size of a pea. Crack seal of vial to relieve pressure and quickly reseal.

   Use a 37°C water bath for thawing. Do not use a bead bath.

8. As the last ice crystal melts, pipette the cells into a 15-mL centrifuge tube containing 3 to 5 mL of 37°C HPLM. Rinse the cryovial with 500 µl HPLM and add to the 15-ml tube.
9. Centrifuge for 5 min at 200 *g*, room temperature.
10. Discard the supernatant. Suspend the pellet in 1 mL of 37°C HPLM.
11. Count the cells with ViaStain as in Basic Protocol 1 (see steps 26 to 28).
12. See Basic Protocol 2 for plating cells (see steps 9 to 12).

Basic Protocol 4: Flow Cytometry

Flow cytometry evaluates whether MSCs meet ISCT minimal definition of positive and negative surface markers [11]. The following procedure was adapted from BD Biosciences human MSC analysis kit protocol. Here, 11 tubes are used to establish settings and compensation.

Subsequent lines evaluated require 4 tubes each. See Table 15 for a layout of the conditions. This kit uses 4-color flow cytometry. Individual stains and fluorescent minus one (FMO) color tests are used to adjust the compensation of each channel. Use Accutase to detach MSCs instead of Trypsin-EDTA for passaging cells prior to flow cytometry (described below). For the positive markers, expression >95% is expected and, for negative markers, expression is less than 2%.

Table 15: Flow Cytometry Antibodies for each Test

Tube	*Test*	*Volume (µL)*	*Testing Reason*	*Notes*
1	Unstained	N/A	Initial Gating	Tested in 2nd line
2	CD90	5	Initial Gating	
3	CD44	5	Initial Gating	Tested in 2nd line
4	CD105	5	Initial Gating	
5	CD73	5	Initial Gating	
6	FMO (-CD90)	5 each (15 total)	Compensation	CD44, CD105, CD73
7	FMO (-CD44)	5 each (15 total)	Compensation	CD90, CD105, CD73
8	FMO (-CD105)	5 each (15 total)	Compensation	CD90, CD44, CD73
9	FMO (-CD73)	5 each (15 total)	Compensation	CD90, CD44, CD105
10	Isotypes (+, -) CD44 isotope	20 each, (+, -) 5	False Positives	Tested in 2nd line
11	Cocktails (+ and -)	20 each, (+, -)	Test for 4 Markers	Tested in 2nd line

Materials

UC-MSCs grown in 75-cm^2 flasks (Basic Protocol 2)

Dulbecco’s phosphate-buffered saline (DPBS; Fisher, cat. no. 14190)

Accutase (Fisher, cat. no. NC9464543)

Human platelet lysate-enriched medium (HPLM; see recipe)

Flow cytometry buffer (FACS buffer; see recipe)

Ice

Antibodies (see Table 15)

4% Paraformaldehyde (see recipe)

Human MSC analysis kit (BD Biosciences, cat. no. 562245)

30-µm cell strainer (Miltenyi, cat. no. 130-098-458)

50- and 15-mL sterile centrifuge tubes

Centrifuge

Cell counting equipment and supplies (see Basic Protocol 1)

4-color flow cytometer (BD Biosciences)

12 × 75–mm clear polystyrene tubes (Evergreen, cat. no. 222-2036-050)

Cell Culture

1. Culture MSCs as described in Basic Protocol 2 (steps 9 to 12) to obtain 11 million cells.

   Two 75-cm^2 flasks provide sufficient surface area to achieve this yield. 500,000 to 1 million cells per each tube. A total of 5.5 to 11 million cells are required for the first test as seen in Table 15 (11 tubes). For additional cell lines, fewer MSCs (4 tubes, 2-4 M cells total) are needed. Thus, one 75-cm^2 flask provides sufficient cells for subsequent testing.

2. When the cells reach 80% to 90% confluency, detach below.

Cell Detachment for Flow Cytometry

3. Wash each 75-cm^2 flask with 10 mL DPBS at room temperature. Discard DPBS in waste.
4. Add 5 mL Accutase to the 75-cm^2 flask. Leave the flask at room temperature for 10 min. Tap the side of the flask to release cells from the surface.
5. Add 5 mL HPLM at room temperature to the 75-cm^2 flask. Pipette up and down 5 times to produce a single-cell suspension.

Strain Cells

6. Remove debris by straining cells through a 30-µm cell strainer into 50-mL centrifuge tube.
7. Wash the strainer with 5 mL FACS buffer.
8. Centrifuge for 5 min at 200 *g*, room temperature. Discard the supernatant.

Counting

9. Suspend MSCs with 1 mL FACs buffer.
10. Count the live cells with ViaStain, as in Basic Protocol 2.
11. Add 5 mL FACs buffer to wash cells.
12. Centrifuge for 5 min at 200 *g*, room temperature. Discard the supernatant.
13. Suspend cells at a concentration of 5 million to 10 million cells per mL in FACs buffer solution. Place on ice until staining.

Staining for Flow Cytometry

14. Add the appropriate amount of antibody from the Human MSC analysis kit (see Table 15).
15. After antibody addition, add 100 µL of cell sample into each tube and incubate in the dark at 4°C for at least 30 min.
16. After 30 min elapsed, add 1 mL of ice-cold FACs buffer solution.
17. Centrifuge for 5 min at 200 *g*, room temperature.
18. Discard the supernatant and suspend cells in 2 mL of ice-cold FACs buffer solution.
19. Centrifuge for 5 min at 200 *g*, room temperature.
20. Discard the supernatant and suspend in 400 µL of ice-cold FACS buffer. Then transfer each sample to a 12 × 75-mm clear polystyrene tube.
21. Add about 100 µL of 4% paraformaldehyde.

    Stained and fixed cells can be stored overnight in the dark at 4°C prior to flow cytometry analysis.

Perform Flow Cytometry

22. Any 4-color flow cytometer from BD Biosciences should work for analysis. We use the BD FACS Calibur with CellQuest software.

    The FACS Calibur requires adjusting the voltage, gain and compensation prior to running the test solutions.

23. After the flow cytometer is adjusted, use FCS Express 5 (or a similar software) to analyze the results and obtain dot plots. Negative control (isotype) staining gates are set to 1.0%. See Figure 47 for an example.

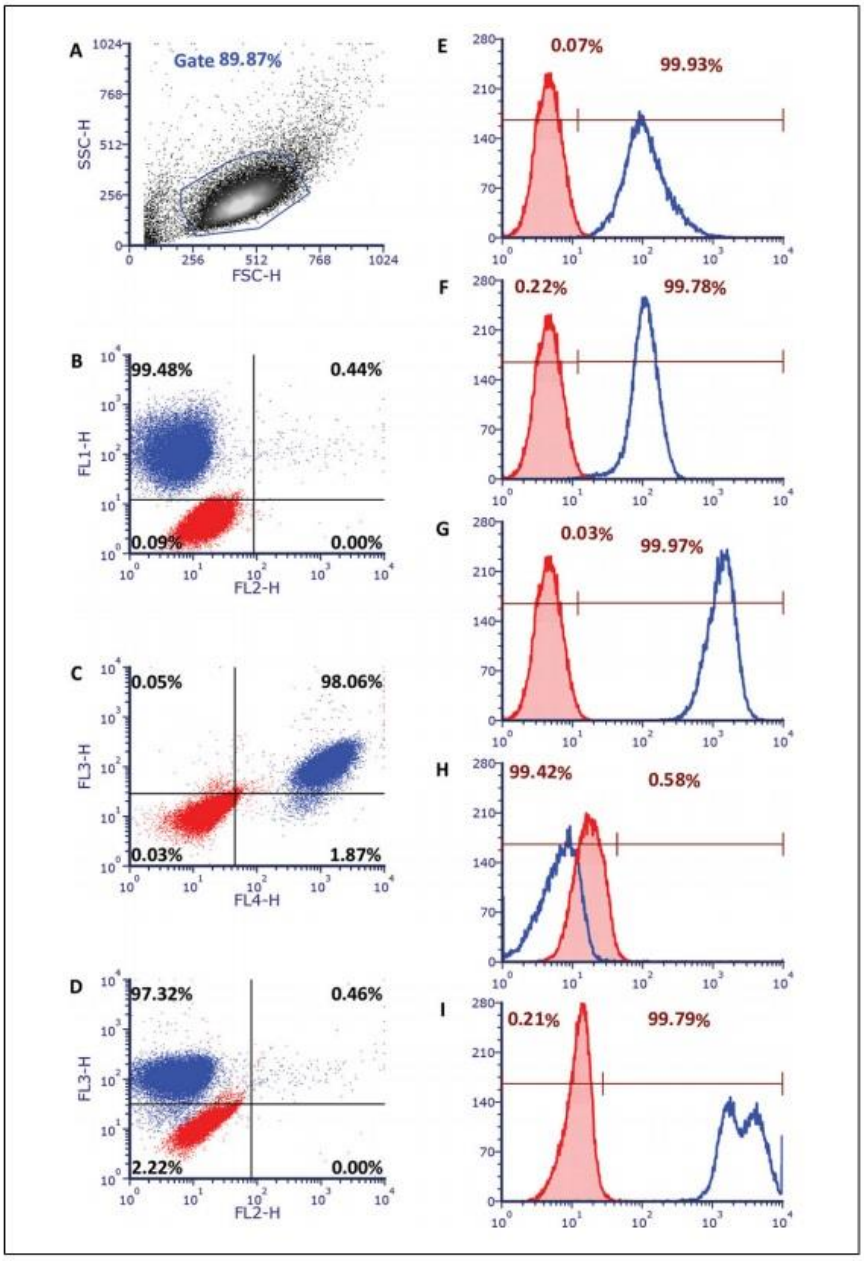

Figure 47: Flow Cytometry Characterization of Human UC-MSCs

Flow cytometry data was initially gated when running samples, gates and quadrants shown here are from previously compensated data. Red = isotype, Blue = test sample result, quadrant values shown are for the test sample. (A) Side scatter vs forward scatter gating for exclusion of doublets and some debris. Density highlight depicting cells primarily inside gate. (B) FL1 channel vs FL2 with quadrant set. (C) FL3 channel vs FL4 with quadrant set. (D) FL3 channel vs FL2 with quadrant set. (E-I) Histograms with isotype (Red) vs. test sample (blue) for positive markers, CD90, CD105, CD73, CD44 and for negative cocktail.

Basic Protocol 5: Osteogenic, Adipogenic, and Chondrogenic Differentiation of UC-MSCs

These protocols were adapted from StemPRO adipogenesis, chondrogenesis and osteogenesis differentiation kit instructions. This protocol will give qualitative evidence that the MSCs can differentiate under those conditions. Figure 48 gives examples of expected growth during differentiation.

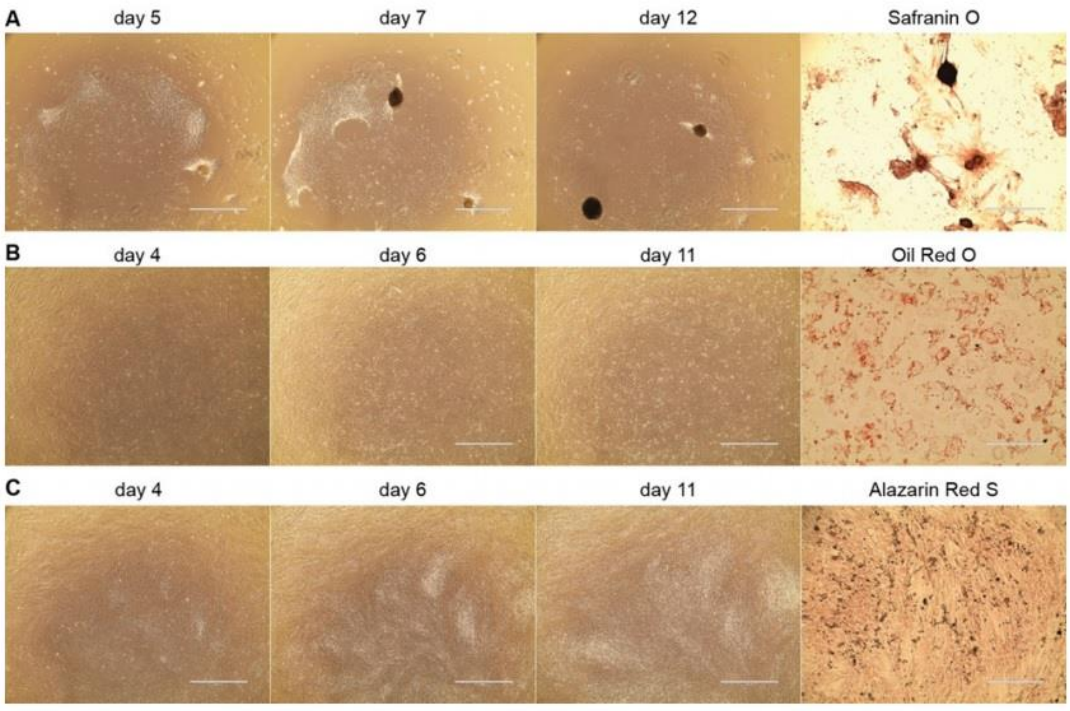

Figure 48: Trilineage Differentiation of Human UC-MSCs

(A) Chondrogenic differentiation at three time points, Safranin O staining after fixation; scale bar for staining represents 1000 µm. (B) Adipogenic differentiation at three time points, Oil Red O staining after fixation; scale bar for staining represents 200 µm. (C) Osteogenic differentiation at three time points, Alizarin Red S staining after fixation; scale bar for staining represents 400 µm. All images for time point data were taken at phase contrast in the same location at the different time points during differentiation. Scale bars represent 1000 µm.

Materials

UC-MSCs (Basic Protocol 2)

StemPro Adipogenesis differentiation kit (Fisher, cat. no. A1007001)

StemPro Osteogenesis differentiation kit (Fisher, cat. no. A1007201)

StemPro Chondrogenesis differentiation kit (Fisher, cat. no. A1007101)

Antibiotic-antimycotic solution (Fisher, cat. no. 15240)

Human platelet lysate-enriched medium (HPLM; see recipe)

50-mL, 0-22 µm filter (Steriflip, Millipore, cat. no. SCGP00525)

12-well plate (CytoOne, USA Scientific, cat. no. CC7682-7512)

37°C, 5% CO_2 incubator

1.5-mL microcentrifuge tubes

Centrifuge

Additional reagents and equipment for counting live cells with ViaStain (see Basic Protocol 1) and for passaging and culturing cells (see Basic Protocol 2).

Cell Culture and Passaging

1. Culture human umbilical cord-derived mesenchymal stromal cells as described in Basic Protocol 2 (see steps 9 to 12).
2. Once wells have reached 70% to 90% confluency, passage the cells.
3. Count live cells with ViaStain, as in Basic Protocol 1 (see steps 26 to 28).

   Each type of differentiation requires a different starting number of MSCs.

Differentiation Media

4. Make the differentiation media (adipogenesis, osteogenesis, and chondrogenesis) following the manufacturer's instructions with one exception: per 100 mL of medium add 1 mL antibiotic-antimycotic, instead of gentamicin.

   We make 50 mL of differentiation medium at a time.

5. 5.Filter the differentiation medium with a 0.22-µm Steriflip. Store up to 1 month at 4°C. Warm to 37°C prior to use.

Adipogenesis

6. Plate the cells as described in Basic Protocol 2 (steps 9 to 10) in a 12-well plate at 10,000 cells/cm^2 in HPLM.
7. After 24 hr in incubator at 37°C, 5% CO_2, replace medium with adipogenesis differentiation medium.
8. Feed cultures every 3 days using adipogenesis differentiation medium. After two weeks, lipid droplet formation should be apparent in cell cytoplasm. Cells will be ready for staining in 2 to 3 weeks.

Osteogenesis

9. Plate the cells as in Basic Protocol 2 (steps 9 to 10) into a 12-well plate at 5,000 cells/cm^2 in HPLM.
10. After 24 hr in incubator at 37°C, 5% CO_2, replace medium with osteogenesis differentiation medium.
11. Feed cultures every 3 days using osteogenesis differentiation medium. After 3 weeks

in culture, calcium deposits will start to form. Cells will be ready for staining after 3 to 4 weeks.

Osteogenesis differentiation takes longer than adipogenesis or chondrogenesis.

Chondrogenesis

A concentration of 8×10^6 cells per mL is required for chondrogenic differentiation. For each well in a 12-well plate, a 5 µL droplet, of 8.0×10^6 cells per mL, will be plated. Calculate the number of cells needed for one more than the number of wells you plan to prepare in case of pipetting error.

12. Determine the number of live cells to add to a sterile 1.5-mL microcentrifuge tube.
13. Centrifuge for 5 min at 200 *g*, room temperature. Discard the supernatant.
14. Add calculated volume of HPLM to the sample to yield 8.0×10^6 cells per mL and mix by pipetting up and down several times.
15. Place 5 µL droplets in the middle of 12-well plates for each sample.
16. Incubate the plates for 2 hr at 37°C, 5% CO_2 and 90% humidity. After the 2 hr, add 1.0 mL of chondrogenesis differentiation medium to the cells.

    Make sure the time is 2 hr, no more. The samples die if left for longer than 2 hr without additional medium.
17. Feed cultures every 3 days using chondrogenesis differentiation medium. The samples start to express chondrogenic-specific markers after 2 weeks. The droplets will be ready to stain in 2 to 3 weeks.

Basic Protocol 6: Staining for MSC Differentiation

MSCs differentiation is confirmed by staining the cells with a specific stain for bone, cartilage or fat. Chondrogenic differentiation is stained with Safranin O to show the GAG proteins associated with cartilage. Alizarin Red S staining visualizes calcium deposits indicating osteogenic differentiation has occurred. Differentiation into adipose cells is confirmed by Oil Red O staining of lipid droplets. See examples for each differentiation in Figure 48.

Materials

UC-MSCs ready to be fixed from Basic Protocol 5

Dulbecco's phosphate-buffered saline with calcium and magnesium (DPBS; Sigma, cat no. 21-030-CV)

4% paraformaldehyde solution (see recipe)

Alizarin Red S solution (see recipe)

Distilled water

Oil Red O working solution (see recipe)

0.1% Safranin O solution (aq.) (Sigma, cat. no. HT904-8FOZ)

Parafilm

Fixing the Cells

1. For a 12-well plate, remove medium and rinse with 500 µl DPBS with Ca++ and Mg++.
2. Add 500 µL of 4% PFA to each well. Fix for 30 min at room temperature.

3. After the fixation, remove PFA and rinse the well twice, each time with 500 µL DPBS with Ca++ and Mg++.

Osteogenic Staining

4. Add 500 µL of filtered 2% Alizarin Red S solution to each well. Stain for 15 min at room temperature.
5. Remove the stain and rinse the wells with distilled water 2 to 3 times.
6. After staining, store the plates in the refrigerator wrapped in Parafilm until photographed.

Adipogenesis Staining

7. Add 500 µL of diluted, filtered Oil Red O stain to each well. Stain for 15 min at room temperature.
8. Remove the stain and rinse the wells with distilled water 2 to 3 times.
9. After staining, store the plates in the refrigerator wrapped in Parafilm until photographed.

Chondrogenic Staining

10. Filter Safranin O 0.1% solution with 0.22-µm syringe filter into a 15-mL tube and protect from light.
11. Add 500 µL filtered Safranin O per well for a 12-well plate. Stain for 15 min at room temperature.
12. Remove the stain and rinse the wells with distilled water 2 to 3 times.

13. After staining, store the plates in the refrigerator wrapped in Parafilm until photographed.

Basic Protocol 7: Colony Forming-Units-Fibroblast (CFU-F)

Colony-forming units can suggest the expansion potential for the particular cell line. We previously found that initial plating numbers and day selections affect colony forming efficiency. The following protocol uses 6 days at 3 different concentrations (50, 100, 500; Figure 49) of cells per 6-well plate. Using three different concentrations ensures one will have countable CFU number per plate in case some lines are more expansive. We found, on average, half the MSCs would form colonies at a plating density of 50 cells, or a CFU-F efficiency of 2 for the UC-MSCs.

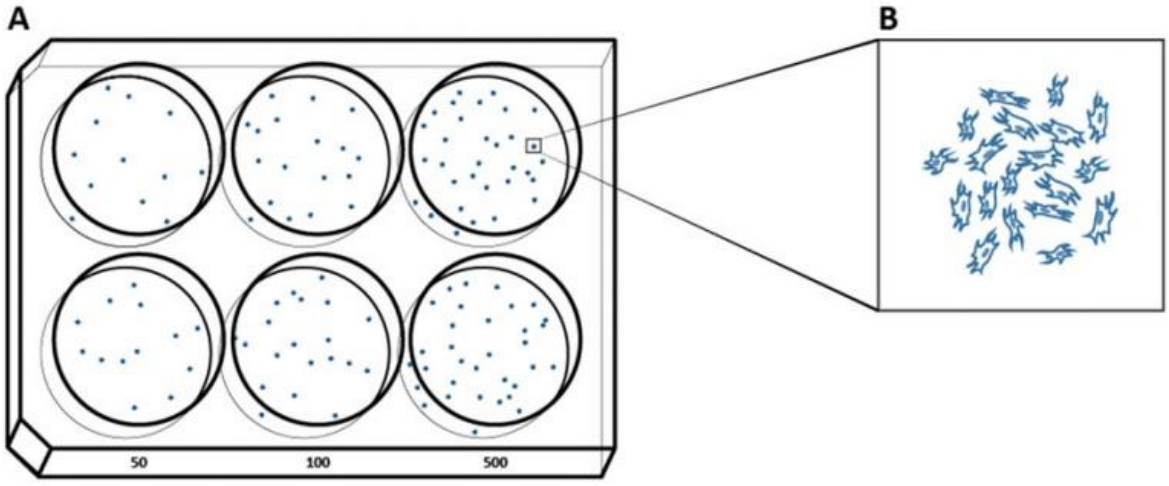

Figure 49: Human UC-MSC CFU-F

(A) Example of a plate with CFUs after they have been fixed and stained with methylene blue according to Basic Protocol 7. (B) A magnified colony, one colony has >10 cells.

Materials

UC-MSCs after passage (Basic Protocol 2)

Dulbecco's phosphate-buffered saline (DPBS; Fisher, cat. no. 14190)

Methanol

1% Methylene Blue solution (aq.), filtered (see recipe)

Distilled water

6-well plates

Phase-contrast illumination, inverted microscope Fisher

EVOS microscope (Life Technologies/Fisher)

Additional reagents and equipment for counting live cells using ViaStain (see Basic Protocol 1, steps 26 to 28)

Cell Culture and Passaging

1. Culture human umbilical cord–derived mesenchymal stromal cells as in Basic Protocol 2 (steps 9 to 12).
2. Once MSCs have reached 70% to 90% confluency, passage the cells as in Basic Protocol 2 (steps 1 to 7).
3. Count the live cells using ViaStain, as in Basic Protocol 1 (steps 26 to 28).

Plating for CFU-F Assay

4. Calculate volume of cell suspension needed for the addition of 50, 100, and 500 cells per well of a 6-well plate (10 cm^2.)

MSC suspension needs dilution to get the cell number into range. We perform this assay in duplicate or triplicates.

5. Grow cells for 6 days. Feed cells on day 3 per Basic Protocol 2.
6. Check the colony size via phase-contrast microscopy every 2 days.

If your MSC lines grow fast, you might need to fix and stain the cells sooner than listed here.

Methanol Fixation

7. Remove the medium and dispose in waste flask.
8. Rinse each well with 1 mL DPBS once.
9. Add 1 mL of 100% Methanol per well and leave for 5 min at room temperature.
10. Remove methanol. Air dry the plate for 5 min at room temperature.

Methylene Blue Staining

11. Add 1 mL methylene blue per well and stain for 15 min at room temperature.
12. Remove the stain and rinse with distilled water about 4 to 5 times until destained.
13. Count the colonies as follows:
    a. Using a dissection microscope, count colonies in each well. Colonies are defined as roughly circular groups of >10 cells.

    OR

    b. Using EVOS microscope to scan entire well, then count each colony by marking on image. Colonies are defined as roughly circular groups of >10 cells.

14. Calculate CFU efficiency by dividing the number of cells plated in the well by the average number of colonies per well.

Reagents and Solutions

Use deionized, distilled water in all recipes.

Alizarin Red S stain, 2%

- Measure 100 mL distilled water into a glass flask
- Add 2 g of Alizarin Red S (Sigma, cat. no. A5533-25 G)
- Mix well using a magnetic stir bar
- After mixing, adjust pH to approximately 4.1-4.3 with 1% NH4OH solution in distilled H_2O (the pH is critical) (works best if adjusted while mixing with the magnetic stir bar)
- Once pH is adjusted, filter the solution using a 0.2-µm syringe filter and protect from light
- Prepare fresh

$CaCl_2$ solution

- Stock: 1 M $CaCl_2 \cdot 2\ H_2O$ solution (FW 147.01)
- Dissolve 147.01 g $CaCl_2$ in 800 ml distilled water
- Adjust volume to 1000 mL with distilled water
- Autoclave $CaCl_2$ stock using liquid cycle
- Store up to 6 months at room temperature

- To use stock to generate 3 mM target: 3:1000 dilution of stock: 3 mL 1 M $CaCl_2$/liter of enzyme solution

DPBS-AA

- Take a freshly opened 500 mL bottle of DPBS without magnesium or calcium (Fisher, cat. no. 14190)
- Add 5 mL of 100× Antibiotic-Antimycotic solution (Fisher, cat. no. 15240)
- Mark DPBS-AA bottle
- Store up to 1 month at 4°C
- Warm to 37°C prior to use

Enzyme solution

Collagenase Type I + Hyaluronidase Enzyme Solution:

Recipe to make 250 ml of solution:

- It is preferable to make the amount you need for each isolation rather than making extra. Enzyme Solution should not be stored in the −20°C freezer. It is good for a day at 4°C after preparation.
- Collagenase Type I (Fisher, cat. no. 17100-017) Target concentration is 562 U/ml. Look up lot enzymatic activity and calculate dilution.

  We have success using both 300 U/ml and 562 U/ml collagenase type I concentration.
- Example: (562 U/ml) × (250 ml) = 140,500 U

  290 U/mg (Lot activity)

  140,500 U (290 U/mg) = 484.5 mg

- Hyaluronidase (MP-Biomedicals, cat. no. 151272) Target concentration is 1 mg/mL. To prepare 250 mL, need 250 mg.
- Calculate amount of each enzyme needed
- Weight amount needed for each enzyme
- Add these to a 50-mL tube (Fisher, cat. no. 05539-6) or a Stericup (Fisher, cat. no. 02-540-10) if making larger amount
- Add DPBS (Fisher, cat. no. 14190) to the enzymes and mix
- Add in 0.75 mL of sterile 1 M $CaCl_2 \cdot 2\ H_2O$
- Sterile filter using 0.22-µm filter
- Divide into 50-mL aliquots
- Store sterile aliquots up to 1 month at −20°C

  To use, thaw and warm to 37°C. Thawed solution is good for 1 day at 4°C

FACS buffer

- Weigh 1 g of bovine serum albumin (BSA; fraction V; Sigma, cat. no. A3912-500G) and add to an Erlenmeyer flask

- Add 100 ml of DPBS (Fisher, cat. no. 14190). Let stand for 10 min so the BSA dissolves. Mixing if necessary to dissolve.

- Solution is good for one day. Make fresh for each use.

Human platelet lysate-enriched medium (HPLM)

For 100 mL combine the following:

- 88 ml DMEM

- 1 g/liter Glucose (Fisher, cat. no. 11885)
- 1 mL of 100× GlutaMAX (Fisher, cat. no. 35030)
- 1 mL of 100× Antibiotic-Antimycotic (Fisher, cat. no. 15240)
- 0.4 mL heparin (1000 USP U/ml)
- 10 mL pooled human platelet lysate (HPL)

Store up to 1 month at 4°C

IMPORTANT: HPL must be added last or the medium may gel. Pooled HPL is a human blood product and may be purchased from a variety of commercial sources or it may be prepared in-house (protocol available upon request).

Methylene blue, 1%

- Add 1 g of Methylene blue to 100 mL distilled water. Allow to stand 5 days prior to use. Store in dark bottle.
- Filter the stain through no. 4 Whatman filter prior to use. Store up to 3 months at room temperature.

Oil Red-O working solution

- Dilute 0.5% Oil Red stock solution (see recipe) with distilled water at a 3:2 ratio and allow to stand for 10 min (e.g., 30 ml of stock plus 20 mL of distilled water)
- Filter the diluted solution and protect from light using 0.2-µm syringe filter
- Prepare fresh

Oil Red-O stock, 0.5%

- Measure 100 ml of 2-propanol into a 100-mL brown glass bottle
- Add 500 mg of Oil Red O powder (Sigma, cat. no. O0652-100 G)
- Protec the solution from light
- Store up to 1 year at room temperature

Paraformaldehyde stock, 10%

- Place 70 mL distilled water at room temperature into a 150-mL Erlenmeyer flask on a stirring hot plate inside a fume hood
- Add 10 g paraformaldehyde (Fisher, cat. no. 04042-500) with stirring
- Heat to 50° to 55°C (do not exceed 60°C)
- Heat and stir for 25 min
- Clear solution with 1 M NaOH added dropwise
- Adjust volume to 100 L with distilled water
- Allow the solution to cool while stirring in fume hood
- Vacuum filter through no. 4 Whatman in fume hood
- Dilute 10% paraformaldehyde (PFA) stock solution to 4% with DPBS with Ca^{++} and Mg^{++}
- Store up to 2 years at −20°C

  It is diluted to 4% with DPBS to use.

Providone-iodine solution

- 195 mL DPBS without magnesium or calcium (Fisher, cat. no. 14190)

- 5 mL providone-iodine solution (10% concentration)
- Final concentration: 0.5% providone-iodine solution in DPBS

  Store up to 1 month at room temperature

Commentary

Background Information

MSCs were first identified in bone marrow as an adherent fibroblastic cell with CFU-F potential [3]. Since that discovery, MSCs have been found in virtually all tissues including adipose, dental pulp, heart, muscle, umbilical cord, amnion, and bone marrow, where they participate in repair of mesenchymal tissues [572, 573]. For these reasons, MSCs have been used as a treatment for numerous diseases and have been a focus for medical research as a regenerative medicine or an immune modulator. Researchers have attempted to ascertain if MSCs from a specific tissue have superior properties for forming bone or cartilage for regenerative medicine, tissue engineering applications, or whether one tissue contains MSCs with superior immune modulatory properties. There are no clear results, likely due to MSCs somewhat plastic response to stimuli. One thing has become clear though, MSCs derived from younger donors proliferate more rapidly than MSCs from older donors [19, 574]. When considering advancing MSCs into clinical production, it may be critical to obtain MSCs from young donors to generate sufficient numbers of cells for treatments.

Depending upon the MSCs tissue source, surgery or other invasive procedures may be needed to obtain them. For this reason, MSCs from a location that does not involve surgery is preferable. The safety and ease of obtaining tissues from a young donor make umbilical cord or

other deciduous tissues of birth a preferable source of MSCs. The present methods generate sufficient MSC yields and expansion for manufacturing of clinically significant numbers for clinical testing.

MSCs have advanced to clinical testing. Trials using bone marrow derived MSCs, or MSCs from amnion, umbilical cord, umbilical cord blood, and adipose tissue are enrolling or have closed enrollment [575]. Umbilical cord-MSCs could be banked, as is umbilical cord blood, and then these banked UC-MSCs could be HLA matched to recipients and used as a source of allogeneic MSC regenerative medicine or tissue engineering treatments.

Research using UC-MSCs has focused primarily on discovering new treatment applications and better understanding their immunological properties in vitro. While many different protocols for isolating, culturing, and expanding UC-MSCs exist there is no single accepted protocol for MSC isolation, expansion or freezing. Even characterization of MSC is not defined [416]. The lack of standardized methods raises questions regarding assay reproducibility between laboratories. For this reason, standardization of MSCs protocol is important. We provide a detailed protocol, here, in the hope that it may lead to further conversation, better uniformity of protocols, better replication across the field, with an end result of more rapid translation into clinic manufacturing and testing.

This protocol addresses some of the issues related to GMP manufacturing, though it falls short in some regards, too. The protocol uses enzymatic digestion and expansion medium containing xenogeneic products. To avoid the digestion step, others have isolated cells from umbilical cord via tissue explants or via mechanical disruption without using enzymes [569, 570, 576]. In our experience, both of these methods result in a lower cell yield and/or a slower startup of the initial culture to first passage; grossly reducing efficiency to produce clinically relevant

numbers of MSCs. We contend that faster start up and reduced passaging are good tradeoff in terms of relative risk to the product. Hyaluronidase is derived from ovine testes. Alternatives are available that are xenogeny-free; we have not tested them yet. Heparin, derived from swine, is one of the most commonly prescribed drugs. Many media use heparin; therefore, we believe its use should not cause a compliance burden [577]. Alternatives to heparin from porcine include synthetic heparin. Heparin was added because the pooled platelet lysate used to supplement the medium can for a gel upon exposure to the calcium rich medium [578]. Another approach is removing fibrin from pooled platelet lysate. Some work indicates that fibrin depleted HPL may improve immunosuppressive properties of the MSCs [579]. We have not investigated the impact of fibrin depletion of HPLM on MSC expansion. An advantage of HPL is, new protocols to improve the safety of platelets by reducing contamination risk are being implemented by the FDA [580]. It is likely that HPLM may be impacted by systems introduced to reduce risk of transfusion transmitted infections, but the actual impact is unknown.

Critical Parameters and Troubleshooting

Several critical parameters affecting isolation have been described [279]. We found variability between donors and between delivery methods that affect the number of cells isolated. For example, the number of cells isolated from umbilical cords after vaginal delivery was larger than the numbers obtained following caesarian section births (Table 13). We stored umbilical cords for up to 4 days prior to isolation. However, we did not notice a difference in the numbers of cells isolated. There does not appear to be an advantage to processing the cord immediately. This finding further supports the notion that establishment of cord processing centers and MSC banking is feasible.

We found that the amount of debris in the initial isolation affected attachment and isolation yield. While some debris from the isolation was always present, too much debris prevented attachment. Our previous isolation protocol produced more debris and had slower attachment and reduced yields. This method did not produce as much debris, so attachment and expansion were more efficient.

Contamination due to red blood cells (RBCs) can be a problem at initial isolation and can affect the attachment and expansion in P0. We saw a trend for RBC contaminated samples to have slower attachment and poorer expansion. The easiest way to prevent RBC contamination is to rinse the blood from the cord before adding the enzyme solution. Performing several extra rounds of rinsing before enzymatic treatment helps more than multiple rounds of RBC lysis at the end of the isolation protocol. Another "trick" is to avoid using parts of the cord that have discoloration associated with blood leaking into the matrix surrounding the blood vessels.

Anticipated Results

This protocol for UC-MSC isolation produces an average yield of 1.88 × 105 (±1.27× 104 SE) cells per gram of cord with an average viability of 63.7% (±1.7% SE) (Table 15). Yields varied which we attribute to variability between donors [279]. It is possible that different portions of the umbilical cord have different numbers of MSCs or different extraction efficiency. We assume that MSCs are uniformly distributed within the umbilical cord and that the cord has uniform extraction efficiency along its length. Thus, sampling from the cord anywhere along its length allows one to estimate theoretically the yield should the whole length be processed.

Cells expand efficiently in 3 to 4 days to reach a confluence for passaging. Upon passage an average viability of 96.9% (±1.52 SD) (Figure 46b) and on average 9.4×10^5 ($\pm 6.2 \times 10^4$ SE)

cells per cm^2 are expected as mentioned in our paper [279]. Figure 46a depicts cells morphology prior to passage at 3 days after plating, these cells were passage 3. Cryostorage with the protocol described allows for storage of MSCs at 5 million cells per ml with little to no cell death over time. We have not been able to test viability after several years yet.

Characterization results demonstrate that this protocol produces MSCs that conform to the ISCT minimal definition [11]. Flow cytometry results indicate that MSC stain for expected positive markers (CD90, CD105, CD73, CD44) with 97% expression and the absence of MSC negative markers ≤2% expression, CD34, HLA-DR, CD11b, CD19, CD and CD45. For the positive markers robust expression is expected for positive and an absence of expression for negative markers (CD45, CD34, CD11b, CD19 HLA-DR) ≤2% expression.

MSCs from umbilical cord have been evaluated in a variety of preclinical models, including, GvHD [581], myocardial infarction [582], and Parkinson's disease [583]. The cells we have isolated from this protocol have been used in preclinical lung injury model [584] and aneurism model (Sharma et al., submitted). Furthermore, expansion of cells using micro-carriers in spinner flasks and a bioreactor demonstrates that large volume, scalable manufacturing of MSCs is feasible; researched using cells isolated via this protocol [571]. These studies demonstrate cells from this protocol have potential to be used for clinical applications and expanded to clinically significant numbers for scale-up.

Time Considerations

Isolation takes 6 hr including 3 to 3.5 hr of enzyme incubation. Passaging takes approximately 30 min. Cryopreservation takes approximately 20 min. Flow cytometry analysis

takes 4 to 5 hr, depending on number of samples. The differentiation assays take about an hour to setup, and three weeks for full differentiation and staining.

Appendix E - Copyright Releases

Chapter 2 Copyright Release

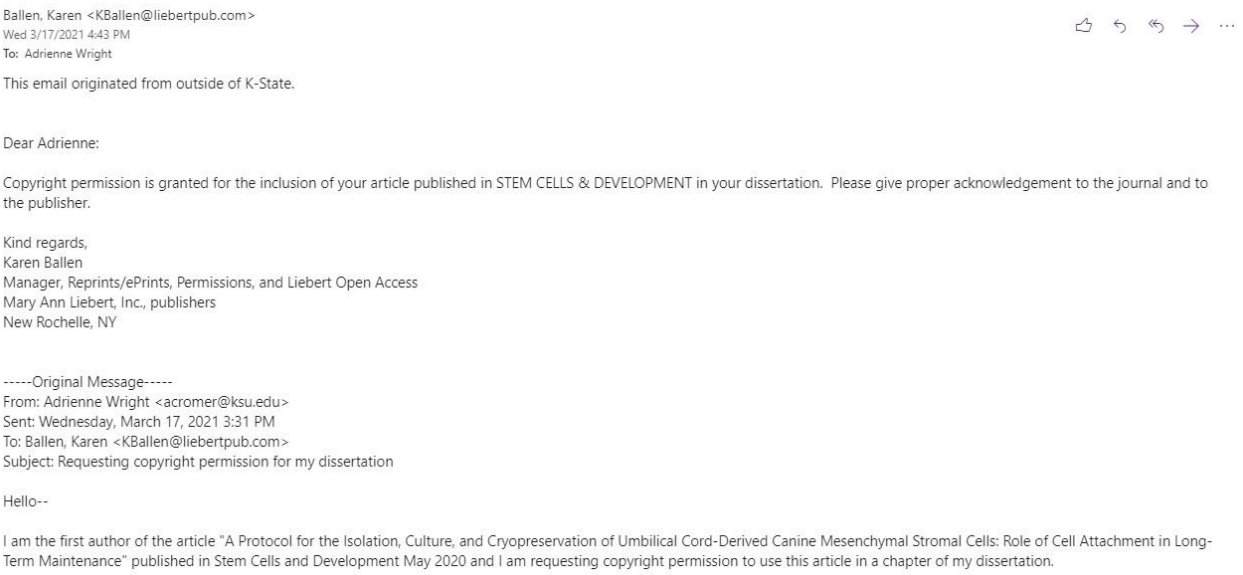

Ballen, Karen <KBallen@liebertpub.com>
Wed 3/17/2021 4:43 PM
To: Adrienne Wright

This email originated from outside of K-State.

Dear Adrienne:

Copyright permission is granted for the inclusion of your article published in STEM CELLS & DEVELOPMENT in your dissertation. Please give proper acknowledgement to the journal and to the publisher.

Kind regards,
Karen Ballen
Manager, Reprints/ePrints, Permissions, and Liebert Open Access
Mary Ann Liebert, Inc., publishers
New Rochelle, NY

-----Original Message-----
From: Adrienne Wright <acromer@ksu.edu>
Sent: Wednesday, March 17, 2021 3:31 PM
To: Ballen, Karen <KBallen@liebertpub.com>
Subject: Requesting copyright permission for my dissertation

Hello--

I am the first author of the article "A Protocol for the Isolation, Culture, and Cryopreservation of Umbilical Cord-Derived Canine Mesenchymal Stromal Cells: Role of Cell Attachment in Long-Term Maintenance" published in Stem Cells and Development May 2020 and I am requesting copyright permission to use this article in a chapter of my dissertation.

Figure 50: Chapter 2 Copyright Release

Chapter 5 Copyright Release

Copyright statement from Frontiers in Cell and Developmental Biology:

"Copyright © 2021 Wright, Arthaud-Day and Weiss. This is an open-access article distributed under the terms of the Creative Commons Attribution License (CC BY). The use, distribution or reproduction in other forums is permitted, provided the original author(s) and the copyright owner(s) are credited and that the original publication in this journal is cited, in